UNIVERSITÀ
DEGLI STUDI
FIRENZE

PhD in
Civil and Environmental Engineering

CYCLE XXXII

COORDINATOR Prof. Borri Claudio

Punching behaviour of R/C flat slabs with openings under seismic loading

Academic Discipline (SSD) ICAR/09

Doctoral Candidate
Dr. Lapi Massimo

_____

Supervisors
Prof. Orlando Maurizio

_____

Prof. Pinho Ramos Antonio

_____

Prof. Spinelli Paolo

_____

Coordinator
Prof. Borri Claudio

_____

Years 2016/2019

Punching behaviour of R/C flat slabs with openings under seismic loading

Abstract

Flat slabs are widely used in many countries thanks to their economic and functional advantages. Although simple in appearance, a flat slab system presents a complex load bearing behaviour, especially in slab-column connections. The punching strength is an important subject in the design of flat slabs, frequently it is the conditioning factor in the thickness design. Nevertheless, the behaviour of flat slabs under the combination of gravity and seismic actions is still not sufficiently studied by the scientific community. The European Code EN1998-1, in 5.1.1(2)P, states: "Concrete buildings with flat slab frames used as primary seismic elements in accordance with 4.2.2 are not fully covered" by the EC8 section on concrete structures. This statement results from the lack of knowledge about the stiffness of slab-column connections and the brittleness of the punching failure. It is also the consequence of insufficient knowledge about the behaviour of slab-column connections under seismic actions. These lacks highlight the need for further researches on the punching strength of slab-column connections under cyclic and dynamic horizontal loading. This research is focused on the seismic response of flat slabs with openings adjacent to the column. The lateral response of slab-column joints in presence of an openings close to the column is poorly investigated. An important part of this work consists in the experimental activity including six specimens 4.15 x 1.85 m with a thickness of 15 cm. Numerical analysis is also included in this research, starting from the experimental results a numerical model is developed in order to predict the behaviour of continuous slab under combined vertical and horizontal loading.

Keywords: Flat slab, punching, seismic behaviour, cyclic loading, openings

CONTENTS

LIST OF FIGURES

LIST OF TABLES

1. INTRODUCTION

1.1 Punching of reinforced concrete flat slab

Reinforced concrete flat slab are very common in structures for residential, commercial and office buildings. This structural system has many advantages, such as: reduced utilization and lower complexity of formwork; easier installation of electrical and mechanical services; reduction in floor height due to the absence of interior beams; versatility and flexibility in space compartmentation and faster construction. Flat-slab structures exhibit a very complex behaviour against bending and shear stresses in the slab-column zone. The transfer of shear forces and bending moments between the slab and the column causes high stresses which can lead to the failure of the slab by punching.

The punching failure is due to a stress concentration along the column perimeter and it is characterized by a collapse surface with a truncated cone shape. This type of failure is rather brittle, and it occurs with limited warning signs. Although a local mechanism, it could bring to a progressive collapse of the entire building, especially if the design of the original slab did not comprise any integrity reinforcement crossing the column. For these reasons the punching issue is primary in the design of R/C flat slab buildings.

The problem of punching in flat slab is even more complex and detrimental when gravity loadings are combined with horizontal cyclic drifts, such as the occurrence of an earthquake. During an earthquake, even if the slab column frames are not considered as primary seismic elements, their connections are subjected to the same drift as the primary elements. These

cyclic drifts, playing a detrimental role on the punching strength of the slab column connections in combination to the presence of gravity loading, could bring to the premature collapse of the slab-column connection.

Nevertheless, the behaviour of flat slab under the combination of gravity and seismic actions is still not sufficiently studied by the scientific community. The European Code EN1998-1 [1], in 5.1.1(2)P, states: “Concrete buildings with flat slab frames used as primary seismic elements in accordance with 4.2.2 are not fully covered” by the EC8 section on concrete structures. This statement results from the lack of knowledge about the stiffness of slab-column connections and the brittleness of the punching failure. It is also the consequence of insufficient knowledge about the behaviour of slab-column connections under seismic actions. These lacks highlight the need for further researches on the punching strength of slab-column connections under cyclic and dynamic horizontal loading.

1.2 Motivation and objective of this research

This research aims at increasing the knowledge on the seismic behaviour of flat slab, that is required for a future development of design recommendations that include seismic actions. The punching capacity of flat slab under seismic actions is not quantified by extensive experimental research. Current formulations for the evaluation of the punching strength were developed from quasi-static tests, and do not take into consideration the degradation caused by cyclic and dynamic loading that happens during an earthquake.

This research is focused on the behaviour of slab column connections with openings adjacent to the column under combined gravity and horizontal loading. The need of a deeper investigation on this topic arises from two considerations: the presence of openings in slabs is always needed for the crossing of mechanical and electrical services and usually the openings are placed adjacent to the columns for architectonical reasons; besides the presence of the openings adjacent to the columns is very common, the effects provided by the openings in case of combined gravity and horizontal loading acting on the slab column connection are scarcely investigated since only a few researches deal with this problem [2,3].

The limited number of experimental results, dealing with this problem, represents the greater problem for a future development of design code provisions. For this reason an important part of this research is devoted to the execution of a new experimental campaign consisting in six specimen 4.15 x 1.85 m with a thickness of 0.15 m. Furthermore, for a correct

interpretation of the experimental results and for their extensions, non-linear numerical analyses are also included in this research.

The aim of this thesis is to provide a better understanding of the role played by the opening placed adjacent to the column on the response of a slab column connection subjected to combined gravity and horizontal loading.

1.3 Organization of the thesis

In the following the organization of the thesis is shown and the content of each chapter is briefly recalled. Besides the introduction and the final conclusions, the thesis consists of four chapters: the literature review (§2), the experimental campaign (§3), the experimental results (§4), the numerical analysis (§5).

The Chapter 2 presents the main analysis methods for slabs laterally loaded and the analytical models for punching prediction of slab column connections under combined gravity and horizontal loading. Then, the experimental campaigns dealing with the presence of opening adjacent to the column, focused on punching failure due to gravity loading or combined gravity-horizontal loading, are shown and the main results provided by these works are presented and discussed. Finally, the main code provisions dealing with the punching of R/C slabs with opening adjacent to the columns under gravity or combined gravity and horizontal loading are presented.

The Chapter 3 describes the characteristics of the new experimental campaign. The test setup is described and analysed then the characteristics of the new specimens are presented. Therefore, the mechanical and geometrical characteristics of aggregates, cement, concrete and reinforcing steel are shown. Finally, the instrumentation and the loading protocol are presented.

The Chapter 4 presents the experimental results according to three different groups: gravity loading tests, combined gravity and horizontal loading tests without shear reinforcement, combined gravity loading tests with shear reinforcement. The test results obtained during this experimental campaign, with opening adjacent to the column, are compared to those provided by reference slabs without openings. Finally, the critical discussion of the results is provided.

The Chapter 5 deals with the numerical analysis performed with the software ABAQUS. Firstly, the calibration of the model is performed then the comparison with the experimental

results is shown and discussed. The effect of gravity loading distribution on the response of the slab column connection is also investigated. Finally, a numerical model of an internal slab column connection is developed and its response, in presence of openings adjacent to the column, is investigated against combined gravity and horizontal loading.

1.4 References

[1] European Committee for Standardization.; Eurocode 8: Design of structures for earthquake resistance - Part 1: General rules, seismic actions and rules for buildings Eurocode, 2004.

[2] El-Salakawy, EF.; Polak, MA.; Soliman, MH.; Reinforced concrete slab-column edge connections with openings, ACI Structural Journal, 1999, Vol. 96: pp. 79–87.

[3] Bu, W.; Polak, MA.; Effect of openings and shear bolt pattern in seismic retrofit of reinforced concrete slab-column connections, Engineering Structures, 2011, Vol. 33: pp. 3329–40.

2. LITERATURE REVIEW

2.1 Introduction

In this chapter a literature review focused on punching strength of slabs with openings is provided. Firstly, the analysis methods for the prediction of the lateral response of slab-column connections are shown, then the analytical models for punching failure with combined gravity and lateral loading are provided. Then, a review of experimental researches dealing with punching failure of slab with opening is proposed. Therefore, the main code provisions about this topic are presented and discussed. Finally, a critical discussion of the literature is presented.

The order of the paragraphs follows the logical design process: firstly vertical forces and unbalanced moments acting on the slab column connections are determined (§2.2) then the punching problem for combined gravity and lateral loading is accounted (§2.3), therefore the presence of the opening is analysed (§2.4), finally the connection is designed according to the code provisions (§2.5).

As shown in the following, the design process is complicated by the fact that the literature about this problem is very scarce. Therefore, nowadays the design of a slab column connection under combined gravity and lateral loading, in presence of openings adjacent to the column, is performed without specific references. More in general, the ACI provisions only provide a method for the design of a slab column connection under combined gravity and lateral loading. Therefore, a deeper investigation about this problem is required.

2.2 Analysis methods for laterally loaded flat slab

The prediction of the lateral response of a flat slab column connection is much more complex than the prediction of the response provided by a beam-column connection. Nowadays, FEM analysis represents an important support for designers, however the need to use analytical methods, that are easy to apply, is still fundamental. Historically, there are two methods for the prediction of the flexural behaviour of slab column connections subjected to lateral loading, the Equivalent Frame Method (EFM) and the Effective Beam Width Method (EBWM). In the following these methods are presented and discussed.

2.2.1 Equivalent Frame Method

The prediction of the lateral load-displacement relationship of slab-column connections was an important challenge for the researchers. One of the first attempts [1] consisted in an elastic model based on a frame analysis. Starting from it, Corley et al. [2] developed the Equivalent Frame Method (EFM) for slab design. Following this approach, also known as the Equivalent Column Method, slab-column connections are modelled as beams and equivalent columns (Figure 2.1).

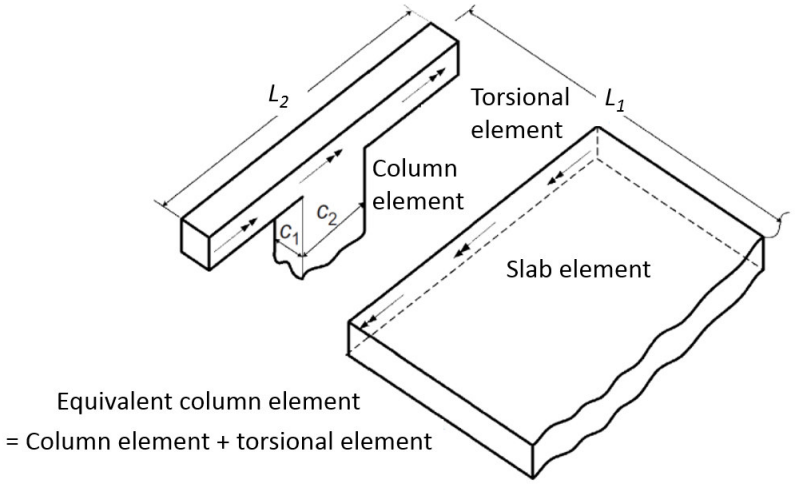

Figure 2.1 – Equivalent column model, adapted from Park et al. [3].

The beams are modelled according to the full slab width. The moment transfer is assumed to occur directly on the column width (c_2) and indirectly via torsional members [4]. The flexibility of the equivalent column is given by:

$$\frac{1}{k_{ec}} = \frac{1}{k_c} + \frac{1}{k_t} \tag{2.1}$$

where k_{ec} is the flexural stiffness of the equivalent column, k_c is the flexural stiffness of the column and k_t is the stiffness provided by the torsional member. Equation (2.1) is a direct consequence of the structural model which assumes that the column and the torsional member are two springs in series. The flexural stiffness of the column is given by:

$$k_c = \frac{4 \cdot E_c \cdot I_c}{H} \tag{2.2}$$

where E_c is the elasticity modulus of concrete, I_c is the moment of inertia of the column cross-section computed based on the gross section and H is the height of the column. The computation of k_t requires some assumptions on the distribution of the unit twisting moment (t_x) along column centreline. Corley and Jirsa [2] proposed a triangular distribution that was still adopted by ACI 318-14 [5]:

$$t(x) = \frac{4}{L_2^2} \cdot x \tag{2.3}$$

the notation used in equation (2.3) and the distribution of external twisting moment are shown in Figure 2.2.

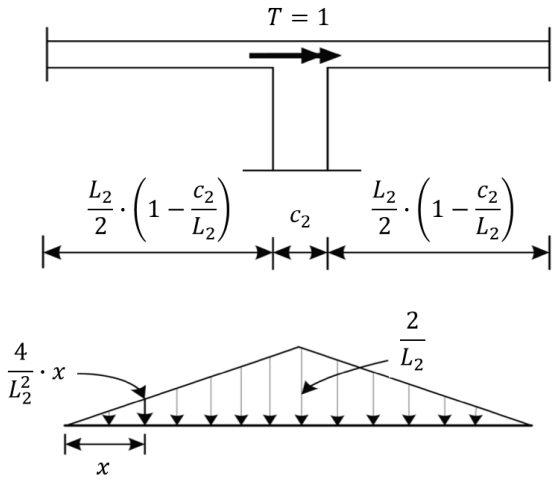

Figure 2.2 – Triangular distribution of twisting moment per unit length, adapted from Park et al. [3].

Integrating over the interval zero to x, follows the twisting moment diagram:

$$T(x) = \int_0^x \frac{4}{L_2^2} \cdot x \cdot dx = \frac{2}{L_2^2} \cdot x^2 \tag{2.4}$$

integrating again and dividing by the torsional stiffness, the unit rotation angle is found:

$$\theta(x) = \int_0^x \frac{T(x)}{C \cdot G} \cdot x \cdot dx = \frac{2}{3 \cdot C \cdot G \cdot L_2^2} \cdot x^3 \tag{2.5}$$

where the torsional constant (C) is taken equal to [2]:

$$C = \sum \left(1 - 0.63 \cdot \frac{x}{y}\right) \cdot \frac{x^3 \cdot y}{3} \tag{2.6}$$

where in this case x and y are the shorter and the longer side of the rectangular cross-section of a torsional element respectively. Assuming that no rotation occurs over the width of the support, the maximum rotation is given by:

$$\theta_{max} = \frac{L_2 \cdot (1 - c_2/L_2)^3}{12 \cdot C \cdot G} \tag{2.7}$$

considering zero the Poisson's ratio and assuming the average rotation angle (ϑ_{avg}) as 1/3 of the maximum rotation (ϑ_{max}) [6] results:

$$\theta_{avg} = \frac{1}{3} \cdot \frac{L_2 \cdot (1 - c_2/L_2)^3}{6 \cdot C \cdot E_c} \tag{2.8}$$

Torsional stiffness (k_t=T/ ϑ_{avg}) is calculated for one half of the torsional element (T=1/2), then the total stiffness is obtained by summing the contribution of each torsional element as follows [6]:

$$k_t = \sum \frac{9 \cdot C \cdot E_c}{L_2 \cdot (1 - c_2/L_2)^3} \tag{2.9}$$

However, this method is limited to elastic analysis and cannot be used for seismic analysis [4].

2.2.2 Effective Beam Width Method

Since the 1960s, as reported by Vanderbilt and Corley [6], the researchers began to develop another model for the prediction of the slab response under lateral loading. In this

model it is assumed that an "effective width" of the slab acts as a beam. Actually, if a moment is applied in the slab-column joint, the slab rotation varies along the slab width. The rotation is maximum close to the column and it becomes smaller with distance (Figure 2.3). The equivalence with a beam is determined by choosing an appropriate effective width ($\alpha \cdot L_2$) that gives:

$$\alpha \cdot L_2 \cdot m_{max} = \int_{-L_2/2}^{L_2/2} m_x \cdot dx \tag{2.10}$$

where m_{max} is the maximum moment acting on the slab width, m_x is the moment at the coordinate x.

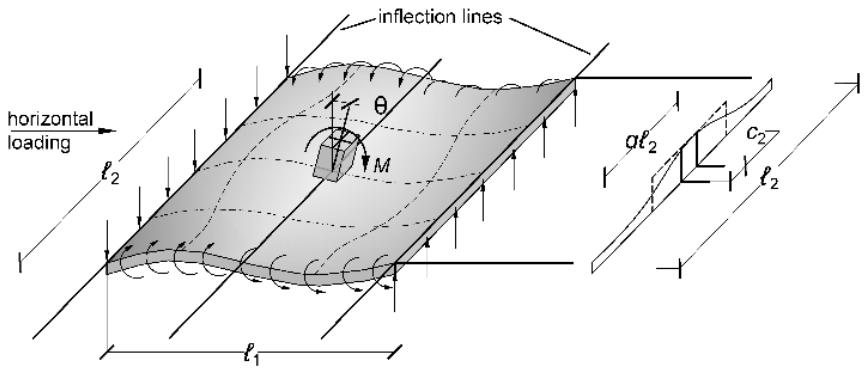

Figure 2.3 – Slab-column structure under lateral loading and moment distribution along the column centreline, adapted from Vanderbilt and Corley [6].

Pecknold [7] solved the elastic problem using the Levy method. The effective width was given as a function of the column size (c) and of the slab dimensions (L_1, L_2). Later, Allen and Darvall [8] provided the effective width coefficients (α) in tabular form, varying the ratios c_1/L_1, c_2/L_2 and L_1/L_2. A summary of previous effective beam width studies is provided by Vanderbilt et al. [6]. In 1987, Banchik [9] showed effective width solutions using the finite element technique. Starting from this work, Hwang and Moehle [10] proposed a simple formula for the effective width, in agreement with the Banchik's results and in accordance with the Westergaard Theory [11]:

$$b = 2 \cdot c_1 + \frac{L_1}{3} \tag{2.11}$$

for exterior frames, the effective width can be approximated as:

$$b = c_1 + \frac{L_1}{6} \tag{2.12}$$

such formulae are also adopted by ASCE/SEI 41-13 [12].

With the increase of lateral loads, cracking in the slab increases and the slab stiffness reduces. To take into account this phenomenon, Vanderbilt and Corley [6] recommended a stiffness reduction factor (β) equal to 1/3 for the equivalent frame analysis. Han et al. [13] provided a summary of all previous studies about the stiffness reduction factor. Luo and Durrani [14] proposed the following formulae:

$$I_e = (M_{cr}/M_a)^3 \cdot I_g + [1 - (M_{cr}/M_a)^3] \cdot I_{cr} \tag{2.13}$$

$$I_g = \frac{\chi \cdot \alpha \cdot L_2 \cdot h^3}{12} \tag{2.14}$$

$$\chi = 1 - 0.4 \cdot \frac{V_g}{V_c} = 1 - 0.4 \cdot \frac{V_g}{\left(\frac{1}{3} \cdot b_0 \cdot d \cdot \sqrt{f_c}\right)} \tag{2.15}$$

where I_e is the reduced effective moment of inertia, I_g is the gross moment of inertia of the effective width slab, V_g/V_c is the gravity shear ratio and χ is a factor accounting for the cracking due to gravity loads (in SI units). The reduction factor is easily obtained as $\beta=I_e/I_g$. A further approximation is provided by Hwang and Moehle [10]:

$$\beta = 4 \cdot \frac{c_1}{L_1} \tag{2.16}$$

2.3 Analytical models for punching failure with combined gravity and lateral loading

2.3.1 Eccentricity of shear

2.3.1.1 Background to ACI 318-19 punching shear provision

Di Stasio and Van Buren [15] introduced the concept of “eccentricity of shear”, where the unbalanced moment between the slab and the column is considered to be transferred by

both flexure and uneven distribution of shear forces around the column. The maximum factored shear stress is given by:

$$v_{u(AB)} = \frac{V}{b_0 \cdot d} + \frac{\gamma_v \cdot M \cdot c_{AB}}{J_c} \tag{2.17}$$

where V is the shear force acting on the critical section, b_0 is the critical perimeter set at d/2 from the column, d is the effective depth, J_c is analogous to the polar moment of inertia, γ_v and γ_f are respectively the portion of unbalanced moment transferred by eccentricity of the shear and by flexure, such as $\gamma_v + \gamma_f = 1$, and c_{AB} is the dimension shown in Figure 2.4.

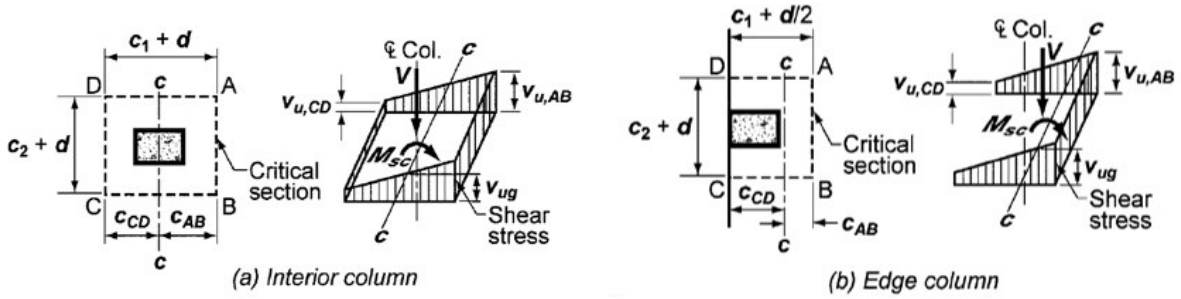

Figure 2.4 – Assumed distribution of shear stress according to ACI 318 – 14 [5]

Later, Moe [16] found that the portion of unbalanced moment transferred by eccentricity of shear is independent from the amount of flexural reinforcement and could be taken equal to 1/3. Starting from 1971, ACI provisions are grounded on Hanson and Hanson's (Hanson and Hanson, 1968) approach which recommended γ_v=0.4. For rectangular columns the following adjustment is provided [5]:

$$\gamma_v = 1 - \frac{1}{1 + (2/3) \cdot \sqrt{b_1/b_2}} \tag{2.18}$$

where b_1 and b_2 are the dimensions of the critical sections.

2.3.1.2 Background to EC2-2004 punching shear provision

In 1970 Mast [17] showed that the plastic distribution of shear stress due to a moment acting between a slab and a column is close to be rectangular [18], as shown in Figure 2.5.

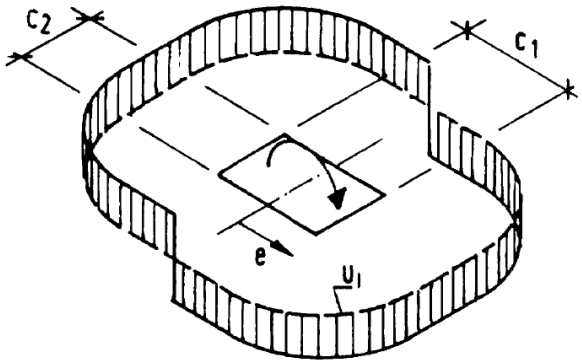

Figure 2.5 – Distribution of shear stresses in slab due to transfer of a moment from a column, adapted from Regan [18].

Later Stamenkovic and Champman [19] provided an interaction curve between vertical loading (V) and unbalanced moment (M):

$$\frac{V}{V_u} + \frac{M}{M_u} = 1 \tag{2.19}$$

The linear interaction is given in terms of V/V_u and M/M_u, where V_u is the failure load when M=0 and M_u is the failure moment when V=0. The interaction curve was also studied by Hawkins et al. [20] who calculated the punching shear stress according to Hanson and Hanson's (Hanson and Hanson, 1968). Starting from these works Regan [18] developed the punching provision for Model Code 1990 [21]:

$$v_{u(AB)} = \frac{V}{b_0 \cdot d} + \frac{K \cdot M}{W \cdot d} \tag{2.20}$$

where M is the transferred moment, K·M is the part transmitted by uneven shear including torsion and W is the integral $W=\int|e|\cdot dl$ extended to the critical perimeter set at 2d from the column, where *dl* is an elementary length of the perimeter and *e* is its distance from the axis about which the moment acts. The values of K given in Model Code 1990 (MC90) [21] primarily depend on the ratio between the column sizes c_1/c_2 (Table 2.1).

Table 2.1 – Ratio of moment transferred to the column by uneven shear

c_1/c_2	0.5	1.0	2.0	3.0
K	0.45	0.60	0.70	0.80

The approach proposed by Regan is also included in the punching shear provision of Eurocode 2 – 2004 (EC2-2004) [22].

2.3.2 Strip model

The strip model, originally called Bond Model [23], describes an internal forces distribution for flat slab that satisfies equilibrium and does not violate either shear or flexural strength limits at any point [24]. The slab is subdivided into two different regions, B-regions dominated by slender flexural behaviour and D-regions dominated by deep beam behaviour. According to this model radial strips are assumed to be D-regions while plate quadrants are assumed to be D-regions (Figure 2.6).

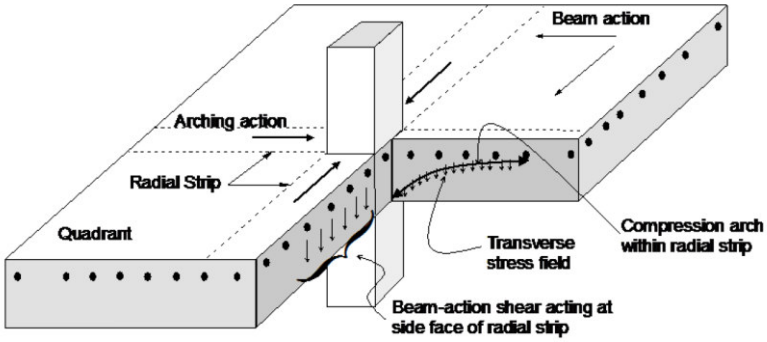

Figure 2.6 – Beam and arching action at column slab-connection, adapted from Alexander [24].

The distribution of load for an internal radial strip, loaded on two faces, is represented in Figure 2.7. The flexural strength of the strip (M_s) is provided by the sum of negative (M_{neg}) and positive (M_{pos}) flexural capacities. The loaded length of the strip (l) is calculated according to equilibrium condition:

$$l = \sqrt{M_s/w} \tag{2.21}$$

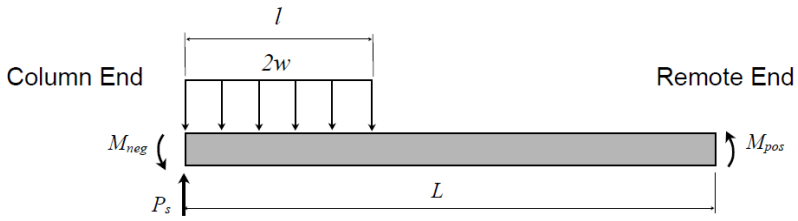

Figure 2.7 – Simplified loading on radial strip, adapted from Alexander [24].

The nominal capacity of the strip is given by:

$$P_s = 2 \cdot \sqrt{M_s / w} \tag{2.22}$$

The total load is provided by adding the individual strip contributions:

$$P_{col} = \sum P_s \tag{2.23}$$

According to the assumption of slender flexural behaviour, the punching failure is reached when the loading term w reaches the unit one-way shear strength of the slab. The latter is calculated according to ACI 318-14 [5] (SI units):

$$w = d \cdot 0.17 \cdot \sqrt{f_c} \tag{2.24}$$

where d is the effective depth and f_c is the concrete compressive strength.

For general case a modified approach, that does not rely on symmetry conditions, is required. Generally radial strips develop in only one direction, in this case the fully enhanced strip is called super strip (Figure 2.8).

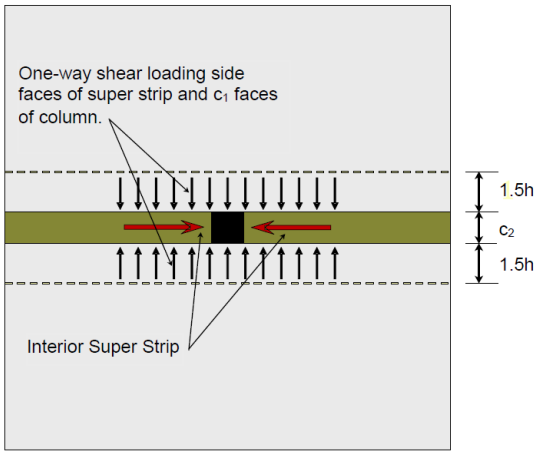

Figure 2.8 – Non-proportional loading, interior super strip, adapted from Alexander [24].

According to Alexander [24] the radial super strip acts like a T-beam in negative moment, with its "stem" equal to c2 and with a "top flange" equal to c2 + 3h. Therefore, the negative reinforcement is calculated according this wider size. The total load transferred to the inner column with this load distribution is given by:

$$P_{col} = \sum P_{ss} + 2 \cdot w \cdot c_1 = 2 \cdot (P_{ss} + w \cdot c_1) \tag{2.25}$$

The non-proportional load distribution is applicable also with unbalanced moment. The load is provided as a combination of symmetric and anti-symmetric contributions (Figure 2.9).

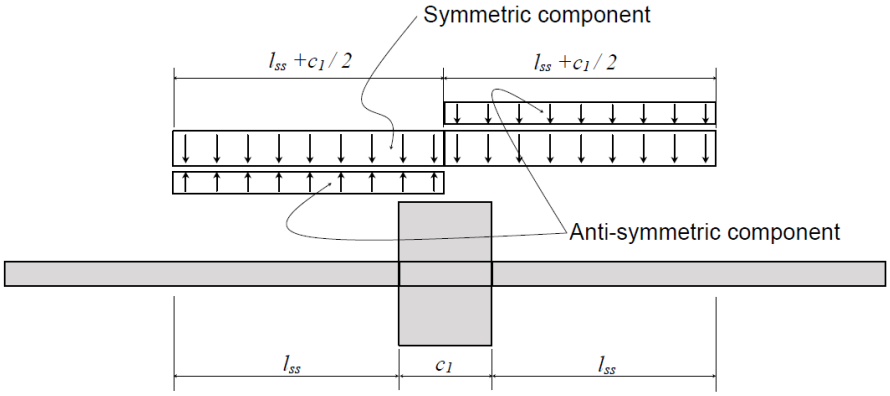

Figure 2.9 – Moment transfer according to the strip model, adapted from Alexander [24].

when the ultimate load, on one side of the connection is reached, the punching failure occurs:

$$\frac{V}{2}+\frac{M}{l_{ss}+c_1/2} \leq P_{ss}+w\cdot c_1 = 2\cdot w\cdot (l_{ss}+c_1/2) \tag{2.26}$$

where w is calculated according to equation (2.24).

2.3.3 Drift versus gravity shear ratio model – Background to ACI 318-19 and 421.2R-10

In the second half of the 80s, several flat slab buildings collapsed due to the earthquakes of Mexico City and Loma Prieta. After these tragic events researchers began to focus on the seismic response of flat slab buildings under combined gravity and lateral loading. In 1989, Pan and Moehle [25], examining the available data from previous experimental campaigns, highlighted the significant effects of gravity load on the ultimate drift capacity of the slab-column connections. The authors, plotting the experimental ultimate drift (DR) versus the gravity shear ratio (V_g/V_c), found that the ultimate drift decreases at the gravity shear ratio increase. Furthermore, since a common form of construction in seismic zones in the United States combines flat slab frames to carry gravity loads with shearwalls to resist the earthquake loads, the authors focused on the capacity of flat slab connection to survive the lateral deformations expected during earthquakes. Assuming 1.5% as a reasonable ultimate drift of a concrete shear wall the authors found that to avoid premature punching failure in the slab column connections, the gravity shear ratio should be limited to $0.4\cdot V_c$.

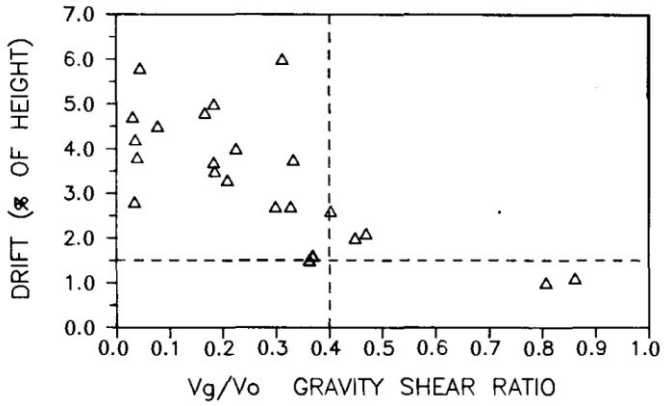

Figure 2.10 – Effect on gravity load on drift, adapted from Pan and Moehle [25].

where V_c is the punching shear strength without shear reinforcement calculated according to the ACI provision [5] (in SI units):

$$V_c = \frac{1}{3} \cdot b_0 \cdot d \cdot \sqrt{f_c} \tag{2.27}$$

where d is the effective depth and f_c is the concrete compressive strength. Pan and Moehle [25] suggested that a minimum ductility factor of 1.2 should be satisfied for ultimate drift equal to 1.5% and gravity shear ratio limited to 0.4.

Later Megally and Ghali [26] highlighted that the concrete shear strength under cyclic moment transfer is less than the strength under monotonic loading. Furthermore, the authors extended the review of experimental campaigns to slab column connections with shear reinforcement. Then, interpolating the experimental ultimate drift at varying of the gravity shear ratio, provided three different curves: one for slab without shear reinforcement, one for slab with stirrups and one for slab with studs (SSR) (Figure 2.11).

In 2000 Megally and Ghali [27] provided a procedure for design slab-column connections in order to avoid premature punching-shear failure. According to this procedure, to ensure a ductile behaviour of the slab-column connection a minimum shear reinforcement is required except when the shear force V_g is less than $0.25\phi V_c$ (where ϕ is the strength reduction factor for shear). The latter unsure an ultimate drift of 2.5%.

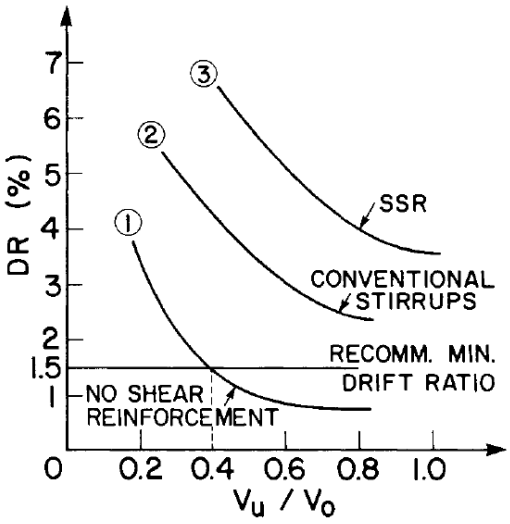

Figure 2.11 – Effects of gravity load on drift capacity, adapted from Megally and Ghali [26].

The minimum amount of shear reinforcement is determined such that the nominal shear stress v_s satisfies the following inequality (in SI units):

$$v_s = \frac{A_v \cdot f_{yv}}{b_0 \cdot s} \geq \frac{1}{4} \cdot \sqrt{f_c} \tag{2.28}$$

Then the authors suggest calculating the design value of unbalanced moment starting from the lateral drift of the primary structure during earthquakes. The flat slab column connection can be modelled as a frame structure as shown in Figure 2.12 according to the equivalent frame method (§2.2.1).

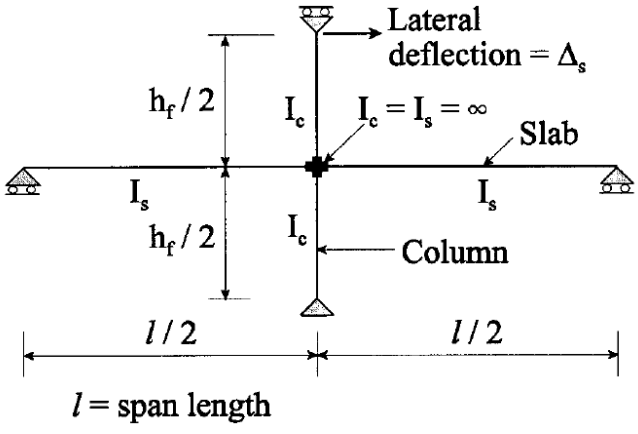

Figure 2.12 – Plane frame idealization of slab-column connection, adapted from Megally and Ghali [27].

Furthermore, the authors provided an upper limit to unbalanced moment (M_u) that cannot be exceed. This upper limit is based on the flexural strength of the slab:

$$M_u \leq \frac{M_{pr}}{\alpha_m} \tag{2.29}$$

where M_{pr} is the sum of the flexural strengths of opposite critical section sides of width cx + d or cy + d when the transferred moment is about the x or y axes respectively. The empirical coefficient α_m for interior connections is expressed as:

$$\alpha_m = 0.85 - \gamma_v - \left(\frac{\beta_r}{20}\right) \tag{2.30}$$

where γ_v is the fraction of moment transferred by vertical shear stresses in the slab and β_r is equal to (c_y+d/c_x+d) or vice versa when the transferred moment is about the x or y axes, respectively.

The value of M_u to be used in punching shear design is the smaller of the design unbalanced moment derived from the elastic drift and the upper limit derived from the flexural strength of the connection. Then the maximum shear stress is calculated according to equation (2.17) and it is compared to the nominal shear strength (v_n). When stud shear reinforcement is provided v_n is given by (in SI units):

$$v_n = v_c + v_s \leq \frac{2}{3} \cdot \sqrt{f_c} \tag{2.31}$$

where the nominal shear strength v_c provided by the concrete is limited to (in SI units):

$$v_c = \frac{1}{8} \cdot \sqrt{f_c} \tag{2.32}$$

The steps of punching shear design of slab column connections subjected to earthquake actions are summarized in Figure 2.13. This procedure represents the background to the ACI 421.2R-10, Guide to Seismic Design of Punching Shear Reinforcement in Flat Plates, that is a reference in this field and also to the section 18.14.5.1 of ACI 318-14 [5].

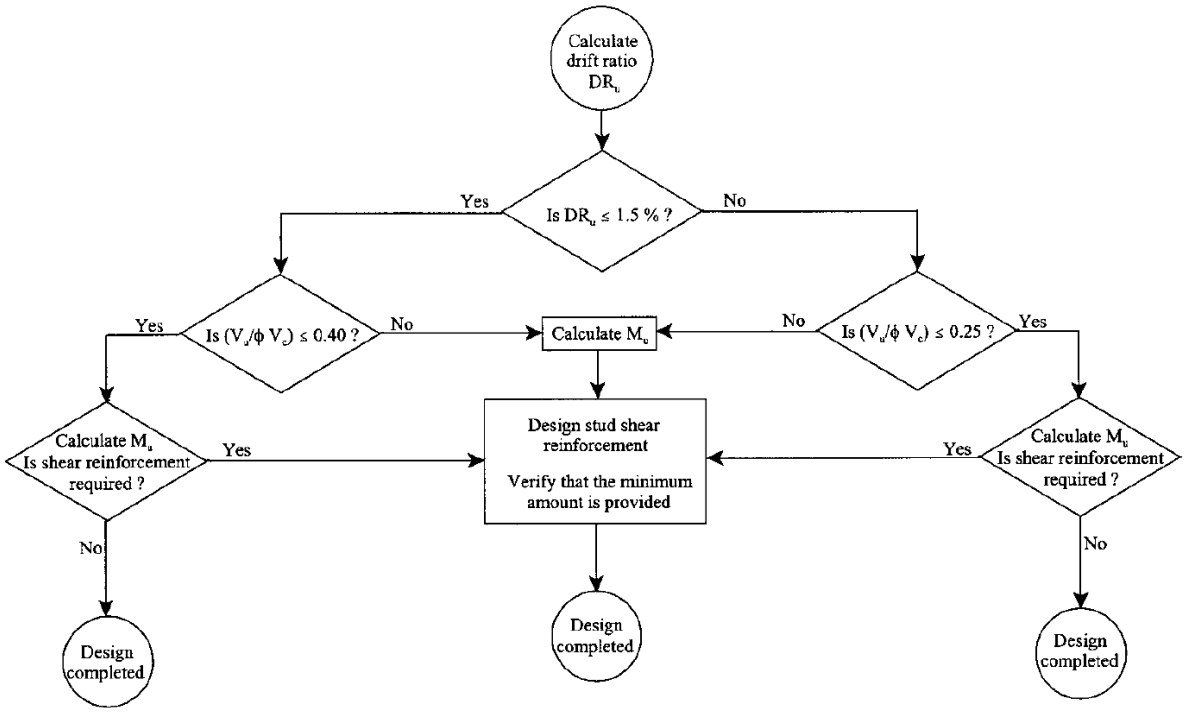

Figure 2.13 - Steps of punching shear design of earthquake-resistant slab-column connections, adapted from Megally and Ghali [27].

2.3.4 Design method for imposed rotations – Broms (2009)

In 2009 Broms [28] proposed a new mechanical model for transfer of unbalanced moment caused by imposed rotation of the slab-column connection. This new method based on imposed rotation arises in contrast to the force-based design methods that presuppose that the unbalanced moment is a defined quantity. Actually, no generally accepted method for accurate prediction of unbalanced moment in slab column connections, during earthquake seems to exist [28]. The failure criterion proposed by the author is based on the limited concrete compression strain capacity of the slab near the column.

For concentric punching the failure the critical value of strain in tangential direction in the slab at the column edge is assumed equal to:

$$\varepsilon_{cpu} = 0.0010 \cdot \left(\frac{0.15}{x}\right)^{1/3} \cdot \left(\frac{25}{f_c}\right)^{0.1} \tag{2.33}$$

where x depth of the compression zone in the slab under elastic conditions:

$$x = d \cdot \frac{E_s}{E_{c10}} \cdot \rho \cdot \left(\sqrt{1 + \frac{2 \cdot E_{c10}}{\rho \cdot E_s}} - 1 \right) \tag{2.34}$$

where E_{c10} is the secant modulus of elasticity to the critical concrete strain 0.0010. The reinforcement strain at the column when punching occurs becomes:

$$\varepsilon_s = \varepsilon_{cpu} \cdot \frac{d - x}{x} \tag{2.35}$$

The punching capacity V_ε is derived from tangential and radial bending moment according to the theory of elasticity (Figure 2.14):

$$V_\varepsilon = m_\varepsilon \cdot \frac{8\pi}{2 \cdot \ln\left(\frac{C}{B}\right) + 1 - \frac{B^2}{C^2}} \tag{2.36}$$

where the critical bending moment at the column edge is:

$$m_\varepsilon = \rho \cdot k_e \cdot E_s \cdot \varepsilon_s \cdot d^2 \cdot \left(1 - \frac{x}{3 \cdot d}\right) \tag{2.37}$$

and $k_\varepsilon = (\varepsilon_y/\varepsilon_s)^{0.2} \leq 1$.

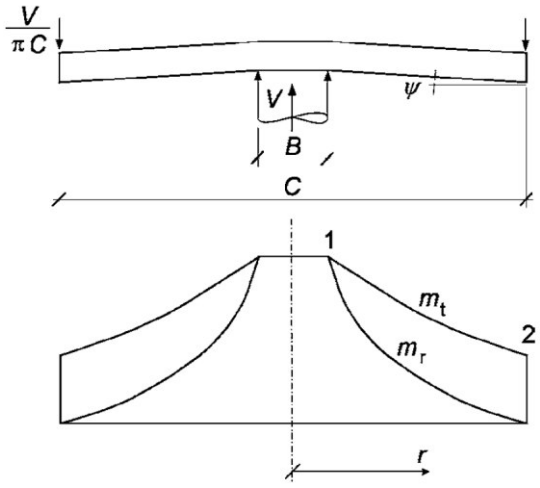

Figure 2.14 – Bending moments and slab inclination according to theory of elasticity for circular slab, adapted from Broms [28].

Upper bound for the shear force is given by the flexural capacity of the slab corresponding to yield of all reinforcement:

$$V_{y2} = m_{y2} \cdot \frac{2\pi}{1 - \frac{B}{C}} \tag{2.38}$$

where m_{y2} is the flexural capacity. The column reaction corresponding to start of reinforcement yield is:

$$V_{y1} = m_{y1} \cdot \frac{8\pi}{2 \cdot \ln\left(\frac{C}{B}\right) + 1 - \frac{B^2}{C^2}} \tag{2.39}$$

where m_{y1} is the yielding moment.

An unbalanced moment is transferred by a combination of eccentric vertical shear, torsional moment and bending moment. For square column the latter contribution could be calculated as:

$$M = 3 \cdot c \cdot (m_T + m_B) \tag{2.40}$$

where c is the size of the column, m_T and m_B are the average values of bending moments per unit width on opposite sides of the column with tension to top and bottom reinforcement respectively. The total unbalanced moment (M_{el}) is provided by the sum of the moments on opposite sides of the column $M_{el}=M_{elT}+M_{elB}$. Since the failure is governed by the negative bending moment M_{elT}, the previous equation in elastic conditions becomes:

$$M_{el} = 2 \cdot M_{elT} = 2 \cdot \left[3 \cdot c \cdot m_\varepsilon \cdot \left(1 - \frac{V}{V_\varepsilon}\right) \cdot \frac{1}{1 - \frac{c}{L_1}}\right] \tag{2.41}$$

where V/V_ε represents the part of critical bending moment m_ε occupied by the vertical loading, while the last term gives the relation between the bending moment at the centreline and that at column edge. The elastic rotation is given by:

$$\theta_{el} = \frac{2 \cdot M_{elT}}{EI \cdot \left(2.8 + 26 \cdot \frac{c}{L_1}\right)} + \left(1 - \frac{V}{V_\varepsilon}\right) \cdot \Phi_u \cdot (2 \cdot d + c) \tag{2.42}$$

where the first term corresponds to the elastic rotation calculated according to Aalami [29] while the second term represents the additional slab rotation due to elongation of

reinforcement over the length 2d provided by the inclined strut (Figure 2.15). The ultimate curvature is calculated as $\phi_u = \varepsilon_{cpu}/x$.

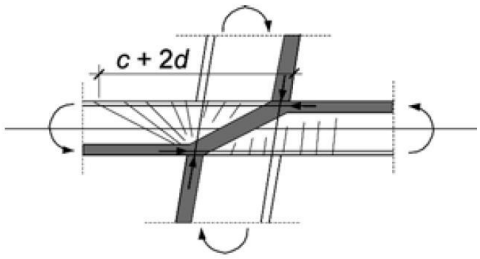

Figure 2.15 – Transfer of unbalanced moment strut and tie mechanism, adapted from Broms [28].

When the reinforcement ratio is moderate the top reinforcement reaches the yield before punching occurs. The ultimate inelastic rotation results [28]:

$$\theta_u = \theta_{el} + \left(\Phi_u - \Phi_y\right) \cdot \frac{2 \cdot 3 \cdot c}{2.8 + 26 \cdot \frac{c}{L_1}} \cdot \frac{1}{1 - \frac{c}{L_1}} \tag{2.43}$$

In this case the elastic part of the ultimate rotation θ_{el} is determined by Eq. (2.41) and (2.42) but with m_ε, V_ε, and ϕ_u replaced by m_{y1}, V_{y1}, and ϕ_y, respectively ($\phi_y = \varepsilon_y/d\text{-}x$).

The results of the parametric study provided by Broms [28], in terms of ultimate drift and gravity shear ratio, are shown in Figure 2.16:

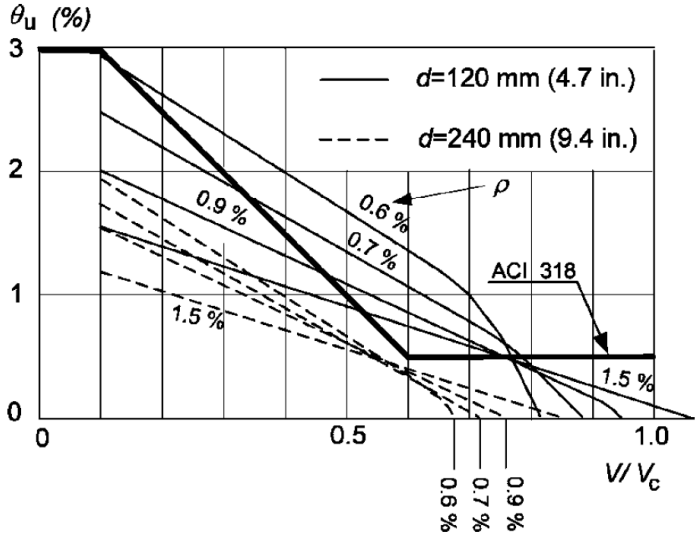

Figure 2.16 – Comparison between ultimate drift vs gravity shear ratio, adapted from Broms [28].

Important size effects due to effective depth and longitudinal reinforcement ratio variation are found. The results obtained for slabs with effective depth equal to 120 mm are non-

conservative for slabs with higher effective depth. Since the ACI 421.2R is grounded on recorded drifts for test slabs with small effective depth, equal to 125 mm or less, it might not be safe for flat slab with greater effective depth [28].

2.3.5 CSCT – Background to Model Code 2010

Starting from 1991, following Kinnunen and Nylander, Muttoni and Schwartz [30] began developing a new mechanical model, with the first draft of this model published in 2003 [31]. In 2008, the final version of the critical shear crack theory (CSCT) was published [32]. The substantial difference with respect to previous models lies in the choice of the CSCT failure criterion, which was inspired by the previous works of Walraven [33] and Vecchio and Collins [34]. They stated that a rough crack can transfer shear by aggregate interlock, which is a function of crack width, compressive strength and aggregate size. Therefore, CSCT describes the relationship between punching strength and the width of the critical shear crack, accounting for its roughness.

The critical state is set at the intersection between two curves: the first describing the failure criterion, accounting for the aforementioned parameters, and the second representing the load–rotation relationship of the flat slab (Figure 2.17). The equation of the failure criterion is provided in the following:

$$\frac{V_R}{b_0 \cdot d \cdot \sqrt{f_c}} = \frac{3/4}{1 + 15 \cdot \frac{\psi \cdot d}{d_{g0} + d_g}} \tag{2.44}$$

where b_0 is the control perimeter set at d/2 from the column edge, d_g is the maximum aggregate size, d_{g0}=16 mm is the reference maximum aggregate size and ψ is the rotation.

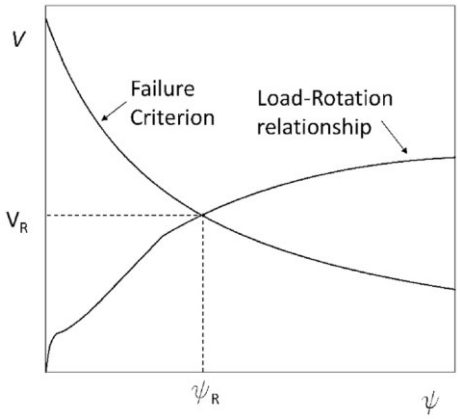

Figure 2.17 – Punching strength according to the CSCT, adapted from Muttoni [32].

The application of the CSCT to non-axisymmetric cases is due to Tassinari [35] and Sagaseta et al. [36]. In particular they focused on non-symmetric layout of longitudinal reinforcement and loading conditions. In such cases the slab exhibits substantially different rotations along different axis, leading to a non-uniform distribution of shear stresses along the critical perimeter. However, the authors found that even for non-axisymmetric conditions the shear stresses around the control perimeter tend to be roughly constant thanks to a plastic redistribution near failure. Since the inherent difficulty to take into account the plastic redistribution, for design purposes they proposed the use of the maximum rotation (ψ_{max}) for calculating the punching strength (Eq. (2.44)), although providing slightly more conservative predictions. For design purpose, the load-rotation relationship could be simplified allowing for a direct expression of the slab rotation [37]:

$$\psi = k_m \cdot \frac{r_s}{d} \cdot \frac{f_y}{E_s} \cdot \left(\frac{m_s}{m_R}\right)^{1.5} \tag{2.45}$$

where k_m is a coefficient that depends on the level of approximation, r_s denotes the position relative to the support axis where the radial bending moment is zero, m_s is the moment acting on the support strip and m_R is the corresponding bending strength. The rotation is calculated for both axis then punching strength is determined according to the maximum value.

According to Muttoni and Ruiz [38] in presence of unbalanced moment the control perimeter should be reduced accounting for the concentration of shear stress. An eccentricity coefficient is introduced:

$$k_e = \frac{1}{1 + e_u/b_u} \tag{2.46}$$

where e_u = M/V is the load eccentricity and b_u is the diameter of a circle with the same area as the region A_c inside the basic control perimeter is $b_u = (4A_c/\pi)^{0.5}$.

2.3.6 CSCT – Mechanical Model for Drift-Induced Punching of Slab-Column Connections

Starting from 2014 Drakatos et al. [39] started to develop an analytical model, based on the CSCT, specifically thought for slab-column connections under seismically induced deformations. The model presents an approach for predicting the moment rotation relationship as well as all the strength mechanisms. The slab is divided into n sector elements, unlike the CSCT each sector is assumed to have a different rotation. The latter explain the arising of torsional

moments and moments due to the eccentricity of shear force. The slab rotation of the sector element at angle φ with regard to the bending axis y is:

$$\psi(\varphi) = \frac{\psi_{max} + \psi_{min}}{2} + \frac{\psi_{max} - \psi_{min}}{2} \cdot \sin(\varphi) \tag{2.47}$$

where ψ_{max} and ψ_{min} are the maximum and the minimum slab rotation for $\varphi = \pi/2$ and for $\varphi = 3\pi/2$, respectively. The authors assumed also that no shear transfer occurs between adjacent sector elements. Furthermore, the tangential moments inside are assumed to be equal to the radial ones in the region inside the critical shear crack, the radius r_0 is assumed equal to the eccentricity e and the quadrilinear moment-curvature relationship is adopted.

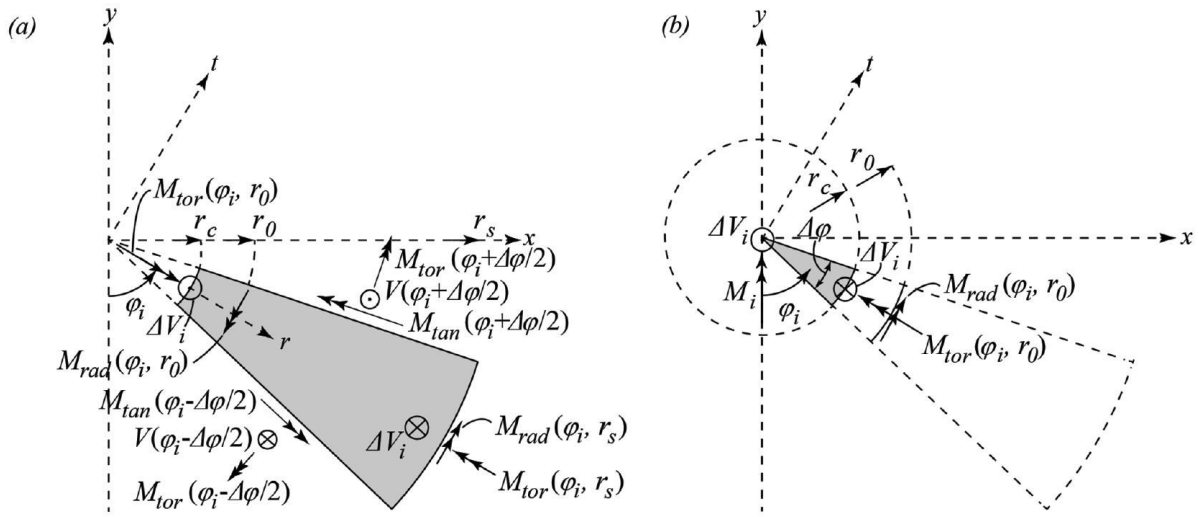

Figure 2.18 – Force distribution of the slab sector: (a) outside the shear rack (b) inside the shear crack, adapted from Drakatos et al. [40].

The integral of the radial moment for a slab sector is:

$$M_{rad}(\varphi_i) = m_r(\varphi_i) \cdot r_0 \cdot \Delta\varphi \tag{2.48}$$

The shear force acting in the sector element is derived by moment equilibrium in the tangential direction with respect to the centre of the column with radius rc:

$$\Delta V_i = \frac{1}{r_q - r_c} \cdot \left\{ M_{rad}(\varphi_i, r_0) - M_{rad}(\varphi_i, r_s) + \left[M_{tan}\left(\varphi_i + \frac{\Delta\varphi}{2}\right) + M_{tan}\left(\varphi_i - \frac{\Delta\varphi}{2}\right) \right] \cdot \sin\left(\frac{\Delta\varphi}{2}\right) \right\} \tag{2.49}$$

the moment equilibrium in the tangential direction gives the torsional moment in each sector:

$$M_{tor}(\varphi_i, r_0) = \left[M_{tan}\left(\varphi_i + \frac{\Delta\varphi}{2}\right) - M_{tan}\left(\varphi_i - \frac{\Delta\varphi}{2}\right)\right] \cdot \cos\left(\frac{\Delta\varphi}{2}\right) + M_{tor}(\varphi_i, r_s) \quad (2.50)$$

where radial and torsional moments at the perimeter of the sector element $M_{rad}(\varphi_i,r_s)$ and $M_{tor}(\varphi_i,r_s)$ are obtained using effective beam width method (Figure 2.19).

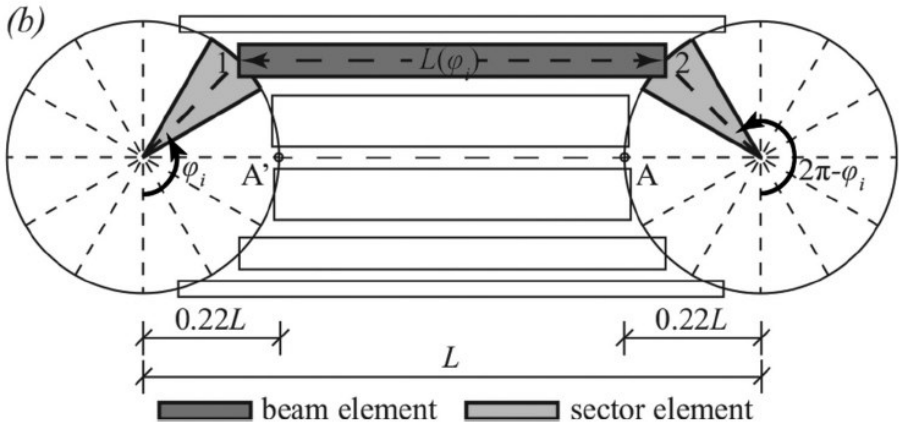

Figure 2.19 – Effective Beam Width Method for calculating contribution of outer slab part to total deformation, adapted from Drakatos et al. [40].

Equilibrium of the shear forces at the column gives the total shear force for the load step k:

$$V_k = \sum_{i=1}^{n} \Delta V_i \quad (2.51)$$

Moment equilibrium at the column edge gives the total moment acting on the connection for the load step k:

$$M_k = \sum_{i=1}^{n} [M_{rad}(\varphi_i, r_0) \cdot \sin(\varphi_i) + M_{tor}(\varphi_i, r_0) \cdot \cos(\varphi_i) + \Delta V_i \cdot r_c \cdot \sin(\varphi_i)] \quad (2.52)$$

the radius r_0 is updated each step k as it is assumed equal to the eccentricity $e_k = M_k/V_k$. Finally the rotation of the connection is calculated as the average of the maximum and minimum local rotations:

$$\psi_{scc,rot} = \frac{\psi_{max} - \psi_{min}}{2} \quad (2.53)$$

The authors provide also a procedure to calculate the contribute of the outer part of the slab ($r > r_s=0.22L$) to the deformation of the connection, however they stated that it contributes approximately to a quarter to the total slab rotation.

Two different failure criterions are provided, for both monolithic and cyclic loading. For monotonically loaded slabs, according to the shear redistribution capacity found by Sagaseta et al. [36], the failure is assumed to occur when the sum of the shear forces acting on the hogging slab half ($0 \leq \varphi \leq \pi$) is equal to the sum of the shear strength of these sectors:

$$V_{R.hog} = \int_0^{\pi} v_R(\varphi) \cdot \left(r_c + \frac{d}{2}(\varphi) \right) d\varphi \tag{2.54}$$

where $v_r(\varphi)$ is the shear strength per unit length:

$$v_R(\varphi) = \frac{0.75 \cdot d(\varphi) \cdot \sqrt{f_c}}{1 + 15 \cdot \frac{\psi(\varphi) \cdot d(\varphi)}{d_g + d_{g0}}} \tag{2.55}$$

For cyclic loading redistribution of shear forces is neglected so it is assumed that the punching failure occurs when for the single sector element that exhibits the maximum rotation ψ_{max}, the acting shear force ΔV_i equals the shear strength V_{Ri}.

$$V_{R.\pi/2} = \frac{0.75 \cdot b_0 \cdot \Delta\varphi \cdot d(\pi/2) \cdot \sqrt{f_c}}{1 + 15 \cdot \frac{\psi_{max} \cdot d(\pi/2)}{d_g + d_{g0}}} \tag{2.56}$$

Drakatos et al. [40] confirmed the observations provided by Broms [28], the rotation capacity decreases with effective depth increasing, highlighting how the ACI 421.2R results unsafe for slab effective depth greater than 240 mm.

2.4 Experimental works on slabs with openings

Almost all slab systems include openings, these may be big, as required by stair-ways and elevators shafts, or they may be of smaller dimensions, like those needed to accommodate the passage of mechanical or electrical service lines. Usually small openings are placed adjacent or close to the column inducing a loss of punching strength.

For vertical loading only, this loss of strength is accounted by reducing the control perimeter. With regards to combined gravity and lateral loading there is no specific calculation about the presence of openings.

In the following the experimental works on slabs with openings are described and discussed. The works are grouped in function of the loading type: vertical loading only or combined gravity and horizontal loading.

2.4.1 Experimental works on slabs with openings – Gravity loading

In 1961 Moe [16] performed the first experimental campaign about punching of R/C slabs with opening. The author investigated five different series of slab, one of this named Series-H included 15 square slabs with openings. The size of the slabs was 1829 x 1829 mm with a thickness of about 152 mm and a concrete cover of 38 mm. The longitudinal reinforcement ratio was assumed equal to 1.5% excepted for a slab that resulted equal to 0.75%. Concrete compressive strength varied from 22.8 MPa to 29 MPa. The size, the position and the number of the openings were the main variables investigated in this series (Figure 2.20).

The author found no significant influence of the opening in the slab deflections. Furthermore, with opening number increasing a clear tendency of punching strength decreasing was found.

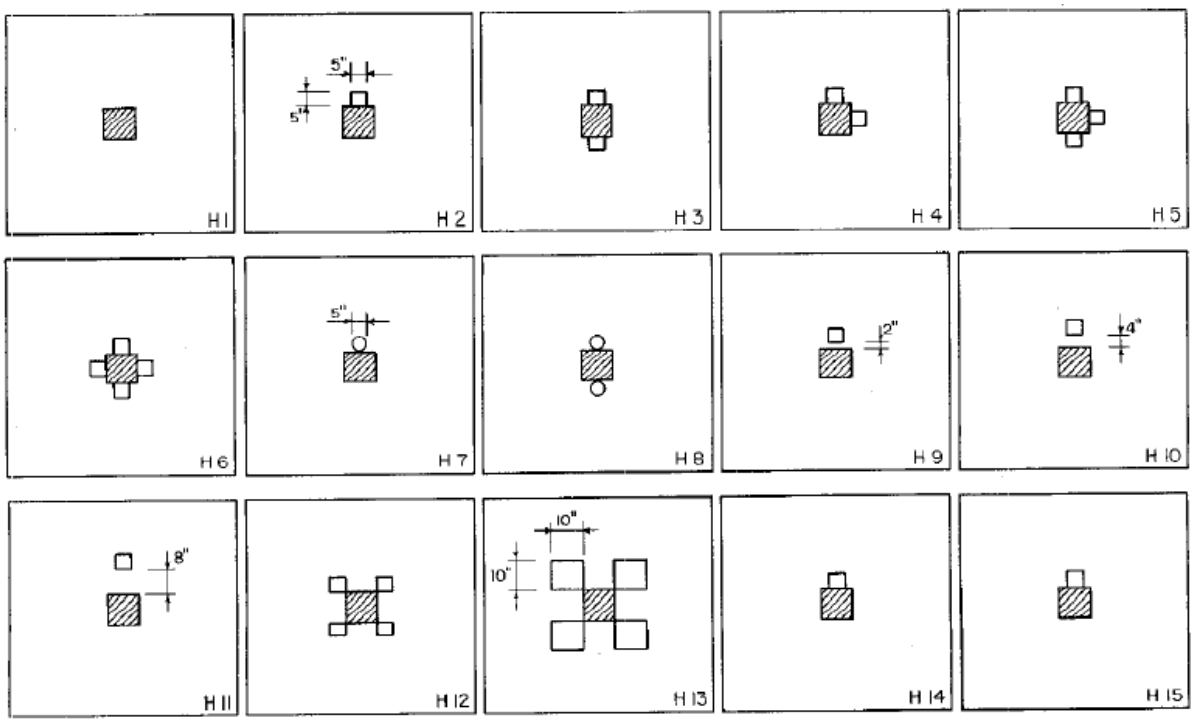

Figure 2.20 – Series H – Opening patterns, adapted from Moe [16].

In 1964 Hognestad et al. [41] performed an experimental campaign about punching of R/C flat slab using lightweight aggregate. During this research three slabs with openings adjacent to all four faces of the column were tested. As shown by Moe [16], the authors noticed an important reduction of the punching strength due to the presence of opening.

Similarly, Mowrer et al. [42] performed a huge experimental campaign with more than 50 specimens. One series of this experimental campaign, named J series, included 25 specimens and investigated the presence of openings. The test results were used by the authors to revise the Moe's [16] equation for punching prediction.

In 1971 Roll et al. [43] focused only on the punching strength of perforated reinforced concrete slabs. The authors concluded that the critical section is around the periphery of the column and provided a new procedure for determining the effective perimeter in presence of opening. The reduced perimeter is calculated excluding the sum of the portions lying within radial projections from the centre of the column to the corners of the holes (Figure 2.21).

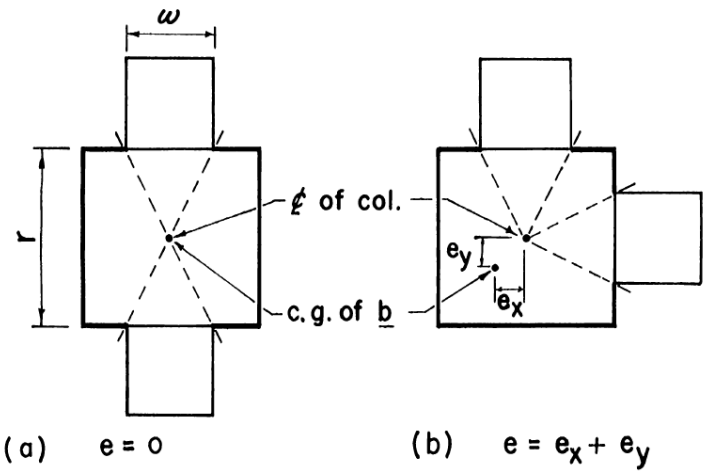

Figure 2.21 – Reduced perimeter of the critical section according to Roll et al. [43].

Later Regan [44] investigated the use of shear reinforcement to enhance the punching strength of slab with opening. In 2004 Teng et al. [45] studied the effect of opening on the punching strength of slabs supported on rectangular columns. The authors tested 20 slabs under concentrated loads founding that if the use of an opening is unavoidable, placing the opening along the longer side of the column represents the best choice. Furthermore, they proposed another procedure to determine the effective critical perimeter. According to the authors the part of the perimeter that is enclosed by the radial projections from the centroid of the end portion of the column to the edge of the openings is ineffective.

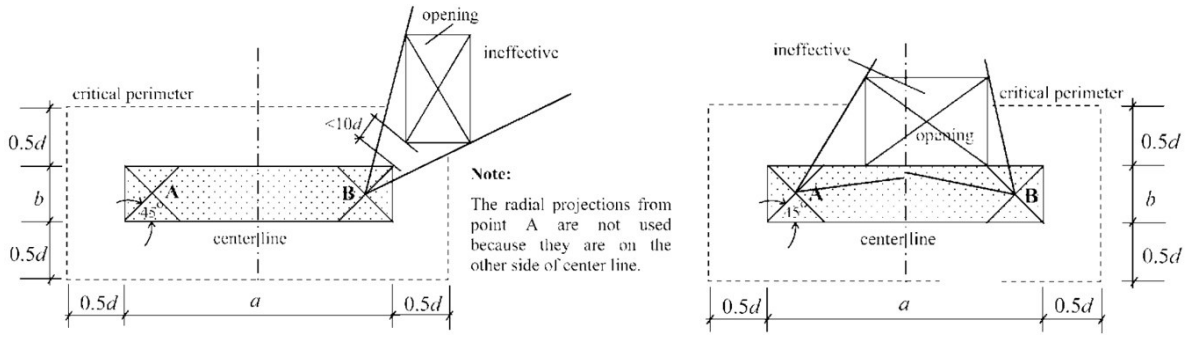

Figure 2.22 – Reduced perimeter according to Teng et al. [45].

The projection lines from one end of the rectangular column section should not cross the center line of the column section. This is because as the column section becomes more elongated, the slab areas around the two ends of the column section behave more independently of each other. Especially when the column cross section is very elongated the projection lines from the centroid of the columns are not suggested.

In 2012 Elshafiey et al. [46] performed a new experimental campaign to evaluate the effect of large opening adjacent to column on the punching capacity of flat slab. The research included seven 1700x1700x150 mm flat slab and investigated different opening size and location. The authors found that for opening dimension higher than one tenth of the span, the load-rotation curve of the slab is also affected.

Later Borges et al. [47] tested 13 flat slab specimens with both symmetrical and non-symmetrical patterns of openings near rectangular columns. The tests also examined the size of the opening and the effects of different arrangements of shear reinforcement for slabs with and without openings. The authors found that to determine the punching strength reduction due to the presence of opening, straight projection of the widths of opening into the control perimeter gave the best results. However, they pointed out the need of further considerations about the effects of eccentricity between the residual control perimeter and the support.

In 2014 Anil et al. [48] performed an experimental campaign including nine flat slab specimens. The authors investigated the influence of position and dimension of the openings. The results showed how the opening situated parallel to the column rather than diagonal to the column led to a reduction of the punching strength, initial stiffness and energy dissipation capacity.

Later, Ha et al. [49] studied the effect on multiple opening near the column on the punching strength. The authors compared the punching failures provided by the experiments with the predictions of the main codes. The results showed that the ratios of effective critical perimeter lengths are generally well matched by the ratios of failure loads. The latter confirmed the validity of the assumption that the reduction in punching shear strength due to the existence of openings is proportional to the loss of critical section perimeter.

Recently, Liberati et al. [50] highlighted the need of further experimental tests about punching strength of slabs with opening close to the column. The authors investigated 12 slabs, eight of these with opening. The experimental evidences resulted aligned to those provided by previous experimental campaigns. Furthermore, the punching predictions provided by the codes resulted always lower than the experimental punching strength.

2.4.2 Experimental works on slabs with openings – Combined gravity and lateral loading

The first research dealing with slab-column connections with openings under combined gravity and lateral loading are due to El-Salakawy et al. [51]. The authors performed an experimental campaign to investigate the response of slab-column edge connections with opening subjected to high moment-to-shear ratio. Four specimens with two different patterns of openings were tested (Figure 2.23).

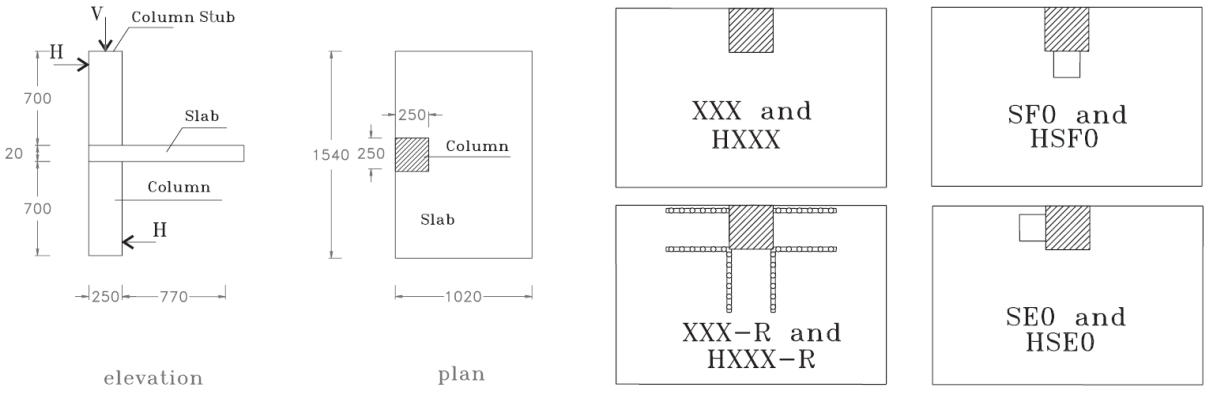

Figure 2.23 – Specimen dimension and plan view, adapted from El-Salakawy et al. [51].

The eccentricity was maintained constant during the test (M/V=e=cost). In the first series, specimens SF0 and SE0, the eccentricity e was kept equal to 0.30 m, while in the second series, specimens HSF0 and HSE0, the eccentricity e was kept equal to 0.66 m. The authors found that the presence of opening decreases the stiffness of the connections. This effect results more pronounced when the opening is placed at the front of the column than at the side of the column.

Later the authors [52] extended the experimental program investigating other three edge slabs with different opening patterns. They found that the opening located in front of the column decreases the punching capacity more than the same size opening placed at the side of the column. Furthermore, they highlighted a progressive reduction in punching strength with reducing the distance of the opening from the column. For the opening placed at 2d from the column the decrease in strength was 4.5%, for a distance of d the reduction was 8%, while for the opening next to the column the reduction was 10%.

However, the only experimental campaign that includes both gravity loading and reversed cyclic lateral loads is due to Bu and Polak [53]. Unlike previous researches the vertical load was maintained constant while the eccentricity was varied by changing the horizontal

load. The experimental program included three slabs with openings, two of these with shear reinforcement (Figure 2.24).

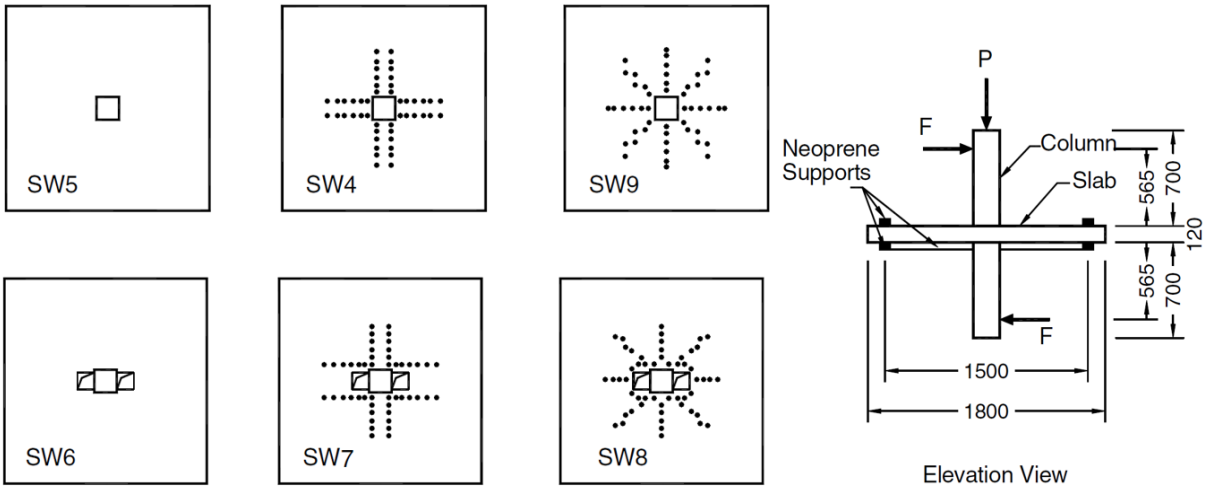

Figure 2.24 – Plan and elevation views of the specimens, adapted from Bu and Polak [53].

The authors found that opening next to the column reduces both punching strength and ductility. Furthermore, the specimens with bolts (SW7-SW8) showed almost the same peak lateral load of SW6, however the presence of shear reinforcement allowed for greater drift ratios.

Then, Oliveira et al. [54] investigated the punching strength in R/C flat slab with opening adjacent to the column in presence of eccentricity of the load. The eccentricity was maintained constant during the test (M/V=e=cost). The authors found that the worst situation, in terms of loss of punching strength, is achieved when the moment transfer is applied towards the opening region, while when the moment is applied in the opposite direction the loss of strength results very low.

2.5 Code provisions

2.5.1 Eurocode 2 – 2004

Beside the punching provision of Eurocode 2 – 2004 (EC2-2004) [22] is strictly empiric it takes into account several effects of the punching phenomenon. The punching strength is defined as:

$$V_{EC2} = \frac{0.18}{\gamma_c} \cdot b_{0,EC2} \cdot d \cdot k \cdot (100 \cdot \rho \cdot f_{ck})^{1/3} \geq \nu_{min} \cdot b_{0,EC2} \cdot d \tag{2.57}$$

where γ_c is the safety coefficient and $b_{o,EC2}$ is the control perimeter placed at 2d from the column (Figure 2.25).

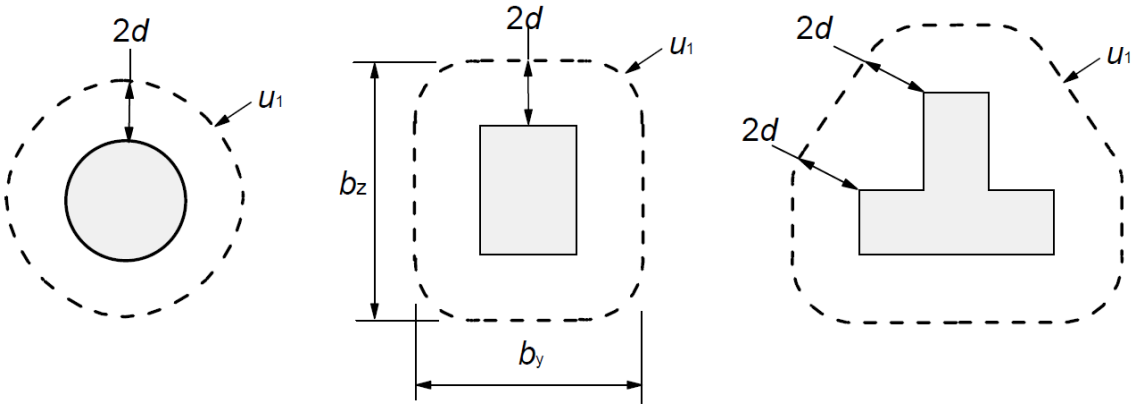

Figure 2.25 – Control perimeters according to EC2 – 2004 [22].

In presence of openings closer than 6d from the column the control perimeter is reduced according to Figure 2.26.

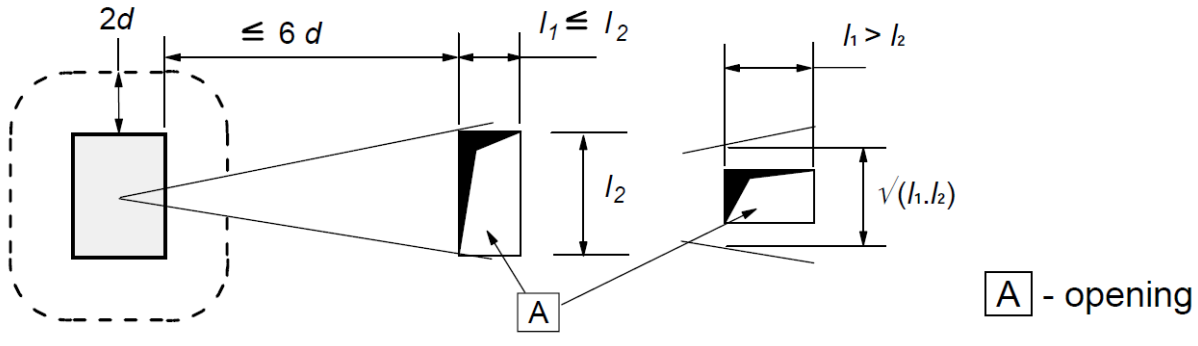

Figure 2.26 – Control perimenter in presence of openings according to EC2 – 2004 [22].

$d=(d_x+d_y)/2$ is the average effective depth of reinforcement in two orthogonal direction (x,y), ρ is the longitudinal reinforcement ratio defined as:

$$\rho = \sqrt{\rho_x \cdot \rho_y} \leq 0.02 \tag{2.58}$$

k is the coefficient that accounts for the size effect:

$$k = 1 + \sqrt{\frac{200}{d}} \leq 2 \tag{2.59}$$

v_{min} is the minimum shear strength:

$$v_{min} = 0.035 \cdot k^{3/2} \cdot f_{ck}^{1/2} \tag{2.60}$$

The punching strength in slabs with shear reinforcement is calculated by adding the concrete and the shear reinforcement contributions. The concrete contribution is taken equal to 75% of the punching strength of slabs without shear reinforcement:

$$V_{EC2,SR} = 0.75 \cdot V_{Rd,c} + 1.5 \cdot A_{sw} \cdot f_{ywd,ef} \cdot \left(\frac{d}{s_r}\right) \cdot \sin\alpha \tag{2.61}$$

where A_{sw} is the cross-sectional area of one perimeter of shear reinforcement around the column, s_r is the distance between the perimeters of shear reinforcement, α is the angle between the shear reinforcement and the average plane of the slabs and $f_{ywd,ef}$ is the effective stress in the shear reinforcement accounting for limited anchorage of the shear reinforcement:

$$f_{ywd,ef} = 250 + 0.25 \cdot d \leq f_{ywd} \tag{2.62}$$

where f_{ywd} is the yield stress of steel shear reinforcement. To prevent the failure of the concrete near the column, the maximum punching strength is defined as:

$$V_{EC2,Crush} = 0.5 \cdot \upsilon \cdot f_{cd} \cdot b_{col} \cdot d \tag{2.63}$$

where $\upsilon=0.6\cdot(1-f_{ck}/250)$ is the strength reduction factor for cracked concrete and b_{col} is the column perimeter.

The maximum punching shear stress is given by:

$$v_{EC2,Ed} = \frac{\beta \cdot V_{Ed}}{b_{0,EC2} \cdot d} \tag{2.64}$$

where β is a coefficient that accounts for the eccentricity of the reaction V_{Ed}:

$$\beta = 1 + k \cdot \frac{M_{Ed}}{V_{Ed}} \cdot \frac{b_{0,EC2}}{W_1} \tag{2.65}$$

where k represents the fraction of unbalanced moment transferred by shear and torsion, function of the ratio between the column dimensions, values of k are listed in Table 2.2.

Table 2.2 – Ratio of moment transferred to the column by uneven shear according to EC2 – 2004 [22].

≤c_1/c_2	0.5	1.0	2.0	≥3.0
K	0.45	0.60	0.70	0.80

W_1 corresponds to a distribution of shear as illustrated in Figure 2.27:

$$W_1 = \int_0^{b_{0,EC2}} |e|\, dl \tag{2.66}$$

where e is the eccentricity. For rectangular column W_1 results equal to:

$$W_1 = \frac{c_1^2}{2} + c_1 \cdot c_2 + 4 \cdot c_2 \cdot d + 16 \cdot d^2 + 2 \cdot \pi \cdot d \cdot c_1 \tag{2.67}$$

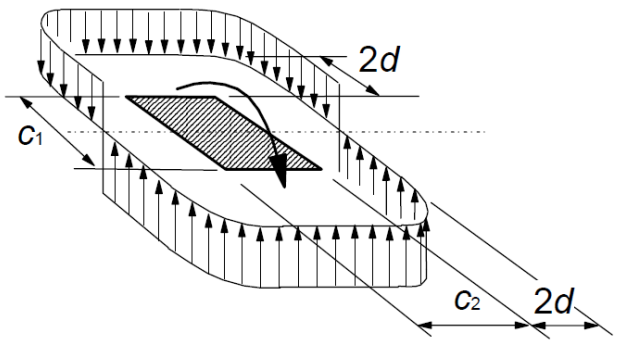

Figure 2.27 – Uneven distribution of shear accorgin to EC2 – 2004 [22].

2.5.2 Model Code 2010

The punching provision of Model Code 2010 [55] is grounded on the CSCT [32]. The punching failure is assumed to depend on the slab rotation. For slab without shear reinforcement the punching strength is defined as:

$$V_{MC} = k_{\psi} \cdot \frac{\sqrt{f_{ck}}}{\gamma_c} \cdot b_{0,MC} \cdot d \tag{2.68}$$

where k_{ψ} depends on the slab rotation ψ the effective depth d and on the maximum aggregate size d_g:

$$k_{\psi} = \frac{\sqrt{f_{ck}}}{1.5 + 0.9 \cdot \psi \cdot d \cdot k_{dg}} \leq 0.6 \tag{2.69}$$

where k_{dg}= 32/(16+d_g) ≥ 0.75 accounts for the influence of the maximum aggregate size d_g. The basic control perimeter $b_{0,MC}$ is set a distance d/2 from the support region with circular corners (Figure 2.28).

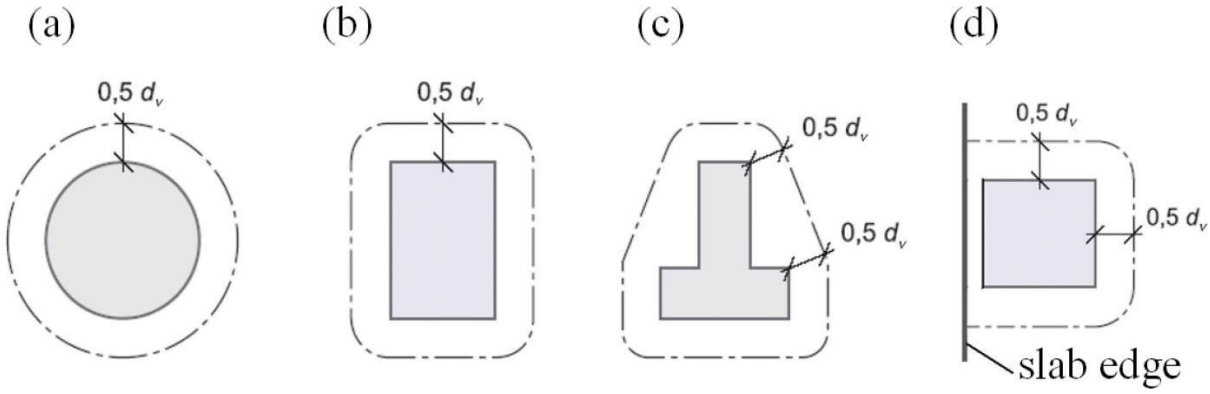

Figure 2.28 – Control perimeter according to Model Code 2010 [55].

The presence of openings is accounted by reducing the control perimeter as shown in Figure 2.29.

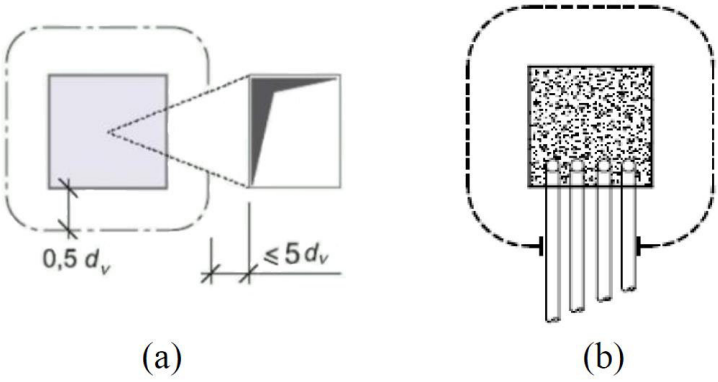

Figure 2.29 – Reduction of the control perimeter in presence of openings and pipings according to Model Code 2010 [55].

Concentration of shear stress due to moment transfer between the slab and the supported is accounted by reducing the control perimeter with the coefficient k_e defined as follows:

$$k_e = \frac{1}{1 + e_u/b_u} \tag{2.70}$$

where e_u is the eccentricity with respect to the centroid of the control perimeter and b_u is the diameter of a circle with the same surface as the region inside the control perimeter. In presence of shear reinforcement, the punching strength is calculated as the sum of the contribution provided by the concrete and that provided by the shear reinforcement. Both these contributions depend on the slab rotation:

$$V_{MC,SR} = k_\psi \cdot \frac{\sqrt{f_{ck}}}{\gamma_c} \cdot b_{0,MC} \cdot d + \sum A_{sw} \cdot k_e \cdot \sigma_{swd} \cdot \sin\alpha \tag{2.71}$$

where ΣA_{sw} is the sum of the cross-sectional area of all shear reinforcement suitably anchored, intersecting the failure surface within the zone bounded by 0.35·d and d from the column (Figure 2.30).

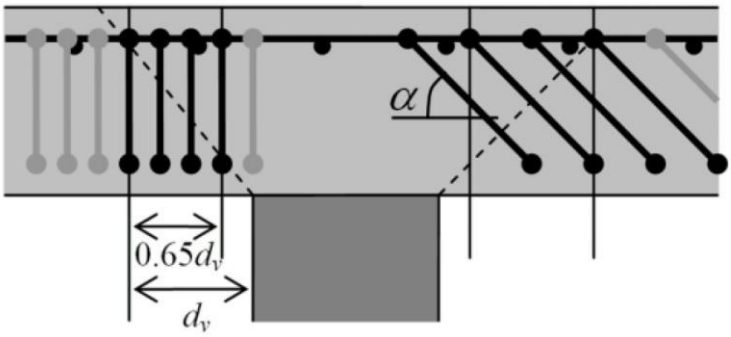

Figure 2.30 – Shear reinforcement activated at faliure according to Model Code 2010 [55].

The stress activated by the shear reinforcement is calculated as follows:

$$\sigma_{swd} = \frac{E_s \cdot \psi}{6} \cdot (\sin\alpha + \cos\alpha) \cdot \left(\sin\alpha + \frac{2 \cdot f_{bd}}{f_{ywd}} \cdot \frac{d}{\emptyset_w}\right) \leq f_{ywd} \tag{2.72}$$

where Es is the steel elastic modulus, f_{bd} is the bond strength provided by the concrete and $\emptyset_w$ is the diameter of shear reinforcement.

The maximum punching shear strength is limited by crushing of the concrete struts in the supported area:

$$V_{MC,Crush} = k_{sys} \cdot k_{\psi} \cdot \frac{\sqrt{f_{ck}}}{\gamma_c} \cdot b_{0,MC} \cdot d \tag{2.73}$$

where k_{sys} accounts the capacity of shear reinforcement to give confinement to compression struts. In absence of other data, a value of k_{sys}=2.0 can be adopted.

For the calculation of the slab rotation different levels of approximations are provided. For Level I of Approximation the rotation at failure is:

$$\psi = 1.5 \cdot \frac{r_s}{d} \cdot \frac{f_{yd}}{E_s} \tag{2.74}$$

where r_s denotes the distance between the point where the radial bending moment is zero and the support axis. For regular flat slab the value of r_s can be approximated as r_s=0.22·L.

For Level II of Approximation the rotation at failure is:

$$\psi = 1.5 \cdot \frac{r_s}{d} \cdot \frac{f_{yd}}{E_s} \cdot \left(\frac{m_{sd}}{m_{Rd}}\right)^{1.5} \tag{2.75}$$

where m_{sd} is the average moment per unit length of the flexural reinforcement in the support strip and m_{Rd} is the related flexural strength. The width of the support strip is calculated as:

$$b_s = 1.5 \cdot \sqrt{r_{s,x} \cdot r_{s,y}} \leq L_{min} \tag{2.76}$$

where r_s could be calculated as for the level I of Approximation. For inner columns the average bending moment over the support strip can be calculated as:

$$m_{sd} = V_{Ed} \cdot \left(\frac{1}{8} + \frac{|e_{u,i}|}{2 \cdot b_s} \right) \tag{2.77}$$

where $e_{u,i}$ is the eccentricity with respect to the centroid of the basic control perimeter in the direction investigated (i = x and y for x and y directions respectively).

For Level III of Approximation the coefficient 1.5 in equations (2.75) and (2.76) can be replaced by 1.2 if both r_s and m_{sd} are calculated using a linear elastic uncracked model.

For Level IV of Approximation the rotation can be calculated using a nonlinear analysis of the structure taking into account, for instance, cracking, tension-stiffening effects and yielding of the reinforcement.

2.5.3 ACI 318 – 19

The punching provision of ACI 318-19 [56] is a semi-empirical formula very easy to apply. For slabs without shear reinforcement the punching strength is provided by the smallest of the following values:

$$V_{ACI} = \frac{1}{6} \cdot \left(1 + \frac{2}{\beta} \right) \cdot \lambda_s \cdot \sqrt{f_{ck}} \cdot b_{0,ACI} \cdot d \tag{2.78}$$

$$V_{ACI} = \frac{1}{12} \cdot \left(\frac{\alpha_s \cdot d}{b_{0,ACI}} + 2 \right) \cdot \lambda_s \cdot \sqrt{f_{ck}} \cdot b_{0,ACI} \cdot d \tag{2.79}$$

$$V_{ACI} = \frac{1}{3} \cdot \sqrt{f_{ck}} \cdot \lambda_s \cdot b_{0,ACI} \cdot d \tag{2.80}$$

where λ_s is the size effect factor:

$$\lambda_s = \sqrt{\frac{2}{1 + 0.004 \cdot d}} \leq 1 \tag{2.81}$$

where β is the ratio between long and short size of the column, α_s is 40 for inner column, 30 for edge column and 20 for corner columns. $b_{0,ACI}$ is the control perimeter set at d/2 from the column. If an opening is located closer than 10·h from the column the control perimeter should be reduced (Figure 2.31).

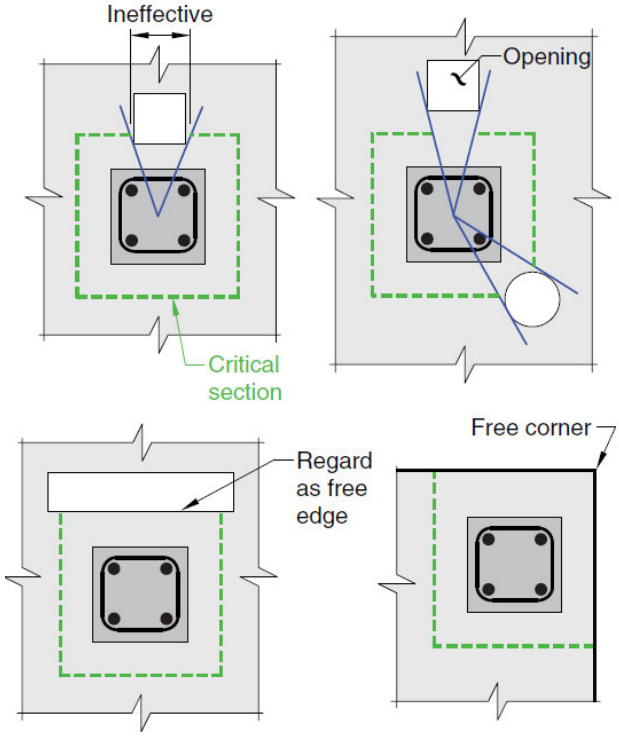

Figure 2.31 – Control perimeter according to ACI 318-19 [56].

In presence of shear reinforcement, the punching strength is calculated by adding concrete and shear reinforcement contributions. There are different formulations in function of the shear reinforcement type, for slabs with stirrups the punching strength results:

$$V_{ACI,SR} = \frac{1}{6} \cdot \sqrt{f_{ck}} \cdot \lambda_s \cdot b_{0,ACI} \cdot d + A_{sw} \cdot f_{yw} \cdot \frac{d}{s_r} \tag{2.82}$$

where A_{sw} is the shear reinforcement area of one periphery and s_r is the distance between two consecutive peripheries. To avoid the crush of the strut, the strength should not be greater than:

$$V_{ACI,Crush} = \frac{1}{2} \cdot \sqrt{f_{ck}} \cdot b_{0,ACI} \cdot d \tag{2.83}$$

In presence of unbalanced moment, the fraction transferred by flexure γ_f is calculated as:

$$\gamma_f = \frac{1}{1 + \left(\frac{2}{3}\right) \cdot \sqrt{\frac{b_1}{b_2}}} \tag{2.84}$$

the effective slab width for resisting this fraction of unbalanced moment is assumed equal to the support size plus 1.5·h on both sides. The fraction of unbalanced moment transferred by eccentricity of shear results equal to $\gamma_v = (1 - \gamma_f)$. The stress distribution is assumed as shown in Figure 2.4. The maximum shear stress is calculated as:

$$v_{u(AB)} = \frac{V_{Ed}}{b_0 \cdot d} + \frac{\gamma_v \cdot M_{Ed} \cdot c_{AB}}{J_c} \tag{2.85}$$

where J_c for inner rectangular columns is calculated as:

$$J_c = \frac{d \cdot (c_1 + d)^3}{6} + \frac{(c_1 + d) \cdot (d)^3}{6} + \frac{d \cdot (c_2 + d) \cdot (c_1 + d)^2}{2} \tag{2.86}$$

The maximum shear stress due to V and M should not exceed the maximum shear strength. In terms of shear forces shall results:

$$v_{u(AB)} \cdot \left(b_{0,ACI} \cdot d\right) \leq \phi \cdot V_{ACI} \tag{2.87}$$

where the shear reduction factor ϕ is placed equal to 0.75.

Unlike EC2 – 2004 and Model Code 2010, ACI 318-19 provides specific rules about flat slab under seismic actions. For flat slab part of a seismic-force-resisting system the shear force shall not exceed $0.4 \cdot \phi \cdot V_c$. Slab-column connection also must satisfy shear and moment strength requirements. However, flat slab-column connections as part of primary system is permitted only for low earthquake risk, corresponding to Seismic Design Categories (SDC) A,B and C. In SDC D, E and F, flat slab buildings need to rely on a lateral-force-resisting system that limits lateral displacement.

For flat slab not designated as part of the seismic-force-resisting system no calculation of induced moments is required. Shear reinforcement shall be provided if:

$$DR \geq 0.035 - (1/20) \cdot \left(\frac{V_{Ed}}{\phi \cdot V_{ACI}}\right) \tag{2.88}$$

where DR is the horizontal drift (Figure 2.32).

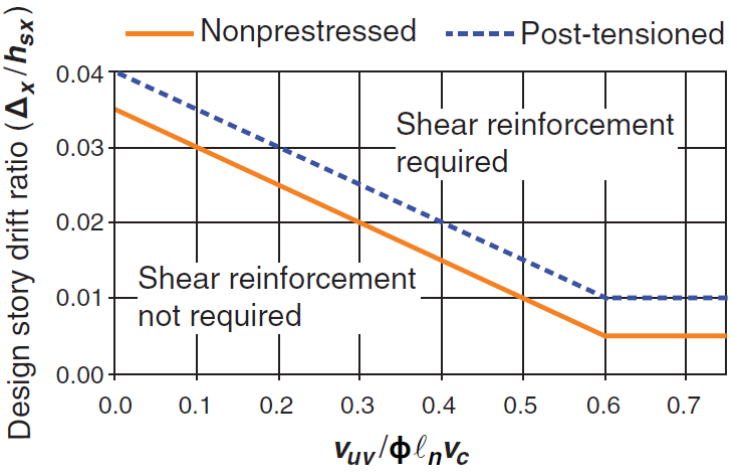

Figure 2.32 – Story drift vs gravity shear ratio criterion according to ACI 318-19 [56].

Required shear reinforcement shall provide:

$$v_s \geq 0.29 \cdot \sqrt{f_{ck}} \tag{2.89}$$

and shall extend at least four times the slab thickness from the column.

2.5.4 ACI 421.2R – 10

ACI 421.2R – 10 [57] focuses on the design of flat slab-column connections subjected to earthquake-induced displacements. This code excludes the design of flat slab column connections as lateral-force-resisting systems. Unlike ACI 318 – 19 [56] this provision requires the calculation of the unbalanced moment and the maximum shear stress is calculated considering both shear and unbalanced moment.

ACI 421.2R – 10 provides a procedure to determine the elastic unbalanced moment acting on the slab column-connection (M_{Ed}). The flat slab-column connection is designed to transfer shear and moments associated with the horizontal drift exhibited by the primary structure. A simplified elastic analysis is proposed as shown in Figure 2.12. The horizontal displacement is introduced at the upper end of the column then the unbalanced moment is calculated. This

provision gives also the upper limit of the unbalanced moment that produces the flexural failure:

$$M_{Ed} \leq \frac{M_{pr}}{\alpha_m} \tag{2.90}$$

where M_{pr} is the sum of flexural strengths of opposite critical section sides (c_1 + d or c_2 + d) and α_m is an empirical coefficient calibrated on finite element results. For inner columns it is expressed by:

$$\alpha_m = 0.85 - \gamma_v - \left(\frac{\beta_r}{20}\right) \tag{2.91}$$

where γ_v is the fraction of unbalanced moment transferred by uneven shear stress and β_r is equal to ℓ_y/ℓ_x or ℓ_x/ℓ_y when the transferred moment is about the x- or y-axis, respectively (see Figure 2.33).

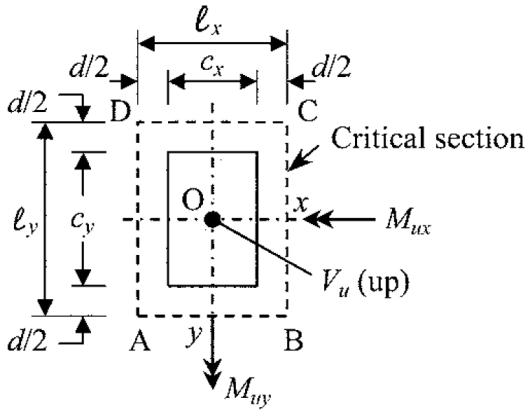

Figure 2.33 – Critical section dimensions, adapted from ACI 421.2R – 10 [57].

The design procedure is summarized in Figure 2.34.

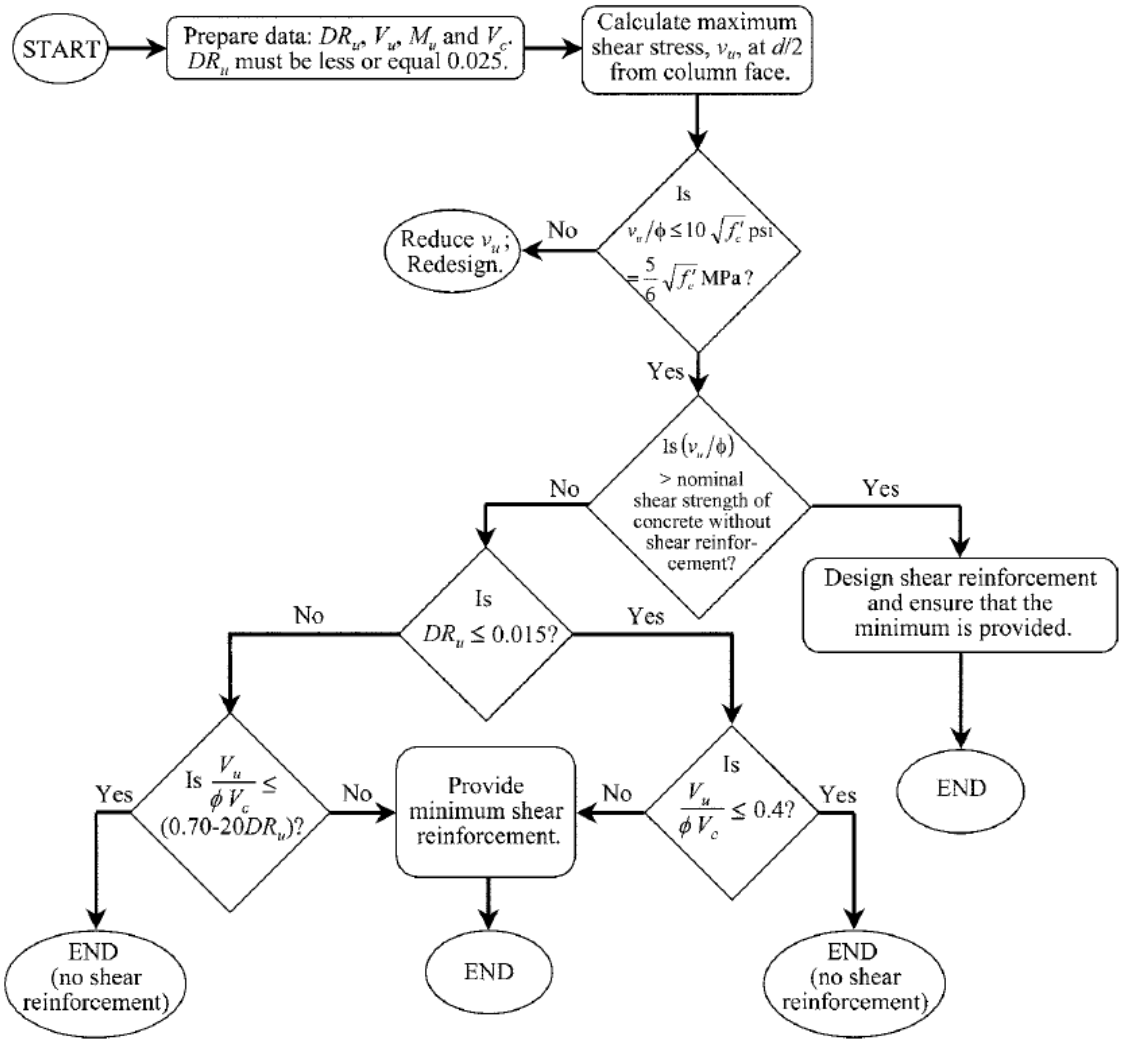

Figure 2.34 – Steps for punching shear design according to ACI 421.2R-10 [57].

where the punching shear strength with or without shear reinforcement are calculated according to ACI 318 – 14 [5]. When shear reinforcement is required the minimum amount is calculated according to the following equation:

$$v_s \geq \frac{1}{4} \cdot \sqrt{f_{ck}} \tag{2.92}$$

2.6 Discussion

2.6.1 Analysis methods for laterally loaded flat slabs

The first step in the design process of a flat slab column connection under combined gravity and lateral loading is represented by the prediction of the connection lateral response. In literature, two methods for the prediction of the flexural behaviour of slab column connections subjected to lateral loading are found: the Equivalent Frame Method (EFM) and the Effective Beam Width Method (EBWM).

Besides, the Effective Beam Width Method (EBWM) could be used for the implementation of a FEM, the presence of the opening makes this method difficult to use. Indeed, the reduction of the effective beam width, due to the presence of the opening, is not known. For instance, the reduced effective beam width could be calculated deducting the opening size from the beam width. However, this approach appears too simplistic since does not consider the position of the opening.

The Equivalent Frame Method (EFM), as the previous method, does not appear perfectly suitable to be used in presence of openings. The presence of the opening could be accounted by reducing the stiffness of the torsional element. For instance, the calculation of the integral of twisting moments could be rearranged to account the presence of the opening. However, also this approach appears too rough.

For these reasons the use of the Finite Element Analysis (FEA) is suggested. The slabs could be modelled with shell elements while the columns as frame elements. The determination of forces and unbalanced moments on the connections could be performed by using static or Response-spectrum analysis. The value of vertical force acting on the slab column connection corresponds with the normal force on the column below the joint. The unbalanced moment acting on the connection corresponds with the sum of the bending moments, on the column, below and above the joint.

2.6.2 Analytical models for punching failure with combined gravity and lateral loading

The first analytical model for punching prediction under combined gravity and lateral loading is the eccentricity of shear. According to this model the unbalanced moment between the slab and the column is considered to be transferred by both flexure and uneven distribution of shear forces around the column. The presence of openings makes the application of this method complicated. Indeed, due to the presence of the opening the distribution of shear around the column should be recalculated for each joint accounting for the size and the position of the opening. Furthermore, the effectiveness of this method for cyclic horizontal loading is questionable.

According to the strip model the slab is subdivided into two different regions, B-regions dominated by slender flexural behaviour and D-regions dominated by deep beam behaviour. The radial strips are assumed to be D-regions, while plate quadrants are assumed to be D-regions. The use of this model in presence of openings appears not possible. Indeed, in presence of two openings placed on both opposite sides of the column along the direction of the lateral loading, the radial strips would be interrupted without any possibility to support unbalanced moments.

The drift versus gravity shear ratio model is directly derived by interpretation of experimental results of slabs without openings. The extension of this method to slabs with openings is questionable. The presence of the opening could be accounted by changing the gravity shear ratio only. However, this procedure could lead to results on the unsafety side.

With regards to the Broms model, the presence of openings appears difficult to be accounted for, therefore the only method that appears more suitable to be implemented in presence of openings is the Drakatos model. In this case both the size and the position of the opening could be accounted identifying an “empty” slab sector. Besides this modification the method could be applied as for the case without openings. However, this model is very complicated and it requires several calculations, and for this reason does not appear suitable for design. Anyway, starting from this model a more code-like method could be developed for design purpose.

2.6.3 Experimental works on slabs with openings

From gravity loading tests arises clearly that the presence of openings near or adjacent to the columns induces a reduction of the punching strength. Furthermore, from the results of the experimental tests emerges that the loss of strength due to the presence of openings could be easily accounted by reducing the control perimeter.

With regards to combined gravity and lateral loading few results are available. Furthermore, there is only one test dealing with cyclic horizontal loading. From this test arises that the presence of the opening plays a detrimental role also for combined gravity and horizontal loading, on both peak load and ductility. However, the determination of this detrimental effect is not easily quantifiable as for gravity loading only, where the reduction in terms of punching strength is proportional to the reduction of control perimeter.

2.6.4 Code provisions

The European code provisions do not deal with slab column connections under seismic loadings. The ACI provisions represent the only reference for design slab column connections under seismic actions. However, the drift versus gravity shear ratio model is directly derived by interpretation of experimental results of slabs without openings. The extension of these results to slabs with openings could lead to an overestimation of the slab column connection capacity. To validate this procedure more experimental results of slabs with openings subjected to combined gravity and cyclic lateral loading are needed.

2.7 Reference

[1] Corley, WG.; Sozen, MA.; Siess, CP.; The Equivalent Frame Analysis for Reinforced Concrete Slabs, Urbana, Illinois: 1961.

[2] Corley, WG.; Jirsa, JO.; Equivalent Frame Analysis For Slab Design, ACI Journal, 1970, Vol. 67: pp. 875–84.

[3] Park, YM.; Han, SW.; Kee, S-H.; A modified equivalent frame method for lateral load analysis, Magazine of Concrete Research, 2009, Vol. 61: pp. 359–70.

[4] Luo, YH.; Durrani, a. J.; Conte, JP.; Equivalent Frame Analysis of Flat Plate Buildings for Seismic Loading, Journal of Structural Engineering, 1994, Vol. 120: pp. 2137–55.

[5] ACI Committee 318.; Building Code Requirements for Structural Concrete (ACI 318M-14) and Commentary (ACI 318RM-14), Farmington Hills, U.S.A.: 2014.

[6] Vanderbilt, MD.; Corley, WG.; Frame analysis of concrete buildings, Concrete International, 1983, Vol. 5: pp. 33–43.

[7] Pecknold, DA.; Slab Effective Width for Equivalent Frame Analysis, ACI Journal, 1975, Vol. 72: pp. 135–7.

[8] Allen, BF.; Darvall, P.; Lateral Load Equivalent Frame, ACI Journal, 1977, Vol. 74: pp. 294–9.

[9] Banchik, CA.; Effective beam width coefficients for equivalent plane frame analysis of flat-plate structures. University of California, Berkeley, 1987.

[10] Hwang, S.; Moehle, JP.; Models for Laterally Loaded Slab-Column frames, ACI Structural Journal, 2000, Vol. 97: pp. 345–53.

[11] Westergaard, HM.; Moments and stresses in slabs, Journal Proceedings, 1921, Vol. 17: pp. 415–538.

[12] ASCE.; Seismic Evaluation and Retrofit of Existing Buildings (ASCE 41-13), ASCE/SEI 4, American Society of Civil Engineers; 2014.

[13] Han, S-W.; Park, Y-M.; Kee, Js-H.; Stiffness Reduction Factor for Flat Slab Structures under Lateral Loads, Journal of Structural Engineering, ASCE, 2009, Vol. 135: pp. 743–50.

[14] Luo, YH.; Durrani, AJ.; Equivalent Beam Model for Flat slab Buildings-Part 1 : Interior Connections, ACI Structral Journal, 1995, Vol. 92: pp. 115–24.

[15] Di Stasio, J.; Van Buren, MP.; Transfer of Bending Moment between Flat Plate Floor and Column, ACI Journal, 1960, Vol. 32: pp. 299–314.

[16] Moe, J.; Shearing Strength of Reinforced Concrete Slabs and Footings under Concentrated Loads., Journal of Portland Cement Association, Research and Development Laboratories, 1961, Vol. D47: pp. 130.

[17] Mast, PE.; Stresses in Flat Plates Near Columns, ACI Journal, 1970, Vol. 67: pp. 761–8.

[18] Regan, PE.; Ultimate limite state principles. In: fib (fédération internationale du béton / the International Federation for Structural Concrete), editor. fib Bull. 2, Struct. Concr. Textb. Behav. Des. Performance; Vol. 2 Basis Des., 1999, p. 320.

[19] Stamenkovic, A.; Chapman, JC.; Local strengthlat column heads in flat slabs subjected t o a combined vertical and horizontal loading, Proceedings of the Institution of Civil Engineers, 1974, Vol. 57: pp. 205–32.

[20] Hawkins, NM.; Bao, A.; Yamazaki, J.; Moment Transfer from Concrete Slabs to Columns, ACI Structural Journal, 1989, Vol. 86: pp. 705–16.

[21] CEB/FIP.; Ceb-Fip Model Code 1990, London: Thomas Telford; 1993.

[22] CEN.; Eurocode 2: Design of concrete structures - Part 1-1: General rules and rules for buildings, Bruxelles: 2004.

[23] Alexander, SDB.; Simmonds, SH.; Bond Model for Concentric Punching Shear, ACI Structral Journal, 1992, Vol. 89: pp. 325–34.

[24] Alexander, SB.; Shear and moment transfer at column-slab connections, ACI Special Publication, 2017, Vol. 315: pp. 1–22.

[25] Pan, A.; Moehle, JP.; Lateral displacement ductility of reinforced concrete flat plates, ACI Structural Journal, 1989, Vol. 86: pp. 250–8.

[26] Megally, S.; Ghali, A.; Design considerations for slab-column connections in seismic zones, ACI Structural Journal, 1994, Vol. 91: pp. 303–14.

[27] Megally, S.; Ghali, A.; Punching Shear Design of Earthquake-Resistant Slab- Column Connections, ACI Structural Journal, 2000, Vol. 97: pp. 720–30.

[28] Broms, CE.; Design method for imposed rotations of interior slab-column connections, ACI Structural Journal, 2009, Vol. 106: pp. 636–45.

[29] Aalami, B.; Moment Rotation Relation Between Column and Slab, ACI Journal, 1972, Vol. 69: pp. 263–9.

[30] Muttoni, A.; Schwartz, J.; Behavior of Beams and Punching in Slabs without Shear Reinforcement, IABSE Colloquium, 1991, Vol. 62: pp. 703–8.

[31] Muttoni, A.; Schubfestigkeit und Durchstanzen von Platten ohne Querkraftbewehrung, Beton- Und Stahlbetonbau, 2003, Vol. 98: pp. 74–84.

[32] Muttoni, A.; Punching shear strength of reinforced concrete slabs without transverse reinforcement, ACI Structural Journal, 2008, Vol. 105: pp. 440–50.

[33] Walraven, JC.; Fundamental analysis of aggregate interlock, Journal of Structural Engineering, ASCE, 1981, Vol. 107: pp. 2245–70.

[34] Vecchio, FJ.; Collins, MP.; The modified compression-field theory for reinforced concrete elements subjected to shear, ACI Journal Proceedings, 1986, Vol. 83: pp. 219–31.

[35] Tassinari, L.; Poinçonnement non symétrique des dalles en béton armé. Ecole

Polytechnique Fédérale de Lausanne, 2011.

[36] Sagaseta, J.; Muttoni, A.; Ruiz, MF.; Tassinari, L.; Non-axis-symmetrical punching shear around internal columns of RC slabs without transverse reinforcement, Magazine of Concrete Research, 2011, Vol. 63: pp. 441–57.

[37] Muttoni, A.; Ruiz, MF.; Bentz, E.; Foster, S.; Sigrist, V.; Background to fib Model Code 2010 shear provisions - part II: punching shear , Structural Concrete, 2013, Vol. 14: pp. 204–14.

[38] Muttoni, A.; Ruiz, MF.; The levels-of-approximation approach in MC 2010: Application to punching shear provisions, Structural Concrete, 2012, Vol. 13: pp. 32–41.

[39] Drakatos, I.; Beyer, K.; Muttoni, A.; Lateral Force Resisting Mechanisms in Slab-Column Connections : an Analytical Approach, 2nd European Conference on Earthquake Engineering and Seismology, 2014: pp. 11.

[40] Drakatos, IS.; Muttoni, A.; Beyer, K.; Mechanical model for drift-induced punching of slabcolumn connections without transverse reinforcement, ACI Structural Journal, 2018, Vol. 115: pp. 463–74.

[41] Hognestad, E.; Elstner, RC.; Hanson, JA.; Shear Strength of Reinforced Structural Lightweight Aggregate Concrete Slabs, Journal Proceedings, 1964, Vol. 61: pp. 643–56.

[42] Mowrer, RD.; Vanderbilt, MD.; Shear Strength of Lightweight Aggregate Reinforced Concrete Flat Plates, Journal Proceedings, 1967, Vol. 64: pp. 722–9.

[43] Roll, F.; Zaidi, STH.; Sabnis, G.; Chuang, K.; Shear Resistance of Perforated Reinforced Concrete Slabs, ACI Special Publication, 1971, Vol. 30: pp. 77–101.

[44] Regan, PE.; Shear Reinforcement of Flat Slabs. Int. Work. Punching Shear Capacit. RC Slab, Stockholm: 2000, p. 99–107.

[45] Teng, S.; Cheong, HK.; Kuang, KL.; Geng, JZ.; Punching shear strength of slabs with openings and supported on rectangular columns, ACI Structural Journal, 2004, Vol. 101: pp. 678–87.

[46] Elshafiey, TMF.; Hussein, M.; Abdel-Aziz, M.; Behaviour of Flat Slabs With Openings Adjacent to Columns. Struct. Faults Repair 14th Int. Conf., Edinburgh: 2012.

[47] Borges, LLJ.; Melo, GS.; Gomes, RB.; Punching Shear Strength of Reinforced Concrete Flat Plates with Openings, ACI Structral Journal, 2013, Vol. 110: pp. 547–56.

[48] Anil, Ö.; Kina, T.; Salmani, V.; Effect of opening size and location on punching shear behaviour of two-way RC slabs, Magazine of Concrete Research, 2014, Vol. 66: pp. 955–66.

[49] Ha, T.; Lee, M-H.; Park, J.; Kim, D-J.; Effects of openings on the punching shear strength of RC flat-plate slabs without shear reinforcement, Structural Design of Tall and Special Buildings, 2015, Vol. 24: pp. 895–911.

[50] Liberati, EAP.; Marques, MG.; Leonel, ED.; Almeida, LC.; Trautwein, LM.; Failure analysis

of punching in reinforced concrete flat slabs with openings adjacent to the column, Engineering Structures, 2019, Vol. 182: pp. 331–43.

[51] El-Salakawy, E.; Polak, MA.; Soliman, MH.; Slab-column edge connections subjected to high moments, Canadian Journal of Civil Engineering, 1998, Vol. 25: pp. 526–38.

[52] El-Salakawy, EF.; Polak, MA.; Soliman, MH.; Reinforced concrete slab-column edge connections with openings, ACI Structural Journal, 1999, Vol. 96: pp. 79–87.

[53] Bu, W.; Polak, MA.; Effect of openings and shear bolt pattern in seismic retrofit of reinforced concrete slab-column connections, Engineering Structures, 2011, Vol. 33: pp. 3329–40.

[54] Oliveira, DC.; Gomes, RB.; Melo, GS.; Punching shear in reinforced concrete flat slabs with hole adjacent to the column and moment transfer, Revista IBRACON de Estruturas e Materiais, 2014, Vol. 7: pp. 414–67.

[55] CEB-FIP.; Model Code 2010 - Volume 2, Lausanne, Switzerland: Internation Federation for Structural Concrete (fib); 2012.

[56] American Concrete Institute.; Building Code Requirements for Structural Concrete (ACI 318-19), 2019.

[57] ACI-ASCE Committee 421.; ACI 421.2R-10 Guide to Seismic Design of Punching Shear Reinforcement in Flat Plates, 2010.

3. EXPERIMENTAL CAMPAIGN

3.1 Introduction

In the following the experimental campaign performed at the Structural Laboratory of the Department of Civil Engineering, NOVA School of Science and Technology is presented. The experimental setup is extensively described and the characteristics of the specimens are provided. Thus, the preparation of the specimens is shown and the material characteristics are presented. Finally, the instrumentation and the loading protocol are provided.

3.2 Description of test setup

The experimental campaign was performed at the Structural Laboratory of the Department of Civil Engineering, NOVA School of Science and Technology in Caparica that is equipped with an innovative test setup. The latter was developed by Almeida et al. [1] and allows for simulating the behaviour of a slab-column connection under combined gravity and horizontal loading. Most of experimental programs setups found in the literature review provide simplified boundary conditions, such as borders that are simply supported, leading to a static position of the zero-moment line and no moment redistribution capacity. The test setup developed at the NOVA School of Science and Technology represents an attempt to overcome these limitations in the existing test setups. This setup allows equal vertical displacements and equal rotations at the opposite N-S slab borders. These boundary conditions are provided by means two different systems (Figure 3.1). The equality of border's vertical displacements is fulfilled

by a passive mechanical see-saw-like system. The equality of border's rotations is fulfilled by a system consisting in a double pinned steel frame suspended on slab's border by two vertical fixed columns.

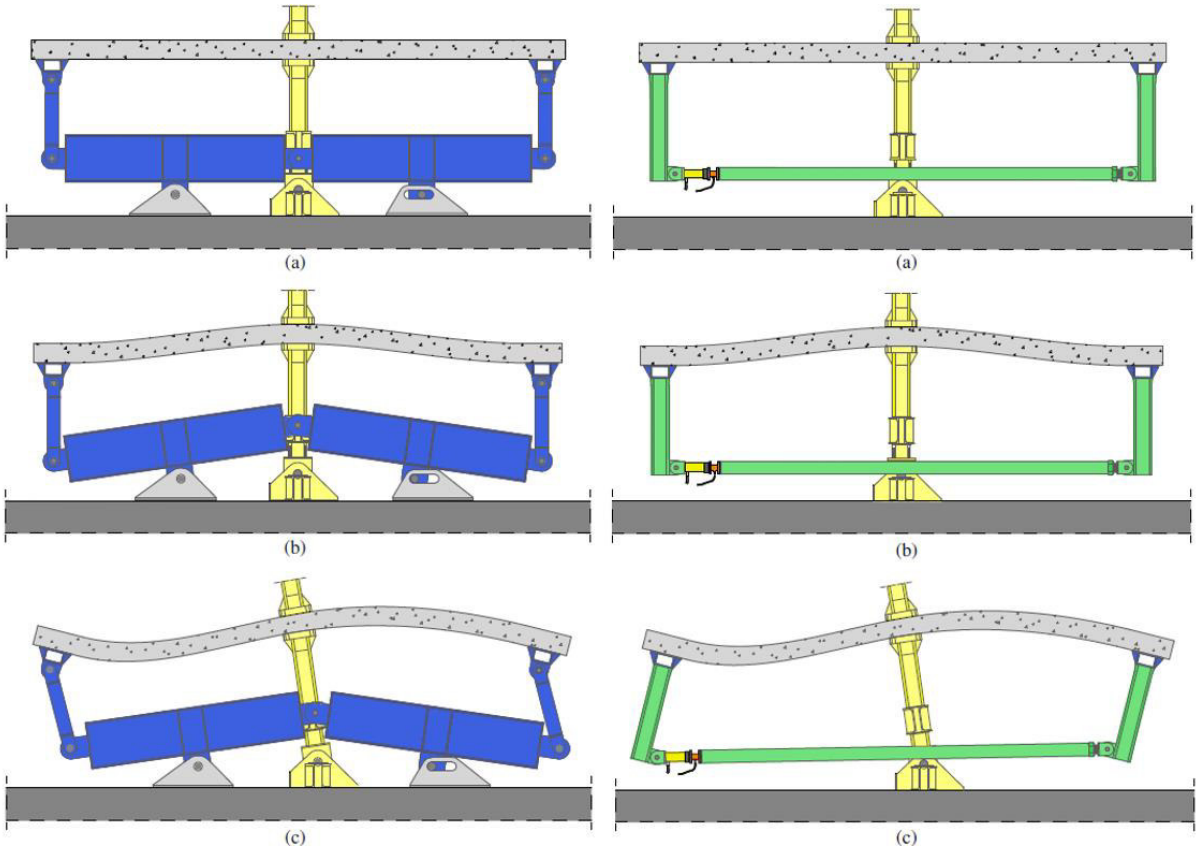

Figure 3.1 – Vertical displacement and rotation compatibilization systems (a) undeformed configuration (b) vertical deformation (c) vertical and horizontal deformation, adapted from Almeida et al. [1].

The vertical load is applied through steel plates to the slab's top surface in eight points to better approximate a uniformly distributed load. For this to be accomplished, a closed structure to apply the vertical load was created using a system of spreader beams and steel tendons that follows the slab horizontal deformation without inducing unintended horizontal forces (Figure 3.2). The connection to the slab is provided by two halves columns made of steel, trough 250x250 mm rigid square plates, using four M24 bolts.

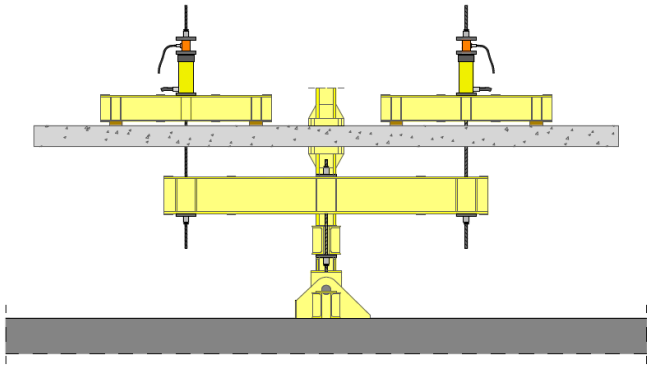

Figure 3.2 – Vertical load application system, adapted from Almeida et al. [1].

The complete test setup, with the three different sub-systems, is shown in Figure 3.3.

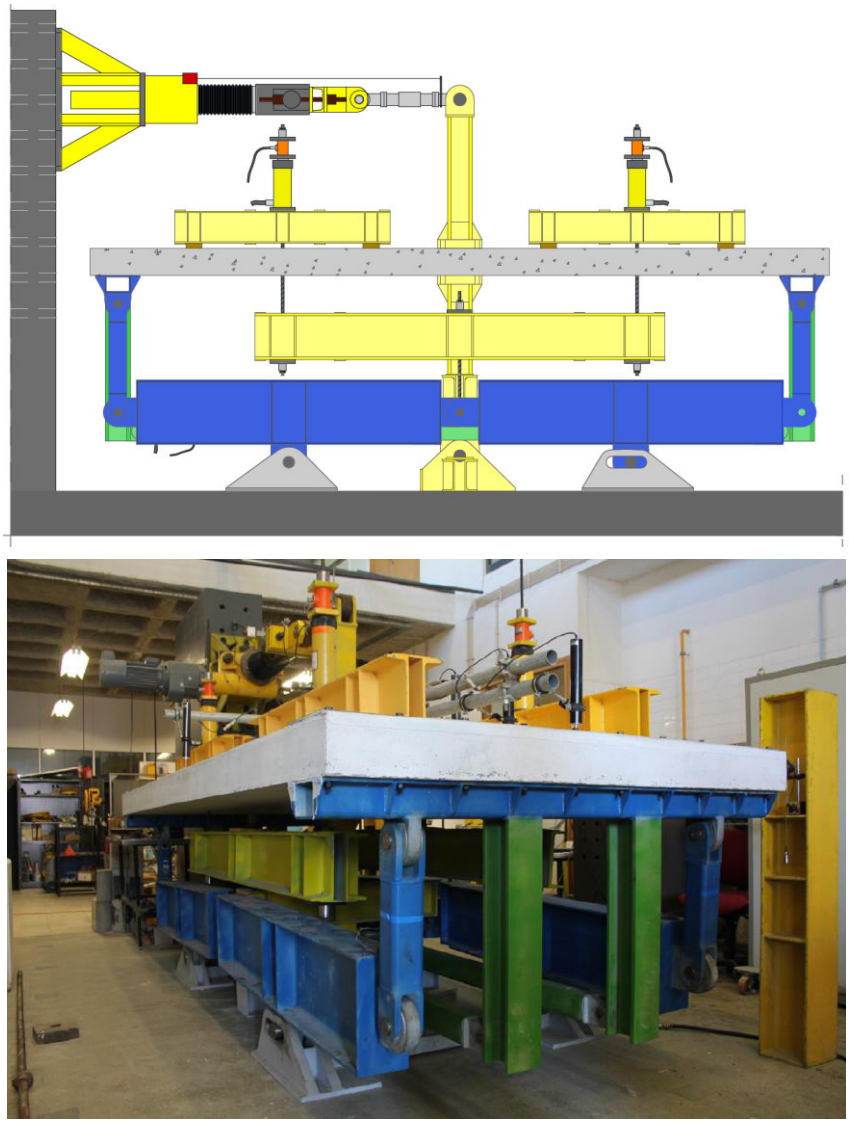

Figure 3.3 – Complete test setup.

The slab specimens are 4150 x 1850 mm in plan, with a thickness of 150 mm. The longer side is placed in N-S direction while the shorter is E-W direction. In N-S direction, where the compatibility of the boundary conditions is provided, the entire slab span (L) approximately equal to four meters is simulated, while in E-W direction the specimen goes to the line of moment contraflexure (0.44·L).

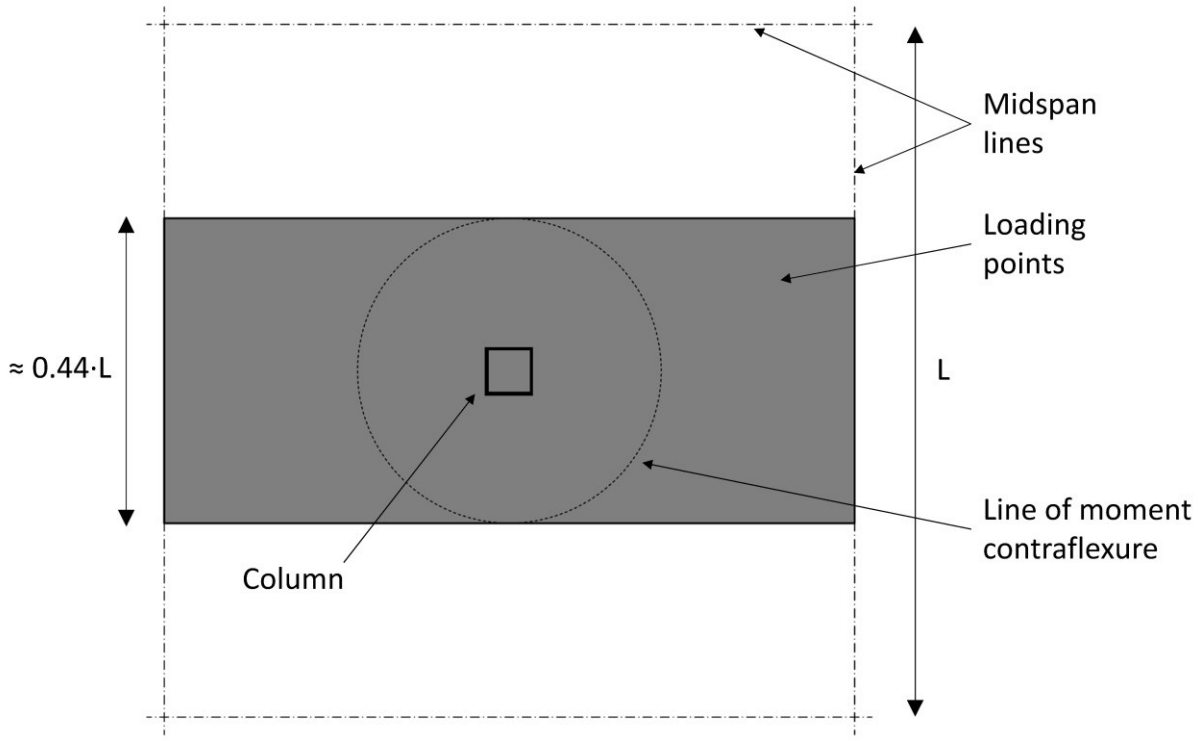

Figure 3.4 – Specimen and idealized flat slab dimensions.

3.3 Finite element linear analysis of test setup

In the following the finite element linear analysis of the test setup is provided. The analysis is focused on comparing the performance of the test setup with the performance of the idealized flat slab that the setup is supposed to represent. The comparison between setup and flat slab is made by means linear FEM in SAP 2000 using shell elements.

The setup is modelled imposing a constraint to the points on N and S borders. The constraint forces the points to have the same vertical displacement and the same rotation along the E-W direction. Considering the steel plates on the borders, the N-S length of the setup model is assumed equal to 4 meters as the flat slab. The E-W length is assumed equal to 1850 mm as the width of the specimen. The 4x4 m flat slab is modelled adopting different constraints along the borders. Indeed, both displacements and rotations vary along the borders

of the flat slab. For this reason, ten different constraints are used on borders N-S and E-W respectively.

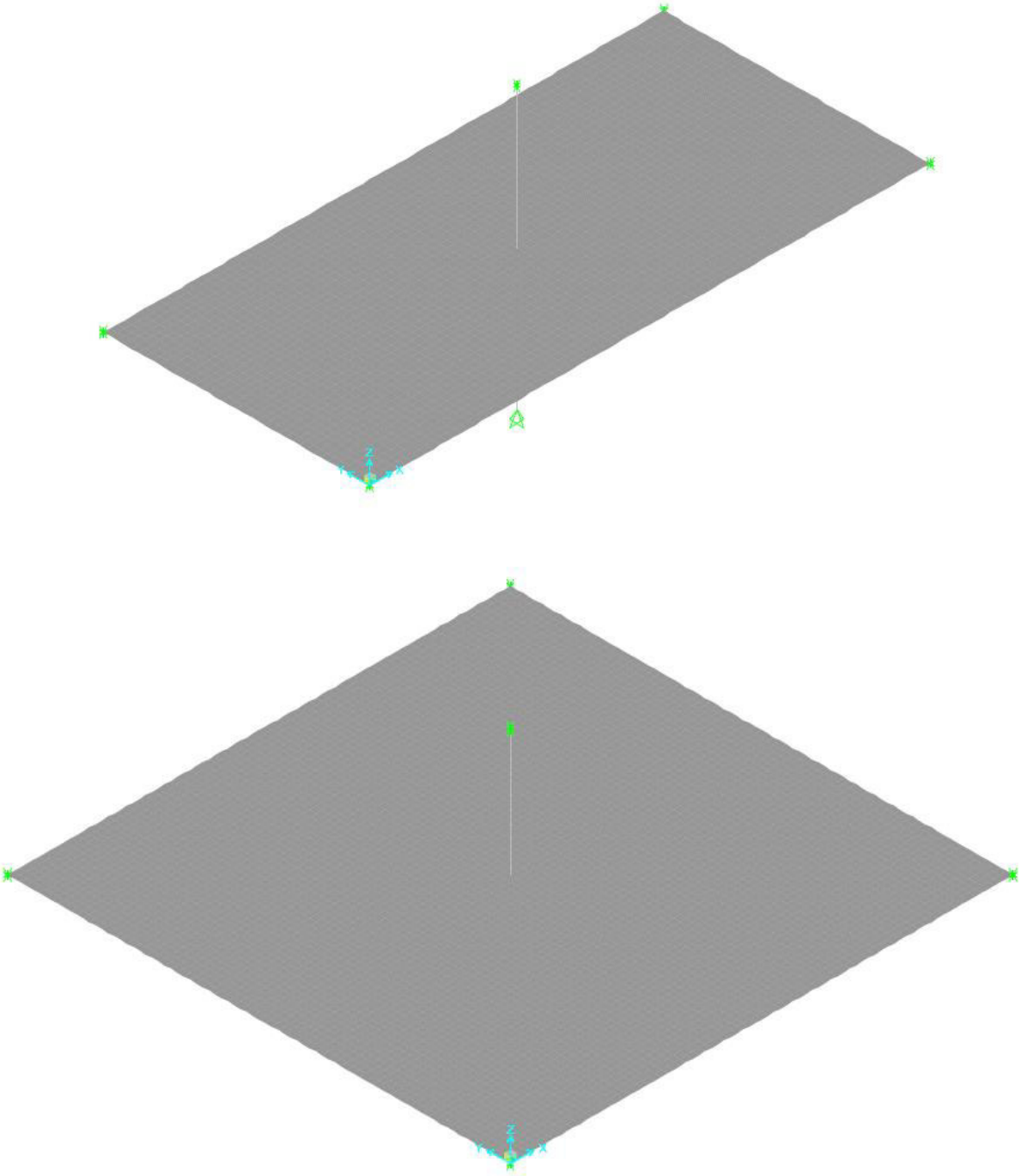

Figure 3.5 – SAP 2000 linear shell models: Lisbon Setup (up) 4x4 m flat slab (down).

In the following a comparison in terms of displacement and bending moments of the two models is provided for different loading conditions. Firstly, a vertical loading of 200 kN is

considered. In the setup model the vertical loading is applied by 8 loading points while in the slab the load is applied uniformly on the entire surface. In Figure 3.6 the comparison between vertical displacements is provided. To make the comparison easier only N-S strip of the 4x4 m slab, with the same width of the setup, is shown.

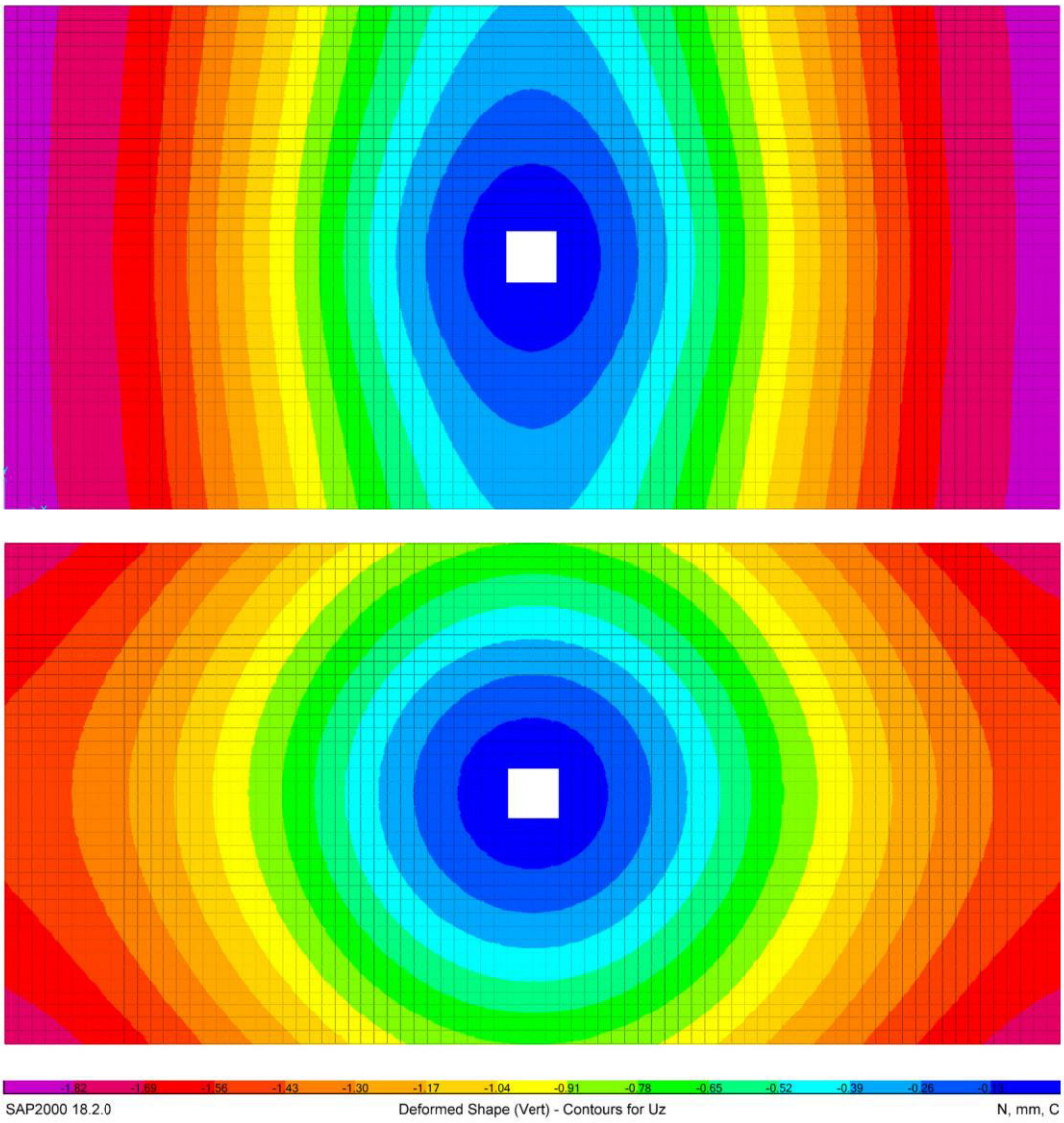

Figure 3.6 – Vertical displacements for the vertical loading: Lisbon setup (up) and flat slab (down).

As shown in the Figure 3.6 the vertical displacements are similar close to the column but tends to diverge in the middle span where the setup appears more flexible. Furthermore, the displacement pattern provided by the setup appear elliptic while that provided by the flat slab is perfectly circular. In Figure 3.7 the comparison of M11 moments, acting in the N-S direction, is shown. In this case the two numerical models provide very similar results.

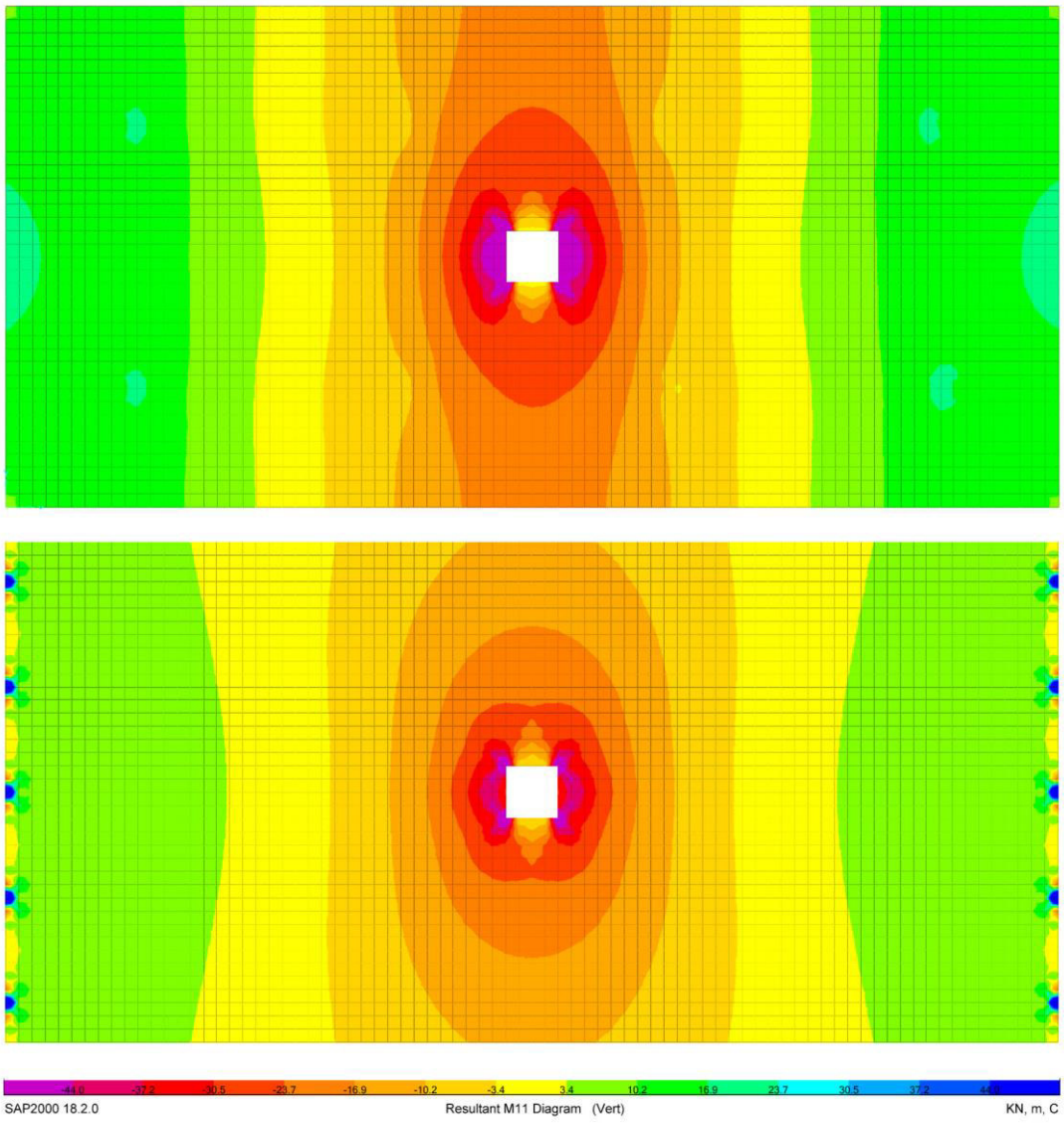

Figure 3.7 – Moments M11 for the vertical loading: Lisbon setup (up) and flat slab (down).

The peaks of stress at the N-S borders provided by the FEM of the flat slab indicate the localised presence of the constraints. As mentioned above ten different constraints are used on borders N-S and E-W respectively, in Figure 3.7 only five constraints are highlighted since the diagram is limited to the N-S middle strip only.

In Figure 3.8 moments M22, acting in the direction E-W, are shown. The difference between the two models is more marked, in particular the moments provided by the Lisbon setup are lower than those provided by the flat slab.

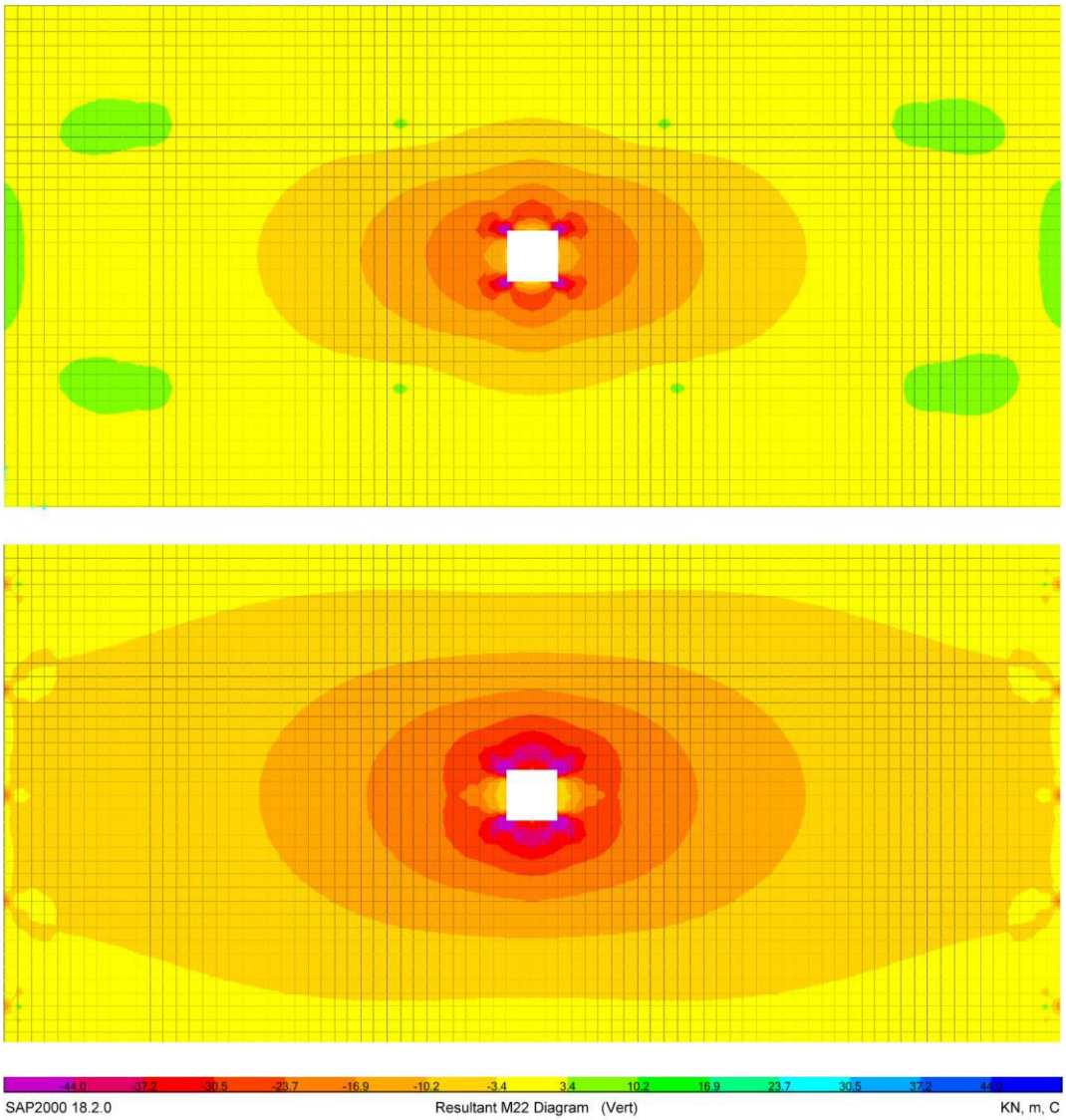

Figure 3.8 – Moments M22 for the vertical loading: Lisbon setup (up) and flat slab (down).

In Figure 3.9 the maximum shear stress (VMAX) between V13 and V23 is shown. In terms of shear stress around the column the two distributions are also quite similar.

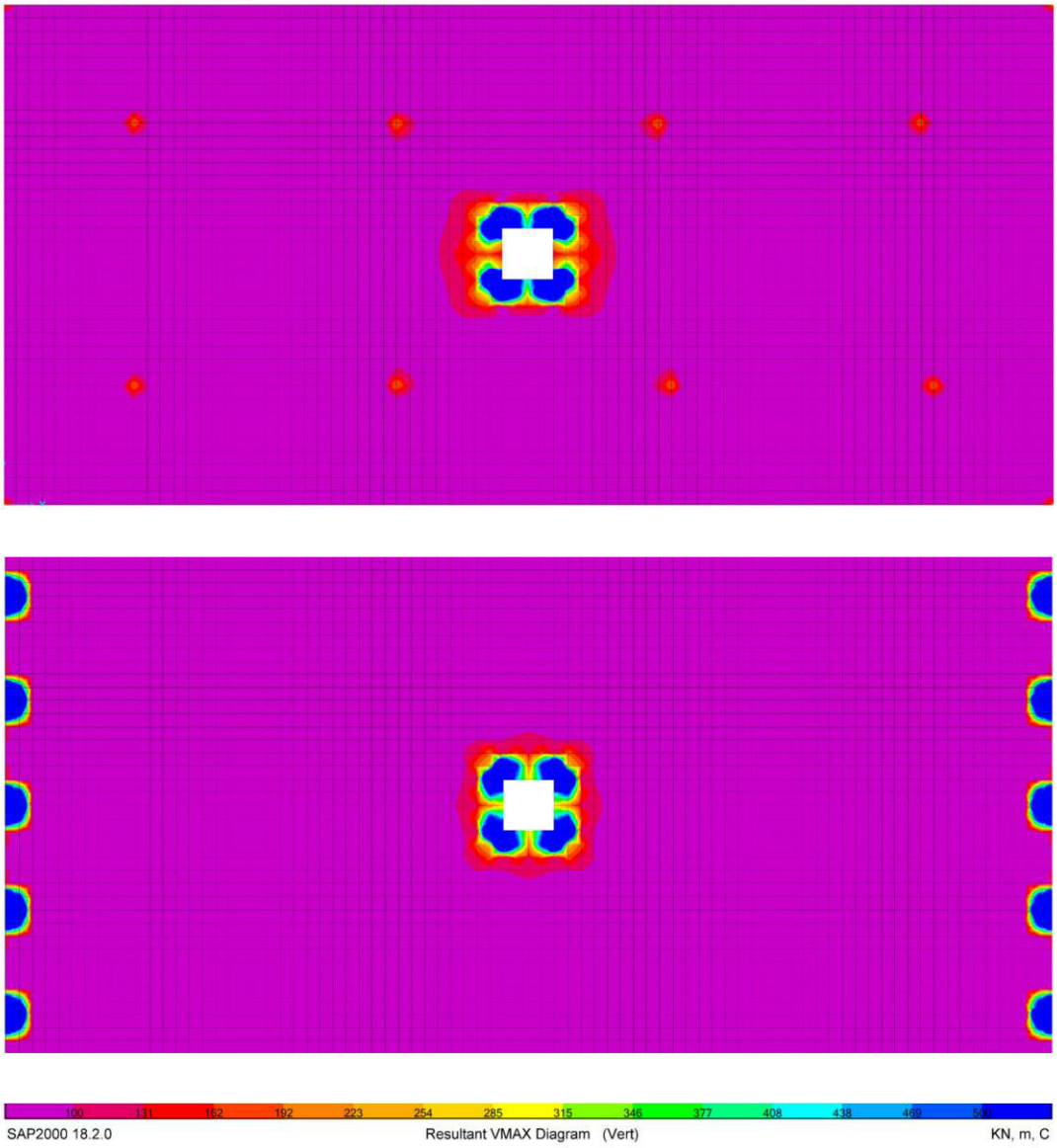

Figure 3.9 – Maximum shear VMAX for the vertical loading: Lisbon setup (up) and flat slab (down).

Therefore, the scenario with horizontal loading is considered. In both model a 60 kN horizontal force is applied in north direction at the top of the column. In Figure 3.10 the vertical displacement provided by both models in this loading configuration are provided. Besides the two patterns of vertical displacement appear different if we consider just the column strip along the direction N-S the two models provide similar results.

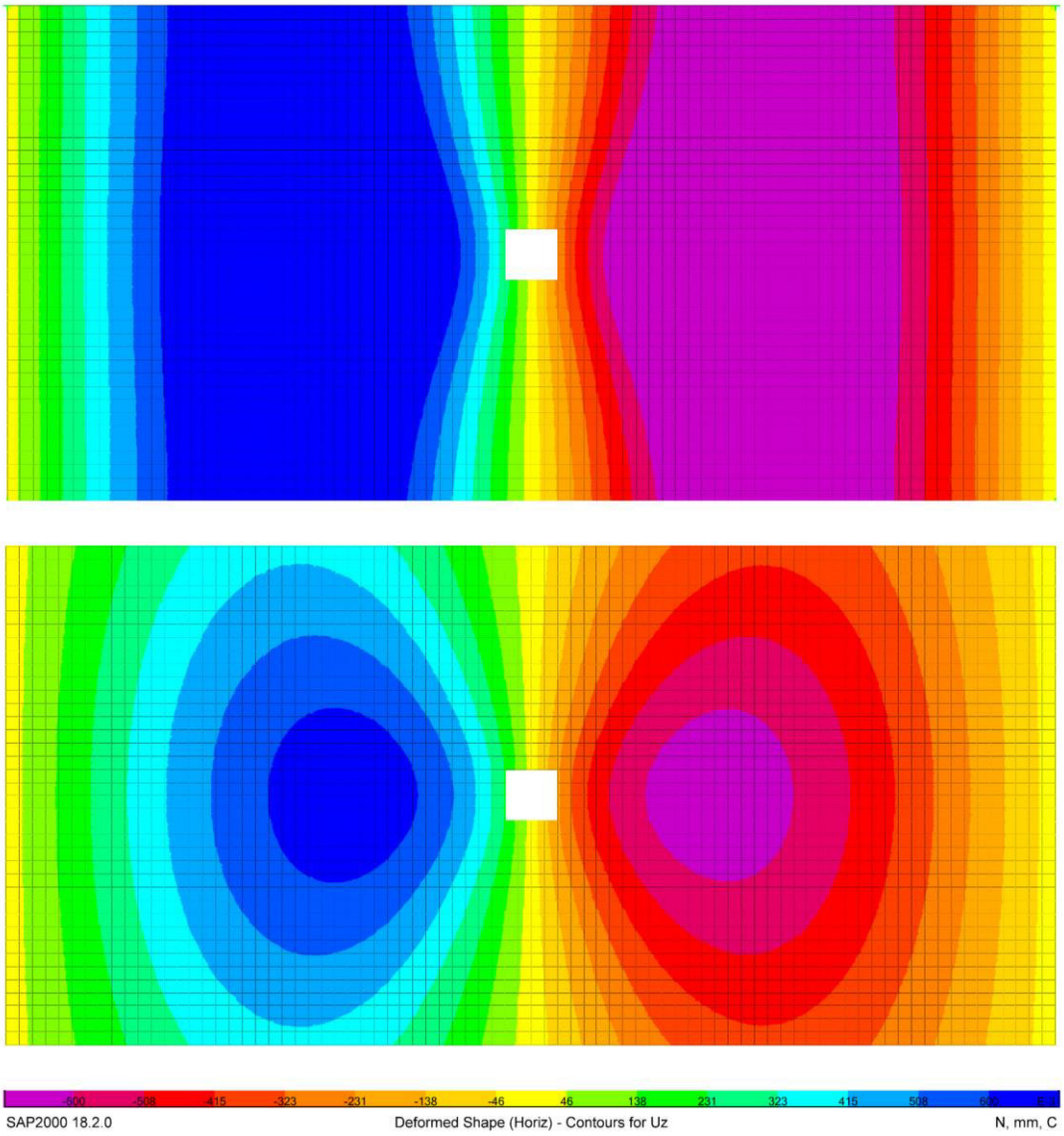

Figure 3.10 – Vertical displacements for horizontal loading: Lisbon (up) and flat slab (down).

In Figure 3.11 the comparison of M11 moments, acting in the N-S direction, is shown. In this case the two models provide very similar results.

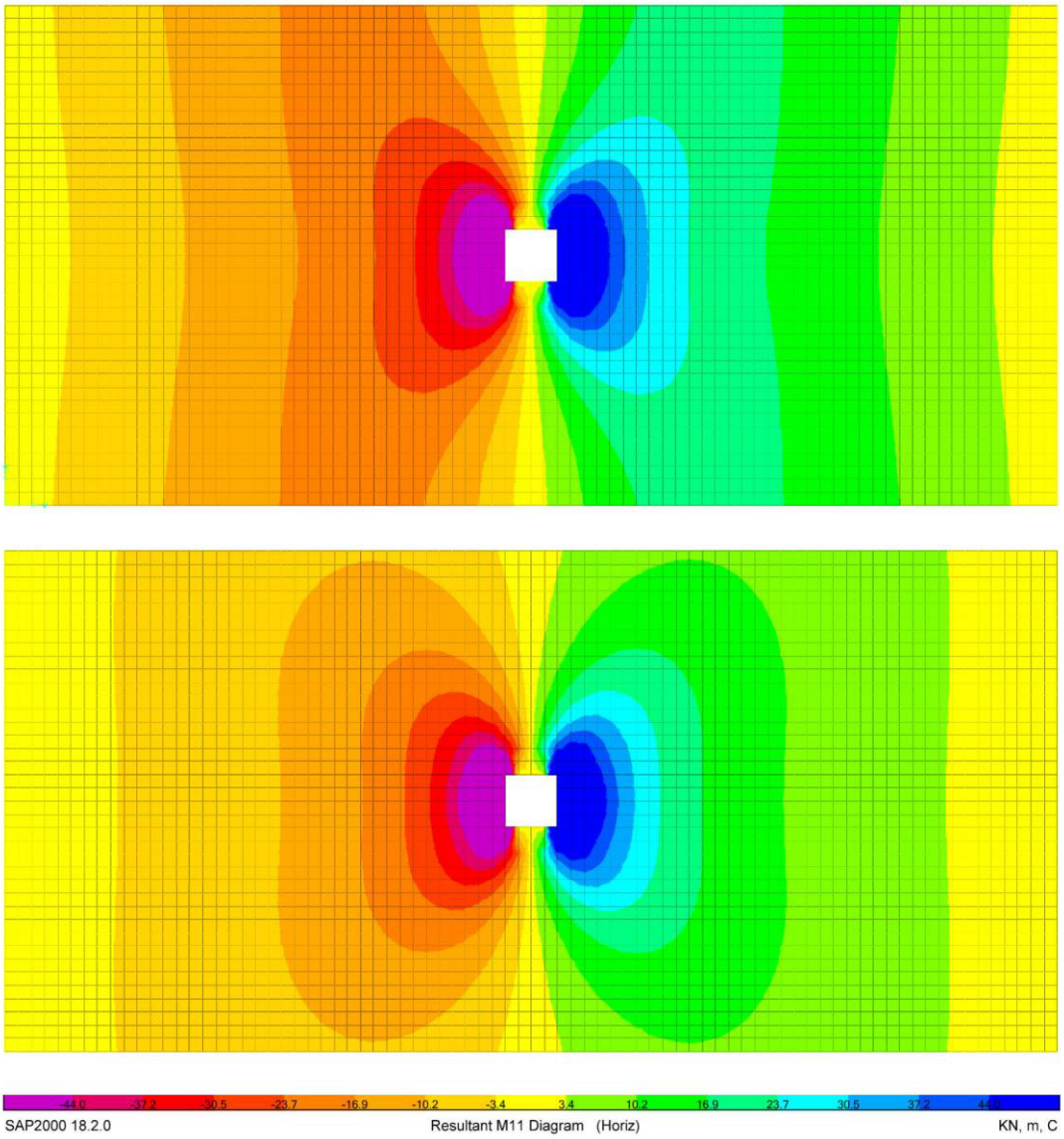

Figure 3.11 – Moments M11 for horizontal loading: Lisbon setup (up) and flat slab (down).

In Figure 3.12 the comparison of M22 moments, acting in the E-W direction, is shown. In this case also the two models provide very similar results.

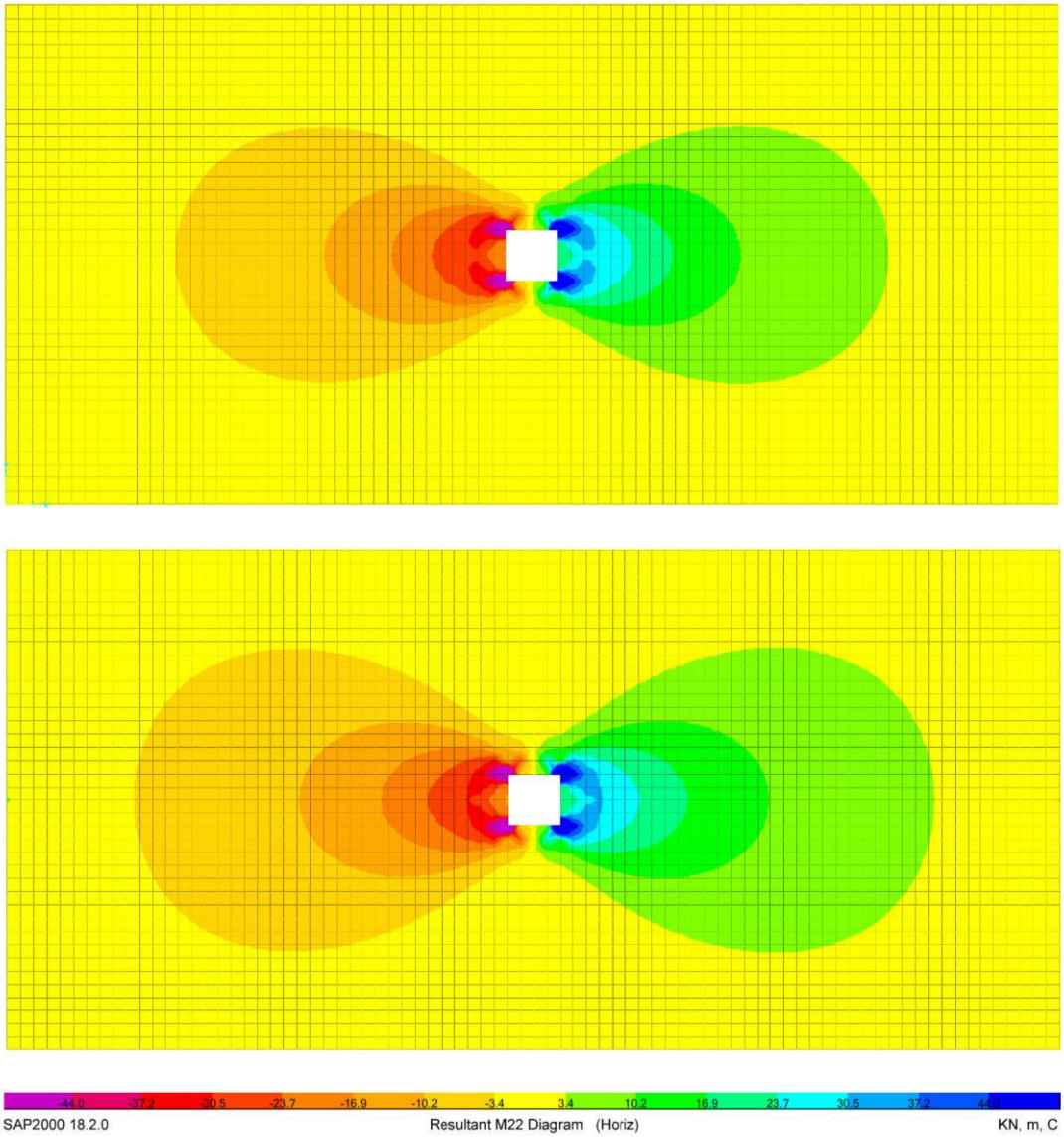

Figure 3.12 – Moments M22 for horizontal loading: Lisbon setup (up) and flat slab (down).

In Figure 3.13 the maximum shear stress (VMAX) between V13 and V23 is shown. In terms of shear stress around the column the two distributions are almost equal.

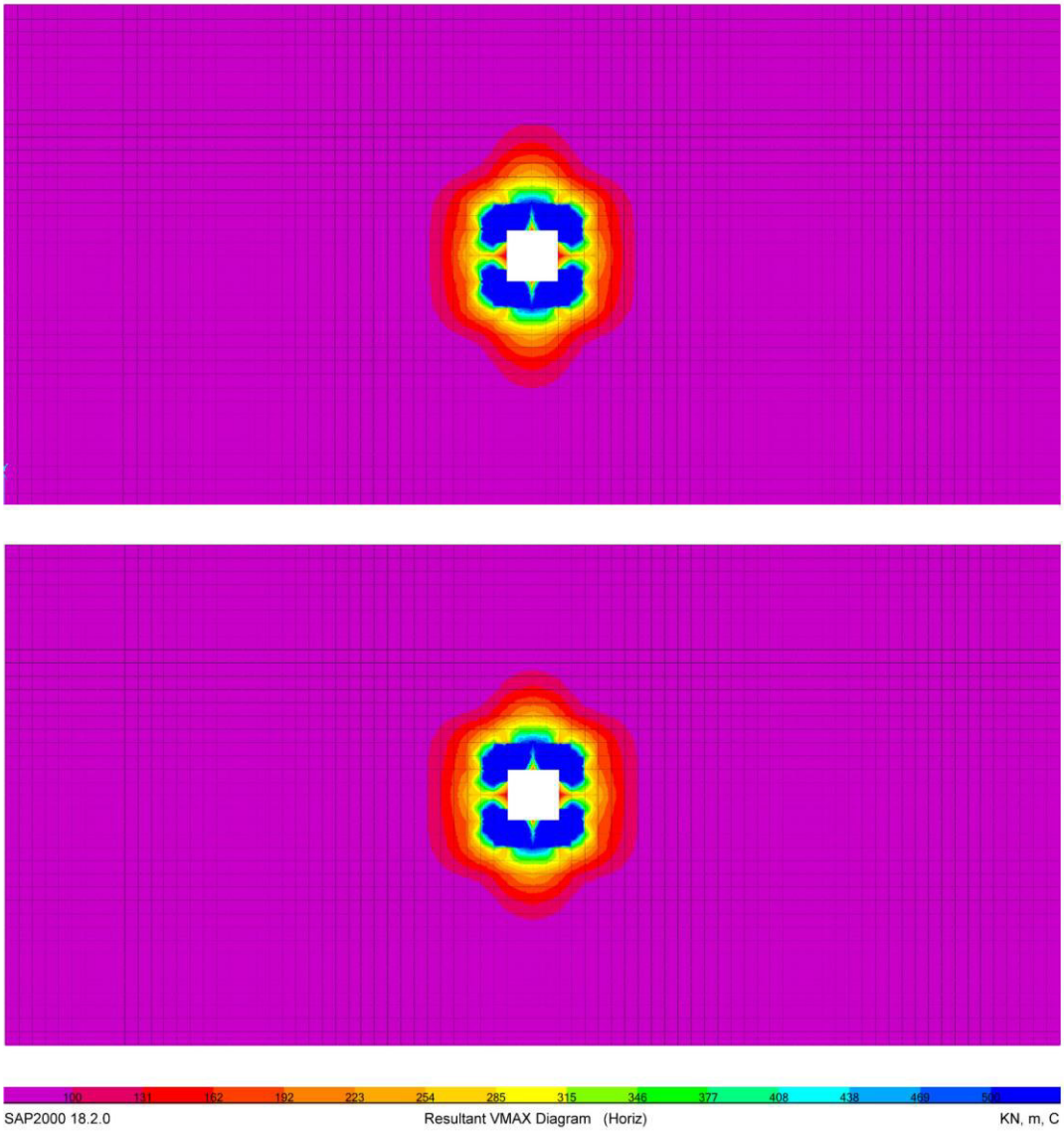

Figure 3.13 – Maximum shear VMAX for horizontal loading: Lisbon setup (up) and flat slab (down).

In conclusion, the linear numerical analysis showed that the Lisbon setup provides a behaviour quite close to that expected by a 4x4 m internal flat slab. The agreement between the Lisbon setup and the flat slab resulted greater for horizontal loading than vertical loading. In general, the matching between the two models resulted higher in terms of maximum shear and bending moments. Conversely the comparison in terms of vertical displacements provides a lower agreement between the two models.

3.4 Description of the specimens

As mentioned above the specimens have overall dimensions 4.15 m × 1.85 m, thickness equal to 0.15 m and a 2.0 m steel column (two halves columns of 1.0 m, one above and one below the slab) with rigid square base plates 0.25 x 0.25 m, connecting the steel column to the concrete slab. The specimens represent in the longitudinal direction the slab between the mid-span lines, while in transverse direction is limited to 22% of the span length. It could be said that the specimens represent a 2/3 scale of a real flat slab 6 x 6 meters span.

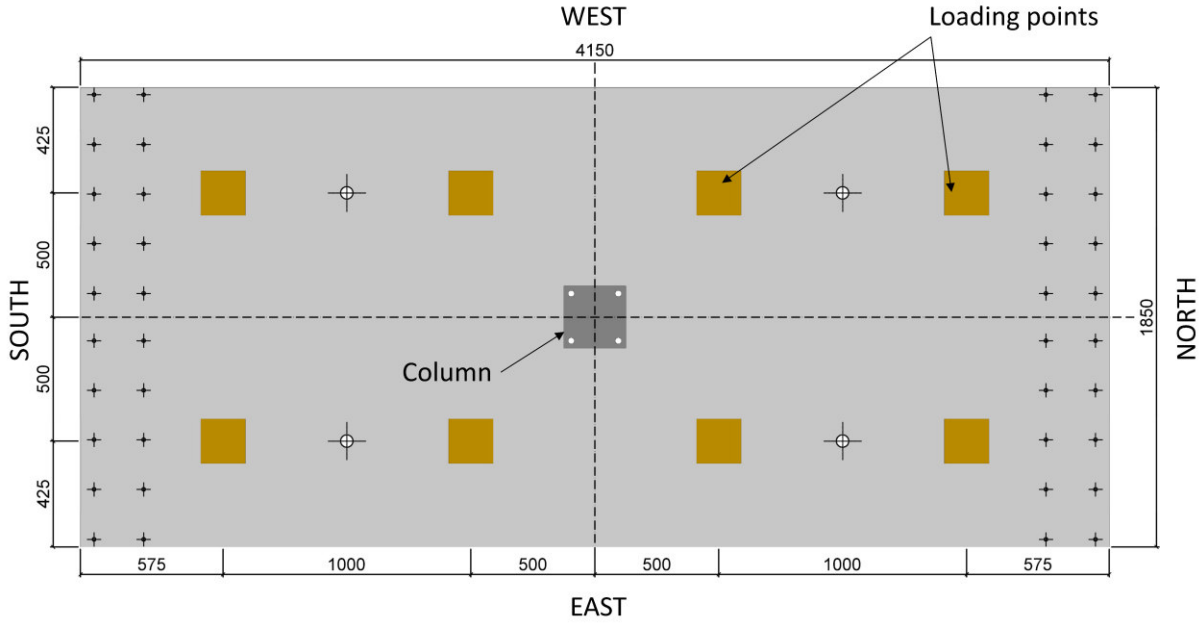

Figure 3.14 – Reference specimen without opening.

The experimental programme consisted of two series, three specimens each, characterized by different positions of the opening with respect to the direction of the seismic loading. In the first series, named SO1, the opening was located in front of the column on the North side (Figure 3.15), in the same direction of the horizontal loading (North-South). In the second series, named SO2, the opening was placed adjacent to the column on the East side (Figure 3.16), along the transverse direction (East-West). Two specimens, one for each series, were only subjected to vertical loading without eccentricity, the others were tested under constant vertical loading and cyclic horizontal loading.

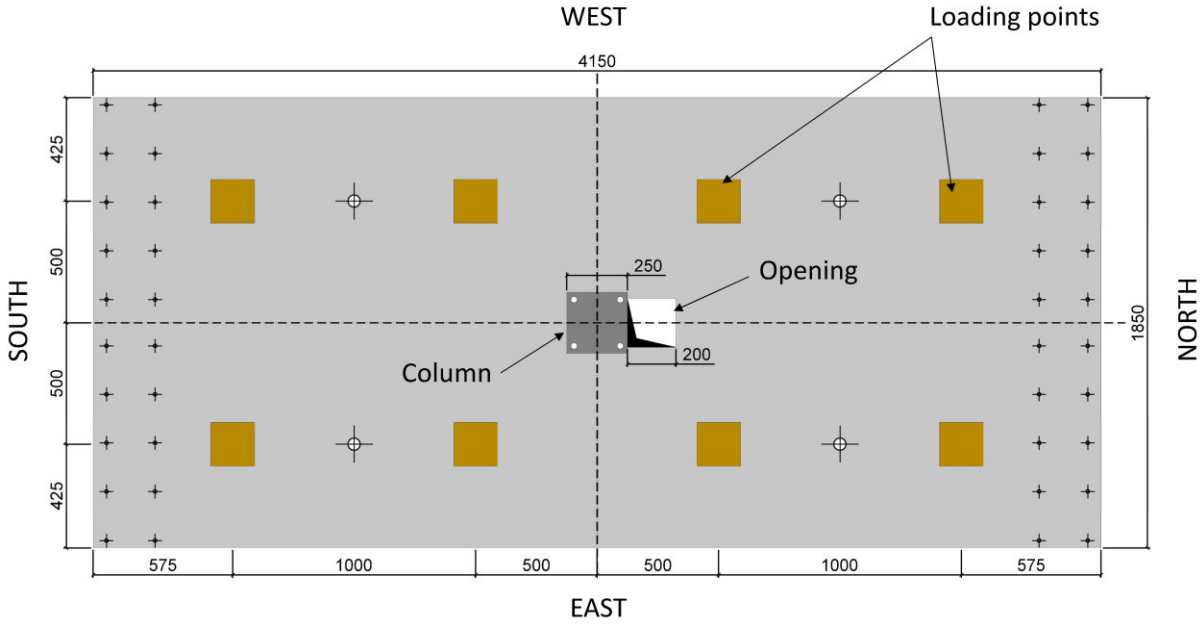

Figure 3.15 – Series SO1: opening placed on the North side of the column.

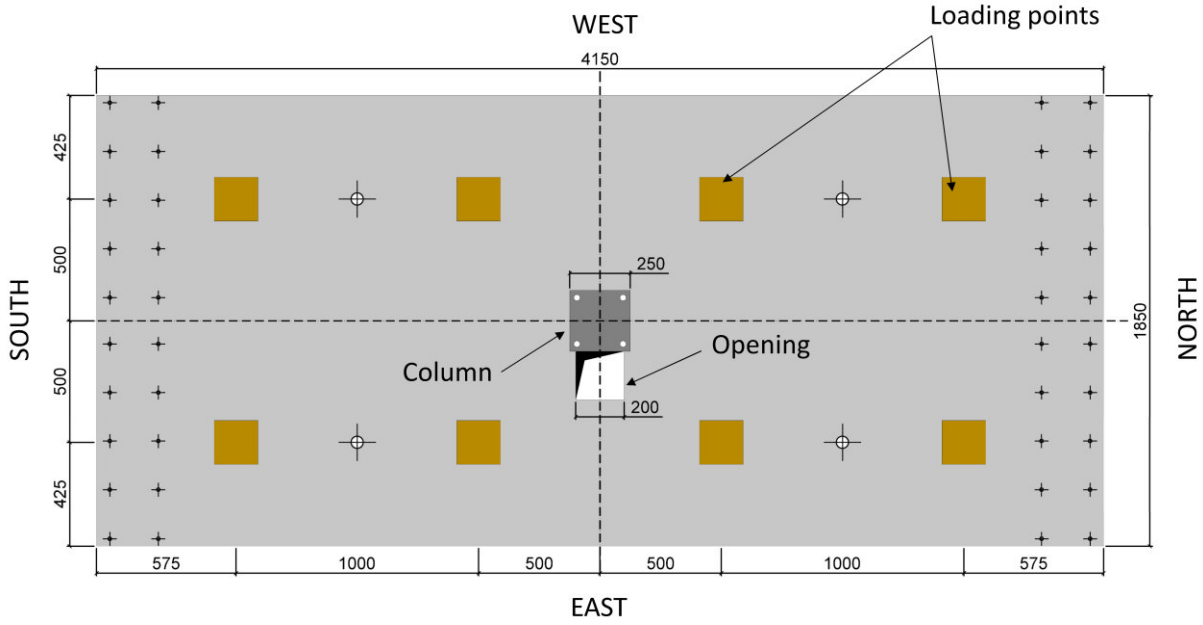

Figure 3.16 – Series SO2: opening placed on the East side of the column.

The nominal clear cover was 20 mm, resulting in average effective depths off 118 mm and 120 mm for top and bottom reinforcement respectively. The top longitudinal reinforcement ratio at the column results about 1%. The higher effective depth was oriented in longitudinal direction.

Detailed information about the longitudinal reinforcement of the first and the second series are provided in Figure 3.17, Figure 3.18, Figure 3.19 and Figure 3.20. The rebars that meet the opening are interrupted and additional rebars are provided on the left and right of the opening to guarantee the continuity of the reinforcement.

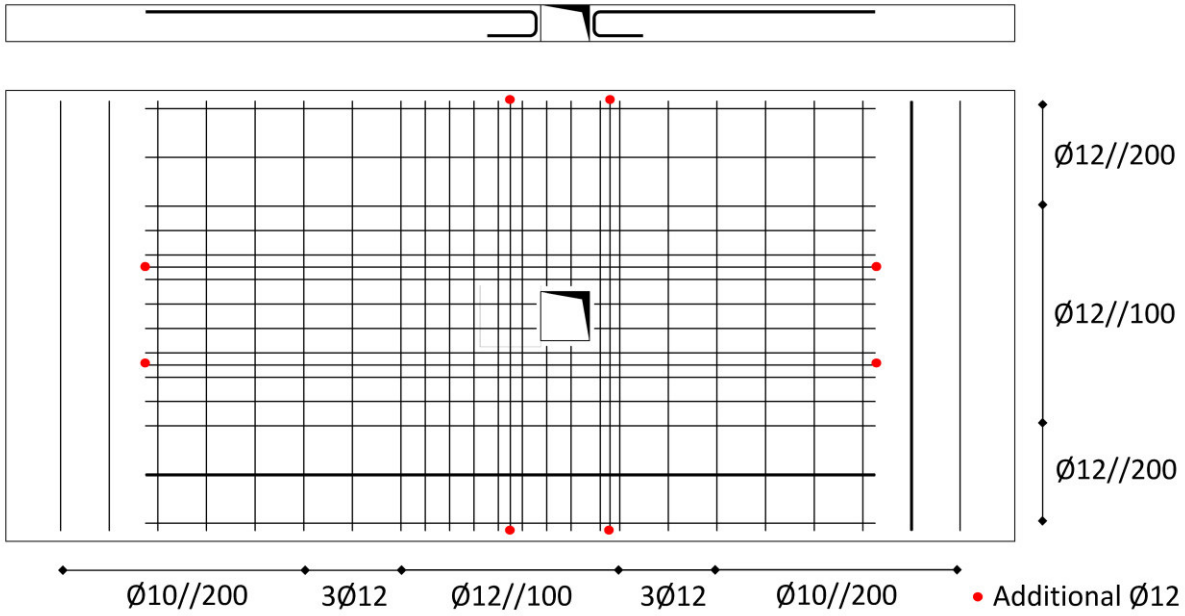

Figure 3.17 – Series SO1: top reinforcement detailing.

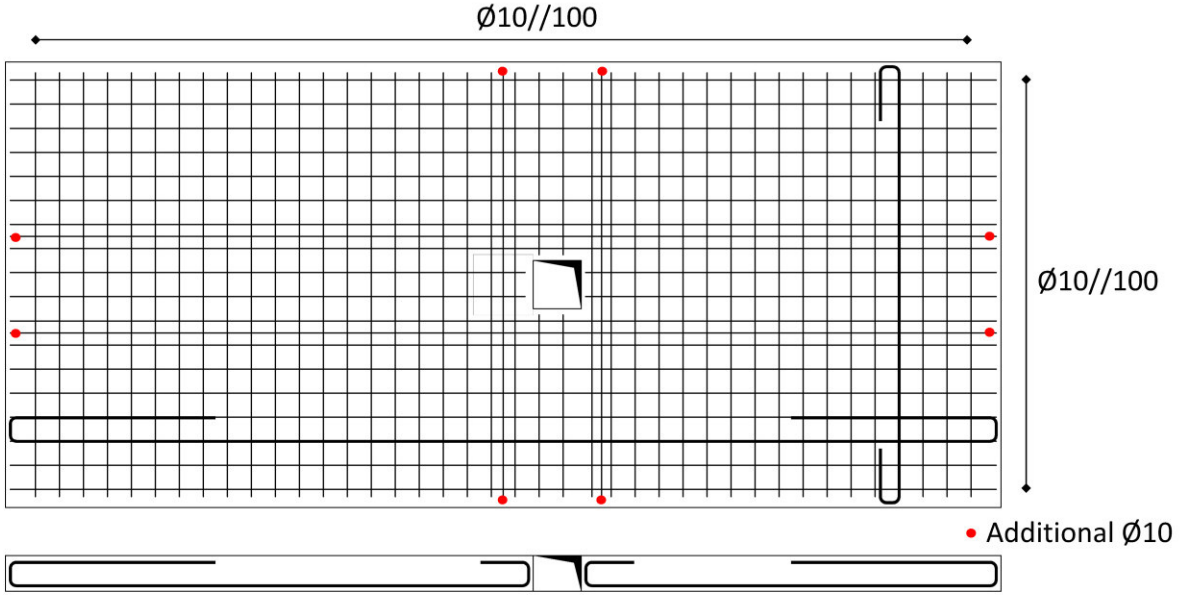

Figure 3.18 – Series SO1: bottom reinforcement detailing.

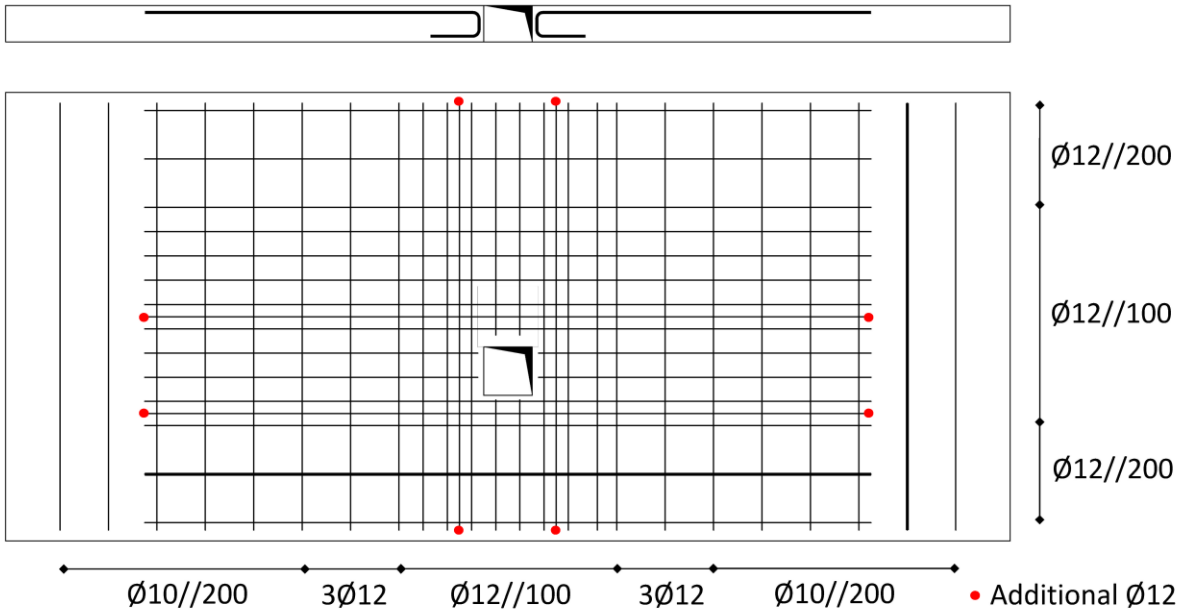

Figure 3.19 – Series SO1: top reinforcement detailing.

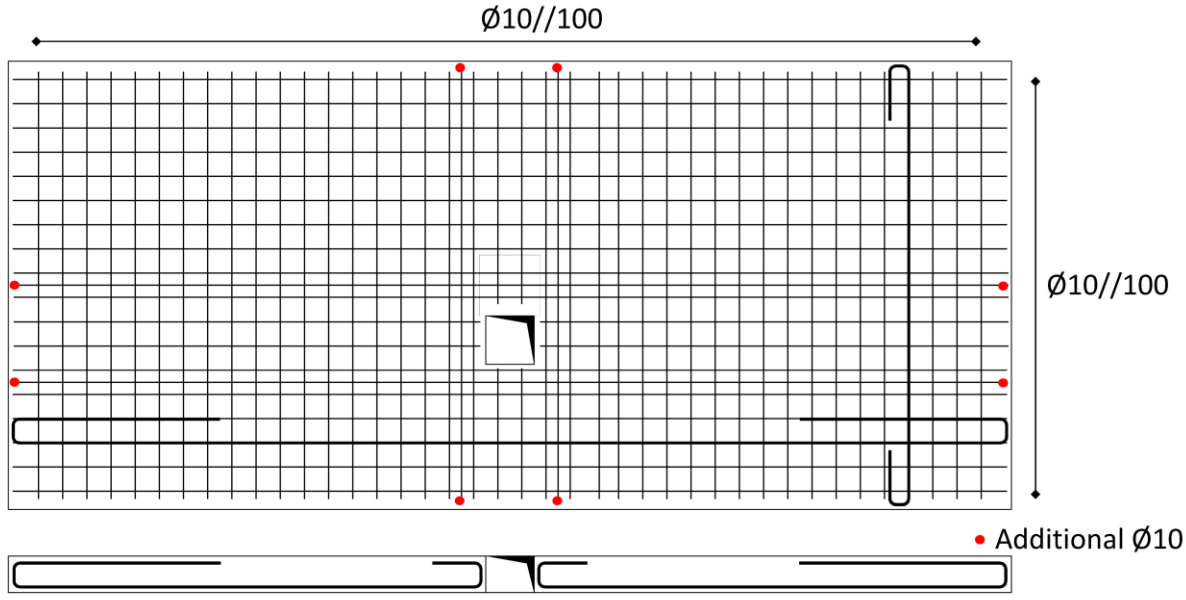

Figure 3.20 – Series SO2: bottom reinforcement detailing.

The third specimen of each series is provided with shear reinforcement. Closed stirrups are placed on three sides of the support column. The arrangement of the shear reinforcement for the specimens SO1-03 and SO2-03 is shown in Figure 3.21 and Figure 3.22 respectively.

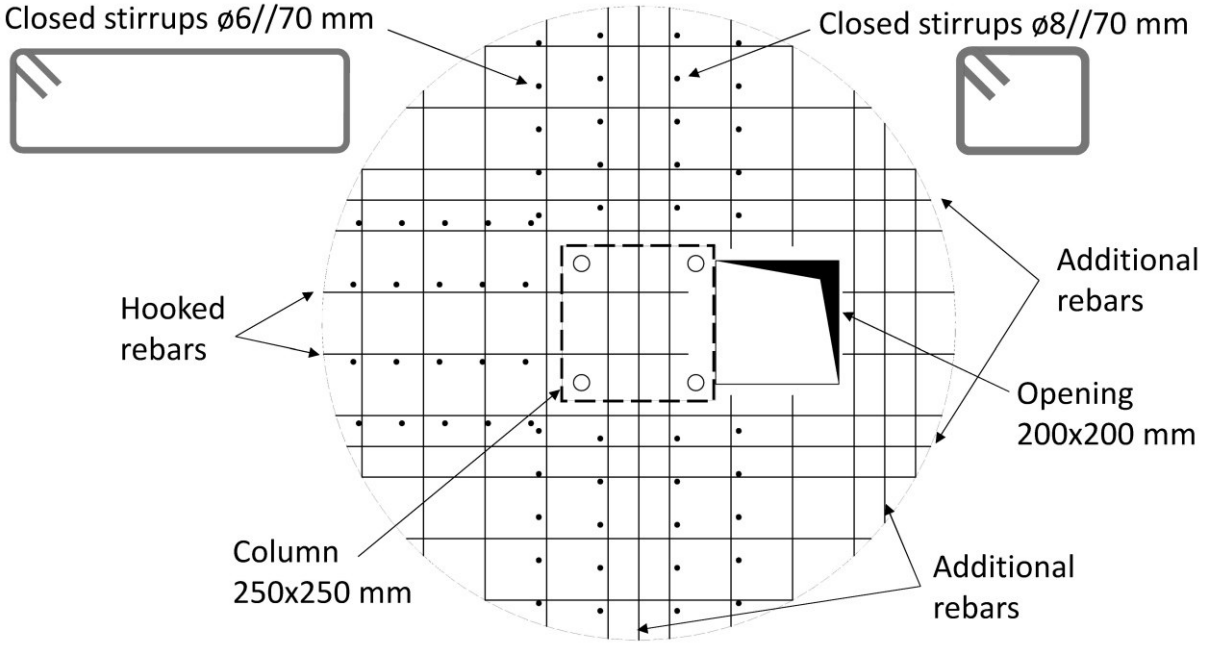

Figure 3.21 - Shear reinforcement arrangement specimen SO1-03.

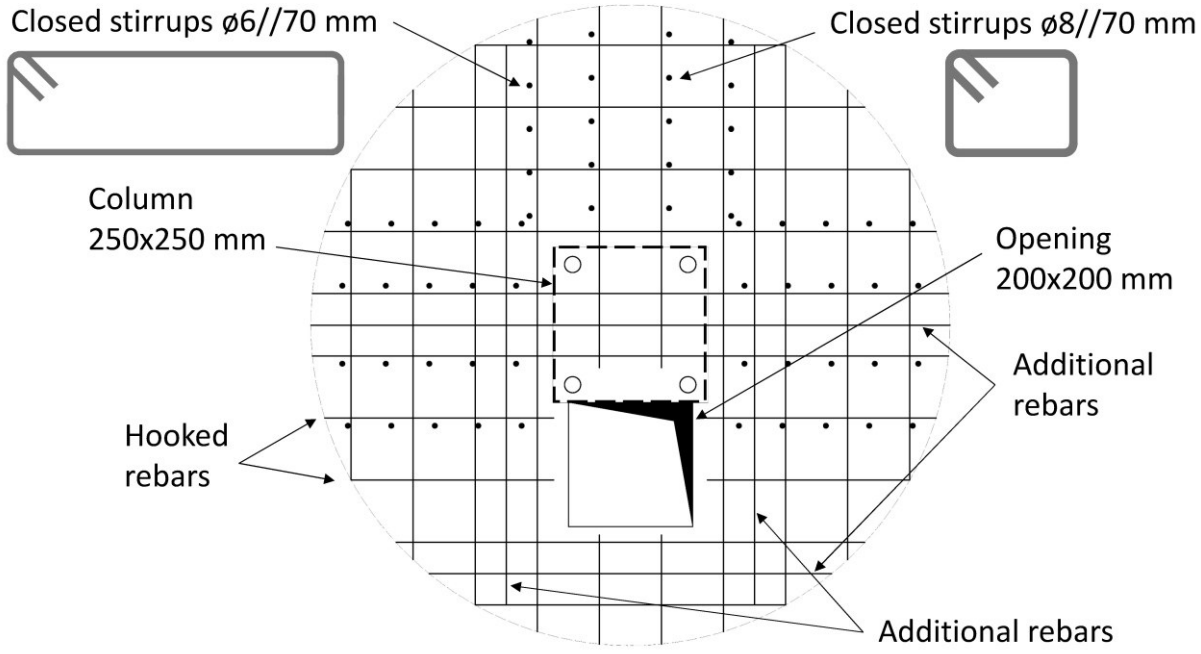

Figure 3.22 - Shear reinforcement arrangement specimen SO2-03.

The main characteristics of the specimens are listed in Table 3.1.

Table 3.1 – Main characteristics of the specimens.

Specimen	Opening position	Shear reinforcement	Loading condition
SO1-01	North	No	Gravity
SO1-02	North	No	Gravity & Horizontal
SO1-03	North	Stirrups	Gravity & Horizontal
SO2-01	East	No	Gravity
SO2-02	East	No	Gravity & Horizontal
SO2-03	East	Stirrups	Gravity & Horizontal

3.5 Preparation of the specimens

All the specimens were prepared in the CONCREMAT precast concrete plant excepted for the shear reinforcement that was prepared at the Structural Laboratory of the Department of Civil Engineering, NOVA School of Science and Technology (Figure 3.23) and then positioned in place before casting.

Figure 3.23 – Stirrups bending.

Before casting, the effective depth of the top reinforcing bars was measured in both directions. The average values for each specimen are summarized in Table 3.2.

Table 3.2 – Effective depth of the specimens.

Specimen	d (mm)
SO1-01	118.4
SO1-02	118.2
SO1-03	119.0
SO2-01	116.4
SO2-02	118.6
SO1-03	118.3

In Figure 3.24 the mould used for casting is shown, the voids are created with plastic tubes while the 200x200 mm opening is created by using a wood mould (Figure 3.25).

Figure 3.24 – Moulds used for the casting.

Specimens were casted on a vibrating platform (Figure 3.26) after the application of a mould-release oil. In Figure 3.27 the detail of the opening after casting is shown.

Figure 3.25 – Detail of the opening mould.

Figure 3.26 – Casting phase.

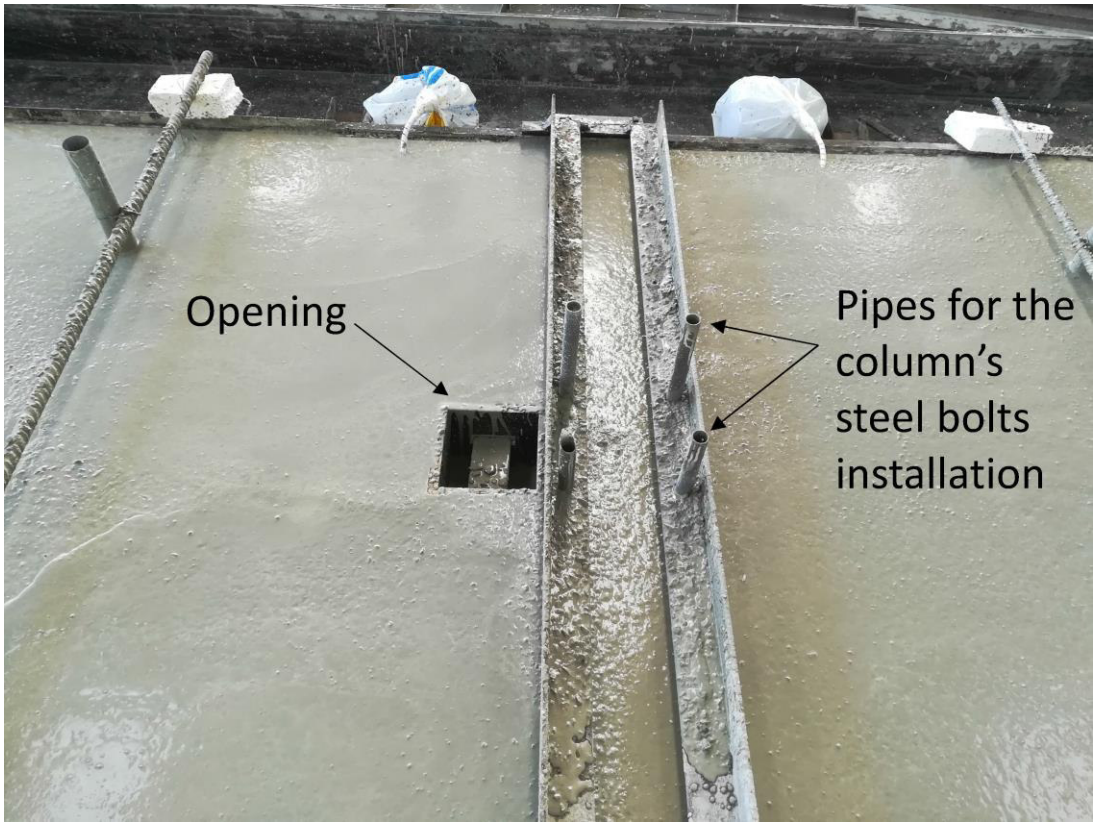

Figure 3.27 – Opening detail after casting.

For each specimen 12 cylinders and 6 cubes were casted (Figure 3.28), the single batch was enough to cast both the specimen and the samples. In Figure 3.29 the cured samples are shown.

Figure 3.28 – Cubes and cylinders casted for each specimen.

Figure 3.29 – Cubes and cylinders after curing.

3.6 Material characterization

3.6.1 Aggregates

According to the CSCT [2] the maximum aggregate size plays a fundamental role in the punching phenomenon. This parameter is included in the failure criterion accounting for the shear that can be transferred across the critical shear crack. The latter is inspired by previous researches provided by Walraven [3] and Vecchio and Collins [4]. They highlighted that a rough crack can transfer shear by aggregate interlock, which is a function of crack width, compressive strength and aggregate size. The maximum aggregate size plays also an important role in the mix design. Usually the maximum aggregate size should be lower than 1/4 of the minimum thickness of the pouring. However, concrete cover and minimum rebar spacing are also affected by this important parameter.

In the following the determination of the maximum aggregate size is shown. The maximum aggregate size is determined by means of a sieve analysis and it usually corresponds with the smallest sieve opening for which less than 10% of the mass is retained. The sieve analysis is provided in Table 3.3.

Table 3.3 – Sieve analysis.

Sieve opening (mm)	Lower bound (%)	Upper bound (%)	Typical value (%)
63			100
40			100
31.5			100
20	100	100	100
16	98	100	100
14			100
12.5	90	99	97
10			74
8	35	65	50
6.3			12
4	0	15	3
2	0	5	1
1			1
0.5			1
0.25			1
0.125			1
0.063	0	1.5	1.1

Therefore, the maximum aggregate size is equal to 12.5 mm.

3.6.2 Cement

The cement used in the concrete mix is a Portland Cement CEM I 42,5 R. The mechanical characteristics of the cement are provided in Table 3.4. The data are determined by the laboratory of the SECIL factory and should be intended as the average strengths determined in the last month and last year of production.

Table 3.4 – Mechanical characteristics of the cement.

Age	Flexural strength (MPa)		Compression strength (MPa)	
(days)	Last month	Last year	Last month	Last year
2	6.3	5.9	31.7	29.8
7	8.8	8.3	49.5	46.2
28	9.3	9.7	60.0	59.0

3.6.3 Concrete

The concrete was characterized by means of four tests: compressive tests on cylinders and cubes, carried out according to EN 12390-3 [5], the test for the determination of the elasticity modulus on cylinders, carried out according to EN 12390-13 [6], and the splitting test performed on cylinders according to EN 12390-6 [7].

The cubic compressive strength ($f_{c,cube}$) was determined as the average compressive strength of six 150 mm cubes (Figure 3.30). The cylinder compressive strength (f_c) was determined as the average compressive strength of six cylinders with diameter of 150mm and height of 300mm (Figure 3.31).

Prior to crushing, three of these cylinders were used to determine the modulus of elasticity of concrete (Figure 3.32). Six other cylinders were used to determine the tensile splitting strength of concrete ($f_{ct,sp}$) (Figure 3.33).

Figure 3.30 – Compressive strength test on cubes.

Figure 3.31 – Compressive strength test on cylinders.

Figure 3.32 – Modulus of Elasticity test.

Figure 3.33 – Splitting test.

The average characteristics of concrete, determined from tests, are summarized in Table 3.5 for each specimen. The tests on cubes and cylinders were always performed in the same day of the slab test, thus the age shown in the table corresponds with the age of the concrete at the time of the slab test.

Table 3.5 – Average concrete properties determined from tests.

Specimen	age (days)	$f_{c,cube}$ (MPa)	f_c (MPa)	$f_{ct,sp}$ (MPa)	E_{cm} (MPa)
SO1-01	54	48.8	46.8	3.4	37.9
SO1-02	51	42.9	40.5	3.3	35.2
SO1-03	54	48.2	44.2	3.3	38.3
SO2-01	42	46.9	38.0	3.2	36.1
SO2-02	41	53.0	49.5	3.3	38.6
SO1-03	37	42.5	35.6	3.2	33.4

3.6.4 Reinforcing steel

Three reinforcing bars were tested in tension in accordance with EN 10080 [8]. Table 3.4 summarizes the yield stress (f_y) as well as the steel strain (ε_y).

Table 3.6 – Average steel properties determined from tests.

Designation	Diameter (mm)	f_y (MPa)	ε_y (%)
Flexural	10	532	0.26
Flexural	12	530	0.27
Stirrups	6	538	0.27
Stirrups	8	534	0.27

The properties are the same for all specimens, since these were made of steel from the same batch.

3.7 Instrumentation

Vertical displacements of the slab were monitored by means of 18 LVDTs placed on the top of the slab. The arrangement of the LVDTs was the same used by Almeida et al. [1] (Figure 3.34) however, due to the presence of the opening, the transducer D8 was not available for series SO1 (Figure 3.35), while for the series SO2 the transducer D17 was placed at 365 mm from the centre instead of 275 mm (Figure 3.36).

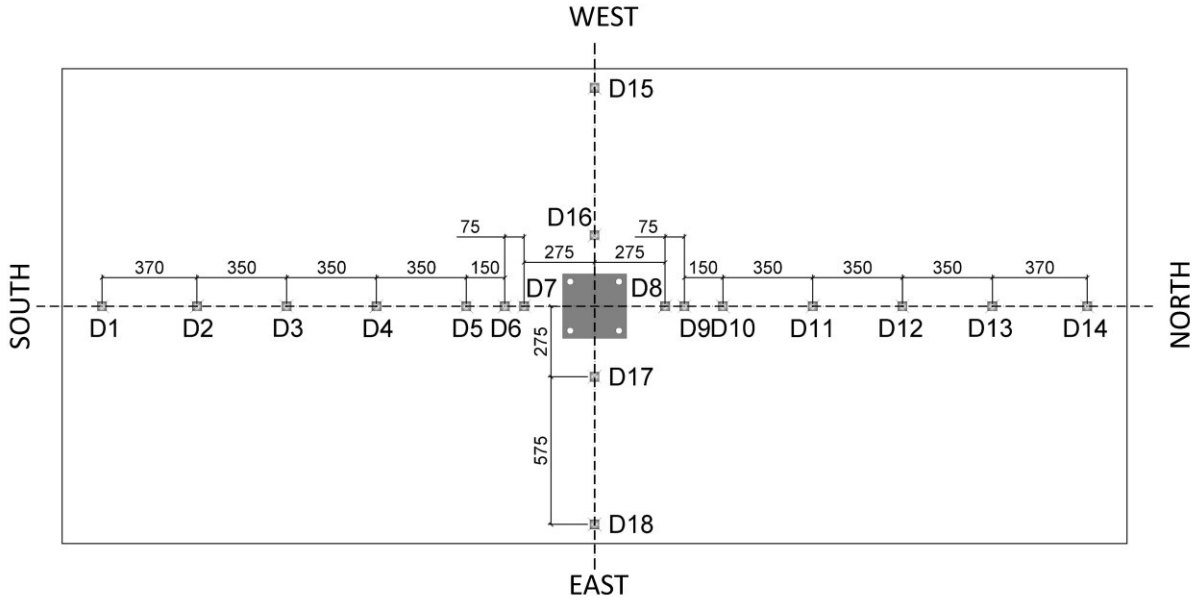

Figure 3.34 – LVDT positions Series without opening.

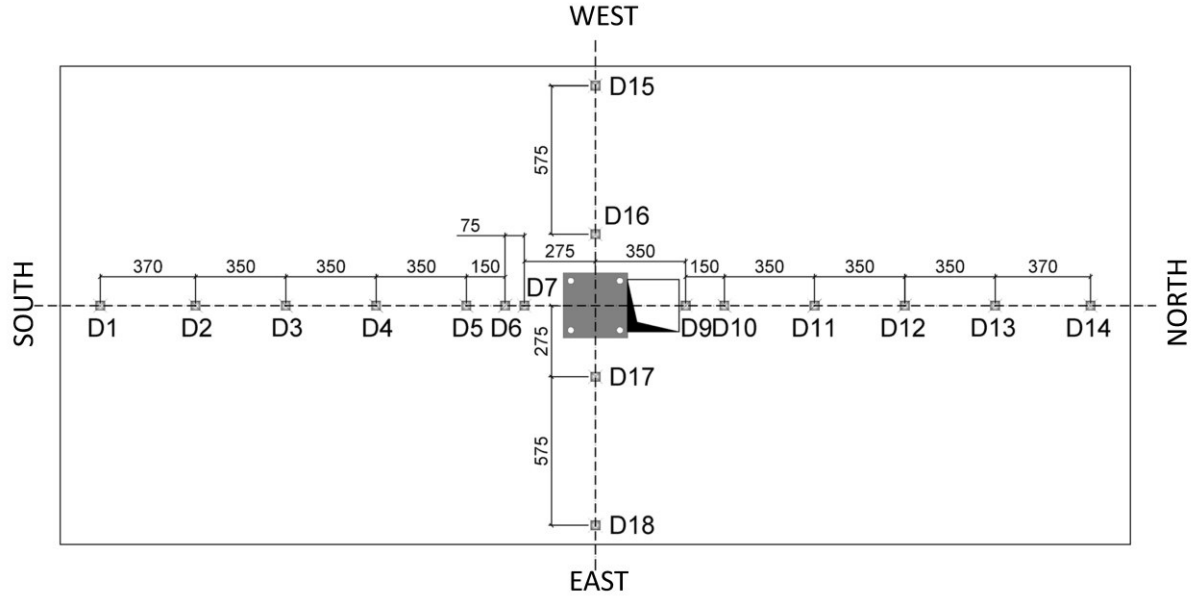

Figure 3.35 – LVDT positions Series SO1.

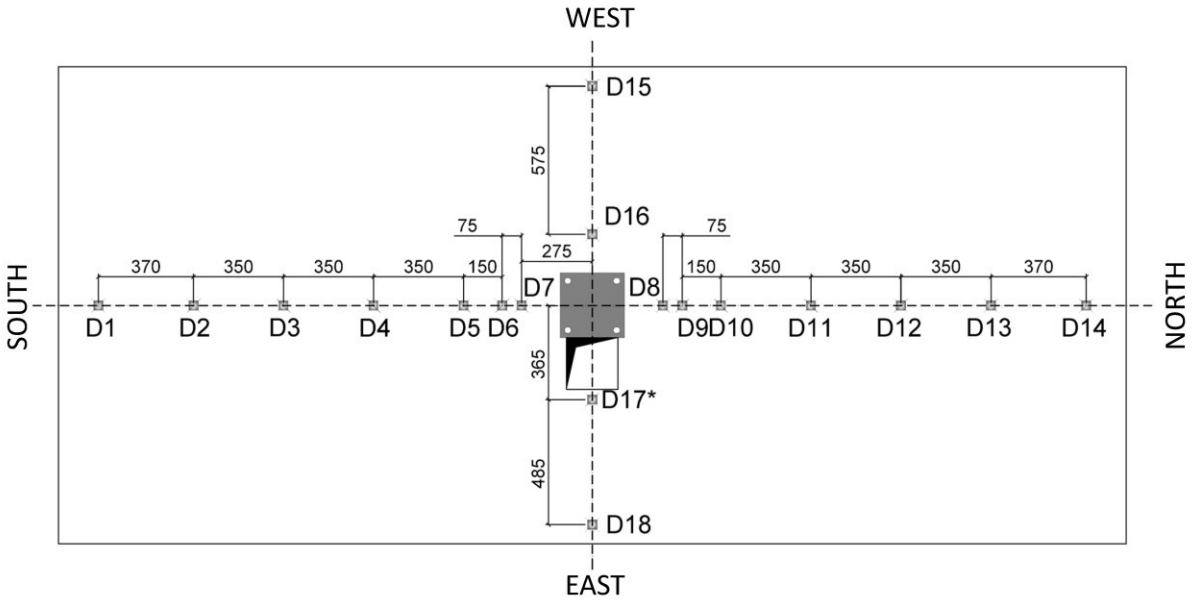

Figure 3.36 – LVDT positions Series SO2.

The actuator was equipped with a tension/compression load cell with a capacity range of 500 kN and a displacement transducer with a measuring range of 500 mm to monitor the horizontal force and displacements during the application of horizontal drifts (Figure 3.37 a).

The vertical load was controlled by eight load cells (Figure 3.37 b), other two load cells were used for assessing the positive moment at the borders through measuring the force in the horizontal struts (Figure 3.37 c). Finally, two inclinometers are placed on the borders to verify the proper working of the system that provides equal rotation at the slab borders (Figure 3.37 d).

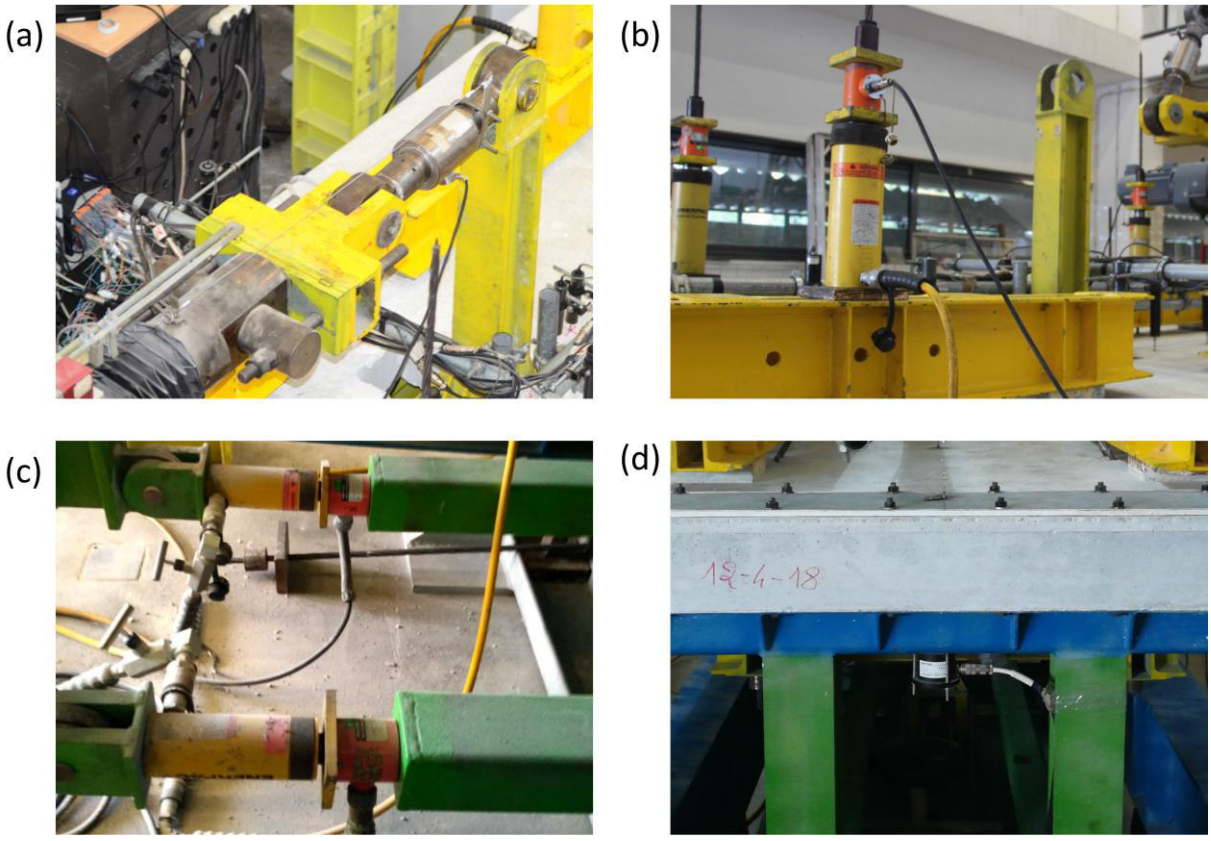

Figure 3.37 – Instrumentation: (a) Actuator LVDT and load cell (b) load cell for gravity loading (c) load cells for controlling bending moments at N-S borders (d) inclinometer.

Strain gauges were installed on both longitudinal reinforcement and shear reinforcement. For the series SO1 the strain gauges placed on top and bottom longitudinal reinforcement are shown in Figure 3.38 and Figure 3.39 respectively, while strain gauges placed in the shear reinforcement for the specimen SO1-03 are shown in Figure 3.40 . For the series SO2 the strain gauges placed on top and bottom longitudinal reinforcement are shown in Figure 3.41 and Figure 3.42 respectively, while strain gauges placed in the shear reinforcement for the specimen SO1-03 are shown in Figure 3.43.

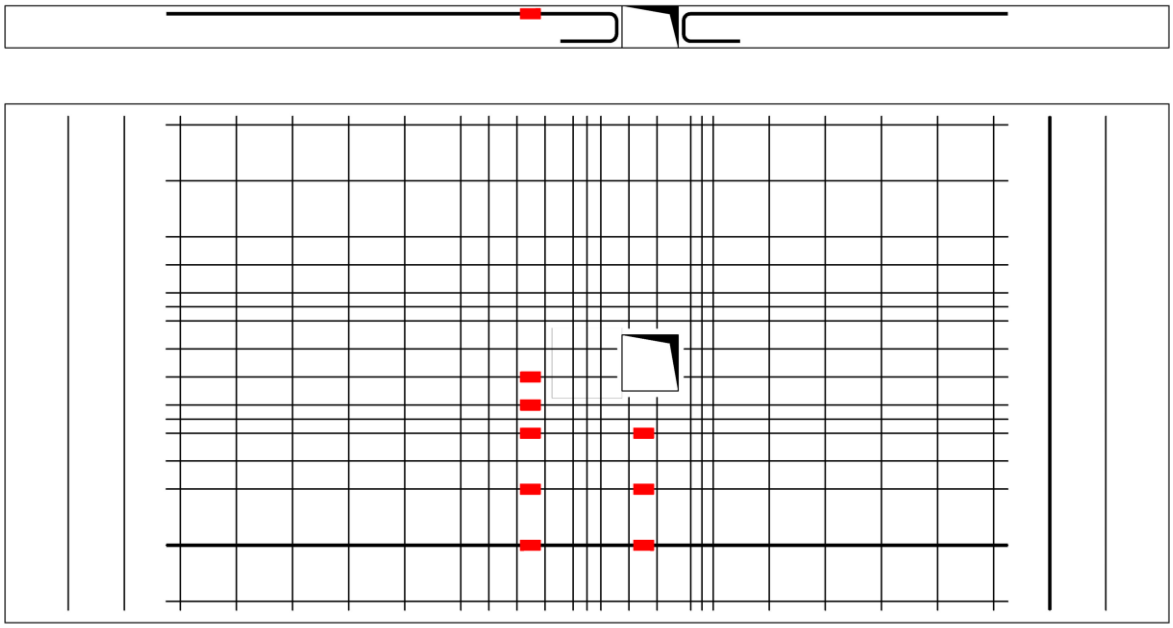

Figure 3.38 – Strain gauge positions Series SO1: top reinforcement.

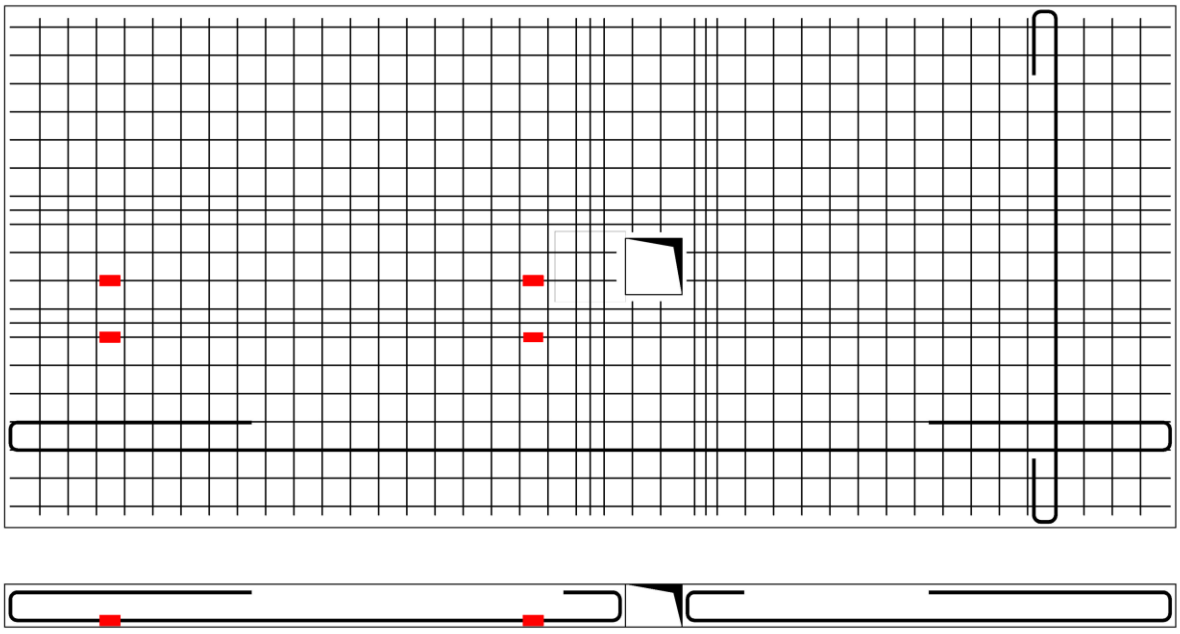

Figure 3.39 – Strain gauge positions Series SO1: bottom reinforcement.

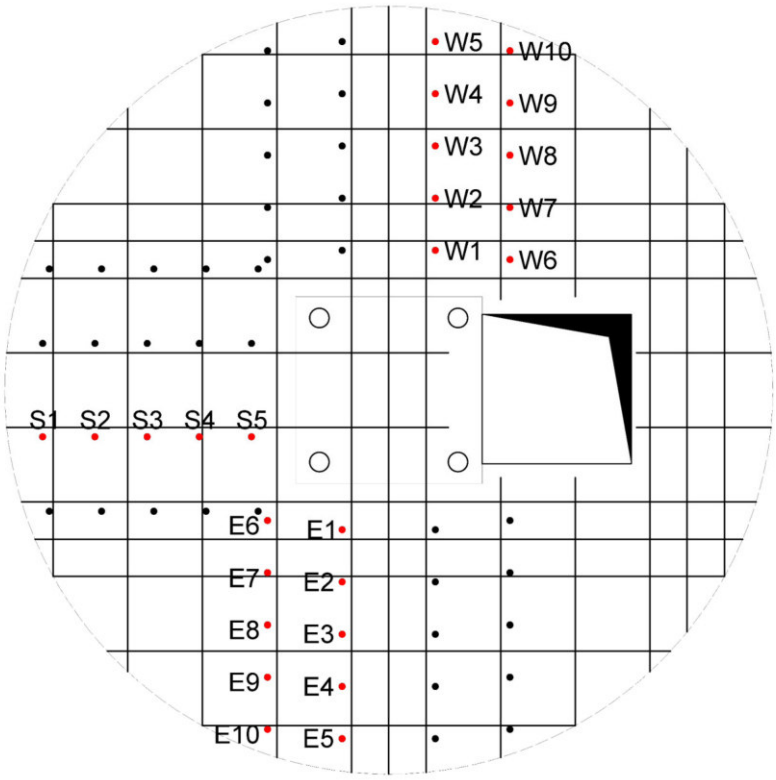

Figure 3.40 – Strain gauge positions Series SO1: shear reinforcement.

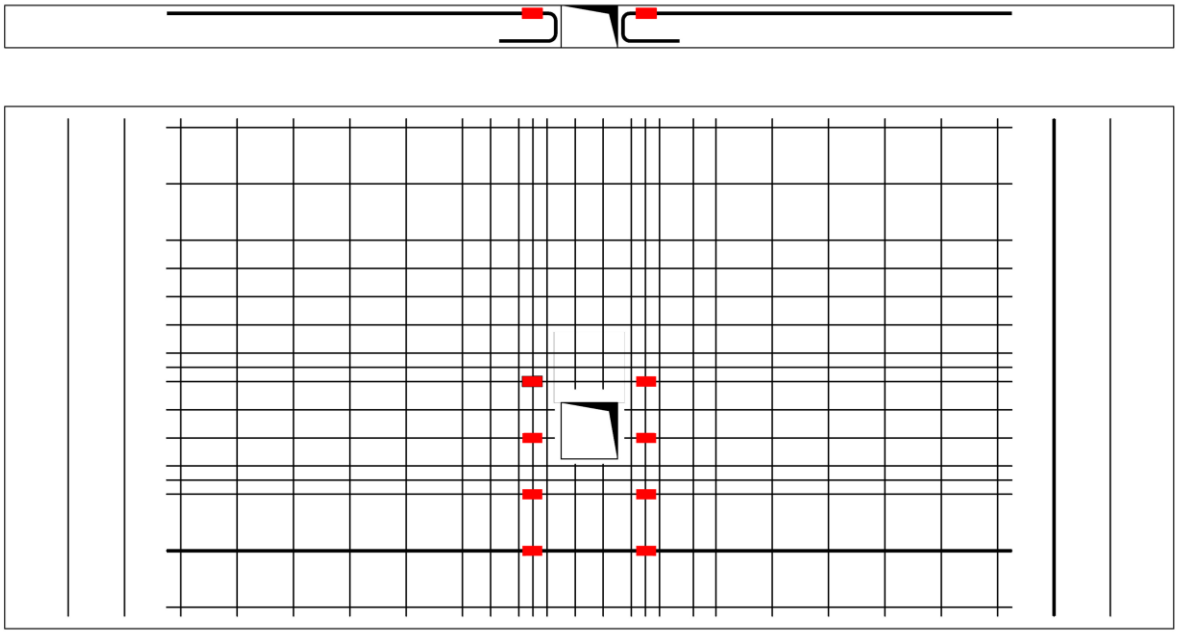

Figure 3.41 – Strain gauge positions Series SO2: top reinforcement.

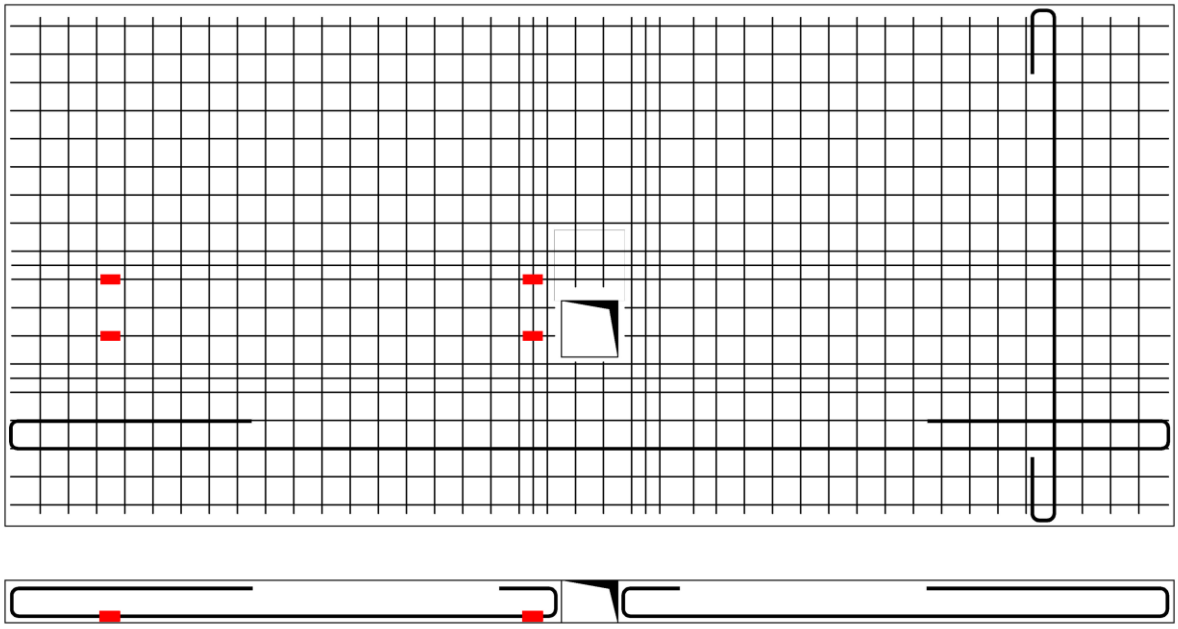

Figure 3.42 – Strain gauge positions Series SO2: bottom reinforcement.

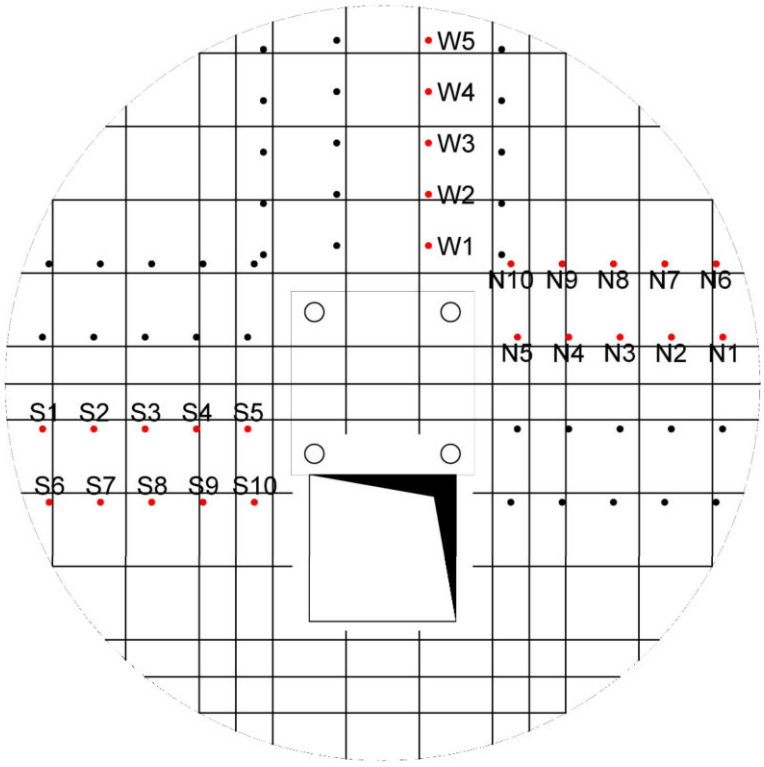

Figure 3.43 – Strain gauge positions Series SO2: shear reinforcement.

3.8 Loading protocol

Specimens SO1-01 and SO2-01 were tested under gravity loading until punching failure, while the others were subjected to both vertical and horizontal loading.

For the specimens tested under vertical and horizontal cyclic loading, and after the application of the target vertical loading, horizontal displacements were applied at the upper end of the steel column. The horizontal drifts protocol is shown in Figure 3.44, for drifts not higher than 3% each cycle is repeated three times, for 4% drift two repetitions are performed, finally for higher drifts only one cycle per drift is provided.

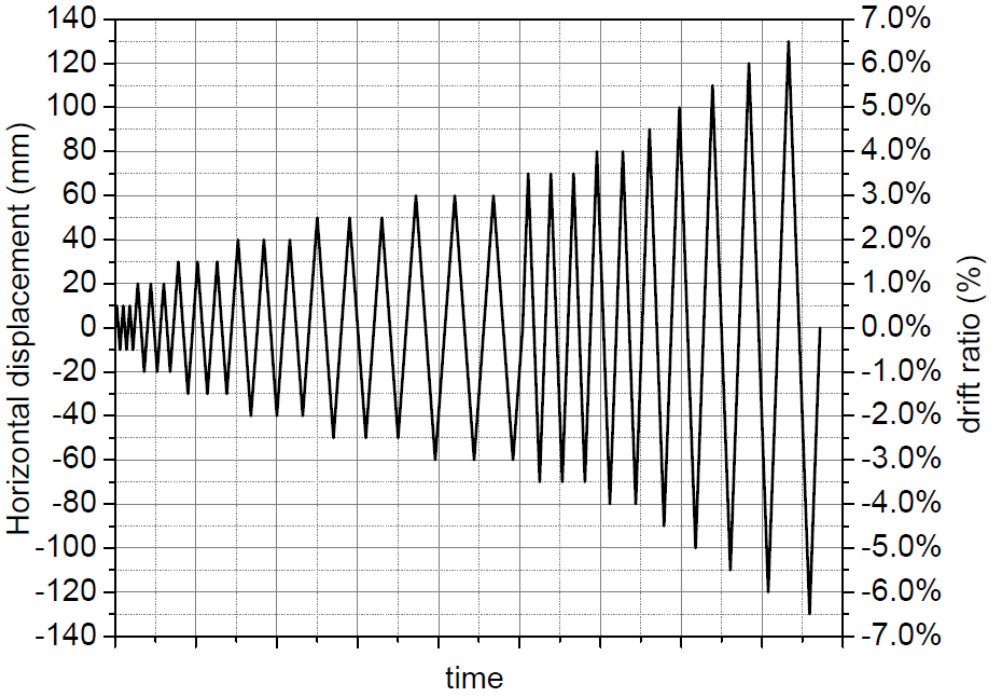

Figure 3.44 – Horizontal drifts protocol.

3.9 Reference

[1] Almeida, AFO.; Inacio, MMG.; Lucio, VJG.; Ramos, AP.; Punching behaviour of RC flat slabs under reversed horizontal cyclic loading, Engineering Structures, 2016, Vol. 117: pp. 204–19.

[2] Muttoni, A.; Punching shear strength of reinforced concrete slabs without transverse reinforcement, ACI Structural Journal, 2008, Vol. 105: pp. 440–50.

[3] Walraven, JC.; Fundamental analysis of aggregate interlock, Journal of Structural Engineering, ASCE, 1981, Vol. 107: pp. 2245–70.

[4] Vecchio, FJ.; Collins, MP.; The modified compression-field theory for reinforced concrete elements subjected to shear, ACI Journal Proceedings, 1986, Vol. 83: pp. 219–31.

[5] CEN.; EN 12390-3 Testing hardened concrete Part 3: Compressive strength of test specimens, Bruxelles: 2009.

[6] CEN.; EN 12390-13 Testing hardened concrete Part 13: Determination of secant modulus of elasticity in compression, Bruxelles: 2013.

[7] CEN.; EN 12390-6 Testing hardened concrete Part 6: Tensile splitting strength of test specimens, Bruxelles: 2000.

[8] European Committee for Standardization.; EN 10080 Steel for reinforcement of concrete - Weldable reinforcing steel - General, 2005.

4. EXPERIMENTAL RESULTS

4.1 Introduction

In this chapter the experimental results of this experimental campaign are presented and compared with the results of previous experimental campaigns without openings [1,2]. For ease of reading the results are listed in three groups: the results of gravity loading tests (§4.2), the results of combined gravity and horizontal loading tests of specimens without shear reinforcement (§4.3) and finally the results of cyclic tests of specimens with stirrups (§4.4).

4.2 Gravity loading tests

In the following the results of the gravity loading tests are shown and compared with those provided by the reference specimen MLS investigated by Almeida et al. [1]. The main results are summarised in Table 4.1. The steel yielding stress is referred to the top reinforcement at the column connection.

Table 4.1 – Main results of gravity loading tests.

Specimen	Opening size (mm)	Opening position	Effective depth (mm)	f_c (MPa)	$f_{ct,sp}$ (MPa)	f_y (MPa)	V_{exp} (kN)
MLS*	-	-	118.0	31.6	2.9	526	324
SO1-01	200x200	North	118.4	46.8	3.4	530	299
SO2-01	200x200	East	116.4	38.0	3.2	530	341

* Almeida et al. [1]

For an effective comparison of the results the concrete compressive strength should be the same for all the specimens while in this case the strengths are quite different. However, for gravity loading is possible to take out the dependence of the punching strength on the concrete compressive strength by considering the following ratio.

$$\frac{V_{exp}}{b_0 \cdot d \cdot f_{cm}^{1/3}} \tag{4.1}$$

where b_0 is the control perimeter calculated according the EC2-2004, d is the effective depth and f_{cm} is the concrete compressive strength. In this case $f_{cm}^{1/3}$ is included in the ratio in accordance with the dependence between punching and concrete strength provided by the EC2-2004 [3]. However, the ratio shown in equation (4.1) could be rewritten considering $f_{cm}^{1/2}$, in accordance with the dependence between punching and concrete strength provided by the MC-2010 [4]. In Table 4.2 a comparison between the failure loads and the punching predictions calculated according to EC2-2004 [3] is proposed.

Table 4.2 – Gravity loading tests – comparison with EC2-2004.

Specimen	Opening size (mm)	Opening position	V_{exp} (kN)	V_{th} (kN)	V_{exp}/V_{th} (-)	$V_{exp}/(b_0 \cdot d)$	$V_{exp}/(b_0 \cdot d \cdot f_{cm}^{1/3})$
MLS*	-	-	324	329	0.99	1.12	0.35
SO1-01	200x200	North	299	296	1.01	1.28	0.36
SO2-01	200x200	East	341	270	1.26	1.51	0.45

* Almeida et al. [1]

In Table 4.2 the control perimeters b_0 of specimens SO1-01 and SO1-02 are calculated considering the presence of the opening as recommended by EC2-2004. The predictions provided by the code are quite accurate except for the specimen SO2-01. Furthermore, if the dependence on the concrete compressive strength is removed by considering the ratio $V_{exp}/b_0 \cdot d \cdot f_{cm}^{1/3}$ arises that the specimen SO2-01 gives higher punching strength than the others. The latter highlights some critical issues about the distribution of vertical loading around the column. The distribution of vertical loading provided by the Lisbon setup follows the North-South direction of the slab, the absence of vertical loading distributed on the East-West direction induces a non-uniform distribution of shear stresses around the column. Probably, the presence of the opening on the East side emphasizes this problem. Indeed, considering the ratio shown in equation (4.1) the results provided by the specimens should be the same since both the dependence on control perimeter and concrete compressive strength were removed. However, some inevitable experimental scatter can also be present and it could be partially responsible of the higher punching strength provided by the specimen SO2-01.

4.2.1 Load-displacement curves

Following figures (Figure 4.1, Figure 4.2 and Figure 4.3) show the load-displacement curves.

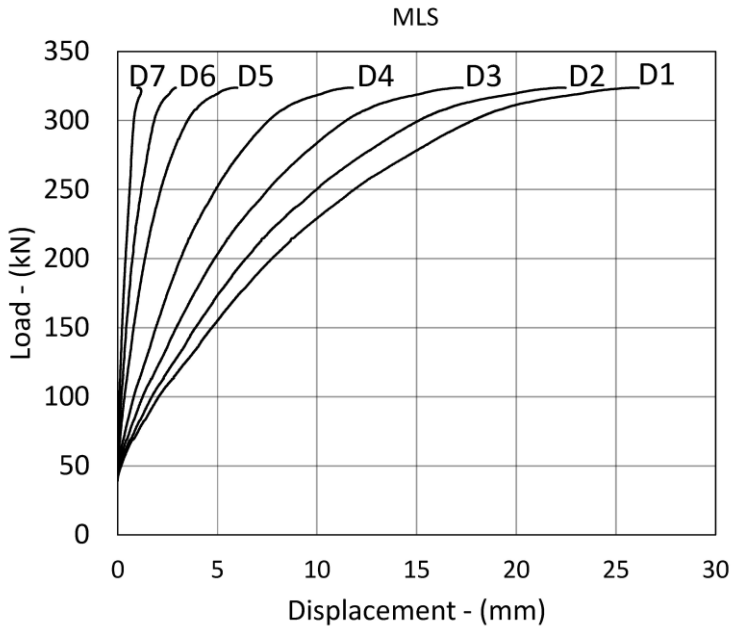

Figure 4.1 – Load-displacement curves. MLS investigated by Almeida et al. [1].

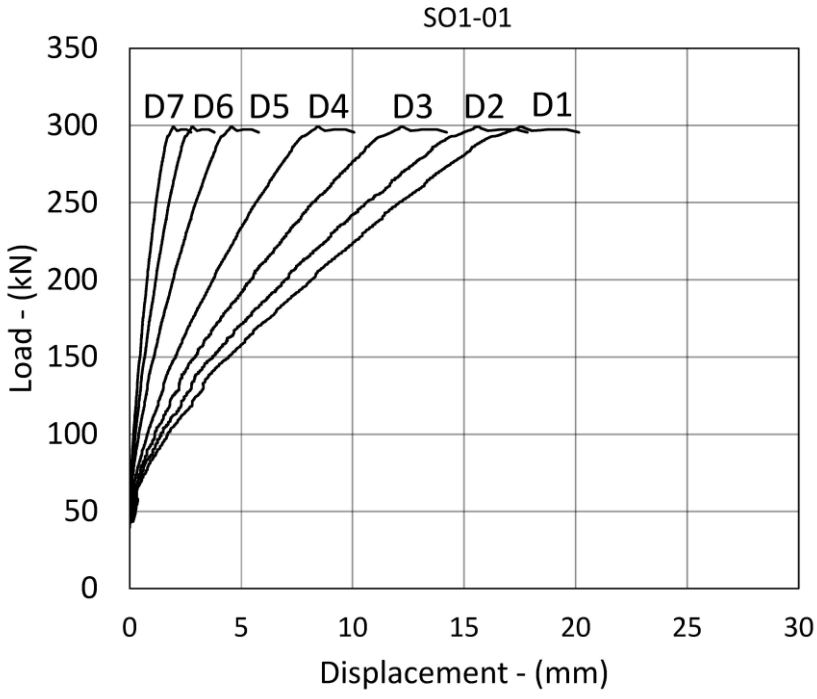

Figure 4.2 – Load-displacement curves. SO1-01.

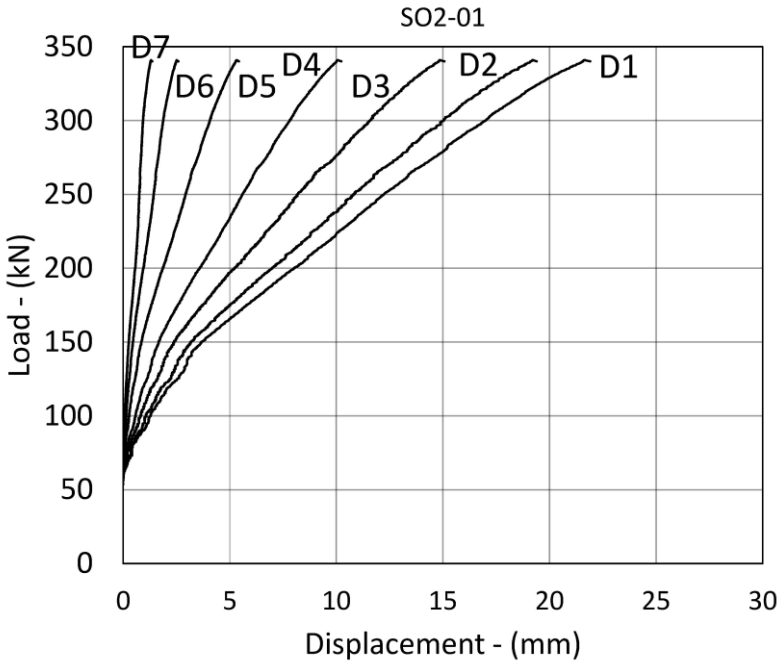

Figure 4.3 – Load-displacement curves. SO2-01.

4.2.2 Slab deflections

The slab deflections in longitudinal and transverse direction at varying the vertical loading are shown in the following. The stiffness loss is evident as equal load steps lead to increasing displacement increments.

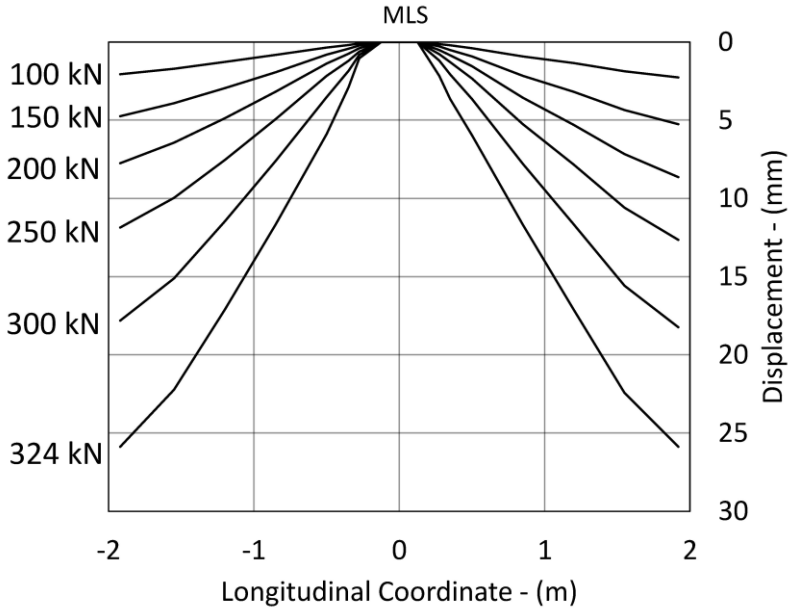

Figure 4.4 – Deflections along N-S direction. MLS investigated by Almeida et al. [1].

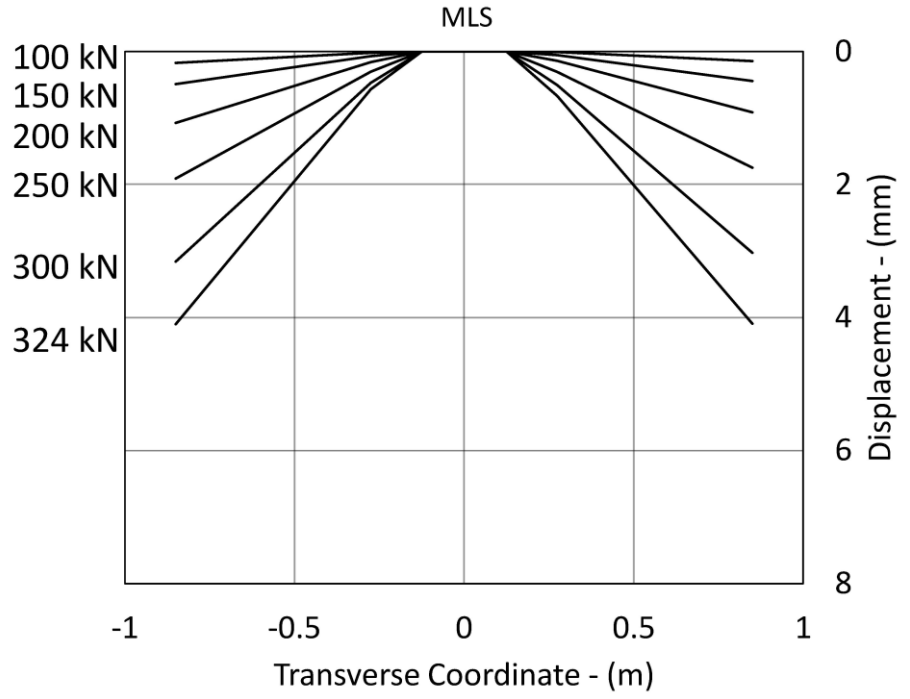

Figure 4.5 – Deflections along E-W direction. MLS investigated by Almeida et al. [1].

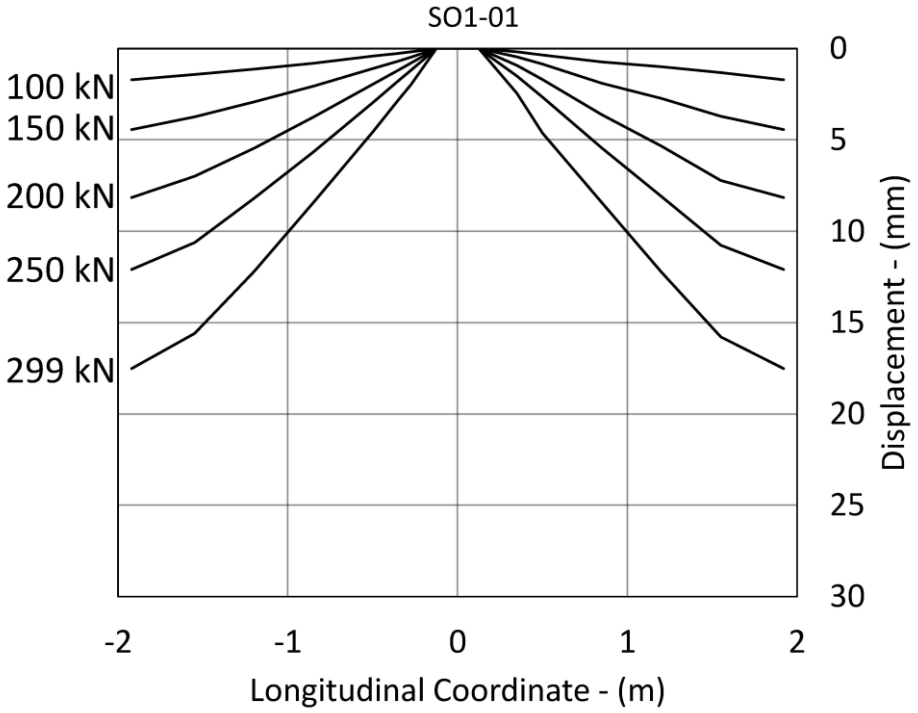

Figure 4.6 – Deflections along N-S direction. SO1-01.

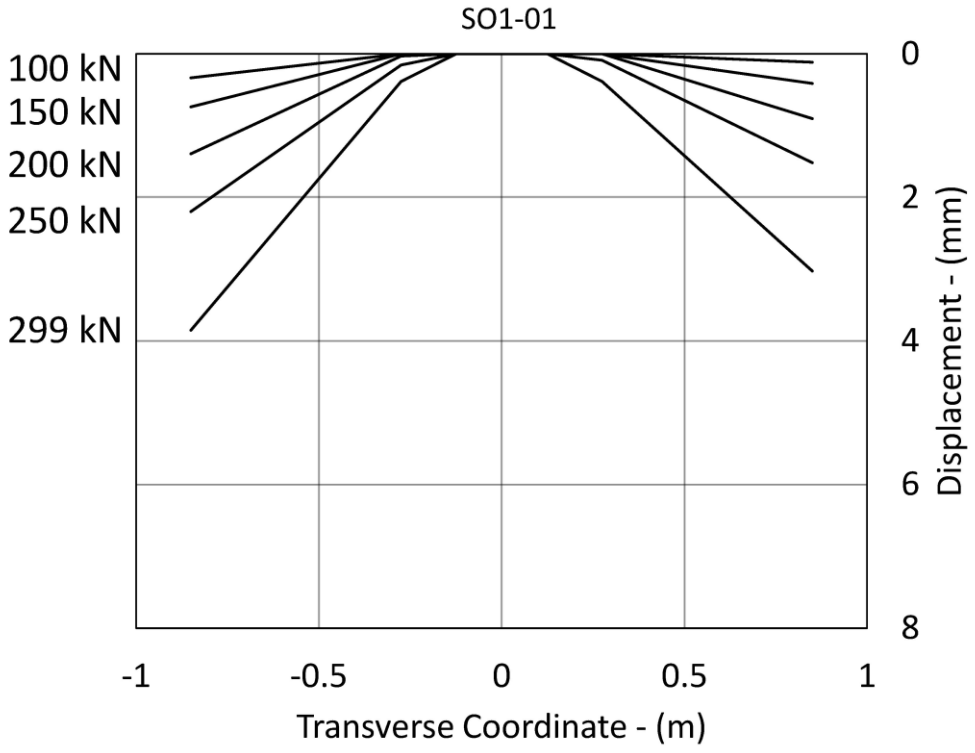

Figure 4.7 – Deflections along E-W direction. SO1-01.

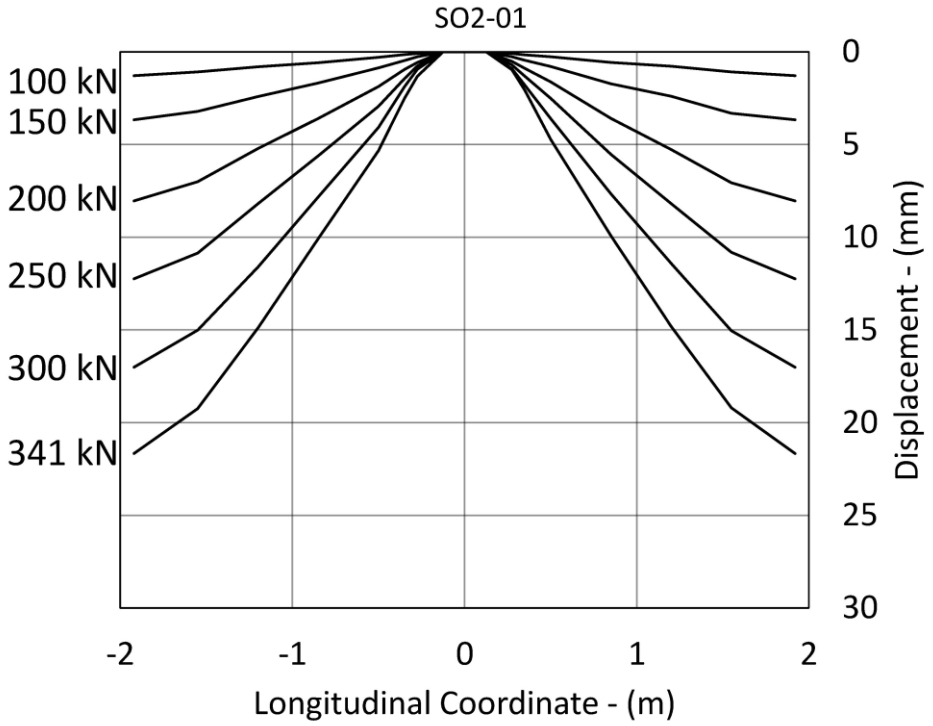

Figure 4.8 – Deflections along N-S direction. SO2-01.

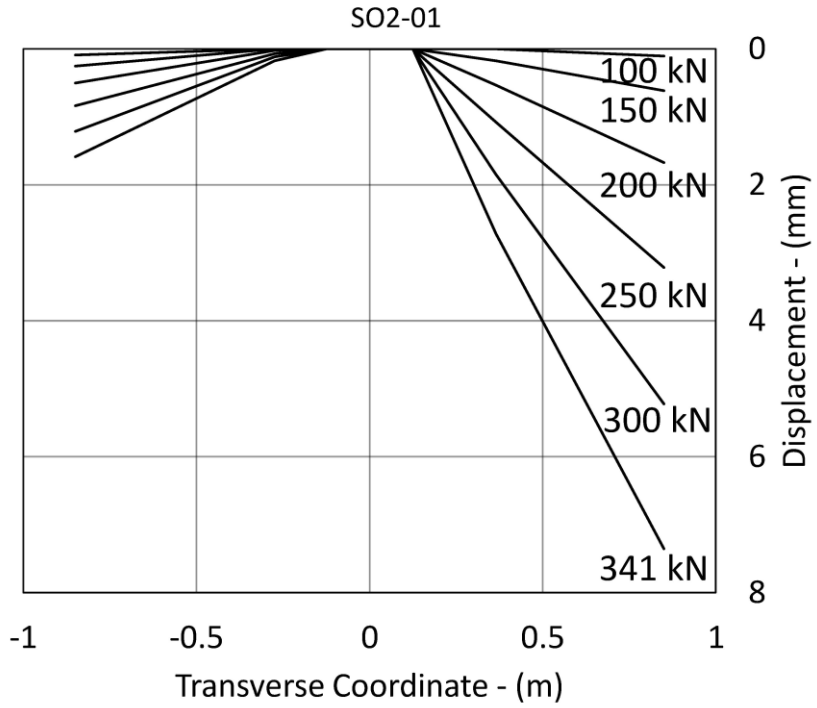

Figure 4.9 – Deflections along N-S direction. SO2-01.

Accounting for the rigid rotation of the slab SO2-01 in transverse direction the deflections become:

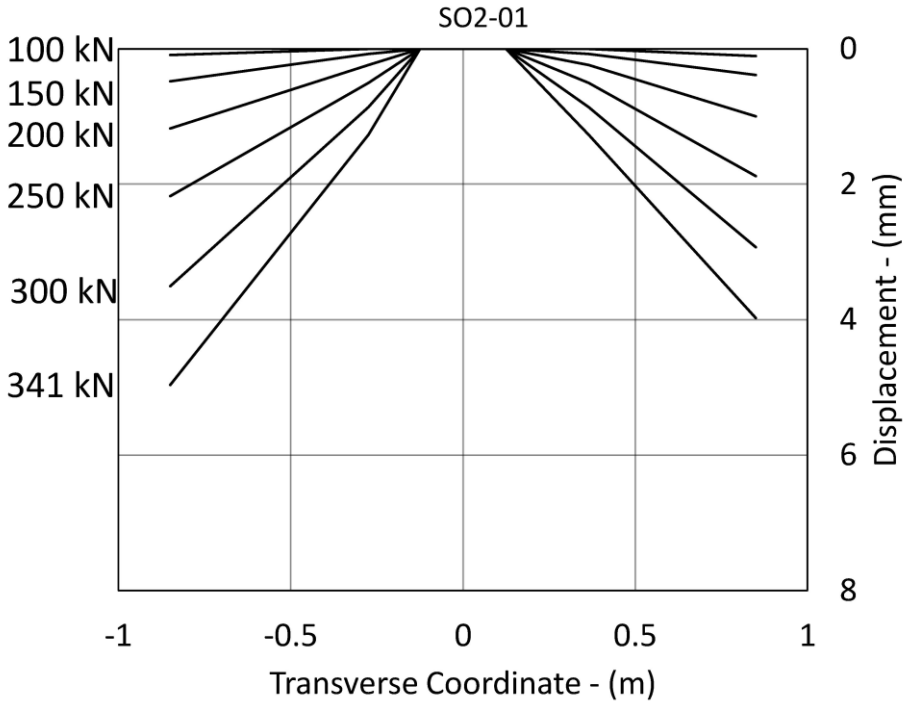

Figure 4.10 – Deflections along E-W direction. SO2-01.

4.3 Combined gravity and horizontal loading tests without shear reinforcement

In the following the results of the combined gravity and horizontal loading tests without shear reinforcement are shown and compared with those provided by the reference specimen C-50 investigated by Almeida et al. [1]. The main results are listed in Table 4.3 considering both North (N) and South (S) loading directions. The ultimate drift Δ_u is considered to be the maximum attained drift before a punching failure or before a drop of the unbalanced moment below 80% of the maximum value.

Table 4.3 – Main results of combined gravity and horizontal loading tests without stirrups.

Specimen	Opening size (mm)	Opening position	Effective depth (mm)	f_c (MPa)	$f_{ct,sp}$ (MPa)	f_y (MPa)	V_g (kN)	M_{unb} (kNm)	Δ_u (%)
C-50*	-	-	118.0	52.4	2.9	526	203	74.8 (S) -73.4 (N)	1.0
SO1-02	200x200	North	118.2	40.5	3.3	530	195	40.3 (S) -75.0 (N)	1.0
SO2-02	200x200	East	118.6	49.5	3.3	530	210	66.9 (S) -71.1 (N)	1.0

* Almeida et al. [1]

Differently from gravity loading only, in this case the dependence of the punching strength on the concrete compressive strength is difficult to remove. Indeed, the combined presence of flexural and shear actions makes this operation not viable.

All the specimens failed by punching for a drift of 1% and the peak loads resulted very similar except for the maximum load exhibited by SO1-02 in south direction. In this case the effect of the opening leads to a reduction of the maximum unbalanced moment of about 46%.

This greater influence provided by the opening placed on the North side when the loading is direct to South is due to the arrangement of longitudinal reinforcement. Indeed, for southward horizontal loading there is no effective top reinforcement passing through the column. Differently for northward horizontal loading two 12mm rebars placed on the top are effective thanks to hooked anchorage.

4.3.1 Load-deformation responses

The load-deformation curves are shown in Figure 4.11, Figure 4.12 and Figure 4.13. In Figure 4.14 the comparison of the backbone curve is provided.

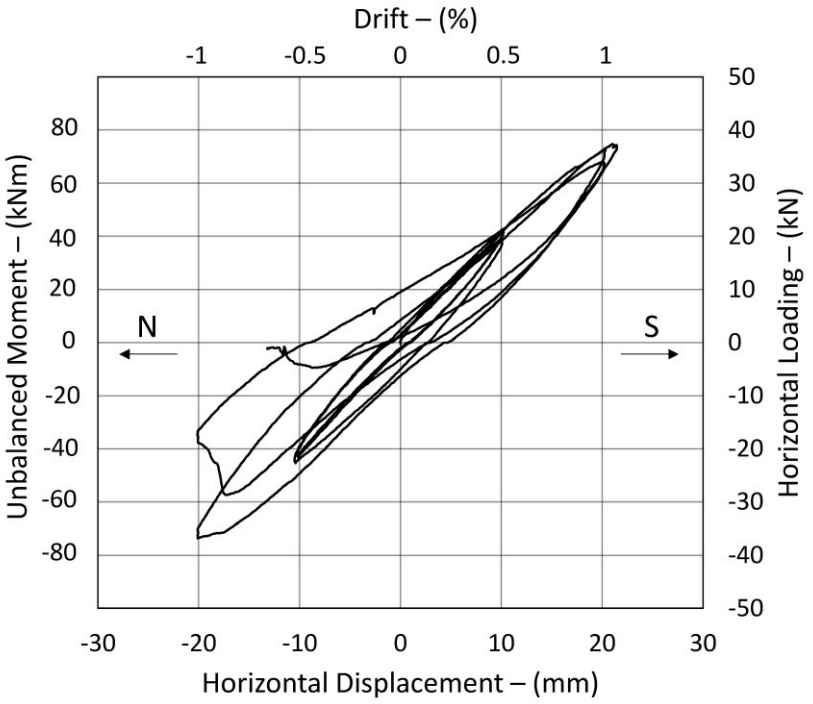

Figure 4.11 – Load-deformation curve. C-50 investigated by Almeida et al. [1].

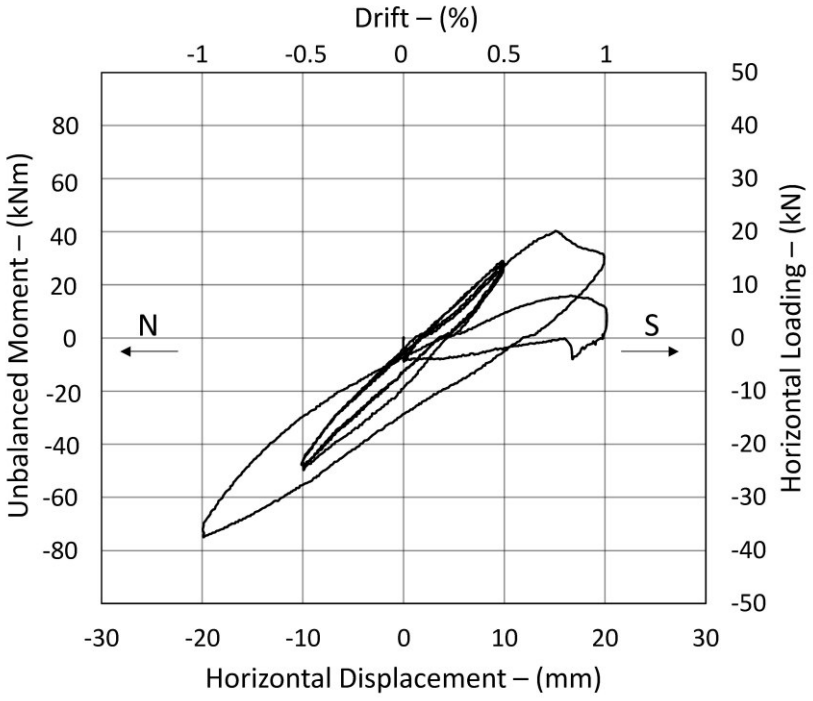

Figure 4.12 – Load-deformation curve. SO1-02.

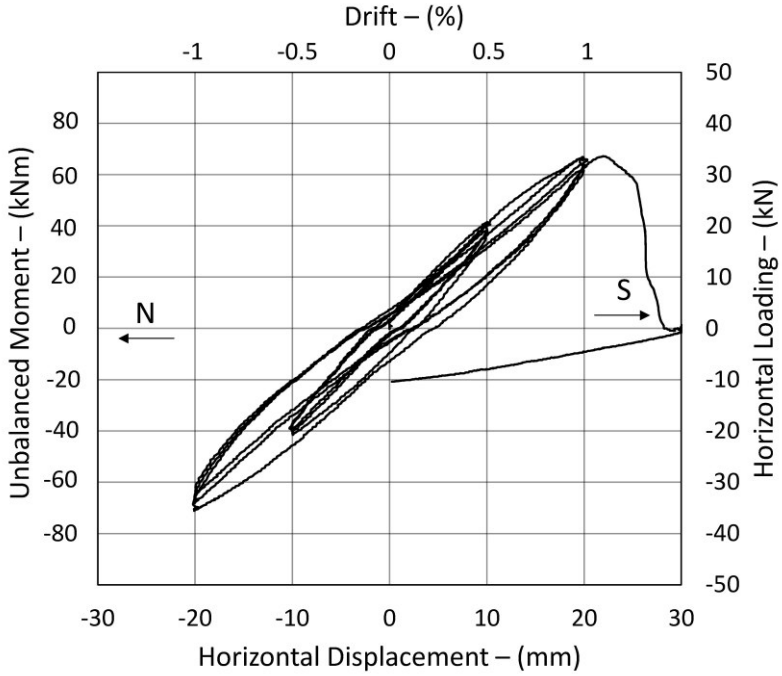

Figure 4.13 – Load-deformation curve. SO2-02.

In the following the envelope curves of the hysteretic cycles are shown for each specimen. As mentioned above, except the SO1-02 for southward horizontal loading, the result provided by the specimens with or without openings is almost the same.

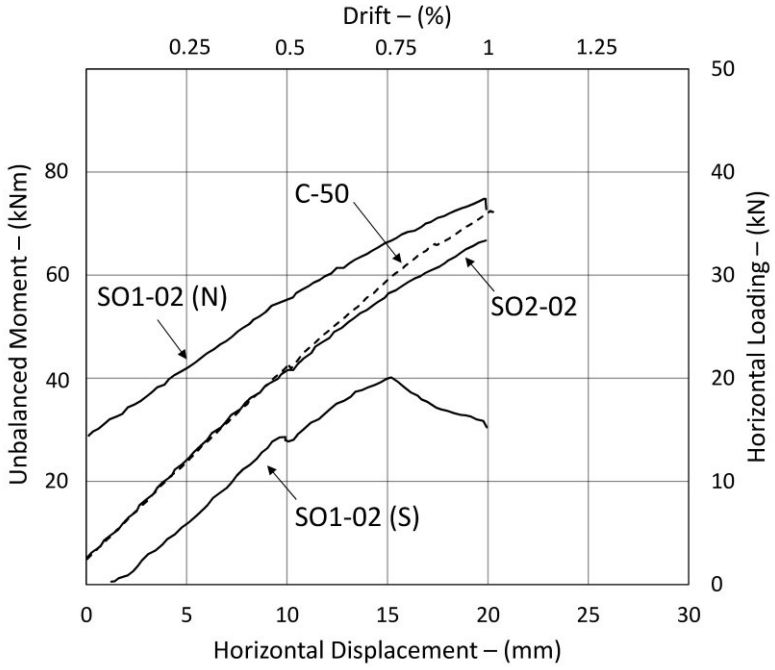

Figure 4.14 – Comparison of envelope curves.

It is interesting to observe that for Southward loading the specimen SO1-02 provides an abrupt change of slope of the backbone for 0.75% of lateral drift. The latter indicates the beginning of the failure that occurs in the second cycle of 1% drift, where a complete loss of stiffness is shown (Figure 4.12).

4.3.2 Slab deflections

In the following the slab deflections exhibited in correspondence of the peak displacement of each cycle, both in North and South directions, are shown. The results of the specimen C-50 are provided in Figure 4.15 and Figure 4.16, those of specimen SO1-02 in Figure 4.17 and Figure 4.18, finally those of specimen SO2-02 are shown in Figure 4.19 and Figure 4.20.

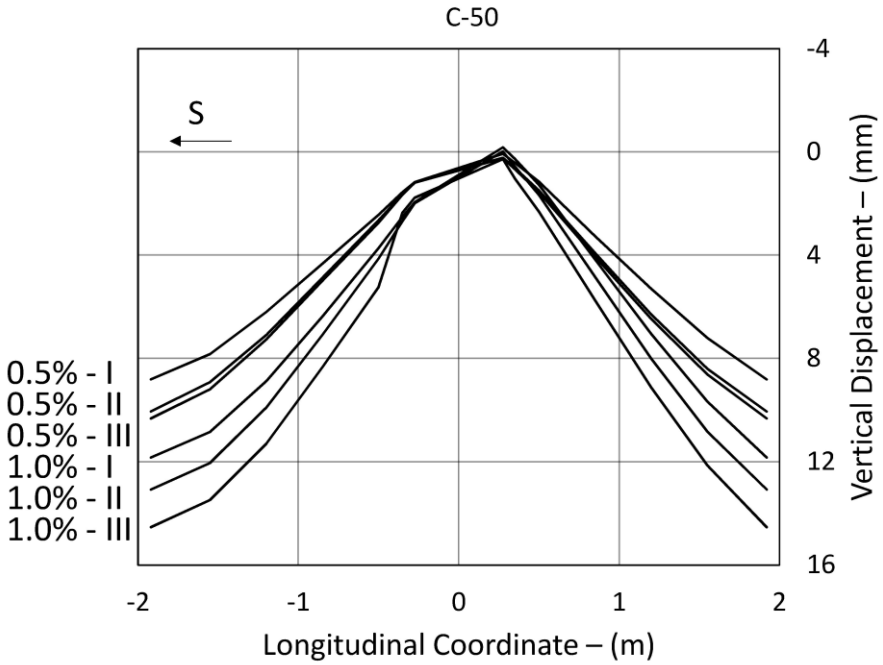

Figure 4.15 – Slab deflection specimen C-50 investigated by Almeida et al. [1]. Cycles in South direction.

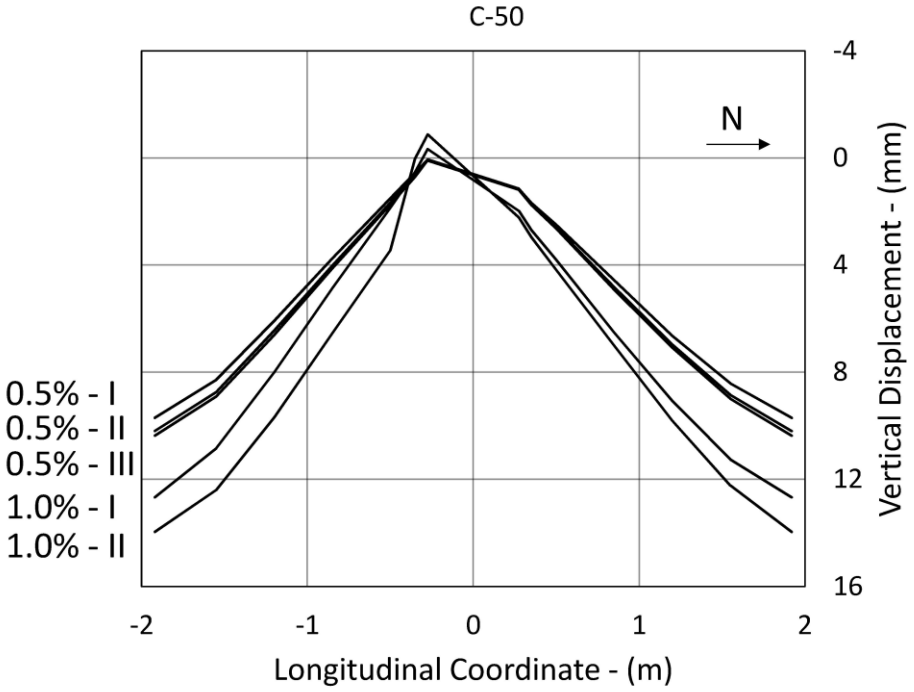

Figure 4.16 – Slab deflection specimen C-50 investigated by Almeida et al. [1]. Cycles in North direction.

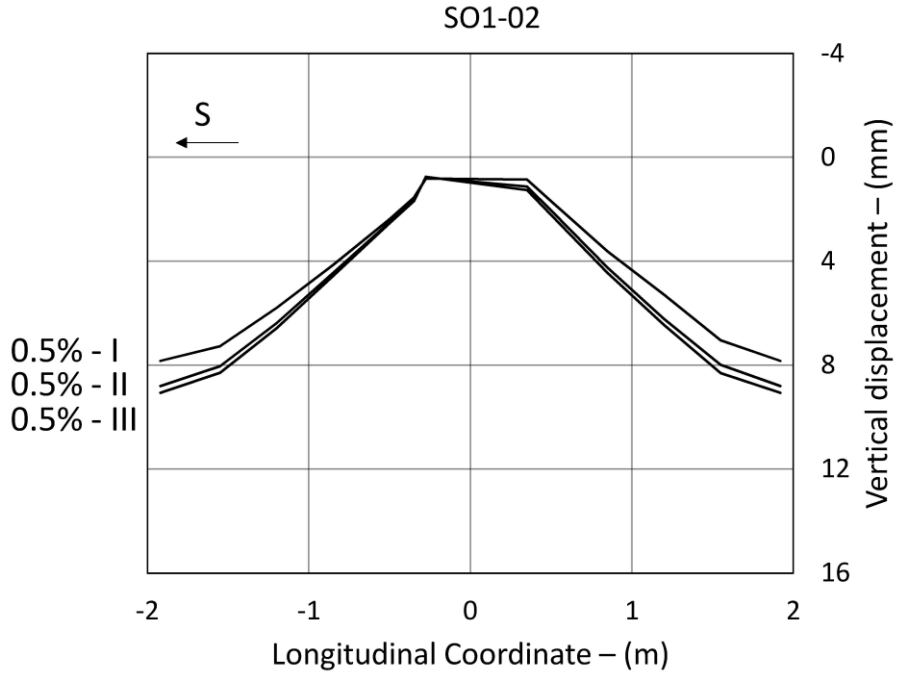

Figure 4.17 – Slab deflection specimen SO1-02. Cycles in South direction.

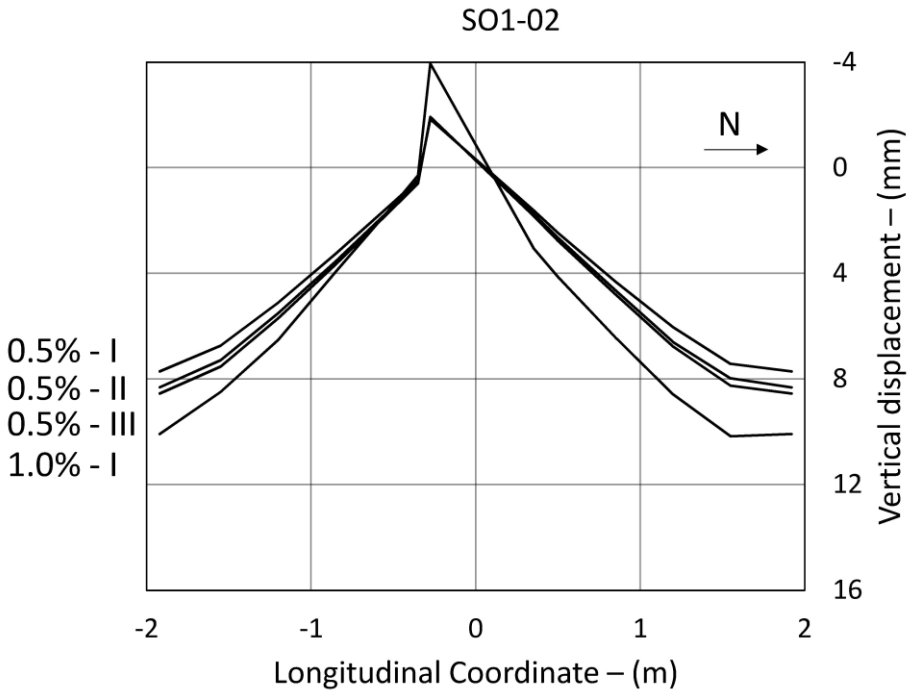

Figure 4.18 – Slab deflection specimen SO1-02. Cycles in North direction.

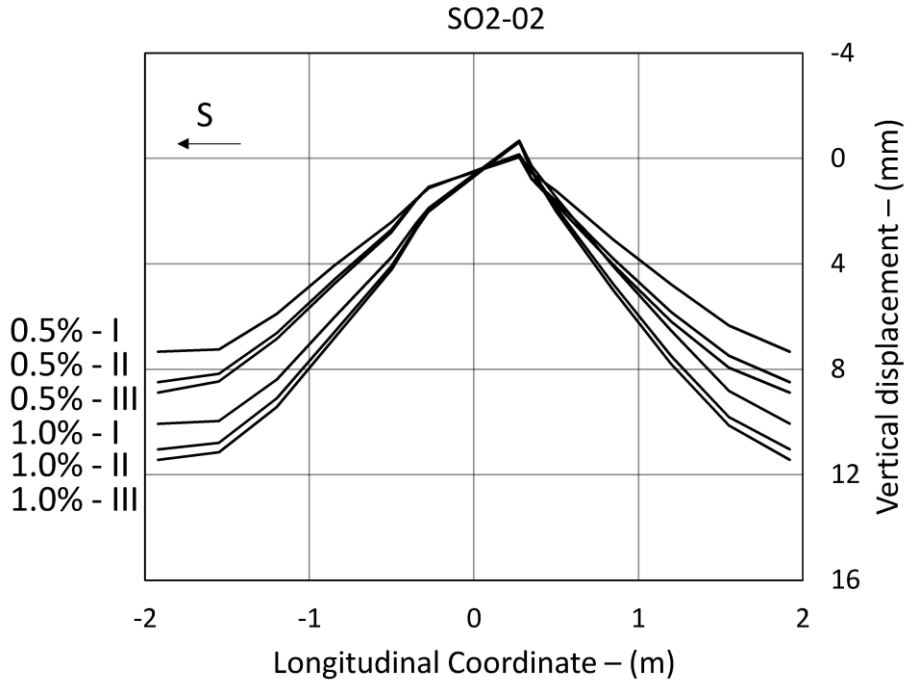

Figure 4.19 – Slab deflection specimen SO2-02. Cycles in South direction.

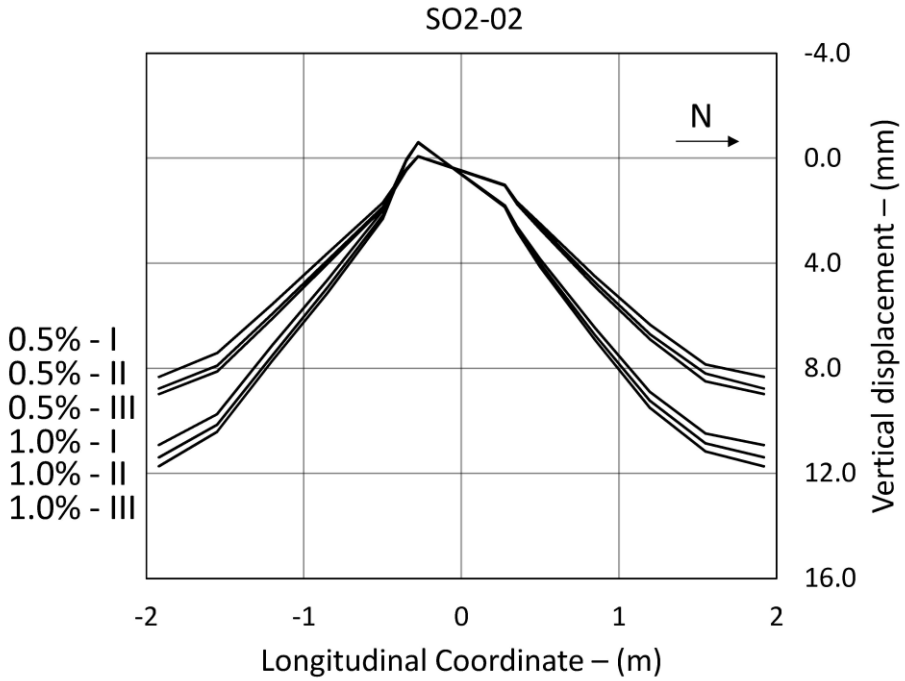

Figure 4.20 – Slab deflection specimen SO2-02. Cycles in North direction.

As shown previously the specimens C-50 and SO2-02 exhibited more cycles than the specimen SO1-02. Furthermore, for the latter specimen in Figure 4.17 three cycles only are shown, since the results for the cycle 1% were not available due to a problem in the acquisition system.

However, the slab deflections show a progressive reduction of the stiffness and a corresponding progressive increasing of the vertical displacements for all the specimens. The latter is particularly evident for the specimens C-50 and SO2-02 since more cycles are available.

4.3.3 Location of the inflection point

Starting from the deflections, the locations of the inflection points have been monitored during the tests. In Figure 4.21, Figure 4.22 and Figure 4.23 the positions of the contraflexure points are plotted against the time.

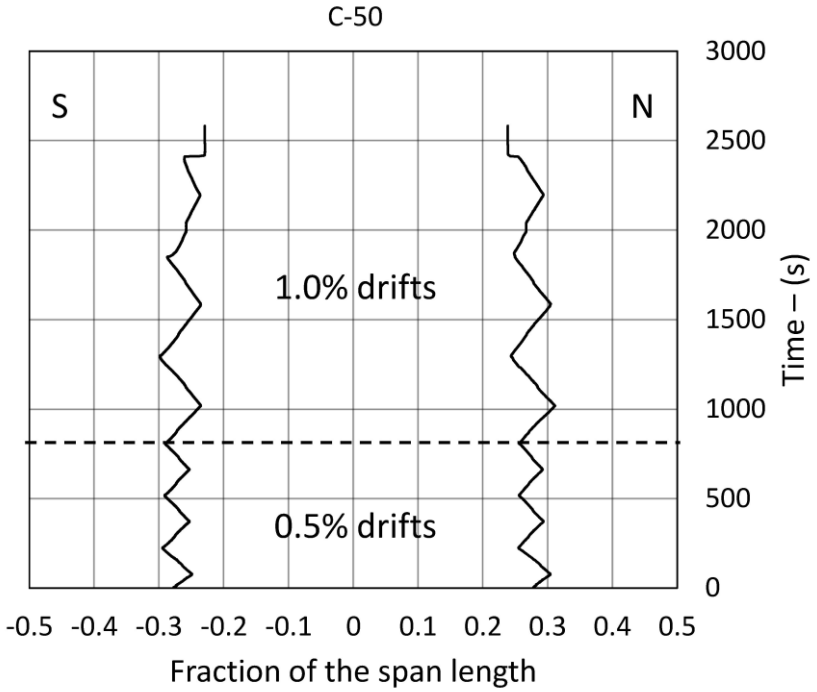

Figure 4.21 – Location of the inflection points during the cyclic loading test. Specimen C-50 investigated by Almeida et al. [1].

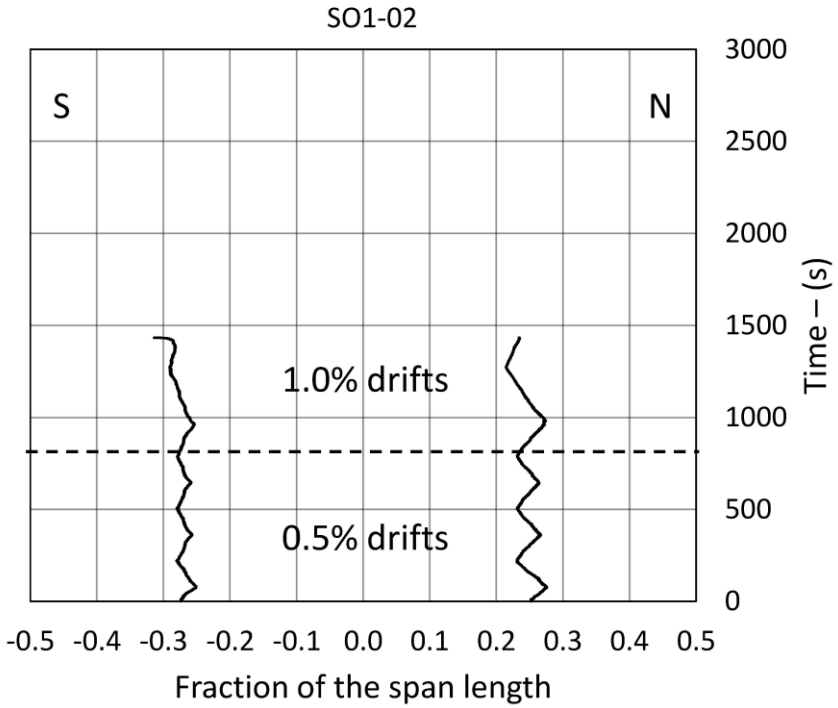

Figure 4.22 – Location of the inflection points during the cyclic loading test. Specimen SO1-02.

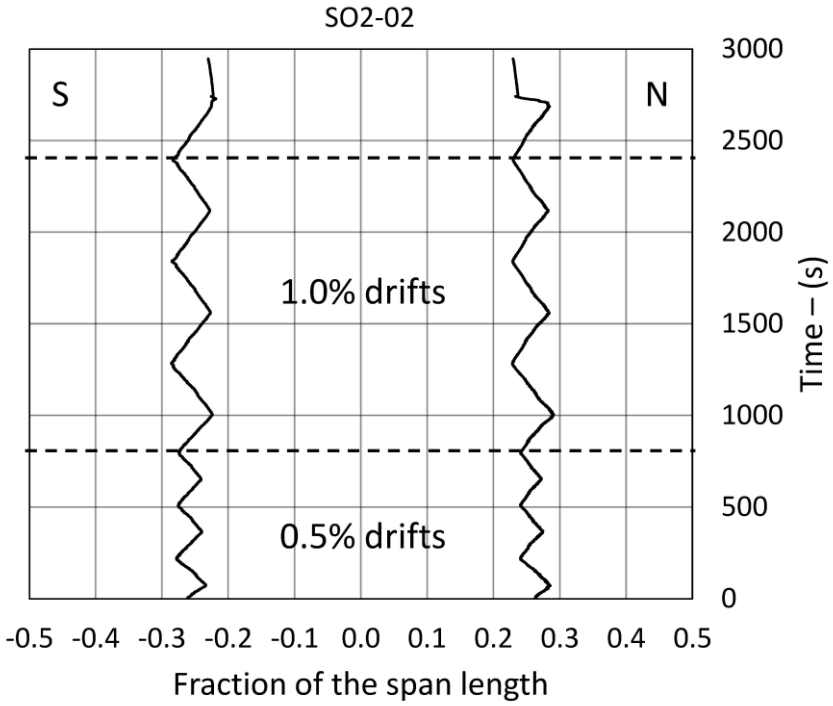

Figure 4.23 – Location of the inflection points during the cyclic loading test. Specimen SO2-02.

At the beginning of the horizontal loading application (for time s=0) the inflection points are placed between 0.2-0.3 the span length. The latter confirm the correct functioning of the setup. For vertical loading only, along the North-South direction, the specimens exhibit the same behaviour of a continuous slab. During the application of the horizontal loading the inflection points move cyclically along the North-South direction.

4.3.4 Lateral stiffness degradation

Another important parameter to be monitored during the cyclic test is the lateral stiffness of the slab column joint. The latter is defined as the ratio between the unbalanced moment and the horizontal displacement at the end of each cycle. In Figure 4.24, Figure 4.25 and Figure 4.26 the lateral stiffness degradation of the specimens C-50, SO1-02 and SO2-02 are shown respectively.

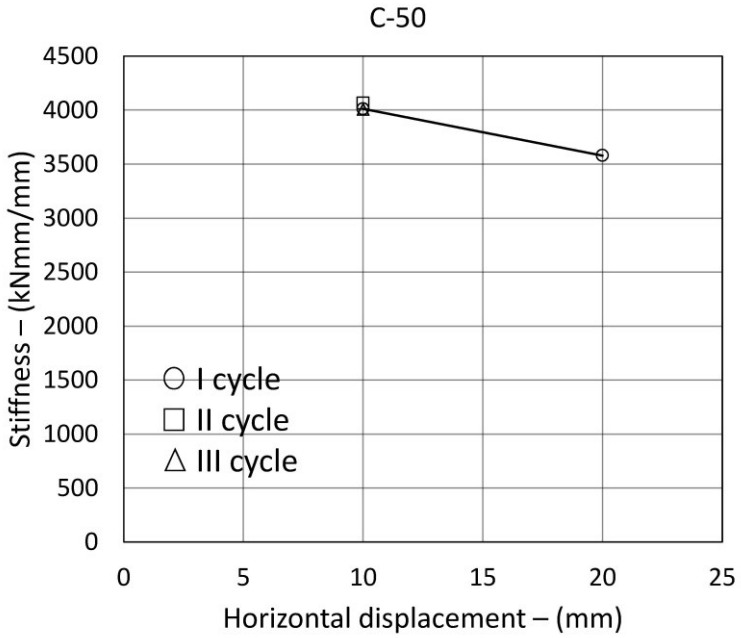

Figure 4.24 – Lateral stiffness degradation. Specimen C-50 investigated by Almeida et al. [1].

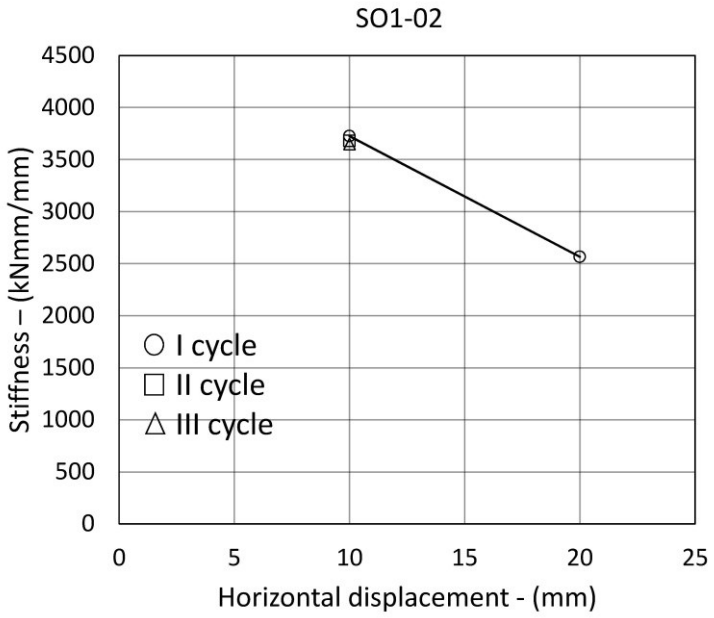

Figure 4.25 – Lateral stiffness degradation. Specimen SO1-02.

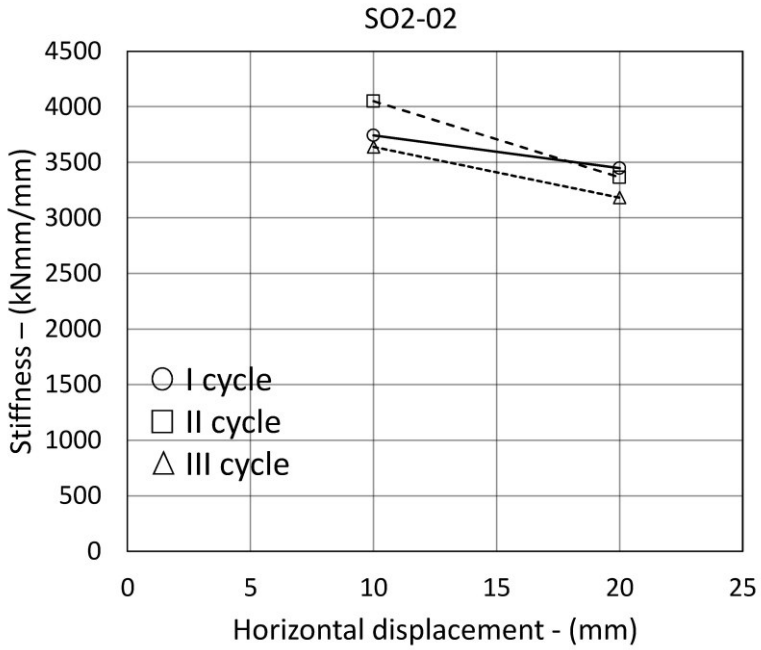

Figure 4.26 – Lateral stiffness degradation. Specimen SO2-02.

In general, a tendency of lateral stiffness degradation is found for all the specimens. However, since the few cycles performed by the specimens without shear reinforcement, an important degradation of the stiffness is not found.

4.3.5 Equivalent viscous damping ratio

To evaluate the dissipation capacity of the specimens an equivalent viscous damping ratio was calculated for each cycle, using equation (4.2):

$$\xi_{eq} = \frac{1}{4 \cdot \pi} \cdot \left(\frac{E_{d1}}{E_{s1}} + \frac{E_{d2}}{E_{s2}} \right) \tag{4.2}$$

where E_{d1} and E_{d2} are the areas within the hysteresis curve for positive and negative displacements respectively. Whereas E_{s1} and E_{s2} are the elastic energies for positive and negative displacements respectively.

In Figure 4.27, Figure 4.28 and Figure 4.29, the evolution of the equivalent viscous damping ratios are shown at varying of the horizontal displacement.

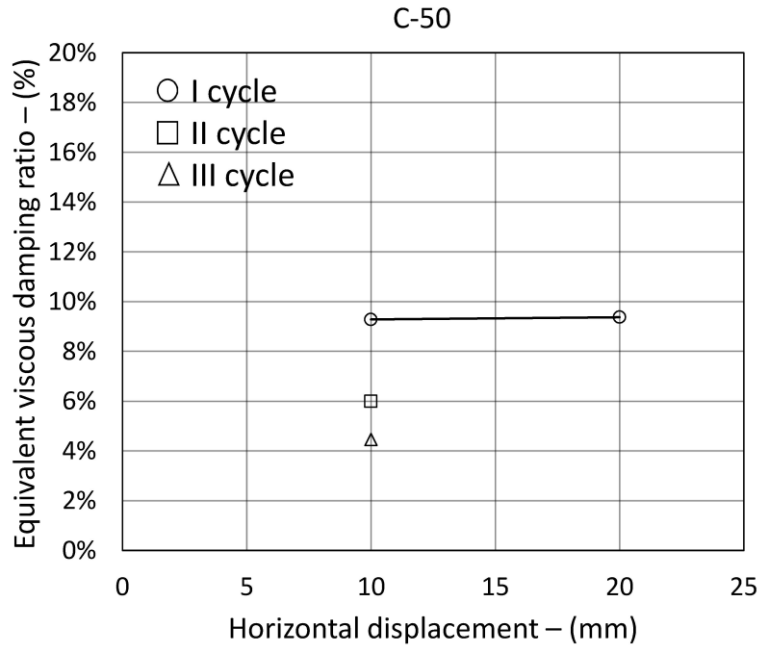

Figure 4.27 – Equivalent viscous damping ratio. Specimen C-50 investigated by Almeida et al. [1].

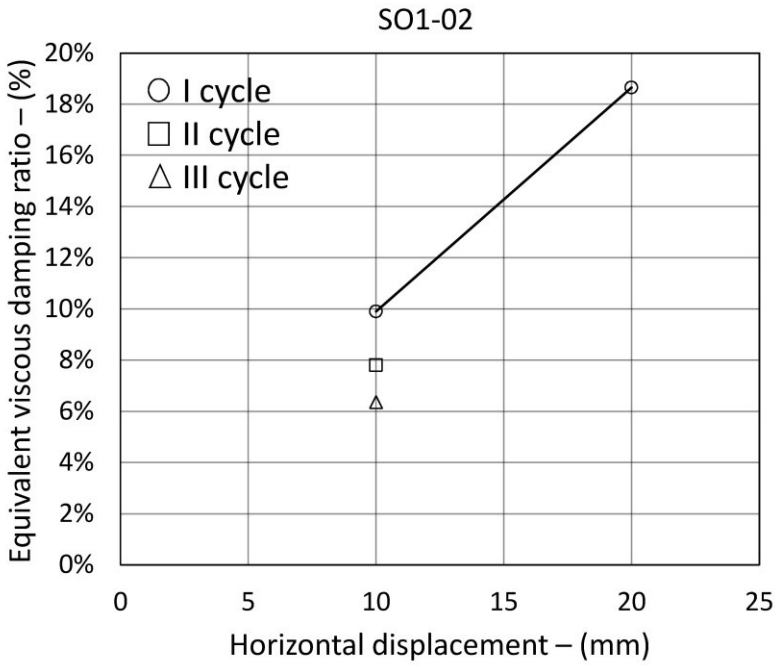

Figure 4.28 – Equivalent viscous damping ratio. Specimen SO1-02.

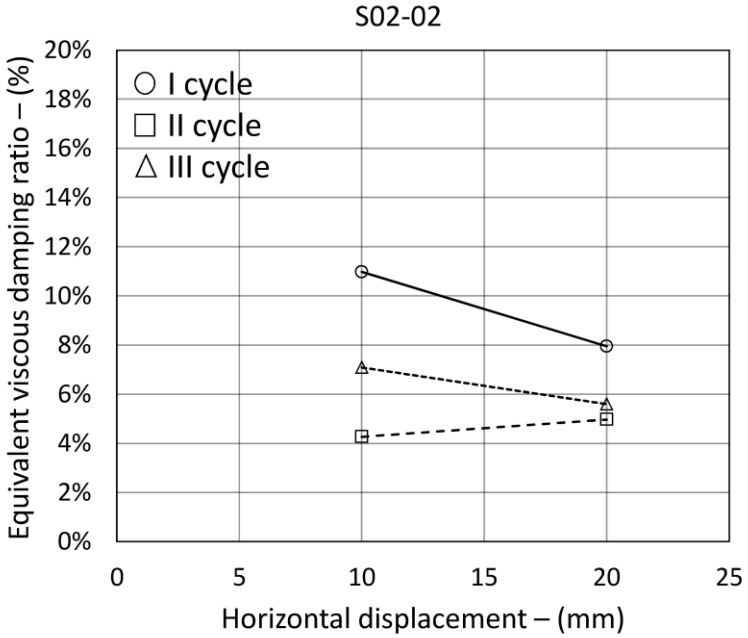

Figure 4.29 – Equivalent viscous damping ratio. Specimen SO2-02.

According to the results provided by the specimens without shear reinforcement is not possible to identify a clear tendency about the variation of the equivalent viscous damping ratio. In general, for a fixed drift, for increasing number of cycles a decrease in terms of equivalent viscous damping ratio is found. However, at drift increasing no tendency is found.

4.4 Combined gravity and horizontal loading tests with shear reinforcement

In the following the results of the combined gravity and horizontal loading tests with shear reinforcement are shown and compared with those provided by the reference specimen C-50 STR4 investigated by Almeida et al. [2]. The main results are listed in Table 4.4.

Table 4.4 – Main results of combined gravity and horizontal loading tests with stirrups.

Specimen	Opening size (mm)	Opening position	Effective depth (mm)	f_c (MPa)	$f_{ct,sp}$ (MPa)	f_y (MPa)	V_g (kN)	M_{unb} (kNm)	Δ_u (%)
C-50 STR4*	-	-	118.0	44.4	3.6	545	196	124.3 (S) -122.5 (N)	4.0
SO1-03	200x200	North	119.0	44.2	3.3	530	214	53.7 (S) -83.3 (N)	2.5
SO2-03	200x200	East	118.3	35.6	3.2	530	194	98.8 (S) -100.4 (N)	5.0

* Almeida et al. [2]

For slab with shear reinforcement, in case of combined gravity and horizontal loading, the presence of the opening clearly affects the flexural capacity of the connection. This detrimental effect is emphasized for the specimen with the opening placed on the north side (SO1-03), especially for southward horizontal loading.

4.4.1 Load-deformation responses

The load-deformation curves are shown in Figure 4.30, Figure 4.31 and Figure 4.32.

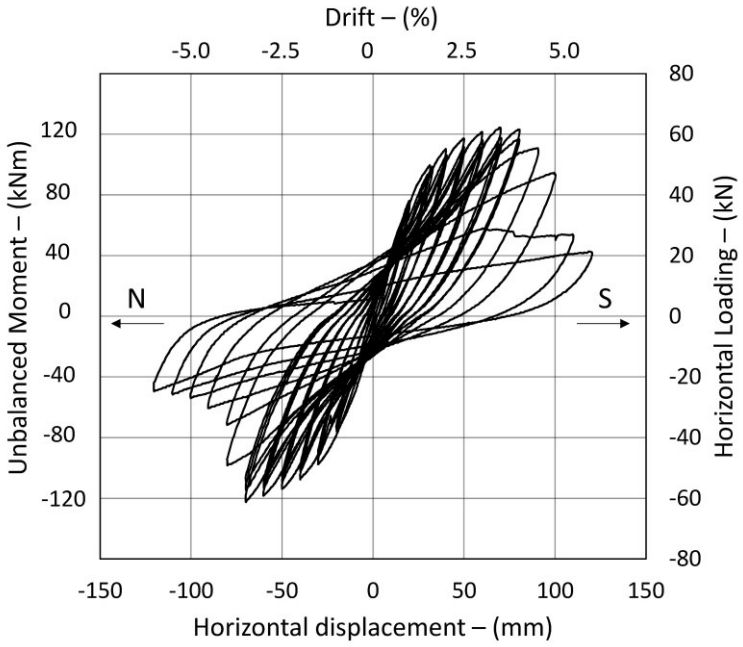

Figure 4.30 – Load-deformation curve. C-50 STR4 investigated by Almeida et al. [2].

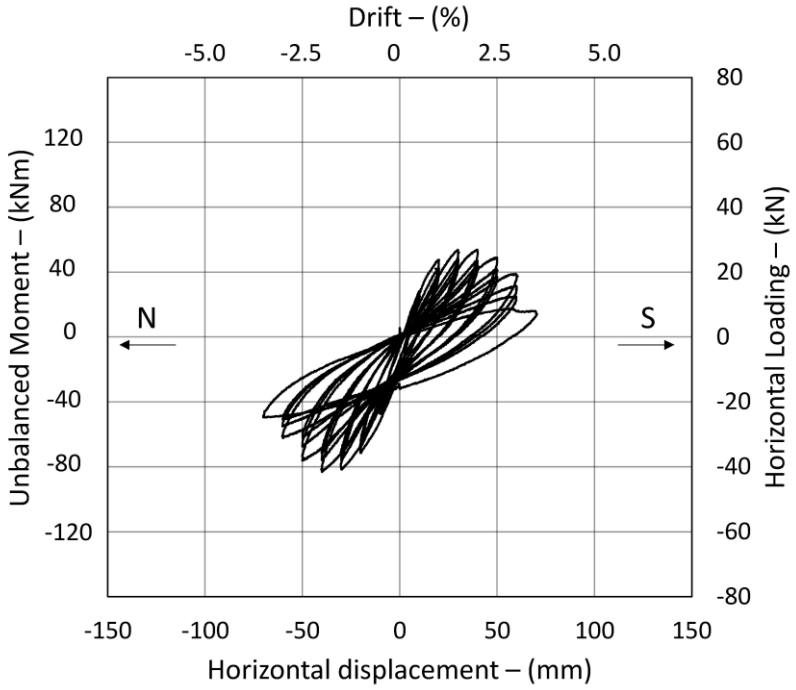

Figure 4.31 – Load-deformation curve. SO1-03.

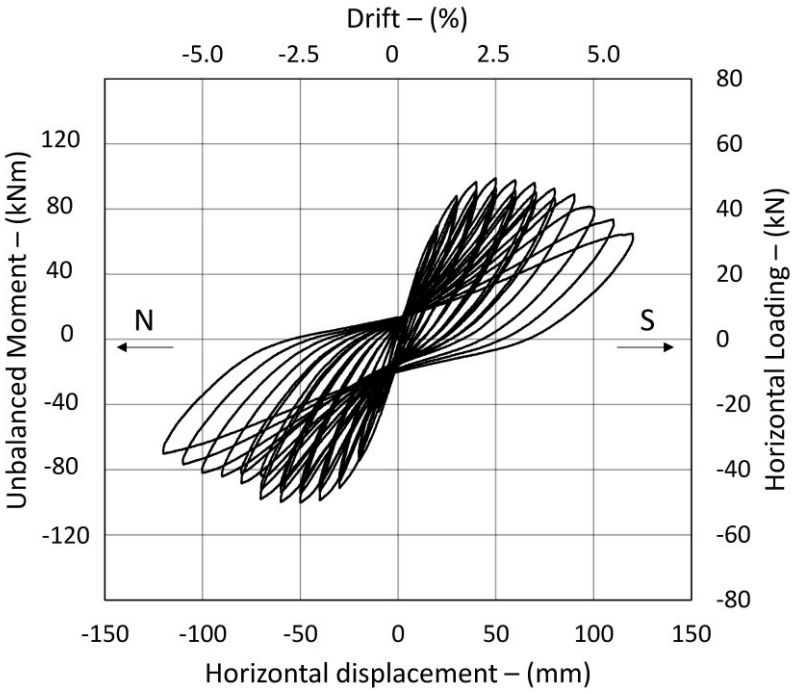

Figure 4.32 – Load-deformation curve. SO2-03.

In Figure 4.33 the envelope curves of the hysteretic cycles are shown for each specimen.

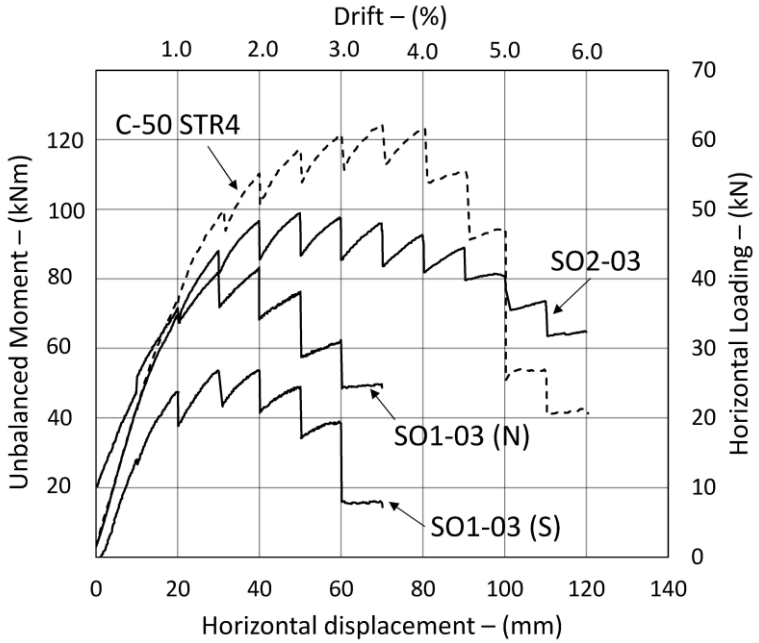

Figure 4.33 – Comparison of envelope curves – Slabs with shear reinforcement.

From the comparison of the envelope curves results evident the detrimental role played by the opening adjacent to the column. Besides all the specimens provided a ductile failure, the specimens with opening showed a lower flexural strength. The latter Is particularly evident in the specimen SO1-03 for southward horizontal loading, due to the present of the opening in the north column´s face.

4.4.2 Slab deflections

Therefore, the slab deflections are shown for both cycles performed in north and south direction. The results of the specimen C-50 STR4 are shown in Figure 4.34 and Figure 4.35, those of specimen SO1-03 in Figure 4.36 and Figure 4.37, finally those of the specimen SO2-03 in Figure 4.38 and Figure 4.39.

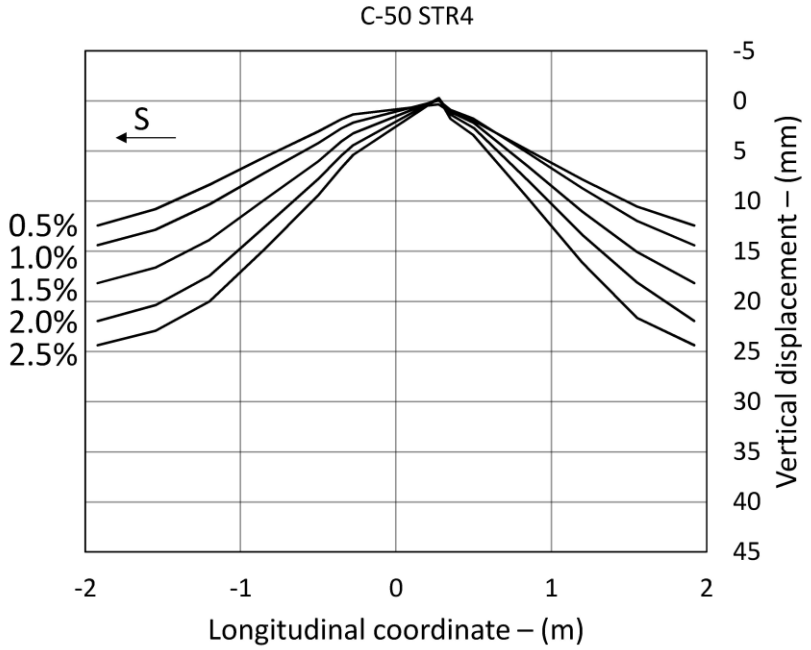

Figure 4.34 – Slab deflection specimen C-50 STR4 investigated by Almeida et al. [2]. Cycles in south direction.

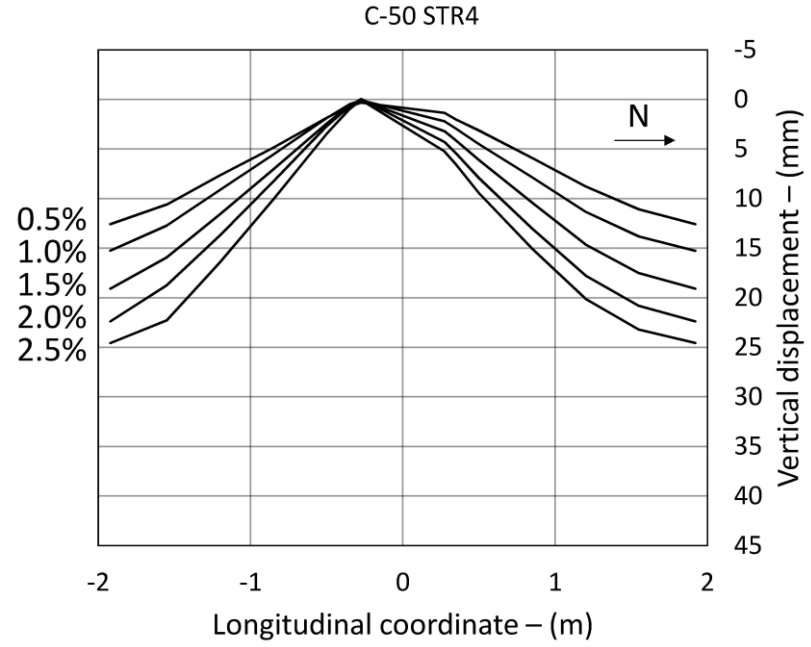

Figure 4.35 – Slab deflection specimen C-50 STR4 investigated by Almeida et al. [2]. Cycles in north direction.

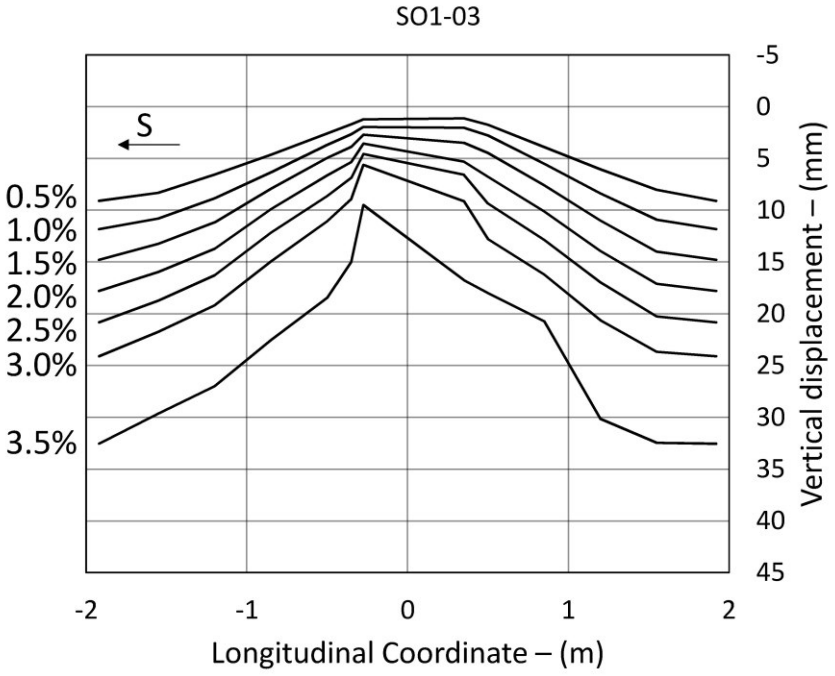

Figure 4.36 – Slab deflection specimen SO1-03. Cycles in south direction.

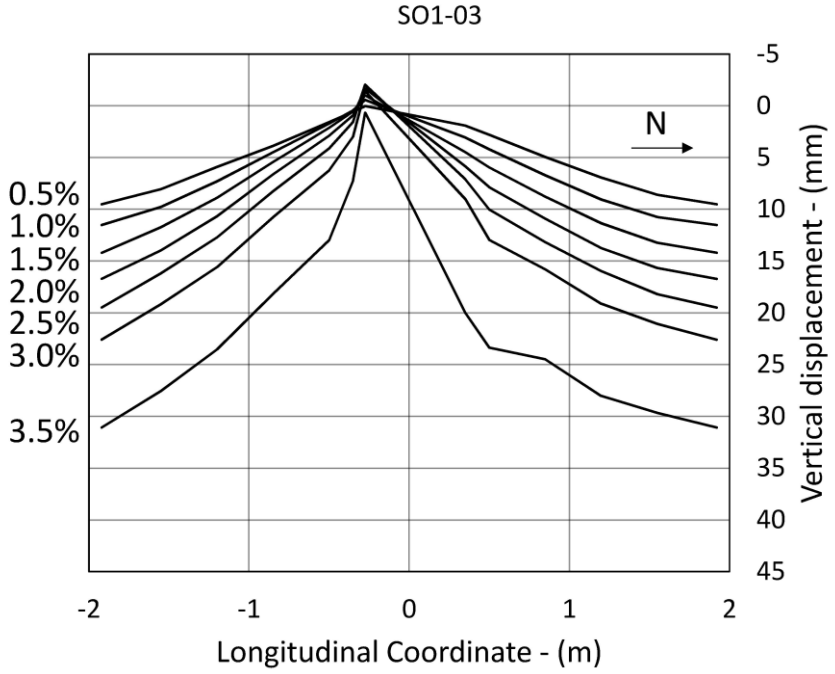

Figure 4.37 – Slab deflection specimen SO1-03. Cycles in north direction.

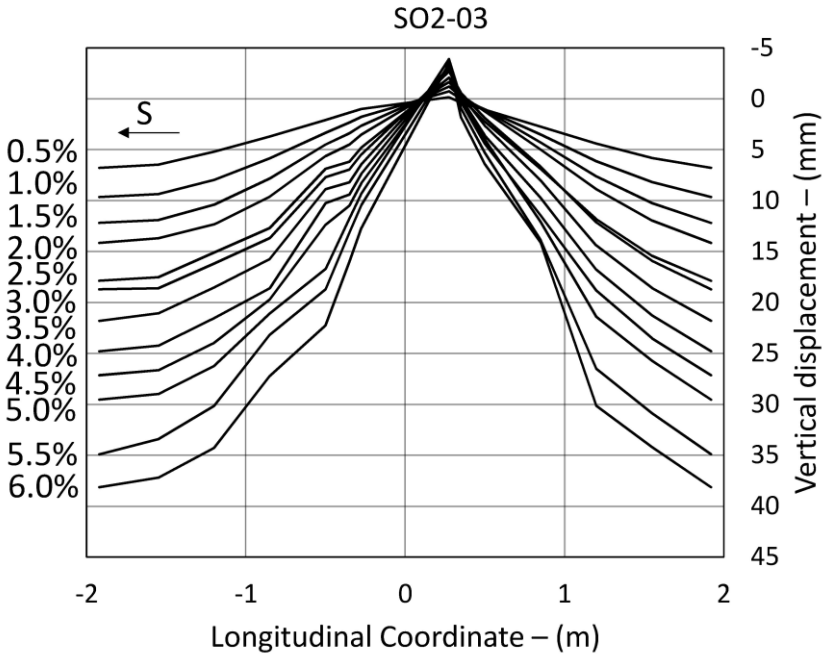

Figure 4.38 – Slab deflection specimen SO2-03. Cycles in south direction

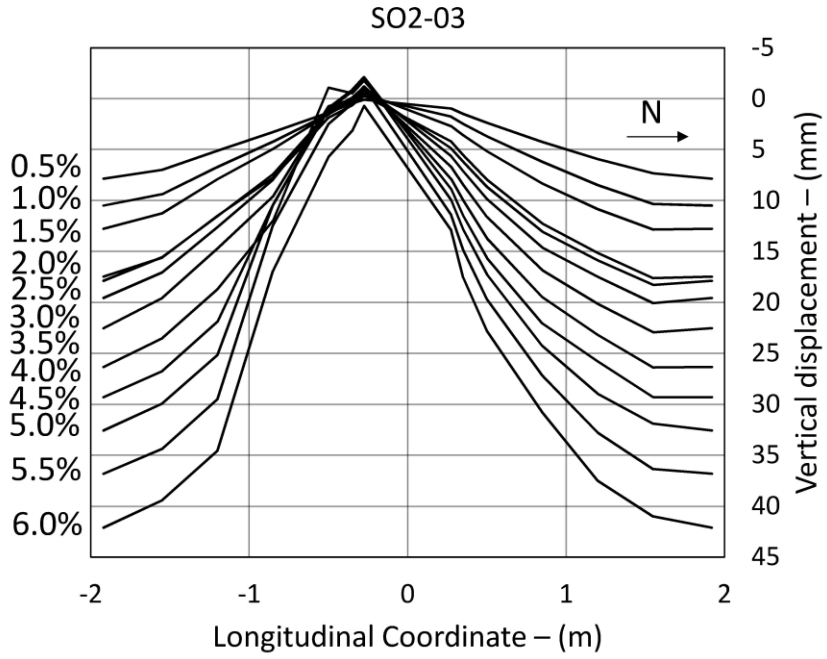

Figure 4.39 – Slab deflection specimen SO2-03. Cycles in north direction.

The slab deflections show a progressive reduction of the stiffness and a corresponding progressive increasing of the vertical displacements for all the specimens. For the specimen SO1-03 a sudden increase of vertical displacements is shown for 3.5% of horizontal drift. The

latter indicates the punching failure of the specimen. Conversely, for the specimen SO2-03 the deflections do not suggest the occurrence of a punching failure.

4.4.3 Location of the inflection point

In Figure 4.40, Figure 4.41 and Figure 4.42 the locations of the inflection points are plotted at varying the time. As for the specimens without shear reinforcement, at the beginning of the horizontal loading application (for time s=0) the inflection points are placed between 0.2-0.3 the span length. Then, during the application of the horizontal loading the inflection points move cyclically along the North-South direction.

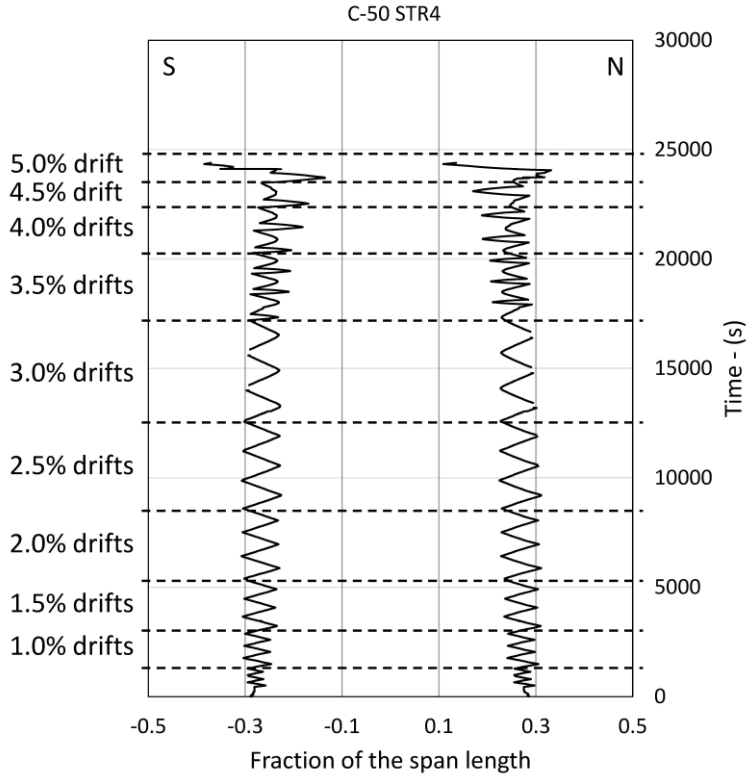

Figure 4.40 – Location of the inflection points during the cyclic loading test. Specimen C-50 STR4 investigated by Almeida et al. [2].

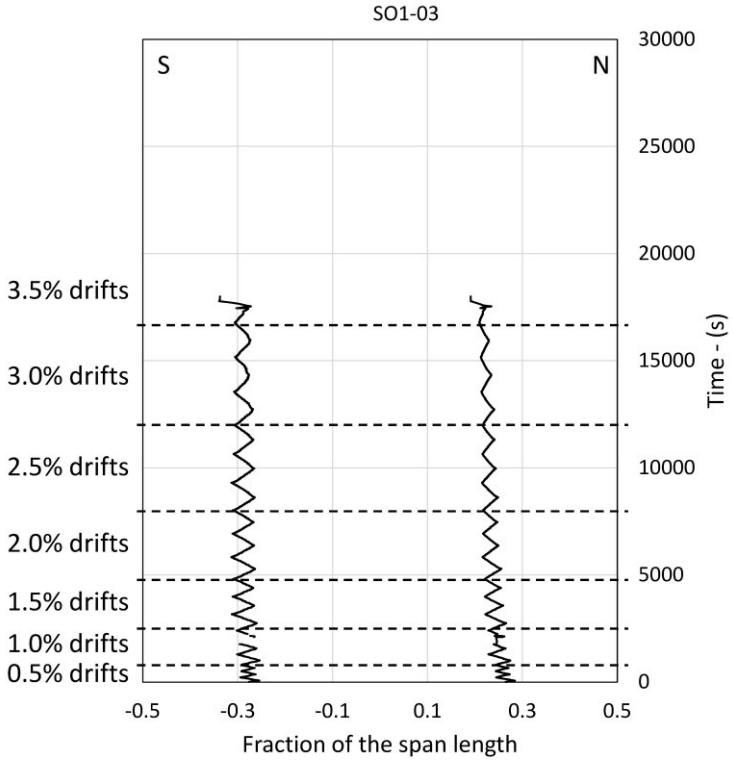

Figure 4.41 – Location of the inflection points during the cyclic loading test. Specimen SO1-03.

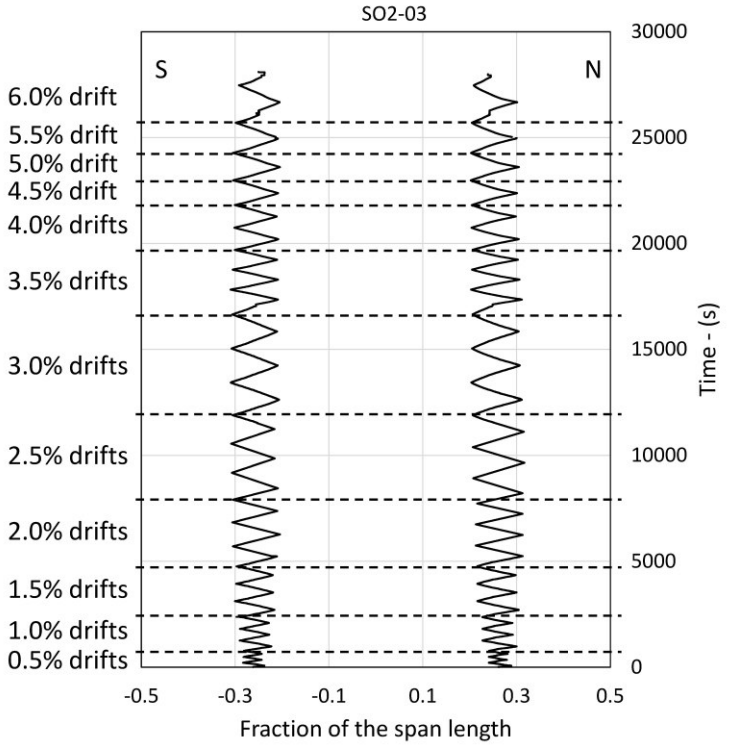

Figure 4.42 – Location of the inflection points during the cyclic loading test. Specimen SO2-03.

4.4.4 Lateral stiffness degradation

In Figure 4.43, Figure 4.44 and Figure 4.45 the lateral stiffness degradation of the specimens C-50 STR4, SO1-03 and SO2-03 are shown respectively.

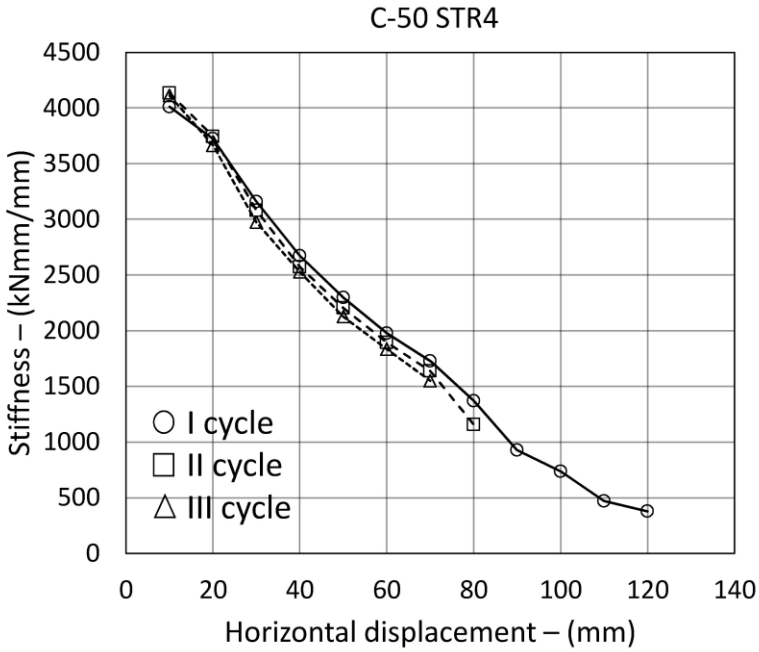

Figure 4.43 – Lateral stiffness degradation. Specimen C-50 STR4 investigated by Almeida et al. [2].

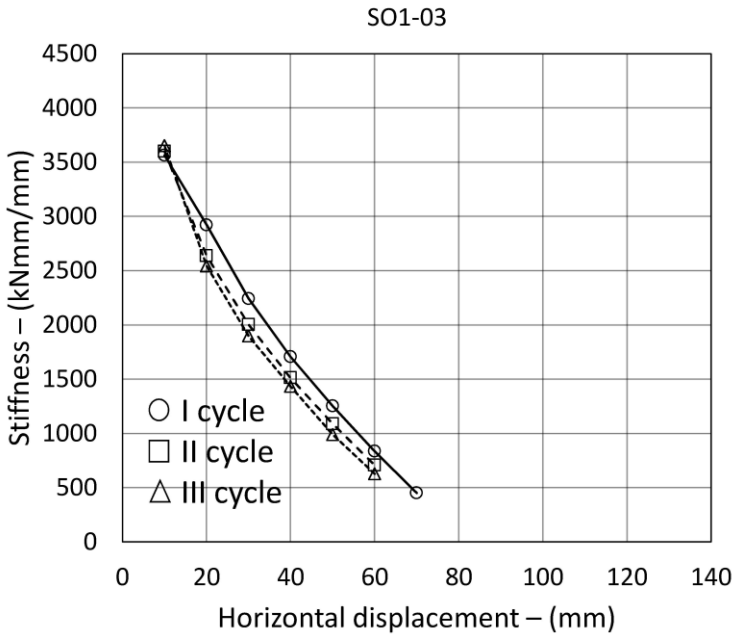

Figure 4.44 – Lateral stiffness degradation. Specimen SO1-03.

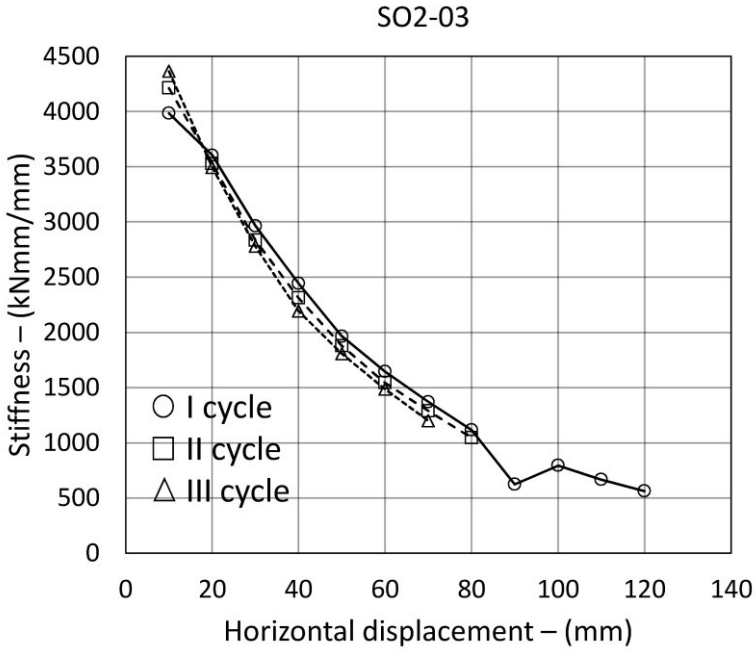

Figure 4.45 – Lateral stiffness degradation. Specimen SO2-03.

In this case, a clear tendency of lateral stiffness degradation is found for all the specimens. The specimen SO2-03 showed almost the same degradation of the lateral stiffness provided by the specimen C-50 STR4.

Conversely, the specimen SO1-03 showed a faster degradation of the lateral stiffness. The latter means that the opening placed along the horizontal loading direction provides a higher detrimental effect when compared to the opening placed in transverse direction.

The reduction of the lateral stiffness for all the specimens achieved the 80%-90% of the initial lateral stiffness.

4.4.5 Equivalent viscous damping ratio

The evolution of the equivalent viscous damping ratio is provided in Figure 4.46, Figure 4.47 and Figure 4.48. For high value of horizontal displacement, a clear tendency of damping increasing at horizontal drift increasing is found. However, for drift lower than 1% (displacement lower than 20 mm) the specimen C-50 STR4 provided a local reduction of the damping ratio.

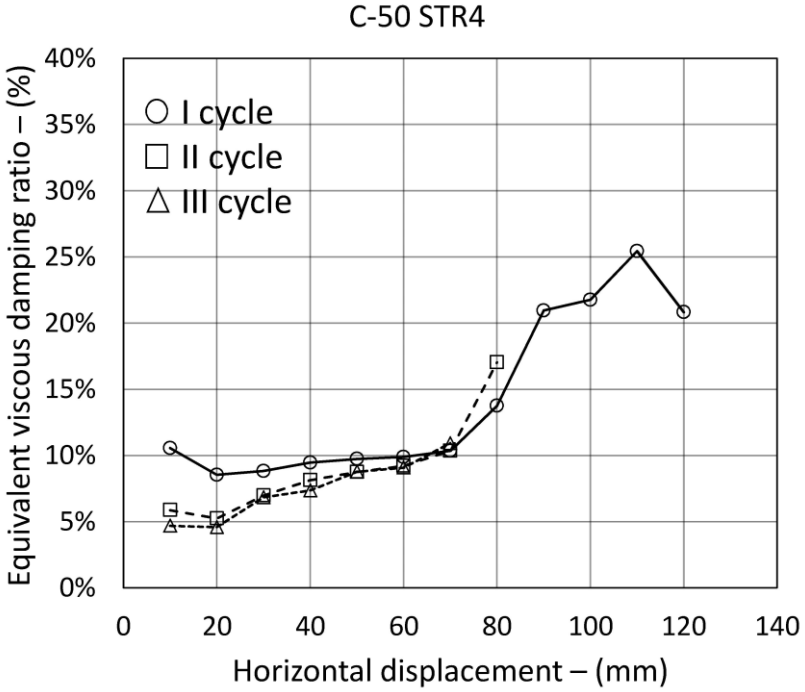

Figure 4.46 – Equivalent viscous damping ratio. Specimen C-50 STR4 investigated by Almeida et al. [2].

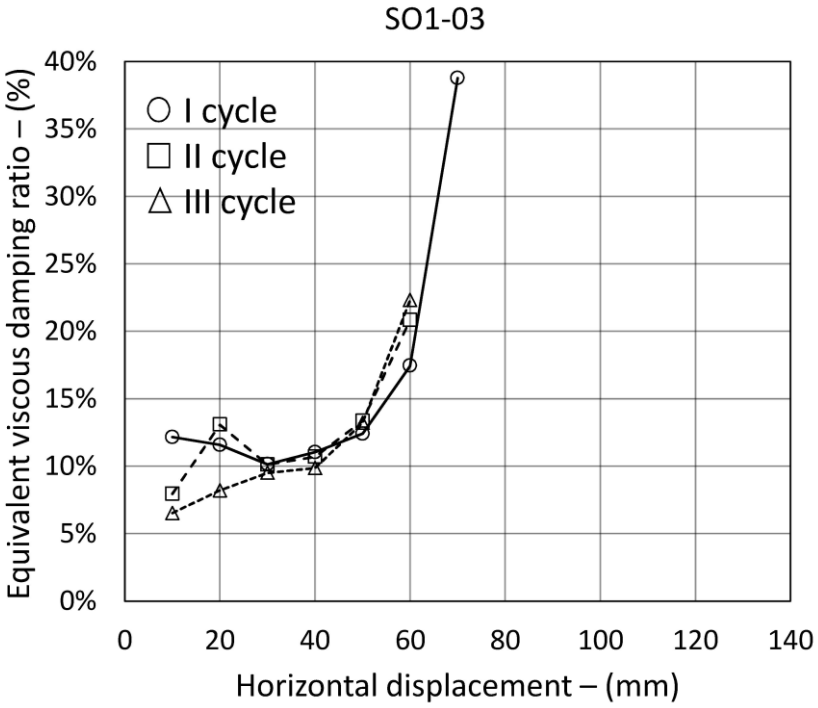

Figure 4.47 – Equivalent viscous damping ratio. Specimen SO1-03.

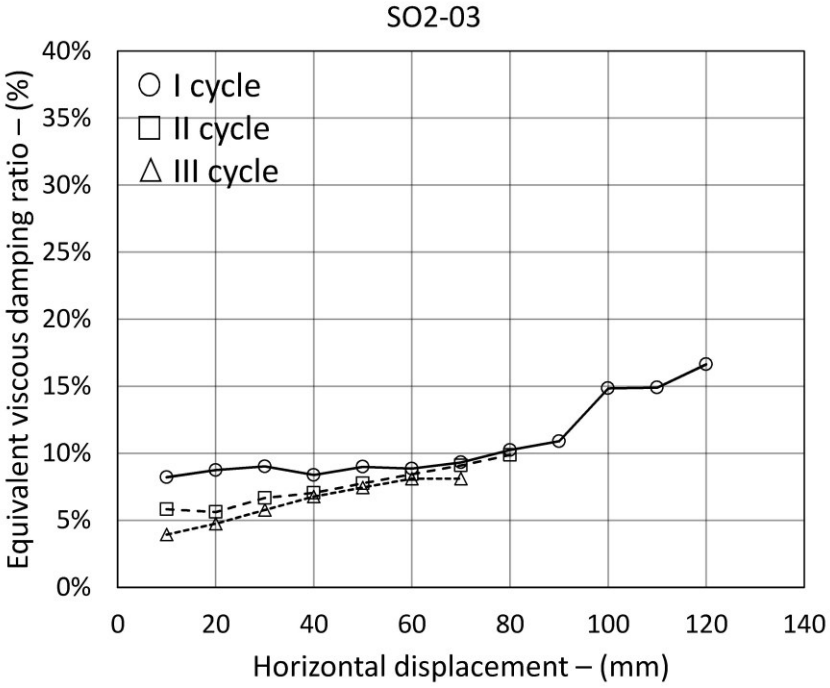

Figure 4.48 – Equivalent viscous damping ratio. Specimen SO2-03.

The specimen SO1-03 provided a huge increase of the equivalent viscous damping ratio between the 3% and the 3.5% of horizontal drift. Indeed, for a drift of 3.5% the specimen SO1-03 failed by punching. Conversely the other specimens showed a more progressive increase of the damping ratio. In particular the specimen SO2-03 provided very stable load cycles with low dissipation of energy when compared to the others.

4.5 Discussion

4.5.1 Gravity loading tests

From the gravity loading tests some contradictory results arose, the specimen SO1-01 showed a sensible reduction of the punching strength due to the presence of the opening when compared to the reference slab MLS, while the specimen SO2-01 apparently was not affected by the opening.

The failure load predictions calculated according to EC2-2004 are accurate excepted for the specimen SO2-01. In this case the ratio between experimental and theoretical punching strength results equal to $V_{exp}/V_{th} = 1.26$. The experimental stress at failure ($V_{exp}/b_0 \cdot d$) calculated for the specimen SO2-01 resulted higher than the others. This anomaly results even more evident if the dependence from the concrete compressive strength (f_{cm}) is removed. Considering the ratio $V_{exp}/b_0 \cdot d \cdot f_{cm}^{1/3}$ the specimens MLS and SO1-01 provide almost the same results while the specimen SO2-01 gives a higher value.

This incongruity is essentially due to an asymmetric distribution of vertical loading along the control perimeter. Since the vertical loads are applied along the north-south direction, the presence of the opening adjacent to the column on the east side is less influential than the opening placed on the north side. For this reason, the specimen SO2-01 provides higher specific punching strength than the other specimens. This issue is also addressed in the next chapter where the results of non-linear analysis are shown and discussed. However, some inevitable experimental scatter can also be present and it could be partially responsible of the higher punching strength provided by the specimen SO2-01.

Therefore, for vertical loading the presence of opening is found to be detrimental for the punching strength. The reduction of punching strength is easily accounted by reducing the control perimeter as suggested by the code provisions.

4.5.2 Combined gravity and horizontal loading tests without stirrups

Differently against gravity loading tests, when combined gravity and horizontal loading are applied to slab without shear reinforcement, the presence of the opening seems to have a lower influence in the punching failure. The specimens with opening SO1-02 and SO2-02 as the reference one C-50 failed by punching for a drift of 1%. The peak loads showed by the three specimens resulted very similar except for the maximum load exhibited by SO1-02 in south direction. The latter is the direct consequence of the opening presence. For southward

horizontal loading there is no effective top reinforcement passing through the column. Differently for northward horizontal loading two 12mm rebars placed on the top are effective thanks to hooked anchorage.

Therefore, when the opening is placed adjacent to the column along the horizontal loading direction, the only presence of the additional reinforcement on both sides of the column is not enough to allow the same punching strength of the reference specimen. On the contrary, the additional presence of effective reinforcement passing through the column allows for the same peak load of the reference specimen. The effectiveness of the top reinforcement anchored in the column is allowed only when the horizontal loading is directed to the opening.

For this reason, when the horizontal loading is northward the peak loads provided by the three specimens are almost the same, while for southward drift the specimen SO1-02 resulted in a lower maximum horizontal loading.

It is important to observe that the vertical loading distribution is less effective for combined gravity and horizontal loading than for vertical loading only. Indeed, in this case the specimen SO2-02 provided the same punching strength of SO1-02. Except for the completion of two cycles more at 1.0% drift, the only difference against the specimen SO1-02 consisted in a symmetric behaviour with respect to the loading direction. The latter is explained by the fact that the top reinforcement passing through the column was not interrupted and the opening was placed along the transverse direction (East-West) allowing for a perfect symmetric response for longitudinal loading (North-South).

Currently the ACI code provisions only give design rules for slab-column connections under combined gravity and seismic loading. The European codes are thought for static actions, so are not useful for cyclic horizontal loading. In Figure 4.49 the experimental horizontal ultimate drifts (Δ_u) are plotted at varying the gravity shear ratio (GSR).

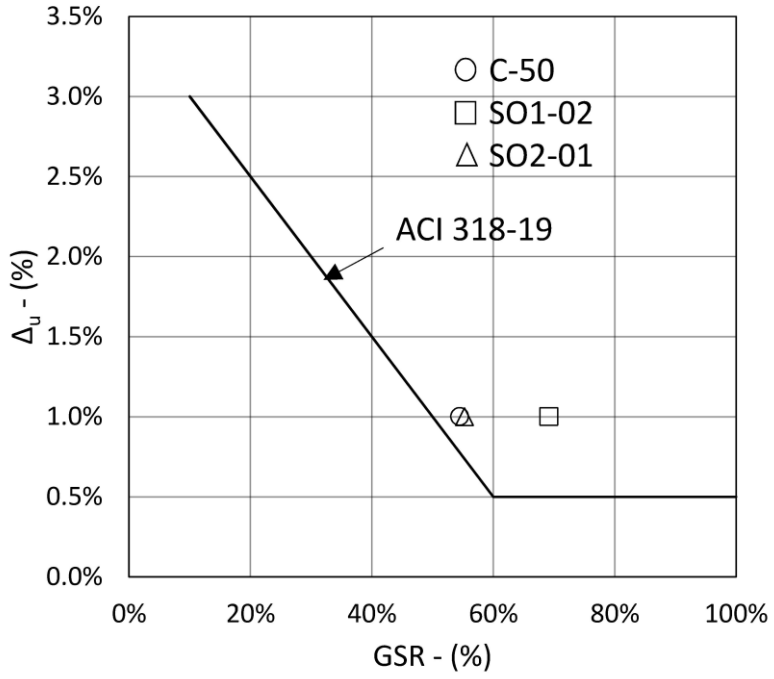

Figure 4.49 – Ultimate horizontal drift (Δ_u) at varying of the gravity shear ratio (GSR) – without shear reinforcement.

The vertical punching strength (V_R) of the specimens C-50, SO1-02 and SO2-02 are derived from those provided by the reference specimens accounting for the different concrete compressive strengths. For instance the vertical punching strength of C-50 is calculated as $V_R=V_{exp,MLS}\cdot(f_{cm,C\text{-}50}/f_{cm,MLS})^{0.41}$. Where the parameter 0.41 was proposed by Mamede et al. [5]: based in a potential regression analysis, they concluded that the punching capacity depends on average on the concrete strength to the power of 0.41. Therefore, the GSR is calculated according to these punching strengths as GSR = V_g/V_R. The experimental ultimate drifts are found on the right side of the curve proposed by ACI 381-19 [6]. According to this first analysis the American design method results effective.

4.5.3 Combined gravity and horizontal loading tests with stirrups

In case of combined gravity and horizontal loading applied to slab with shear reinforcement, the presence of the opening affects the flexural capacity and, as consequence, the punching strength of the connection. The lower maximum unbalanced moment exhibited by SO1-03 and SO2-03 when compared to C-50 STR4, proved the detrimental effect provided by the presence of the opening. This detrimental effect is emphasized for the specimen with the opening placed on the north side (SO1-03), in particular for southward horizontal loading. For

the same reasons discussed above, the flexural capacity of the specimen SO1-03 is higher for northward loading and lower for southward loading. However, even considering northward drifts the maximum unbalanced moment achieved by the specimen SO1-03 (83.3 kNm) resulted lower than that achieved by the specimen SO2-03 (100.4 kNm).

However, this difference in terms of flexural capacity has been probably accentuated by the higher gravity loading of the specimen SO1-03 ($V_{g,SO1-03}$ = 214 kN, $V_{g,SO2-03}$ = 194 kN) and by the higher cyclic damaging effect due to the presence of the opening on the north side.

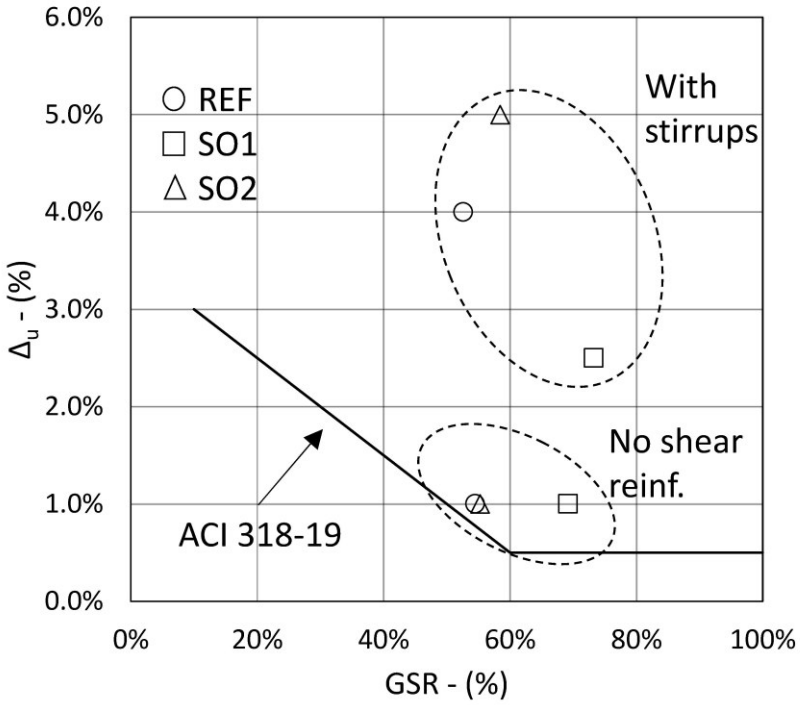

Figure 4.50 – Ultimate horizontal drift (Δ_u) at varying of the gravity shear ratio (GSR) – with and without shear reinforcement.

Differently from the unbalanced moment capacity, the ultimate drift capacity provided by the three specimens resulted similar. It could be said that the ductility of the slab-column connection is not much affected by the presence of the opening adjacent to the column.

4.6 Reference

[1] Almeida, AFO.; Inacio, MMG.; Lucio, VJG.; Ramos, AP.; Punching behaviour of RC flat slabs under reversed horizontal cyclic loading, Engineering Structures, 2016, Vol. 117: pp. 204–19.

[2] Almeida, A.; Marreiros, R.; Ramos, AP.; Ornelas, M.; Alcobia, B.; Behaviour of RC Flat Slabs with Stirrups under Reversed Horizontal Cyclic Loading, Magazine of Concrete

Research, 2019.

[3] CEN.; Eurocode 2: Design of concrete structures - Part 1-1: General rules and rules for buildings, Bruxelles: 2004.

[4] CEB/FIP.; Model Code 2010 - Volume 1, Bulletin 6, Lausanne, Switzerland: Internation Federation for Structural Concrete (fib); 2012.

[5] Mamede, N.; Ramos, A.; Faria, D.; Experimental and Parametric 3D Nonlinear Finite Element Analysis on Punching of Flat Slabs with Orthogonal Reinforcement, Engineering Structures, 2013, Vol. 48: pp. 442–57.

[6] American Concrete Institute.; Building Code Requirements for Structural Concrete (ACI 318-19), 2019.

5. NUMERICAL ANALYSIS

5.1 Introduction

In this chapter results of several numerical analyses are shown and discussed. The model calibration is performed using the experimental results of the specimen MLS, investigated by Almeida et al. [1] in the Lisbon setup, then the numerical model of the Lisbon setup is used to simulate the experimental tests of the present experimental campaign. Finally, starting from the calibrated model of the Lisbon setup, a new numerical model representing the slab-column connection is developed. According to this model the presence of the opening adjacent to the column is accounted for. Analyses are performed using the software ABAQUS.

5.2 Concrete damage plasticity (CDP)

The software ABAQUS adopts the Concrete Damage Plasticity (CDP) model which was developed by Lubliner et al. [2] and then was improved by Lee and Fenves to account for effects provided by cyclic loading [3]. The CDP model implemented in ABAQUS adopts the yield criterion proposed by Lubliner et al. [2] (Barcelona model) and accounts also for different evolution of damage in tension and compression as proposed by Lee and Fenves [3]. The yield function for the Barcelona model is:

$$F(\boldsymbol{\sigma}) = \frac{1}{1-\alpha}\left[\sqrt{3J_2} + \alpha I_1 + \beta\langle\sigma_{max}\rangle - \gamma\langle-\sigma_{max}\rangle\right] \tag{5.1}$$

The yielding condition is reached when:

$$F(\boldsymbol{\sigma}) = c(k) \tag{5.2}$$

where *c* is the cohesion. The evolution of the cohesion is determined by a plastic-damage-variable *k*. For undamaged condition k=0, the cohesion results equal to the initial yield strength in uniaxial compression f_{c0}. After that, due to strain-softening, the cohesion decreases, and it vanishes for *k*=1. When the cohesion reaches the maximum value, equation (5.2) describes the failure surface [2]. The plastic-damage-variable, for the uniaxial case is defined as:

$$k = \frac{1}{g}\int_0^{\varepsilon^p} \sigma \, d\varepsilon^p \tag{5.3}$$

where *g* corresponds to the area under the experimentally derived stress-plastic strain (σ-ε^p) diagrams for uniaxial tension (g_t) and compression (g_c) (Figure 5.1).

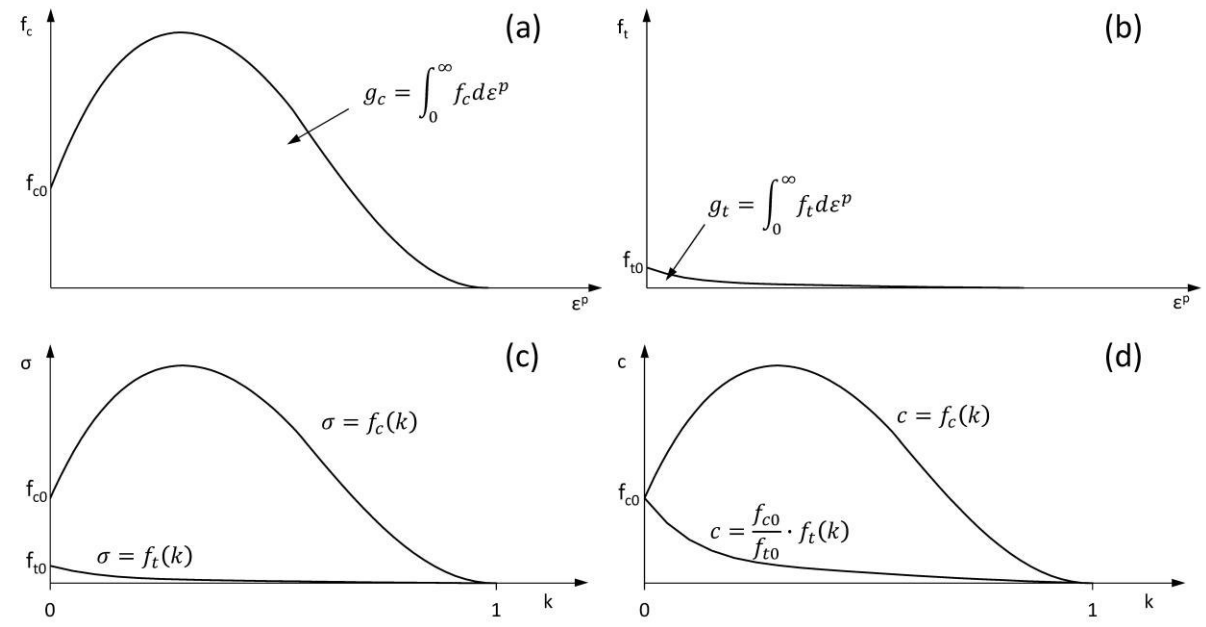

Figure 5.1 – Uniaxial curves: (a) compressive stress-plastic strain curve, (b) tensile stress-plastic strain curve, (c) compressive and tensile-plastic damage variable curves, (d) compressive and tensile cohesion-plastic damage variable curves (adapted from [2])

The curve (b) could be converted into a function $\sigma=f_t(k)$, such that $f_t(0)=f_{t0}$ and $f_t(1)=0$. For the compression case results $\sigma=f_c(k)$, such that $f_c(0)=f_{c0}$ and $f_c(1)=0$. However, the cohesion

is not taken as a function of the damage parameter k, but it is assumed to be an internal variable governed by the rate equation. For the uniaxial case the rate equation of the damage is obtained by deriving equation (5.3):

$$\dot{k} = \frac{1}{g} f(k) \dot{\varepsilon}^p \tag{5.4}$$

for the multiaxial state of stresses, the rate equation is given in terms of principal stress and plastic strain:

$$\dot{k} = \frac{r(\boldsymbol{\sigma})}{g_t} f_t(k) \dot{\varepsilon}_1^p - \frac{1 - r(\boldsymbol{\sigma})}{g_c} f_c(k) \dot{\varepsilon}_3^p \tag{5.5}$$

where r(σ) is a weight factor defined as:

$$r(\boldsymbol{\sigma}) = \frac{\sum_{i=1}^{3} \langle \sigma_i \rangle}{\sum_{i=1}^{3} |\sigma_i|} \tag{5.6}$$

and $\langle \sigma_i \rangle = ½ (|\sigma_i| + \sigma_i)$. Therefore, the rate equation of the cohesion is given by:

$$\dot{c} = c \left[\frac{r(\boldsymbol{\sigma})}{f_t(k)} f_t'(k) - \frac{1 - r(\boldsymbol{\sigma})}{f_c(k)} f_c'(k) \right] \dot{k} \tag{5.7}$$

Actually, as mentioned above, Lee and Fenves [3] introduced two different damage variable $\boldsymbol{k}(k_t,k_c)$ accounting for two different cohesion values in tension c_t and compression c_c respectively, thus the yield function becomes:

$$F(\boldsymbol{\sigma}, \boldsymbol{k}) = \frac{1}{1 - \alpha} \left[\sqrt{3J_2} + \alpha I_1 + \beta(\boldsymbol{k}) \langle \sigma_{max} \rangle - \gamma \langle -\sigma_{max} \rangle \right] - c_c(\boldsymbol{k}) \tag{5.8}$$

where:

$$\alpha = \frac{(f_{b0}/f_{c0}) - 1}{2(f_{b0}/f_{c0}) - 1} \tag{5.9}$$

$$\beta(\boldsymbol{k}) = \frac{c_c(\boldsymbol{k})}{c_t(\boldsymbol{k})}(1-\alpha) - (1-\alpha) \tag{5.10}$$

$$\gamma = \frac{3(1-K_c)}{2K_c - 1} \tag{5.11}$$

$$K_c = \frac{\left(\sqrt{J_2}\right)_{TM}}{\left(\sqrt{J_2}\right)_{CM}} \tag{5.12}$$

where σ_{b0}/σ_{c0} is the ratio of initial equibiaxial compressive yield stress to initial uniaxial compressive yield stress and K_c is the ratio between the square root of the second stress invariant on the tensile meridian, to that on the compressive meridian. If degradation of the elastic stiffness is not accounted for, the elastic-plastic strain decomposition could be written as:

$$\boldsymbol{\varepsilon} = \mathbf{D}^{-1}\boldsymbol{\sigma} + \boldsymbol{\varepsilon}^{\boldsymbol{p}} \tag{5.13}$$

where **D** is the elastic stiffness tensor, the flow rule governs the plastic strain evolution:

$$\dot{\boldsymbol{\varepsilon}}^{\boldsymbol{p}} = \dot{\lambda}\boldsymbol{g} = \dot{\lambda}\frac{\partial G}{\partial \boldsymbol{\sigma}} \tag{5.14}$$

$\boldsymbol{g}$ is the plastic flow vector normal to the plastic potential surface G and $\dot{\lambda}$ is the plastic loading factor. The plastic potential function implemented in ABAQUS is the Drucker-Prager hyperbolic function [4]:

$$G(\boldsymbol{\sigma}, \Psi) = \sqrt{(\epsilon f_{t0}\tan\Psi)^2 + q^2} - p\tan\Psi \tag{5.15}$$

and Ψ is the dilation angle that indicates the direction of the plastic flow in the p-q plane and ε is the flow potential eccentricity that defines the rate at which the flow potential approaches the asymptote.

Therefore, the evolution of the failure surface is governed by two hardening variables: the plastic strains in tension and compression. The softening branches that characterize the uniaxial concrete behaviour both in tension and compression are determined according to the fracture energy (G_f) and the crushing energy (G_c), respectively. However, as highlighted by

Lubliner et al. [2], if the fracture energy (G_f) is usually considered as a property of the material, the same importance is not given to the crushing energy. First, because the fracture energy results fundamental whenever the shear strength comes into play, while the crushing energy has not the same importance. Furthermore, the determination of the crushing energy is quite uncertain since it is affected by the specimen slenderness and by the boundary restraint [5],[6]. For these reasons the softening behaviour in compression is usually provided without an explicit reference to the crushing energy.

5.2.1 Main parameters

Parameters that come into play in the CDP model are several, however for some of them default values are usually assumed. The flow potential eccentricity is usually placed equal to ε=0.10 [7], the ratio of initial equibiaxial compressive yield stress to initial uniaxial compressive yield stress is assumed equal to σ_{b0}/σ_{c0}=1.16 according to Kupfer et al. [8], while the ratio of the second stress invariant on the tensile meridian to that on the compressive meridian is usually placed equal to K_c=2/3 [4]. Therefore, besides the two softening laws in tension and compression, the remaining parameter to be defined is the dilation angle (Ψ). In this work the concrete behaviour under uniaxial compression is subdivided into four parts (Figure 5.2): A-B linear-elastic behaviour, B-C non-linear behaviour according to Eurocode 2 – 2004 (EC2) [9], C-D sinusoidal behaviour and D-E linear behaviour until the ultimate strain. The first part A-B is defined according to EC2 [9], the linear behaviour is assumed until $0.4 \cdot f_{cm}$ adopting a secant elastic modulus that results slightly lower than the initial tangential modulus E_{cm}. The non-linear behaviour of the B-C part is given by the following expression:

$$\sigma_c(\varepsilon_c) = f_{cm} \cdot \frac{k \cdot \eta - \eta^2}{1 + (k-2) \cdot \eta} \, , \varepsilon_{cB} < \varepsilon_c \leq \varepsilon_{cC} \tag{5.16}$$

where $\sigma_{cB} = \sigma_c(\varepsilon_{cB}) = 0.4 \cdot fcm$, $\eta = \varepsilon_c/\varepsilon_{c1}$, and $k = 1.05 \cdot E_{cm} \cdot |\varepsilon_{c1}|/f_{cm}$, where ε_{c1} is the strain in correspondence of the stress peak f_{cm}, determined according to [10]. Then the compression stress-strain curve is extended beyond the nominal ultimate strain (ε_{cC}= 3.5 ‰), according to Pavlovic et al. [11], adopting a sinusoidal curve:

$$\sigma_c(\varepsilon_c) = f_{cm} \cdot \left[\frac{1}{\beta} - \frac{\sin(\mu^{\alpha_{tC}} \cdot \alpha_{tD} \cdot \pi/2)}{\beta \cdot \sin(\alpha_{tD} \cdot \pi/2)} + \frac{\mu}{\alpha} \right] \, , \varepsilon_{cC} < \varepsilon_c \leq \varepsilon_{cD} \tag{5.17}$$

where $\mu = (\varepsilon_c - \varepsilon_{cC})/(\varepsilon_{cD} - \varepsilon_{cC})$, $\alpha = f_{cm}/f_{cD}$, $\beta = f_{cm}/f_{cC}$, α_{tD} and α_{tE} are factors affecting the tangent angle in points D and E. The behaviour of the part C-E is assumed to be linear:

$$\sigma_c(\varepsilon_c) = [f_{cD} \cdot (\varepsilon_{cE} - \varepsilon_c) + f_{cE} \cdot (\varepsilon_c - \varepsilon_{cD})]/(\varepsilon_{cE} - \varepsilon_{cD}) \, , \varepsilon_{cD} < \varepsilon_c \leq \varepsilon_{cE} \tag{5.18}$$

In this work, the residual compressive strengths f_{cD} and f_{cE} are assumed equal to 1/70 and 1/100 of the average compressive strength f_{cm}, respectively, and strains in correspondence of points D and E are assumed equal to ε_{cD}=0.6% and ε_{cD}=1%, respectively. Furthermore, factors α_{tD} and α_{tE} are assumed equal to 1 to allow for smooth transitions at points C and D (Figure 5.2).

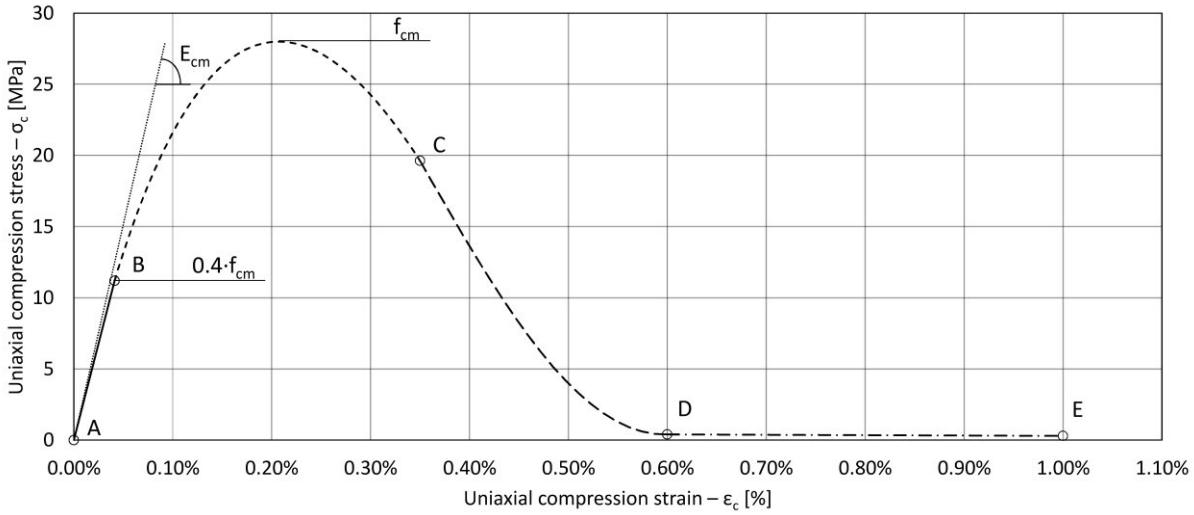

Figure 5.2 – Stress-strain relationship for concrete under uniaxial compression, C20/25

The proposed stress-strain relationship is quite similar to that provided by Eurocode 2 – 2004 [9] except for the gradual loss of strength from point C to point D and for the presence of the point E with a residual strength of one hundred of f_{cm}. The latter is needed to avoid potential numerical problems: even when this small residual strength is not provided, ABAQUS enforces a lower limit on the post-failure stress equal to one hundred of the initial failure stress [4]. With regards to the softening behaviour in tension, the Hordijk's model [12] is assumed. The latter has been preferred to others since it gives a very smooth curve that allows for numerical problems to be reduced. Furthermore, it only requires values of the concrete tensile strength and fracture energy (G_F) to be defined:

$$\frac{\sigma_t}{f_{ctm}} = \left[1 + \left(c_1 \cdot \frac{w}{w_c}\right)^3\right] \cdot e^{-\left(c_2 \cdot \frac{w}{w_c}\right)} - \frac{w}{w_c} \cdot (1 + c_1^3) \cdot e^{-(c_2)} \tag{5.19}$$

where c_1=3, c_2=6.93 and w_c=5.14·G_F/f_{ctm}. The stress-crack opening relationship under uniaxial tension is shown in Figure 5.3, also in this case ABAQUS enforces a lower limit equal to f_{ctm}/100.

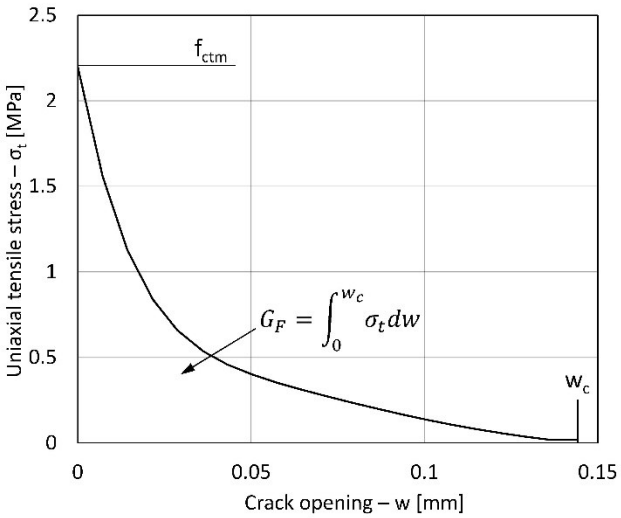

Figure 5.3 – Stress-crack opening relationship for concrete under uniaxial tension, C20/25

Finally, according to above hypotheses, main parameters are the dilation angle (Ψ) and the fracture energy (G_F). The dilation angle governs the plastic volumetric changes and deeply affects the non-linear response of concrete structures. Particularly, it predominantly comes into play when failure is governed by shear or punching-shear. In literature values of the dilation angle for concrete range from 15° to 55°. Lubliner et al. [2] suggested Ψ=30°, however when the dilation angle is calibrated on shear tests or punching tests it generally varies between 35° and 40° (Table 5.1).

Table 5.1 – Literature values of dilation angle for concrete calibrated on shear or punching tests.

References	Dilation angle Ψ
Jankowiak and Lodygowski [13]	38°
Pavlović et al. [11]	36°
Genikomsou and M. A. Polak [14]	40°
Bompa and T. Onet [15]	40°
Najafgholipour et al. [16]	35°
Nana et al. [17]	37°
Russell et al. [18]	35°
Navarro et al. [19]	36°

In the following the dilation angle is assumed equal to Ψ=38°, which is intermediate between 35° and 40°, so the fracture energy is the only parameter to be calibrated. The fracture energy of concrete G_F is the energy required to propagate a tensile crack of unit area. This amount mainly depends on water-cement ratio, maximum aggregate size and age of concrete. Furthermore, its experimental determination is affected by curing conditions and specimen size. The latter are the cause of a significant scattering between the fracture energy values experimentally determined. However, a tendency of fracture energy increasing with compressive strength is usually observed [20]. For numerical analyses the fracture energy is usually calculated, starting from the concrete compressive strength, according to Model Code 1990 [21] or Model Code 2010 [22].

In the following the fracture energy is calibrated according to experimental results provided by the specimen MLS investigated by Almeida et al. [1]. Then the model is used to replicate the experimental results of the current experimental campaign. Since the concrete compressive strength of each specimen is different from that one provided by MLS, the calibrated value of fracture energy was updated considering the power law provided Model Code 1990 [21] $G_F = G_{F,MLS} \cdot (f_c/f_{c,MLS})^{0.7}$.

The numerical model is calibrated on the results provided by a specimen without openings in order to obtain a more consistent analysis of the specimen with openings.

5.3 Model calibration

As mentioned above the Lisbon setup was developed by Almeida et al. [1] at the NOVA School of Science and Technology and represents one of the few attempts to comply the boundary conditions of a continuous flat slab subjected to combined gravity and horizontal loading. This setup allows equal vertical displacements and equal rotations at the opposite N-S slab borders. These boundary conditions are provided by means of two different systems (Figure 5.4). The equality of border's vertical displacements is fulfilled by a passive mechanical see-saw-like system (Blue system). The equality of border's rotations is fulfilled by a system consisting in a double pinned steel frame suspended on slab's border by two vertical fixed columns (Green system).

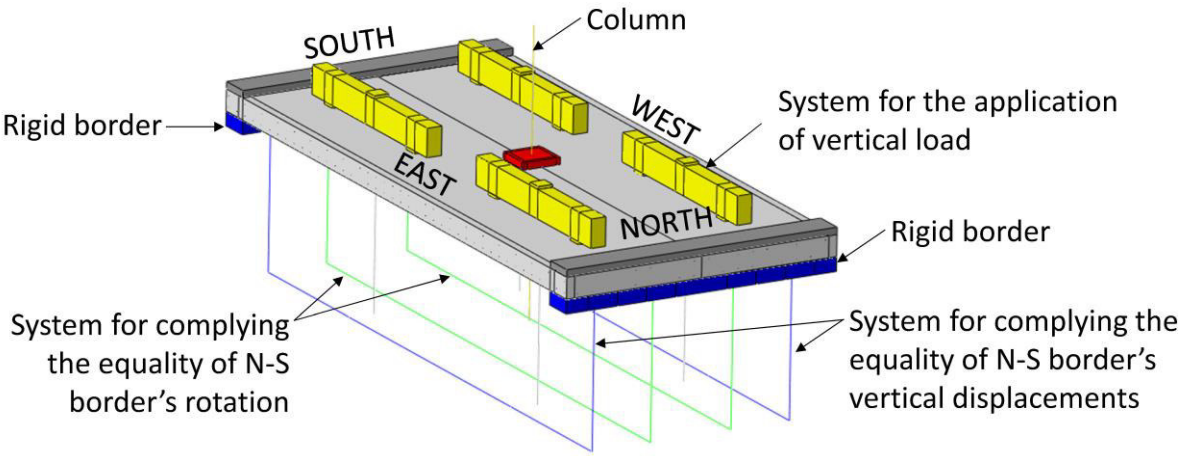

Figure 5.4 – Numerical model of the Lisbon setup.

The vertical load is applied through 200x200 mm steel plates to the slab's top surface in eight points to better approximate a uniformly distributed load. For this to be accomplished, a self-balanced structure to apply the vertical load was created using a system of spreader beams and steel tendons that follows the slab horizontal deformation without inducing unintended horizontal forces (Figure 5.4).

After a mesh sensitivity analysis, the size of brick elements was limited to 30 mm, so eight mesh elements were used through the thickness of the slab (31.25x30x30 mm). As explained in §5.2.1, the only parameter to be calibrated is the fracture energy. The calibration was performed starting from experimental results of the test MLS performed by Almeida et al. [1] then the reliability of the calibrated model was checked with experimental tests of the present experimental campaign.

The matching between experimental and numerical results is monitored by means the control points shown in Figure 5.5.

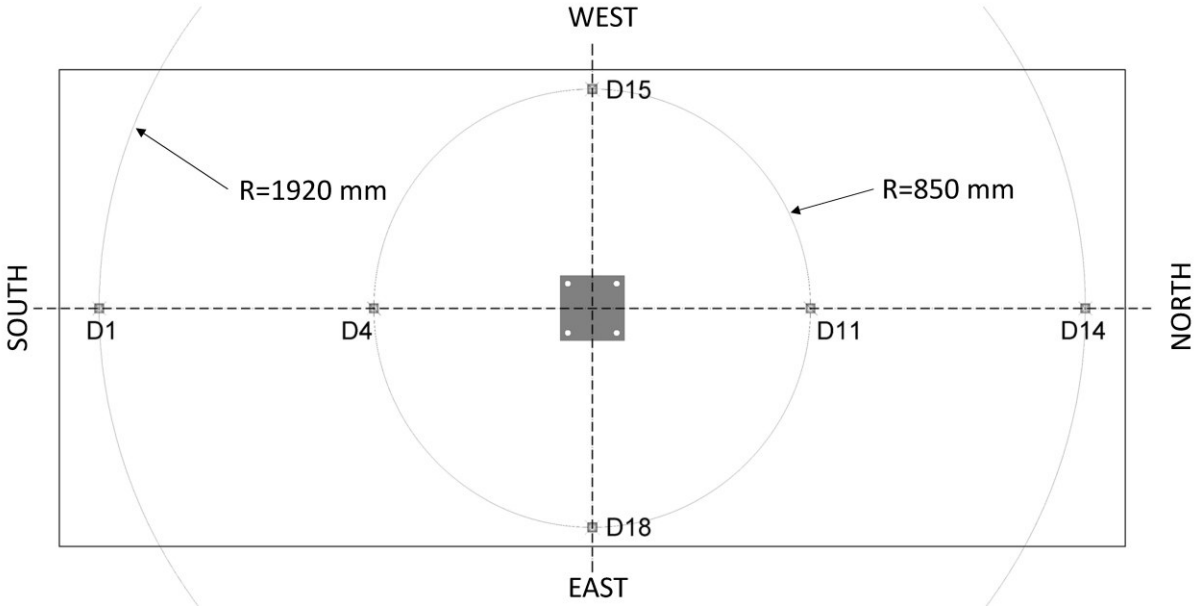

Figure 5.5 – Control points.

As mentioned above the specimen MLS was tested under monotonic vertical loading until failure. In Figure 5.6 both experimental and numerical load-displacement curves of the control point D1 are provided. The fracture that provided the best matching between FEM and experimental test resulted equal to $G_{F,MLS}$ = 67 N/m.

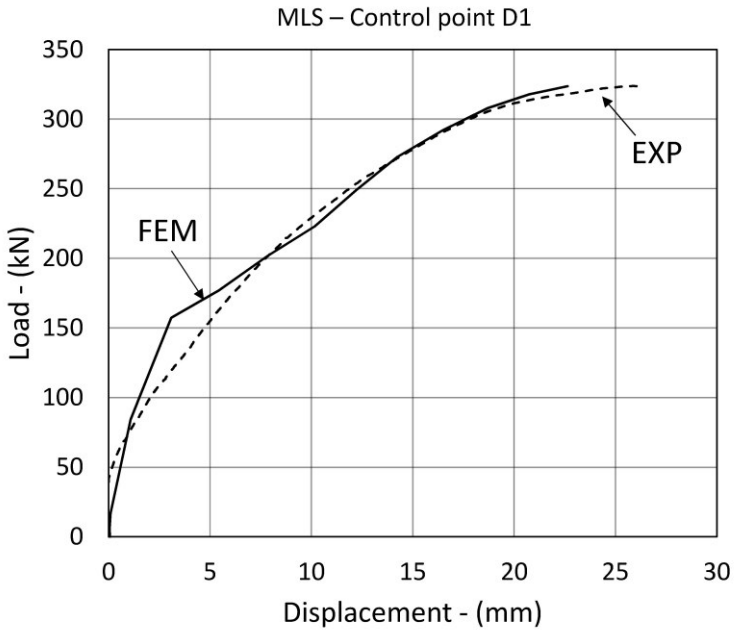

Figure 5.6 – Specimen MLS, load-displacement curves of control point D1.

The calibrated numerical model provides almost the same punching load of the experimental test, being also the ductility results very similar. The only difference is placed in the behaviour before cracking, the finite element model exhibits a stiffer behaviour than the test. In Figure 5.7 the comparison of load-displacement curves of control points D4 and D18 is provided.

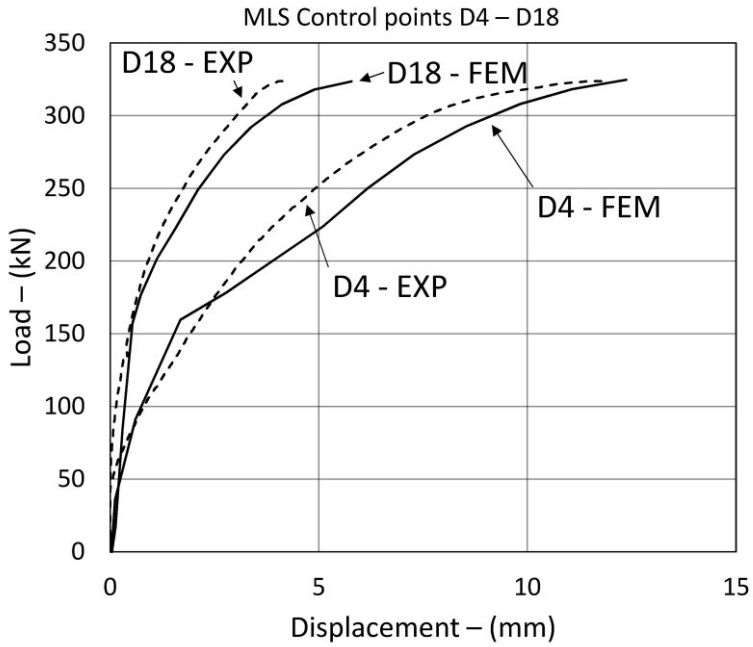

Figure 5.7 – Specimen MLS, load-displacement curves of control points D4 and D18.

For these points, the agreement between experimental and numerical load-displacement curves is even better. Both load-displacement curves D4 and D18 are very well replicated by the numerical model. Furthermore, it is important to observe that D4 provides much greater displacement than D18. This non-symmetric behaviour was expected and for that reason required to investigate the effects of gravity loading distribution on punching strength.

5.4 Comparison with experimental results

In the following the calibrated model is used to simulate experimental tests of the present experimental campaign. Firstly, the comparison between numerical and experimental tests is provided for specimens subjected to vertical loading only, then for specimens subjected to combined gravity and horizontal loading with and without shear reinforcement.

5.4.1 Vertical loading

In Table 5.2 a comparison between numerical (V_{FEM}) and experimental (V_{exp}) failure loads of specimens subjected to vertical loading only is provided. Numerical (δ_{FEM}) and experimental (δ_{exp}) ultimate displacements evaluated in correspondence of transducer D1 are also shown.

Table 5.2 – Gravity loading tests – comparison between numerical and experimental results.

Specimen	Opening size (mm)	Opening position	V_{exp} (kN)	V_{FEM} (kN)	δ_{exp} (mm)	δ_{FEM} (mm)	V_{exp}/V_{FEM} (-)	$\delta_{exp}/\delta_{FEM}$ (-)
SO1-01	200x200	North	299	256	17.5	13.8	1.168	1.268
SO2-01	200x200	East	341	314	21.7	23.3	1.086	0.931
MLS*	-	-	324	324	25.9	22.6	1.000	1.146
						Avg	1.085	1.115
						COV	7.74%	15.23%

* Almeida et al. [1]

The correspondence between experimental and numerical failure loads is quite accurate the average ratio between experimental and numerical failure loads results equal to 1.085 with a coefficient of variation (COV) equal to 7.74%. The agreement between ultimate displacements is lower; the average ratio between experimental and numerical ultimate displacements results equal to 1.115 with a coefficient of variation (COV) equal to 15.23%. In Figure 5.8 and Figure 5.9 the comparison between numerical and experimental load displacement curves of specimens SO1-01 and SO2-01, respectively, are shown.

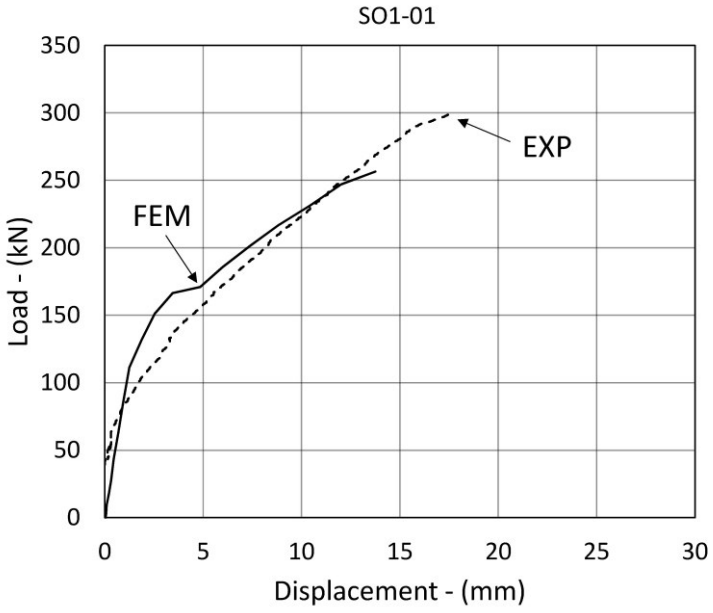

Figure 5.8 – Specimen SO1-01: Load-displacement curves.

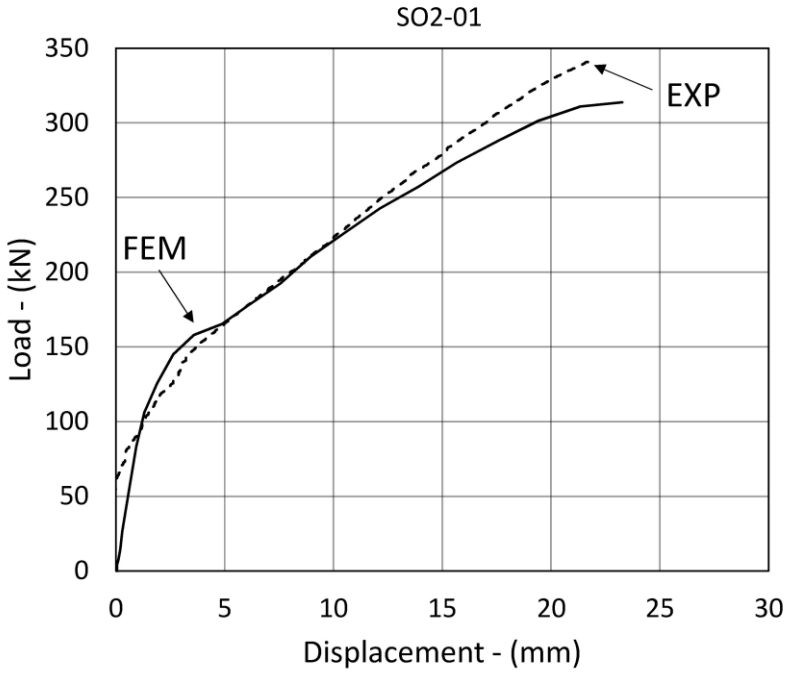

Figure 5.9 – Specimen SO2-01: Load-displacement curves.

5.4.2 Combined vertical and horizontal cyclic loading - without shear reinforcement

Experimental tests including both gravity and horizontal loading are performed adopting a constant vertical load combined with cyclic horizontal drifts. Since the numerical analyses are performed adopting a monotonic horizontal loading, instead of cyclic drifts, the capacity provided by the numerical model is expected to be higher than the experimental since in the numerical model the degradation of the punching strength due to the cyclic drifts is neglected. For this reason, the comparison between numerical and experimental results should be intended just for a qualitative matching between the backbone curves.

Indeed, in general the backbone curve provided by a monotonic test is expected to follow that provided by the cyclic test, the difference consists in the higher capacity provided by the monotonic test compared to the cyclic test [23].

In Figure 5.10 the comparison between numerical and experimental curves is provided for the specimen C-50 investigated by Almeida et al. [1]. The matching between the load-displacement curves is convincing and as expected the capacity provided by the numerical model results higher. The same result is found for the specimen SO1-02 when northward drifts are considered (Figure 5.11).

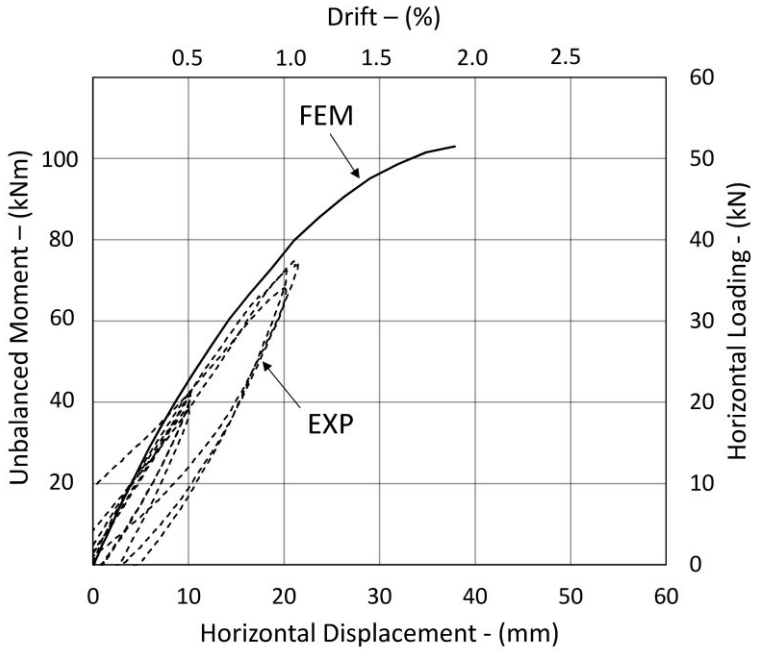

Figure 5.10 – Specimen C-50 investigated by Almeida et al. [1]: Load-deformation curves.

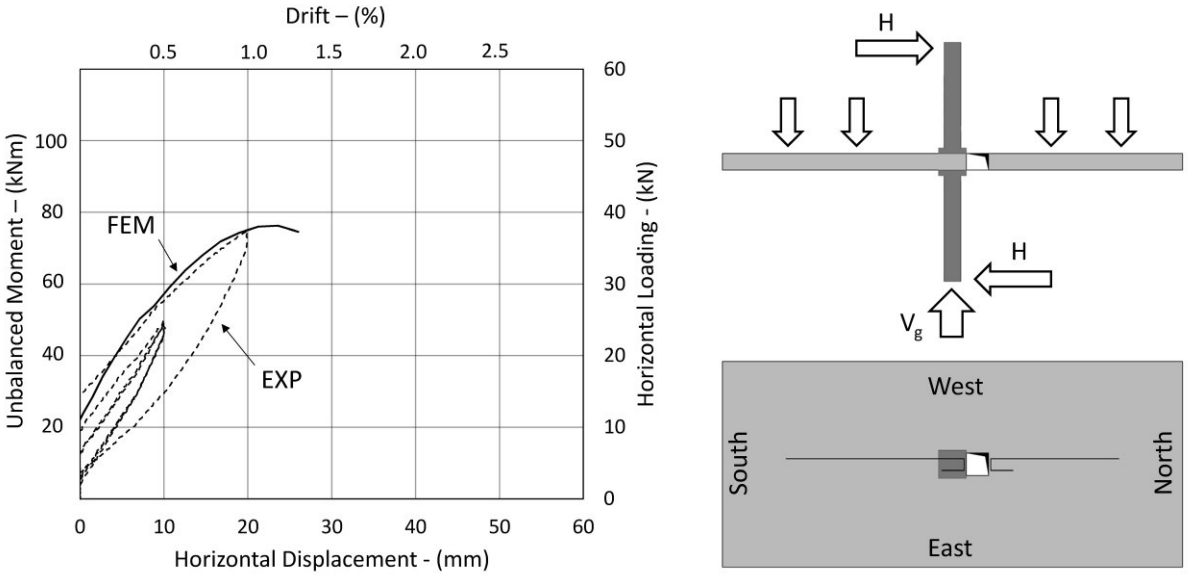

Figure 5.11 – Specimen SO2-01 northward loading: Load-deformation curves.

For southward loading the comparison provided in Figure 5.12 shows that in this case the numerical model underestimates the capacity of the specimen. In this case the numerical model is highly affected by the presence of the opening, more than the experiment.

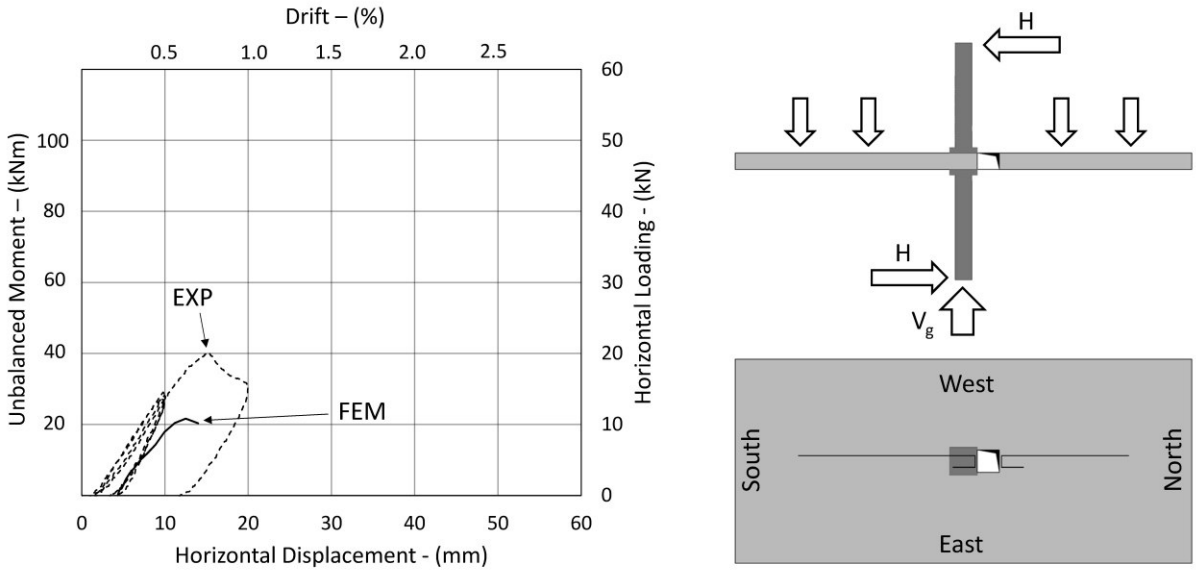

Figure 5.12 – Specimen SO2-01 southward loading: Load-deformation curves.

Then the comparison between numerical and experimental backbone curves, referred to the specimen SO2-02, is provided (Figure 5.13). In this case the matching between the curves is very good and the capacity provided by the numerical model results higher than that provided by the experiment as expected.

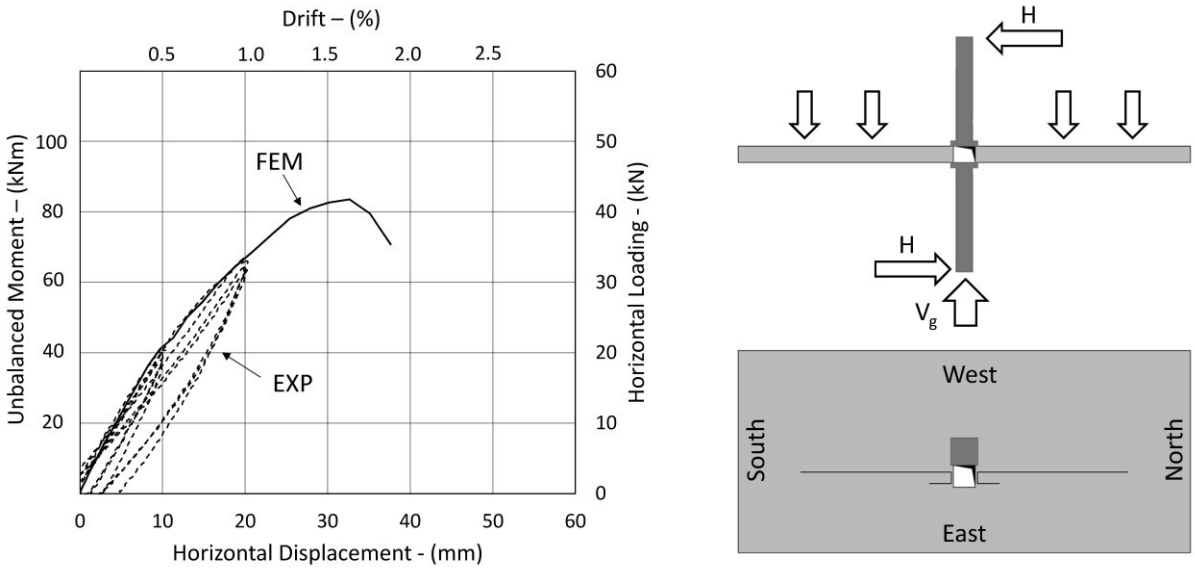

Figure 5.13 – Specimen SO2-02: Load-deformation curves.

5.4.3 Combined vertical and horizontal loading - with shear reinforcement

As for the previous case, numerical analyses are performed adopting a monotonic horizontal loading, while experiments were performed under cyclic horizontal drift. However, in this case thanks to the presence of shear reinforcement, specimens reached the flexural capacity, therefore the comparison between the experimental and numerical maximum unbalanced moment could be performed.

Conversely the ultimate horizontal drifts achieved experimentally results lower than that calculated by means of numerical analysis, since the first is affected by the higher degradation of the punching capacity due to cyclic drifts.

In Table 5.3 a comparison between numerical (M_{FEM}) and experimental (M_{exp}) maximum unbalanced moments is provided.

Table 5.3 – Combined gravity and horizontal loading tests – specimens with shear reinforcement – comparison between numerical and experimental results.

Specimen	Opening size (mm)	Opening position	Loading direction	M_{exp} (kNm)	M_{FEM} (kNm)	M_{exp}/M_{FEM} (-)
C-50 STR4*	-	-	-	124.3	140.7	0.883
SO1-03	200x200	North	Southward	53.7	55.7	0.964
			Northward	83.3	103.4	0.806
SO2-03	200x200	East	-	98.8	105.4	0.937
					Avg	0.898
					COV	7.79

* Almeida et al. [24].

The correspondence between experimental and numerical failure loads is quite accurate, the average ratio between experimental and numerical maximum unbalanced moments results equal to 0.898 with a coefficient of variation (COV) of 7.79%.

In Figure 5.14 the comparison between experimental and numerical backbone curves is provided for the specimen C-50 STR4 investigated by Almeida et al. [24]. The matching between the backbone curves is very high until the flexural plateau, then the experimental curve drops down due to the detrimental effect of the cyclic loading while the numerical model attains larger horizontal displacements and higher unbalanced moments.

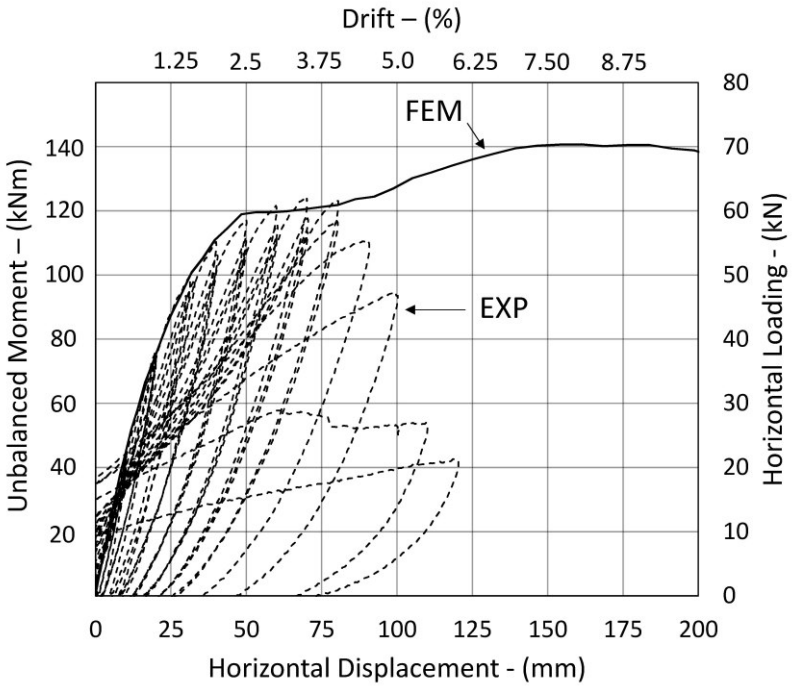

Figure 5.14 – Specimen C-50 STR4: Load-deformation curves.

In Figure 5.15 the comparison between experimental and numerical backbone curves of specimen SO1-03, for northward loading is proposed. In this case the matching between the curves is less accurate, the flexural plateau achieved by the numerical model is higher than that achieved experimentally.

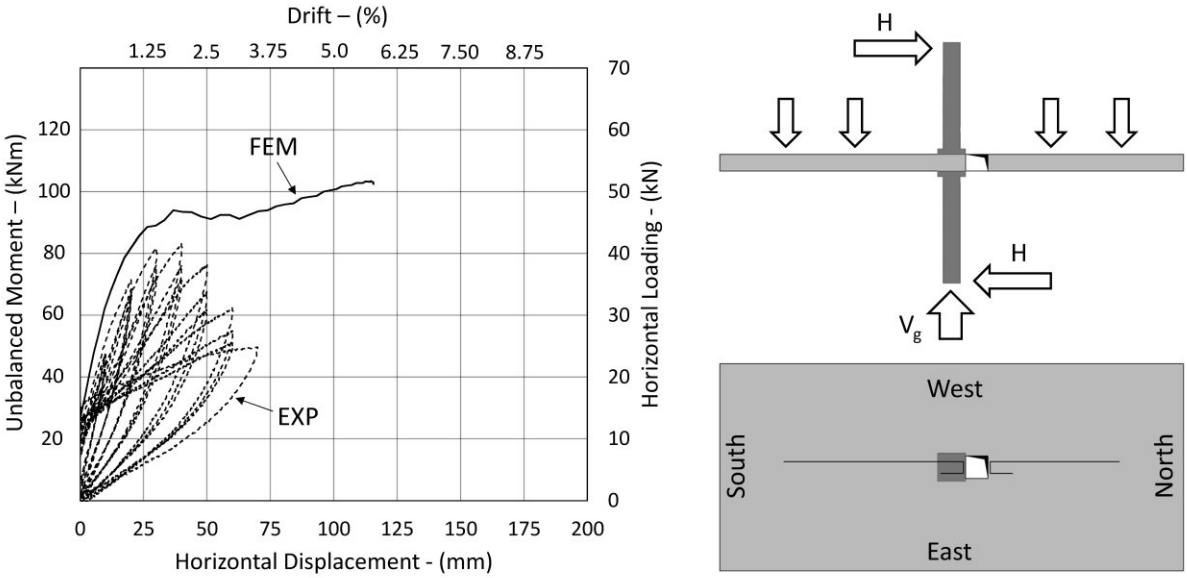

Figure 5.15 – Specimen SO1-03 northward loading: Load-deformation curves.

In Figure 5.16 the comparison between experimental and numerical backbone curves of specimen SO1-03, for southward loading, is shown. In this case the flexural plateau achieved by the numerical model is very close to that achieved in the experiment, furthermore the matching between curves is good.

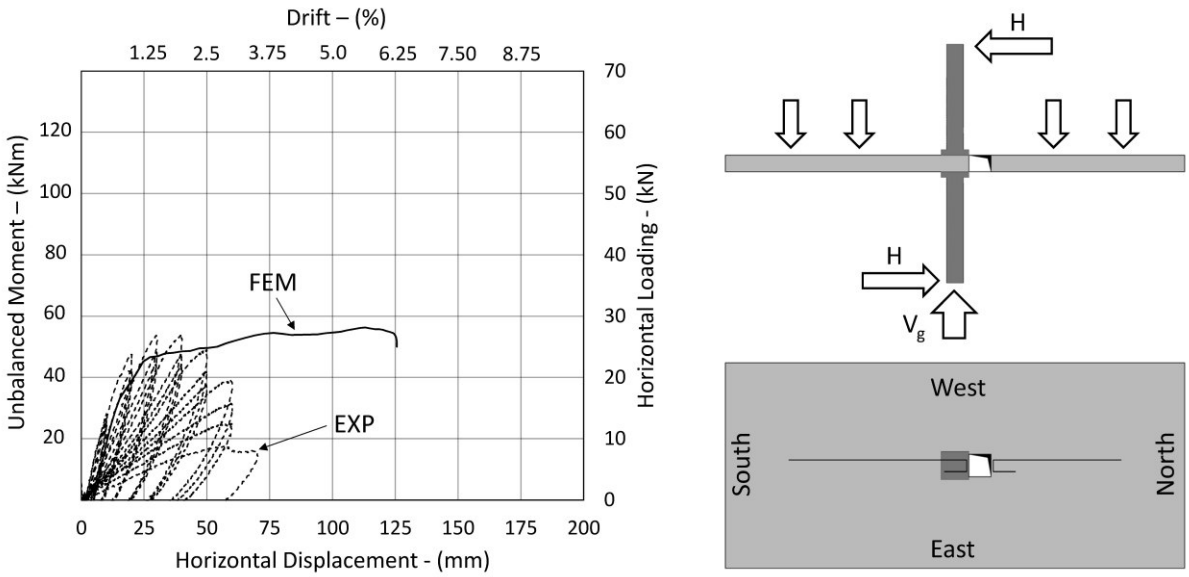

Figure 5.16 – Specimen SO1-03 southward loading: Load-deformation curves.

Finally, in Figure 5.17 the comparison between experimental and numerical backbone curves of specimen SO2-03 is proposed. The matching between curves is very good until reaching the flexural plateau, then the experimental curve drops down due to the detrimental effect of the cyclic loading, while the numerical model attains larger horizontal displacements showing a hardening behaviour.

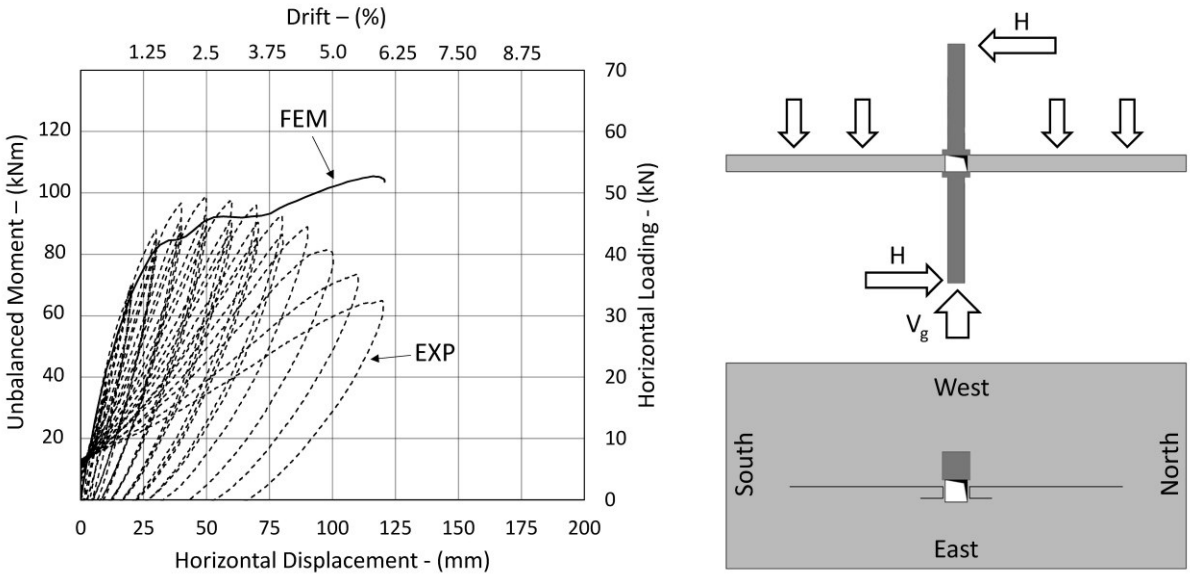

Figure 5.17 – Specimen SO2-03: Load-deformation curves.

5.5 Effects of gravity loading distribution on punching strength

5.5.1 Introduction

As shown in the previous chapters, from the gravity loading tests some contradictory results arose, the specimen SO1-01 showed a sensible reduction of the punching strength due to the presence of the opening when compared to the reference slab MLS, while the specimen SO2-01 apparently was not affected by the opening. This inconsistency is essentially due to the distribution of gravity loading around the support.

In the Lisbon setup the vertical loading is provided by eight points equally distributed along the N-S direction. However, it could be noticed that the specimen is continuous in the N-S direction while it is isolated in the E-W direction. Usually for continuous setup loading points are equally distributed while for isolated specimens loading points are concentrated along a circle. In this case both type of loading patterns should be adopted, distributed for the N-S direction and concentrated for the E-W direction.

Furthermore, if the continuous slab is simplified considering the two column strips, 50% of the vertical load is distributed along the N-S direction and 50% is distributed along the E-W direction (Figure 5.18).

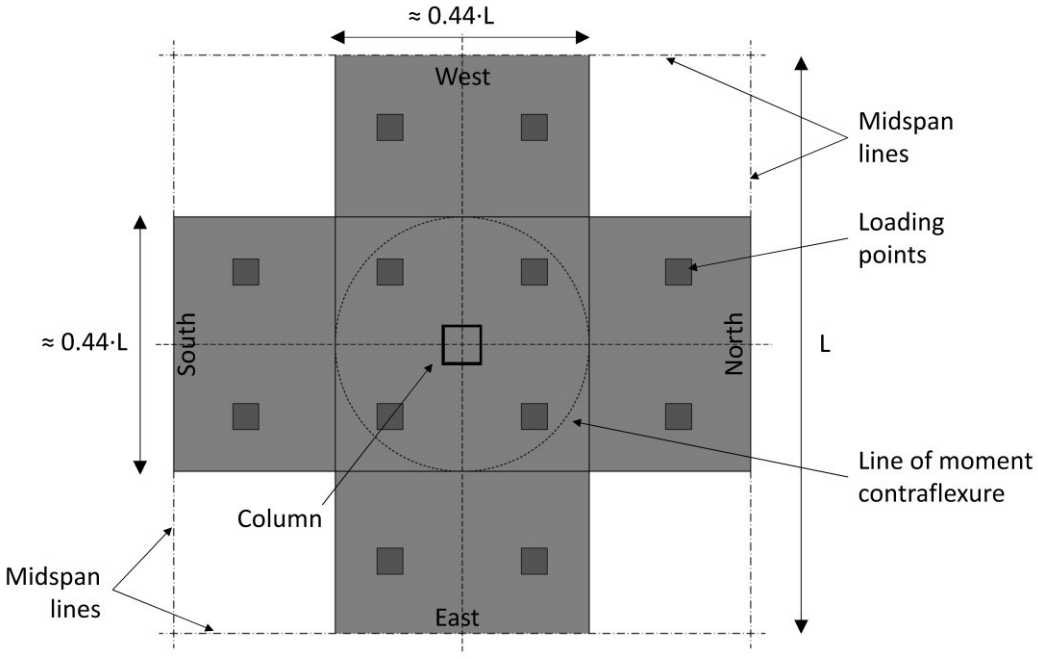

Figure 5.18 – Simplification of the continuous slab into column two strips.

Since the Lisbon setup provides all the vertical loading to the N-S strip, the flexural behaviour in this direction is supposed to be more flexible compared to the continuous slab. To reduce this inconsistency a modified version of the Lisbon setup, in which both distributed and concentrated loads are considered, is proposed.

In this case 50% of the vertical load is provided by eight points as for the Lisbon setup, while the other 50% of the vertical loading is provided by four additional loading points placed in the E-W direction. The final pattern of loading points is shown in Figure 5.19.

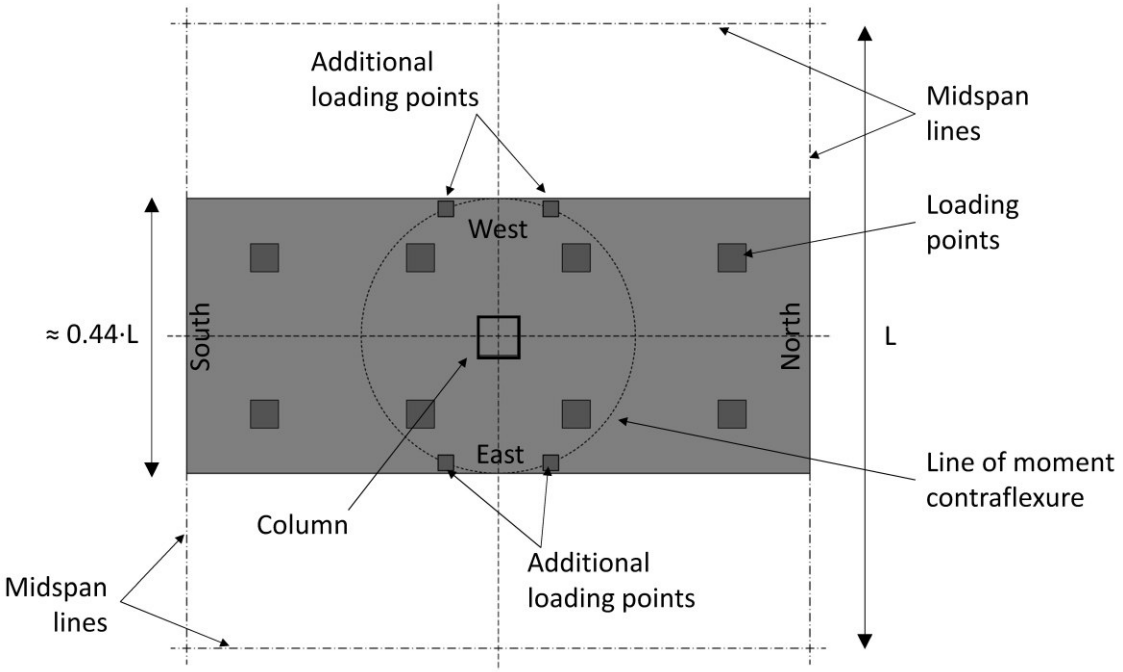

Figure 5.19 – Loading points of the modified Lisbon setup.

The numerical model of the modified Lisbon setup is shown in Figure 5.20. In the following the results provided by this setup are compared with those provided by the Lisbon setup with the aim to evaluate the influence of the distribution of vertical loading on the punching strength. The analyses are performed using the material characteristics of the specimen MLS investigated by Almeida et al. [1].

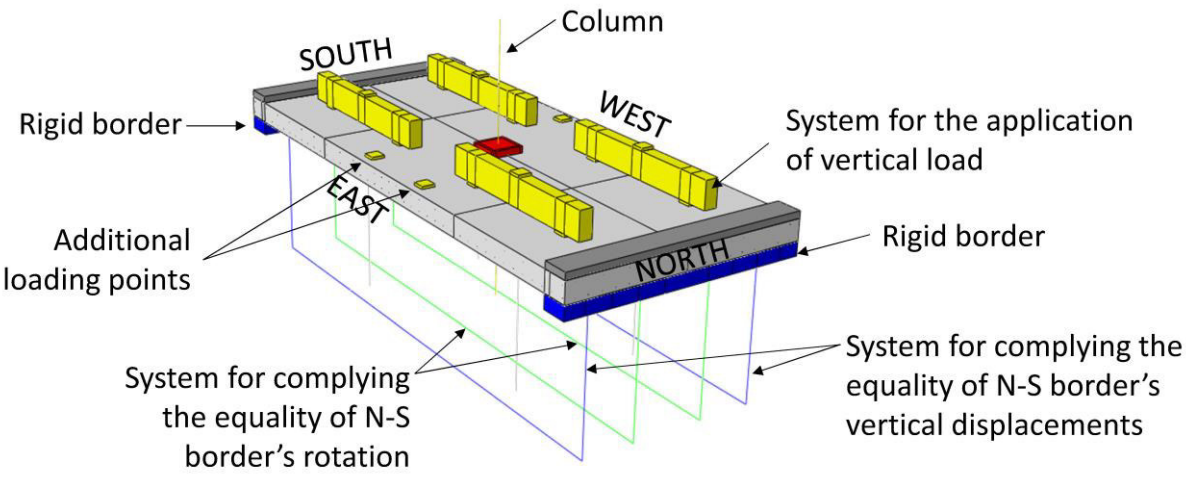

Figure 5.20 – Numerical model of the Modified Lisbon setup.

5.5.2 Vertical loading

In Table 5.4 both numerical failure loads and numerical ultimate displacements, provided by the Lisbon setup and Modified Lisbon setup, are listed.

Table 5.4 – Gravity loading tests – Comparison between numerical results provided by the Lisbon setup and the modified Lisbon setup.

Specimen	Opening size (mm)	Opening position	Setup	V_{FEM} (kN)	δ_{FEM} (mm)	$V/V_{MLS\text{-}Lisb}$	$\delta/\delta_{MLS\text{-}Lisb}$
SO1-01-Lisb	200x200	North	Lisbon	221	12.2	0.682	0.540
SO1-01-Mod	200x200	North	Modified	255	10.0	0.787	0.442
SO2-01-Lisb	200x200	East	Lisbon	289	21.2	0.892	0.938
SO2-01-Mod	200x200	East	Modified	258	10.0	0.796	0.442
MLS-Lisb	-	-	Lisbon	324	22.6	1.000	1.000
MLS-Mod	-	-	Modified	321	13.5	0.991	0.597

As expected, the Lisbon setup provides different results in terms of punching strength and ultimate displacement for the two series SO1 and SO2. The presence of the opening on the East side of the column is less affecting the punching strength than the same opening of the North side. This effect is due to the non-uniform distribution of vertical loading along the support column provided by the Lisbon setup.

On the contrary, it is interesting to observe that the Modified Lisbon setup provides almost the same punching strength and ultimate displacement for the series SO1 and SO2. Compared to the specimen MLS the reduction of punching strength for both series results about 20%.

This value corresponds to the reduction of the control perimeter calculated according to EC2-2004 [9].

With regards to the specimen without opening, both setups provide almost the same results in terms of punching strength, while the ultimate displacement is quite different. As expected, the Modified Lisbon setup provides a stiffer behaviour when compared to the Lisbon setup. Therefore, the different vertical loading distribution provided by the two setups affects the punching strength in presence of the opening only. In Figure 5.21 the comparison of load-displacement curves is provided.

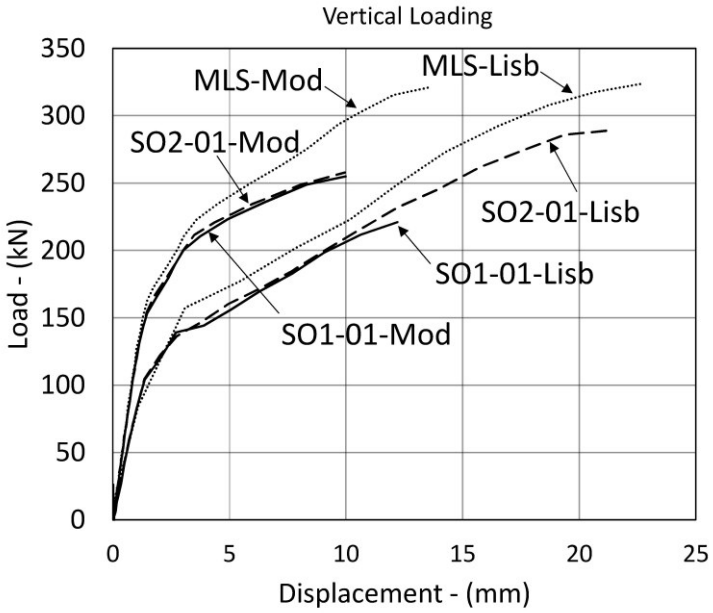

Figure 5.21 – Load-displacement curves. FEM results for vertical loading provided by the Lisbon setup and the Modified Lisbon setup adopting the material characteristics of MLS.

5.5.3 Combined gravity and horizontal loading without shear reinforcement

In Table 5.5 both maximum unbalanced moments and ultimate horizontal drifts, provided by Lisbon setup and Modified Lisbon setup, are shown. The gravity loading is assumed equal to V_g=190 kN, the gravity shear ratios (GSR) are calculated according to the punching strengths (V_R) found in the previous section (§5.5.2) as GSR=V_g/V_R.

Table 5.5 – Combined gravity and horizontal loading tests – Comparison between numerical results provided by the Lisbon setup and the Modified Lisbon setup.

Specimen	Opening size (mm)	Opening position	Loading direction	Setup	GSR (%)	M_{FEM} (kNm)	Δ_{FEM} (%)	M/M_{REF} (-)	Δ/Δ_{REF} (-)
SO1-02-N-Lisb	200x200	North	North	Lisbon	86%	64.0	0.88%	0.82	0.67
SO1-02-N-Mod	200x200	North	North	Modified	75%	67.3	1.37%	0.86	1.05
SO1-02-S-Lisb	200x200	North	South	Lisbon	86%	16.4	0.62%	0.21	0.47
SO1-02-S-Mod	200x200	North	South	Modified	75%	35.0	0.82%	0.45	0.63
SO2-02-Lisb	200x200	East	-	Lisbon	66%	61.8	1.16%	0.79	0.89
SO2-02-Mod	200x200	East	-	Modified	74%	63.2	1.31%	0.81	1.00
C-50-Lisb	-	-	-	Lisbon	59%	78.4	1.31%	1.00	1.00
C-50-Mod	-	-	-	Modified	59%	78.6	1.59%	1.00	1.21

For combined gravity and horizontal loading, the influence of the distribution of vertical loading along the support results lower than for gravity loading only. In Figure 5.22 the numerical load-displacement curves of the specimen C-50 are provided for both setups.

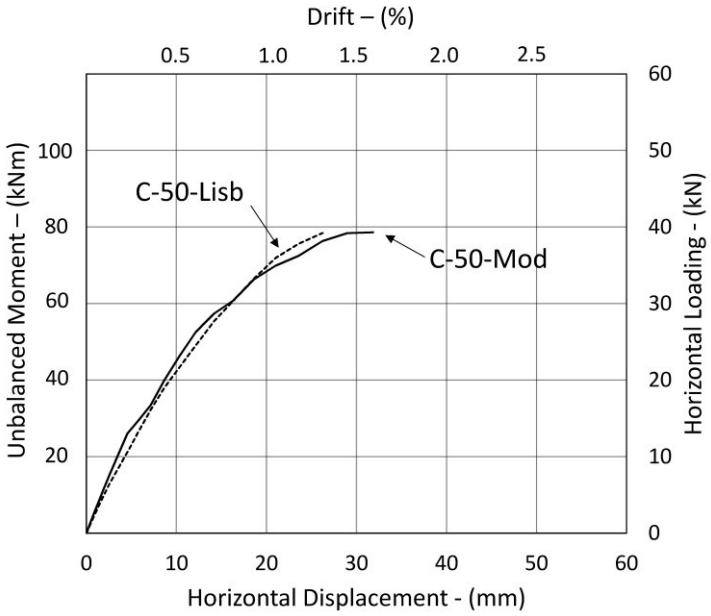

Figure 5.22 – Load-displacement curves. FEM results specimen C-50 provided by the Lisbon setup and the Modified Lisbon setup adopting the material characteristics of MLS.

For the series SO1 the maximum unbalanced moment provided by the Lisbon setup is almost the same provided by the Modified Lisbon setup, except when southward loading is considered. In this case the Modified Lisbon setup provides a maximum unbalanced moment about two times the unbalanced moment provided by the Lisbon setup (Figure 5.23).

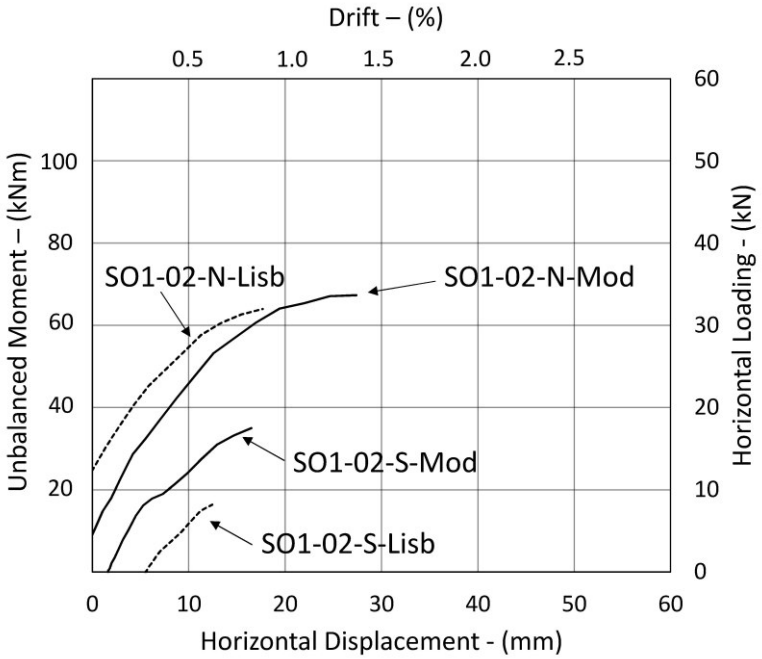

Figure 5.23 – Load-displacement curves. FEM results specimen SO1-02 provided by the Lisbon setup and the Modified Lisbon setup adopting the material characteristics of MLS.

In general, the Modified Lisbon setup reduces the initial eccentricity that arises from the presence of the opening along the North-South direction. The opening placed on the North side introduces a reduction of the flexural stiffness, inducing a Southward drift to the column when the vertical loading is applied. The Modified Lisbon setup reduces this drift thanks to a different distribution of vertical loading.

For the series SO2 the influence of the setup results in a very small difference in terms of both maximum unbalanced moment and ultimate drift between the Lisbon setup and the Modified Lisbon Setup (Figure 5.24).

In general, for northward loading the presence of the opening provides a reduction of the maximum unbalanced moment of about 20% while for southward loading the series SO1 results in a higher reduction (Figure 5.25) due to the detrimental presence of the opening on the north side, as discussed in the previous chapter.

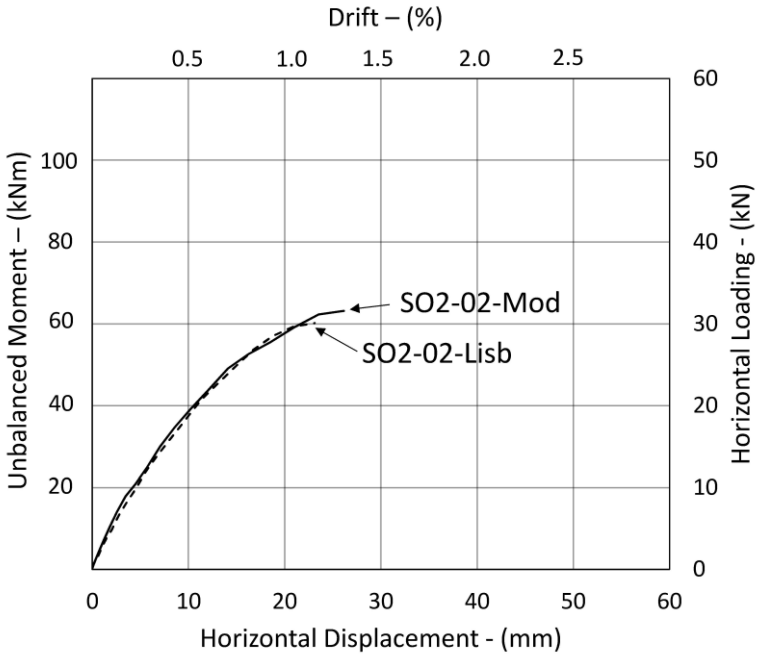

Figure 5.24 – Load-displacement curves. FEM results specimen SO2-02 provided by the Lisbon setup and the Modified Lisbon setup adopting the material characteristics of MLS.

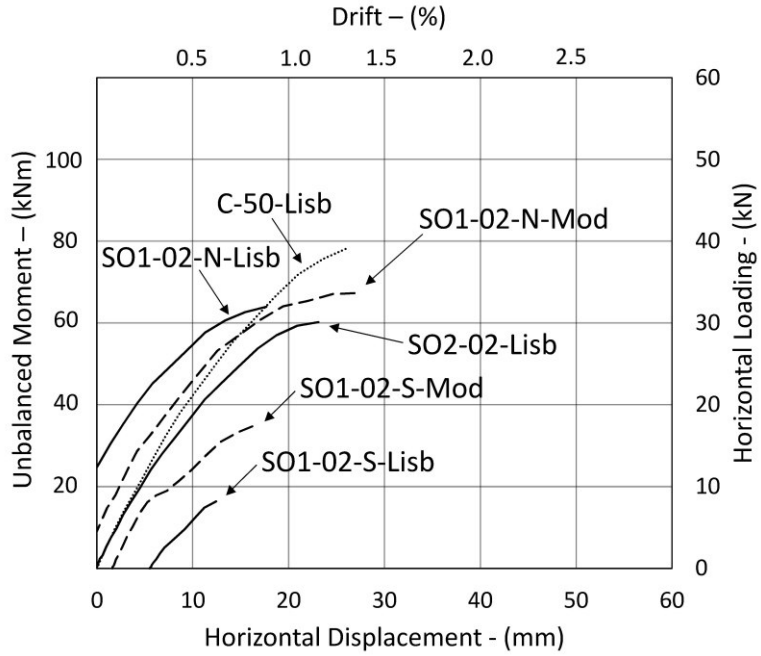

Figure 5.25 –Load-displacement curves. Comparison between all the curves provided by the Lisbon setup and the Modified Lisbon setup adopting the material characteristics of MLS.

5.5.4 Combined gravity and horizontal loading with shear reinforcement

In Table 5.6 a comparison between the maximum unbalanced yielding moment provided by Lisbon setup and Modified Lisbon setup is provided. The comparison is performed in terms of yielding moment only, since results in terms of ultimate drift are less reliable. For large drifts (>10%) the Lisbon setup is pushed to the limit reducing the effectiveness of the constraints. Indeed, for very large drifts the compliance of the boundary conditions results less effective.

Table 5.6 – Combined gravity and horizontal loading tests with shear reinforcement – Comparison between numerical results provided by the Lisbon setup and the modified Lisbon setup.

Specimen	Opening size (mm)	Opening position	Loading direction	Setup	GSR (%)	M_{FEM} (kNm)	M/M_{REF} (-)
SO1-03-N-Lisb	200x200	North	North	Lisbon	86%	92.6	0.727
SO1-03-N-Mod	200x200	North	North	Modified	75%	99.4	0.781
SO1-03-S-Lisb	200x200	North	South	Lisbon	86%	50.9	0.400
SO1-03-S-Mod	200x200	North	South	Modified	75%	54.3	0.427
SO2-03-Lisb	200x200	East	-	Lisbon	66%	96.5	0.758
SO2-03-Mod	200x200	East	-	Modified	74%	100.0	0.786
C-50-STR4-Lisb	-	-	-	Lisbon	59%	127.3	1.000
C-50-STR4-Mod	-	-	-	Modified	59%	128.2	1.007

In Figure 5.26 results of both Lisbon and Modified Lisbon setup are provided for the specimen C-50-STR4.

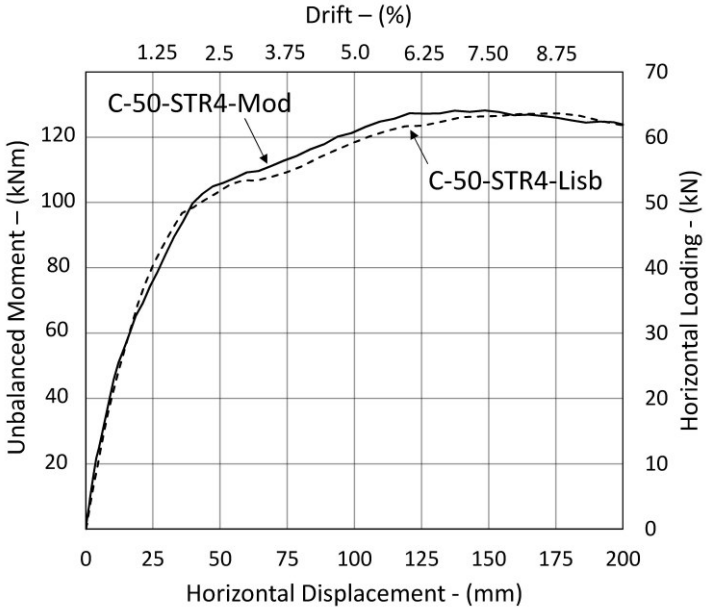

Figure 5.26 – Load-displacement curves of specimen C-50-STR4 provided by the Lisbon setup and the Modified Lisbon setup adopting the material characteristics of MLS.

The effect of the vertical loading is practically negligible, the difference between Lisbon and Modified Lisbon setup in terms of yielding moment and ultimate drift are minimal. In Figure 5.27 and Figure 5.28 results of the first and the second series are shown.

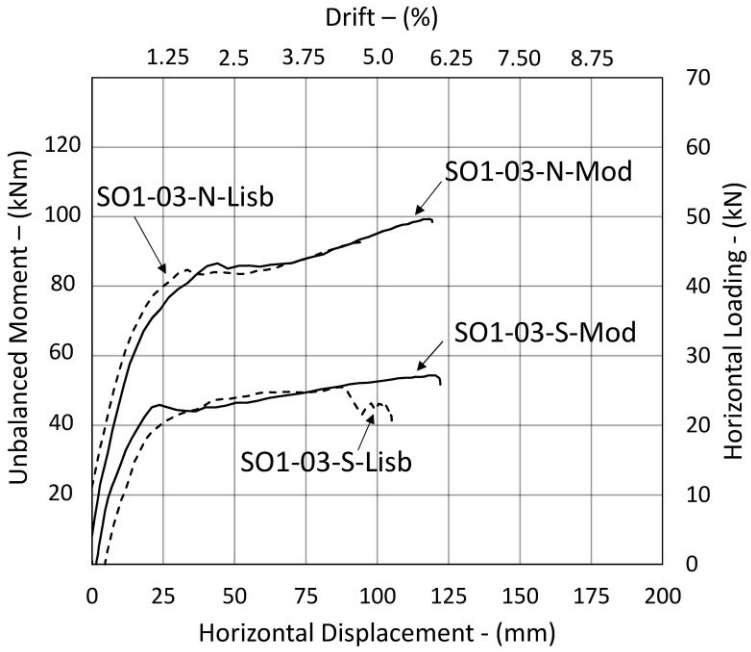

Figure 5.27 –Load-displacement curves of the specimen SO1-03 provided by the Lisbon setup and the Modified Lisbon setup adopting the material characteristics of MLS.

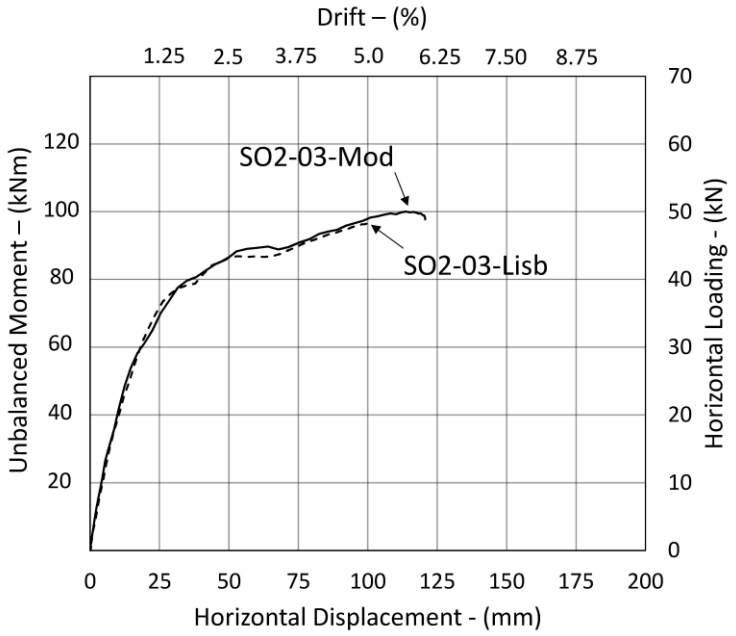

Figure 5.28 –Load-displacement curves of series of the specimen SO2-03 provided by the Lisbon setup and the Modified Lisbon setup adopting the material characteristics of MLS.

In presence of the opening the distribution of vertical loading is still effective, however the modification in terms of yielding moment and ultimate drift is limited. The Modified Lisbon setup provides about 7% and 4% higher yielding moments, for the first series and second series respectively, when compared to the Lisbon Setup.

Finally, in Figure 5.29 a comparison between all the specimens of the Lisbon setup is provided.

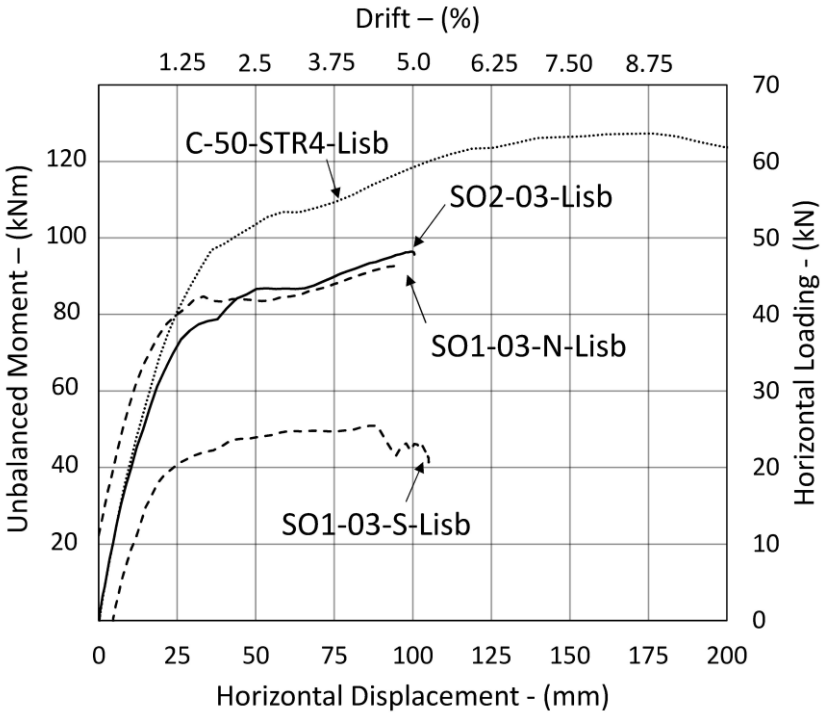

Figure 5.29 – Load-displacement curves. Comparison between all the curves provided by the Lisbon setup adopting the material characteristics of MLS.

For northward loading the presence of the opening provides a reduction of the yielding moment of about 25%, while for southward loading the series SO1 leads to a reduction equal to 60%.

5.6 Slab-column connection with openings adjacent to the column

5.6.1 Introduction

In the following the response of the slab-column connection is investigated by means of the development of a new numerical model of a Continuous setup. The Continuous setup is the attempt to replicate the actual behaviour of an internal slab-column connection. The slab is modelled from midspan to midspan in both directions as shown in Figure 5.30.

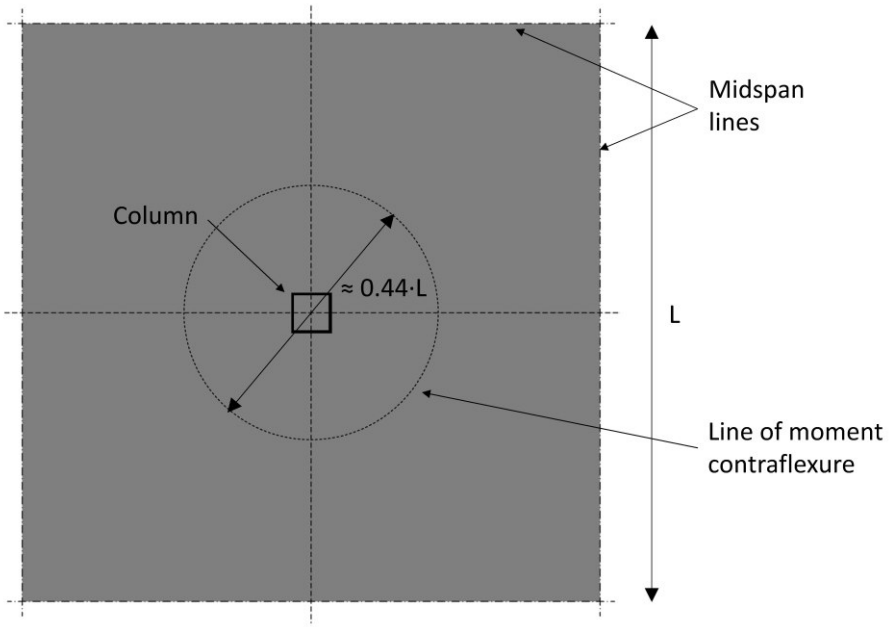

Figure 5.30 – Continuous internal slab.

The boundary conditions are compiled thanks to the use of couple of constraints placed on the borders of the specimen. The idea is to replicate the systems of the Lisbon setup along the borders of the setup. In the E-W borders six couple of constraints for the equality of the rotation are placed, while in the N-S borders constraints for the equality of both rotation and vertical displacement are placed. The presence of the latter is needed because the horizontal load is applied along the N-S direction. Conversely in the E-W borders there is no need of these constraints since the equality of the vertical displacement is provided by the symmetrical loading condition. Unlike the Lisbon setup, different rotations along the borders are allowed. Indeed, in the continuous setup, the constraints work in couple, each point is constrained to the point placed in the front, while in the Lisbon setup the rotation and the vertical displacement along the borders N-S are constants. The numerical model of the Continuous setup is shown in Figure 5.31.

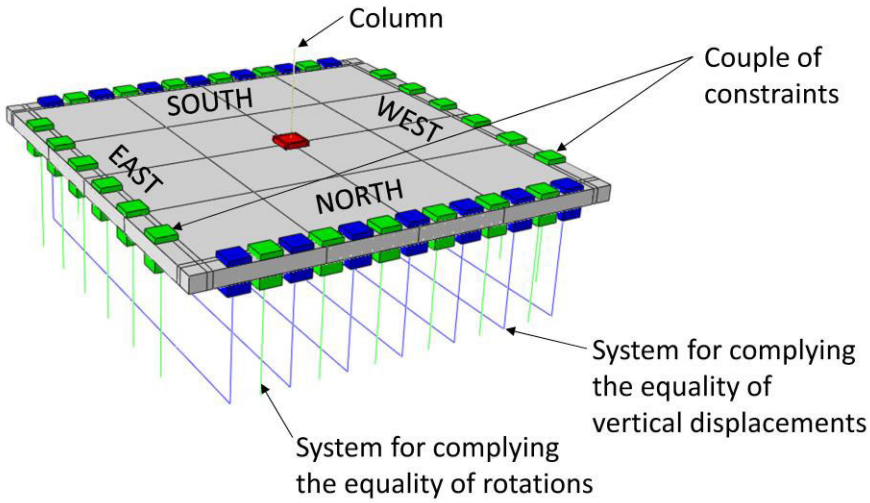

Figure 5.31 – Numerical model of the Continuous setup.

5.6.2 Vertical loading

In Table 5.7 both failure loads and ultimate displacements, provided by Lisbon setup and Continuous setup, are listed.

Table 5.7 – Gravity loading tests – Comparison between numerical results provided by the Lisbon setup and the Continuous setup.

Specimen	Opening size (mm)	Opening position	Setup	V_{FEM} (kN)	δ_{FEM} (mm)	V/V_{REF}	δ/δ_{REF}
SO1-01-Lisb	200x200	North	Lisbon	221	12.2	0.682	0.540
SO1-01-Cont	200x200	North	Continuous	304	8.7	0.934	0.385
SO2-01-Lisb	200x200	East	Lisbon	289	21.2	0.892	0.938
SO2-01-Cont	200x200	East	Continuous	301	11.1	0.929	0.491
MLS-Lisb	-	-	Lisbon	324	22.6	1.000	1.000
MLS-Cont	-	-	Continuous	374	15.7	1.154	0.695

The Continuous setup provides a punching load 15% higher than that provided by the Lisbon setup. Series SO1 and SO2 result almost in the same punching strength when investigated with the Continuous setup. Furthermore, the opening provides a reduction of the punching strength almost equal to 20% when compared to the case without opening. The latter is aligned to the result of the Modified Lisbon setup. In general, the Continuous setup provides a stiffer behaviour when compared to the Lisbon setup, as found with the Modified Lisbon setup. The ultimate displacement achieved with the Continuous setup for the specimen MLS results about 40% lower than that provided by the Lisbon setup. In Figure 5.32 the load-displacement curves for vertical loading are shown.

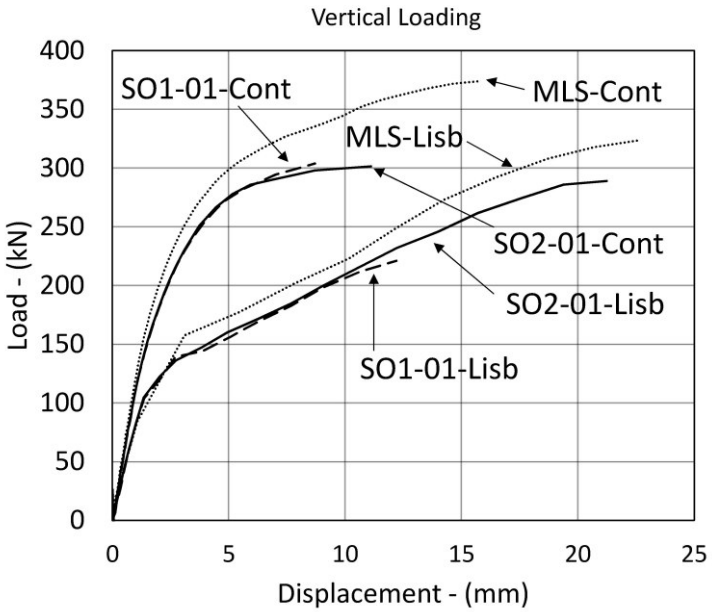

Figure 5.32 – Load-displacement curves. FEM results for vertical loading provided by the Lisbon setup and the Continuous setup adopting the material characteristics of MLS.

5.6.3 Combined gravity and horizontal loading without shear reinforcement

In Table 5.8 both maximum unbalanced moments and ultimate horizontal drifts, provided by Lisbon setup and Continuous setup, are shown. The gravity loading is assumed equal to V_g=190 kN, the gravity shear ratios (GSR) are calculated according to the punching strengths (V_R) found in the previous section (§5.6.3) as GSR=V_g/V_R.

Table 5.8 – Combined gravity and horizontal loading tests – Comparison between numerical results provided by the Lisbon setup and the Continuous setup.

Specimen	Opening size (mm)	Opening position	Loading direction	Setup	M_{FEM} (kNm)	GSR (%)	Δ_{FEM} (%)	M/M_{REF} (-)	Δ/Δ_{REF} (-)
SO1-02-N-Lisb	200x200	North	North	Lisbon	64.0	86%	0.88%	0.816	0.671
SO1-02-N-Cont	200x200	North	North	Continuous	98.6	63%	1.33%	1.258	1.015
SO1-02-S-Lisb	200x200	North	South	Lisbon	16.4	86%	0.62%	0.209	0.473
SO1-02-S-Cont	200x200	North	South	Continuous	63.3	63%	0.80%	0.807	0.611
SO2-02-Lisb	200x200	East	-	Lisbon	61.8	66%	1.16%	0.788	0.885
SO2-02-Cont	200x200	East	-	Continuous	100.4	63%	1.24%	1.281	0.947
C-50-Lisb	-	-	-	Lisbon	78.4	59%	1.31%	1.000	1.000
C-50-Cont	-	-	-	Continuous	135.9	51%	1.59%	1.733	1.213

For combined gravity and horizontal loading, the Continuous setup provides higher maximum unbalanced moment when compared to the Lisbon setup. For the specimen C-50 the increase in terms of peak load results about 73%, while the increase in terms of ultimate drift

results about 21%. In Figure 5.33, Figure 5.34 and Figure 5.35 load-displacement curves for the specimen C-50, SO1-02 and SO2-02 are shown.

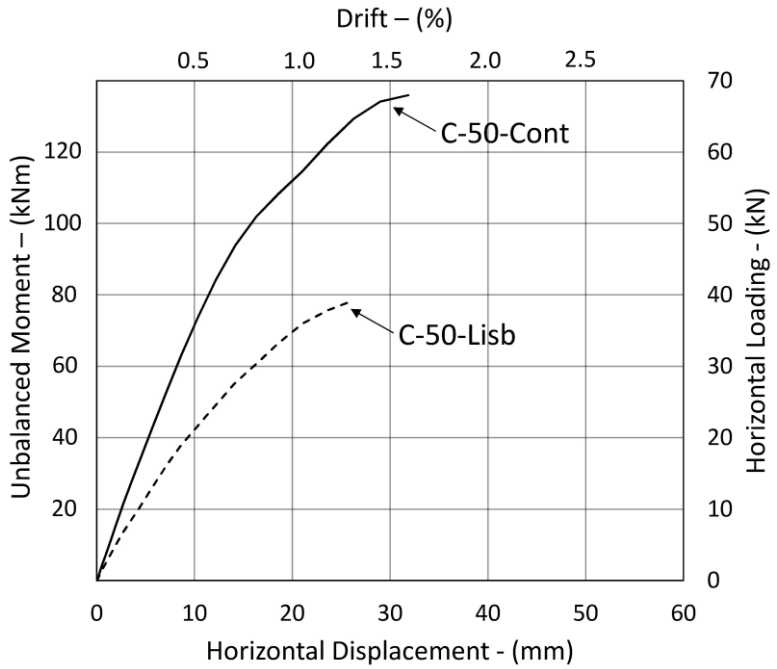

Figure 5.33 – Load-displacement curves. FEM results specimen C-50 provided by the Lisbon setup and the Continuous setup adopting the material characteristics of MLS.

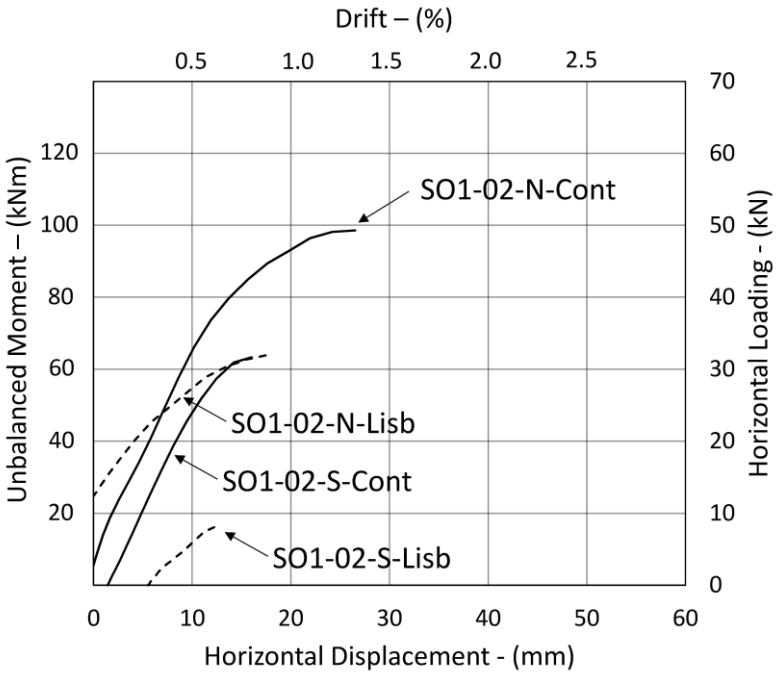

Figure 5.34 – Load-displacement curves. FEM results specimen SO1-02 provided by the Lisbon setup and the Continuous setup adopting the material characteristics of MLS.

In presence of the opening the scenario is similar to the case without opening: the Continuous setup provides higher maximum unbalanced moments than those provided by the Lisbon setup. In Figure 5.36 results provided by the Continuous setup are shown.

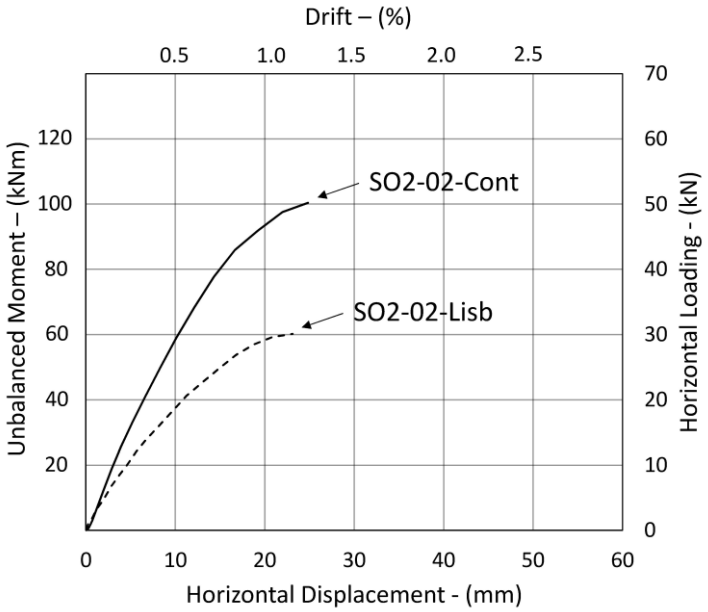

Figure 5.35 – Load-displacement curves. FEM results specimen SO2-02 provided by the Lisbon setup and the Continuous setup adopting the material characteristics of MLS.

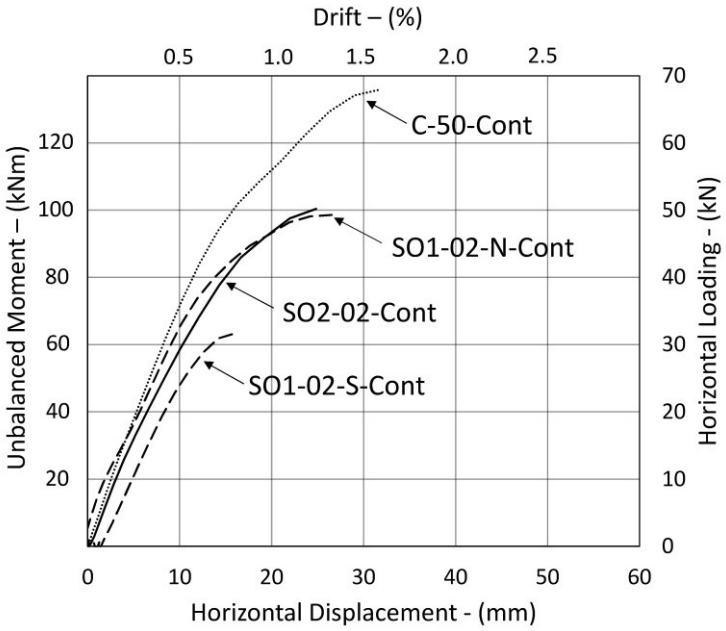

Figure 5.36 – Load-displacement curves. Comparison between all the curves provided by the Continuous setup adopting the material characteristics of MLS.

5.6.4 Combined gravity and horizontal loading with shear reinforcement

In Table 5.9 a comparison between the maximum unbalanced yielding moment provided by Lisbon setup and Continuous setup is provided. In this case the comparison is performed in terms of yielding moment only since, results in terms of ultimate drift are less reliable. For large drifts (>10%) the Lisbon setup is pushed to the limit reducing the effectiveness of constraints. Indeed, for very large drifts the compliance of the boundary conditions results less effective.

Table 5.9 – Combined gravity and horizontal loading tests with shear reinforcement – Comparison between numerical results provided by the Lisbon setup and the Continuous setup.

Specimen	Opening size (mm)	Opening position	Loading direction	Setup	M_{FEM} (kNm)	M/M_{REF} (-)
SO1-03-N-Lisb	200x200	North	North	Lisbon	92.6	0.727
SO1-03-N-Cont	200x200	North	North	Continuous	124.2	0.976
SO1-03-S-Lisb	200x200	North	South	Lisbon	50.9	0.400
SO1-03-S-Cont	200x200	North	South	Continuous	75.1	0.590
SO2-03-Lisb	200x200	East	-	Lisbon	96.5	0.758
SO2-03-Cont	200x200	East	-	Continuous	127.8	1.004
C-50-STR4-Lisb	-	-	-	Lisbon	127.3	1.000
C-50-STR4-Cont	-	-	-	Continuous	171.3	1.346

In Figure 5.37 results of both Lisbon and Continuous setup are provided for the specimen C-50-STR4. The flexural plateau provided by the Continuous setup results about 35% higher than that achieved by the Lisbon setup.

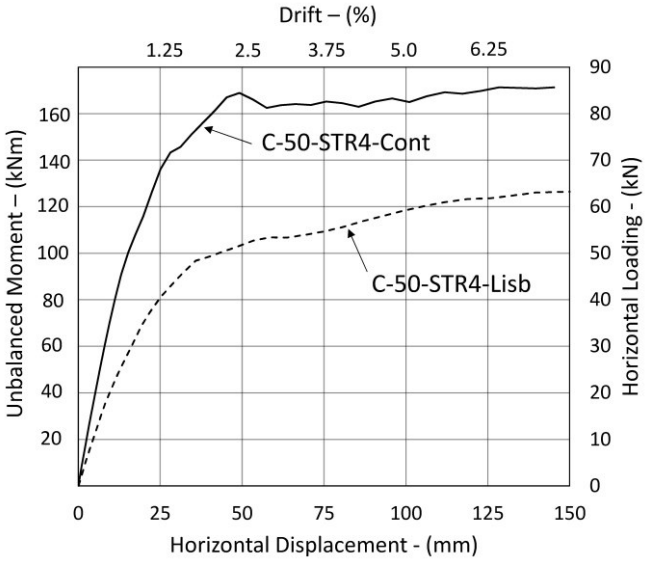

Figure 5.37 –Load-displacement curves of specimen C-50-STR4 provided by the Lisbon setup and the Continuous setup adopting the material characteristics of MLS.

Similar increases also occur in presence of opening, in Figure 5.38 and Figure 5.39 the results of the first and the second series are shown.

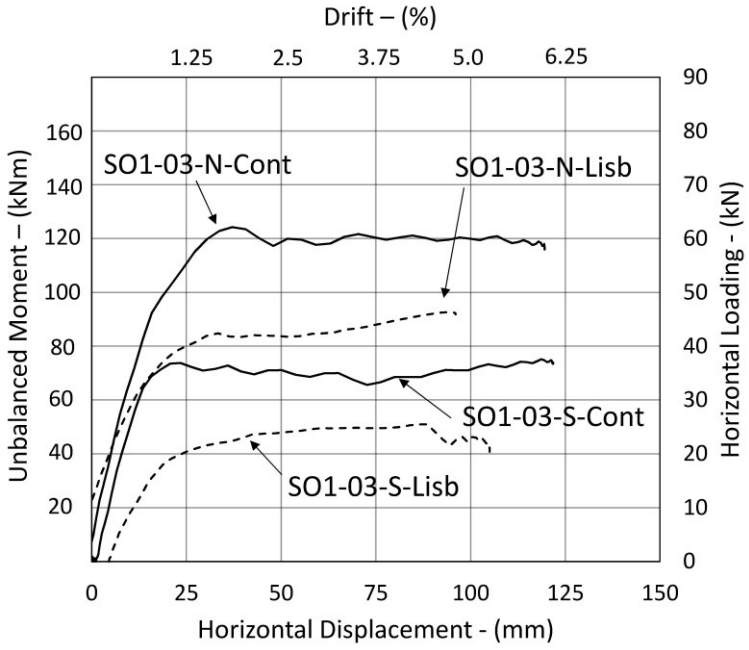

Figure 5.38 –Load-displacement curves of specimen SO1-03 provided by the Lisbon setup and the Continuous setup adopting the material characteristics of MLS.

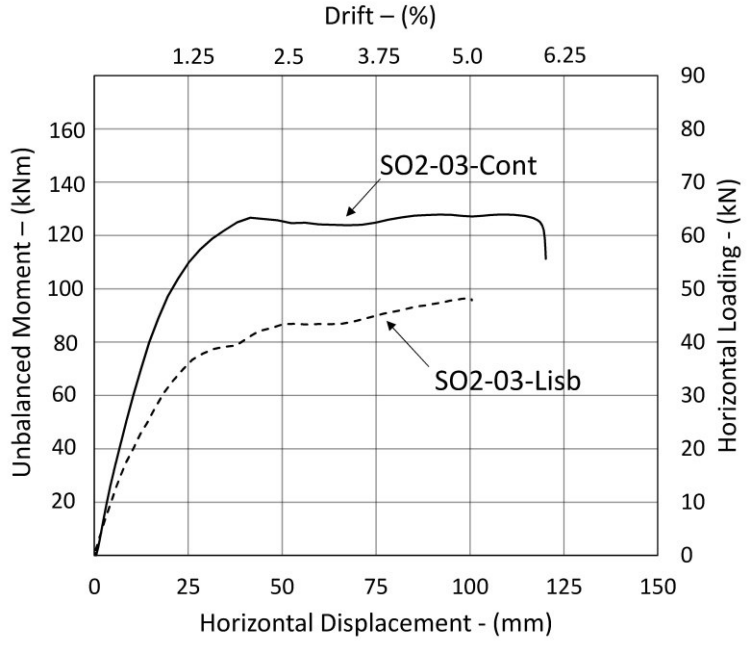

Figure 5.39 –Load-displacement curves of specimen SO2-03 provided by the Lisbon setup and the Continuous setup adopting the material characteristics of MLS.

In Figure 5.40 the load-displacement curves provided by the Continuous setup are shown. Similarly to the Lisbon setup, the Continuous setup in presence of the opening shows lower yielding moment compared to the case without opening. For northward loading the presence of the opening provides a reduction of the yielding moment of about 25%.

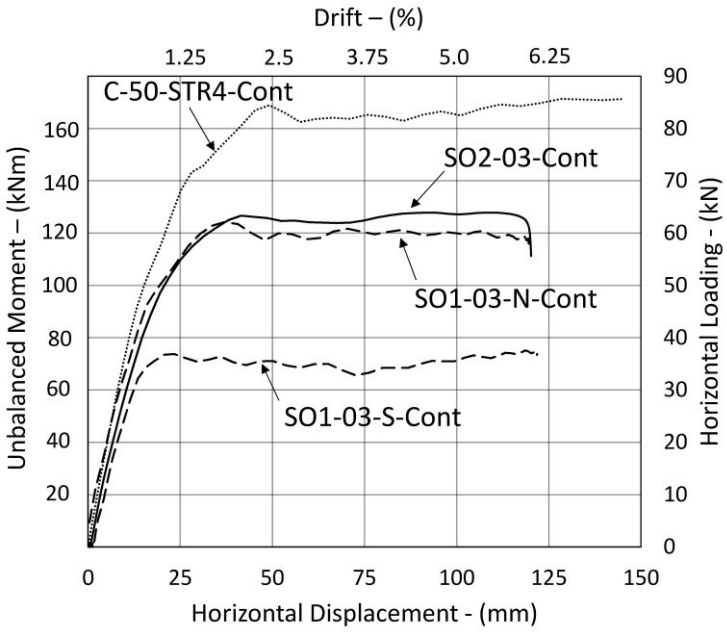

Figure 5.40 – Load-displacement curves. Comparison between all the curves provided by the Continuous setup adopting the material characteristics of MLS.

For southward loading the series SO1 leads to a reduction almost equal to 55% similarly to the Lisbon setup.

5.7 Discussion

The numerical analysis allowed for evaluating various scenarios not supported by the experimental activity. The numerical model was calibrated on the test MLS, then the reliability of the FEM was checked with results provided by the present experimental campaign. Actually, the direct comparison in terms of failure load and ultimate displacement was possible for vertical loading only. For combined vertical and horizontal loading without shear reinforcement the comparison between numerical and experimental results was not possible since the numerical model was calibrated for monotonic loading only, while tests were performed under cyclic loading. For combined vertical and horizontal loading with shear reinforcement the comparison was performed in terms of yielding moment only, since the latter is supposed to be almost the same for cyclic and monotonic loading.

In terms of vertical loading the agreement between experimental and numerical results is quite good. The average ratio between experimental and numerical failure loads results equal to 1.085 with a coefficient of variation (COV) of 7.74%, while the average ratio between experimental and numerical ultimate displacements results equal to 1.115 with a coefficient of variation (COV) of 15.23%.

For combined vertical and horizontal loading with shear reinforcement the numerical model achieved higher yielding moments than those provided experimentally. The average ratio between experimental and numerical yielding moments is equal to 1.085 with a coefficient of variation (COV) of 7.74%, while the average ratio between experimental and numerical ultimate displacements results equal to 0.898 with a coefficient of variation (COV) of 7.79%.

Therefore, numerical results could be considered enough reliable to be extended to other scenarios. Two different scenarios were investigated, the Modified Lisbon setup with a more realistic distribution of vertical loading and the Continuous setup, that aims to reproduce the actual behaviour of an internal slab-column connection. In order to make easier the comparison of results, all the analyses were performed adopting the material characteristics of the specimen MLS.

Differently from the Lisbon setup, the Modified Lisbon setup provided the same vertical punching load for the two series SO1 and SO2. This result shows how the distribution of vertical loading affects the punching strength in presence of the opening. However, for combined vertical and horizontal loading the distribution of vertical loading seems to have a lower influence on both maximum unbalanced moment and ultimate drift. Indeed, both Lisbon and Modified Lisbon setup give almost the same results.

For both setups, considering northward loading, the presence of the opening provides a reduction of the maximum unbalanced moment of about 20% when compared to the case without opening. For southward loading, the series SO1 gives a reduction of 79% for the Lisbon setup and a reduction of 55% for the Modified Lisbon setup.

In presence of shear reinforcement, the scenario is very similar to the case without shear reinforcement: the two setups provide almost the same results. Therefore, the influence of the vertical loading distribution is very limited. For both setups the opening induces a substantial reduction of the yielding moment, for northward loading this reduction results about equal to 25% while for southward loading the series SO1 leads to a reduction equal to 60%.

Finally, the Continuous setup shows the behaviour of the internal slab-column connection. Compared to the Lisbon setup, the Continuous setup provides a punching load for vertical loading 15% higher. Furthermore, the punching strength results independent from the position of the opening (North or East) and the detrimental effect provided by the latter results about 20% of the punching strength provided by the slab-column connection without opening, as found for the Modified Lisbon setup. This value corresponds to the reduction of control perimeter calculated according to EC2-2004 [9].

For combined gravity and horizontal loading without shear reinforcement, the Continuous setup leads to an enhancement in terms of maximum unbalanced moment up to 73%. Considering northward loading, the presence of the opening provides a reduction of the maximum unbalanced moment of about 25% when compared to the case without opening, while for southward loading, the series SO1 gives a reduction of 55% for the Continuous setup.

With shear reinforcement the Continuous setup gives yielding moments about 35% higher than those provided by the Lisbon setup. For the Continuous setup the opening induces a substantial reduction of the yielding moment, for northward loading this reduction results about equal to 25% while for southward loading the series SO1 leads to a reduction equal to 55%.

5.8 References

[1] Almeida, AFO.; Inacio, MMG.; Lucio, VJG.; Ramos, AP.; Punching behaviour of RC flat slabs under reversed horizontal cyclic loading, Engineering Structures, 2016, Vol. 117: pp. 204–19.

[2] Lubliner, J.; Oliver, J.; Oller, S.; Oñate, E.; A plastic-damage model for concrete, International Journal of Solids and Structures, 1989, Vol. 25: pp. 299–326.

[3] Lee, J.; Fenves, GL.; Plastic-Damage Model for Cyclic Loading of Concrete Structures, Journal of Engineering Mechanics (ASCE), 1998, Vol. 124: pp. 892–900.

[4] Simulia.; Abaqus 6.11 Theory Manual 2011: pp. 1172.

[5] Van Mier, JGM.; Part II : Load-Histories, Materiaux et Constructions, 1986, Vol. 19: pp. 190–200.

[6] Van Mier, JG.; Shah, SP.; Arnaud, M.; Balayssac, J.; Bascoul, A.; Choi, S.; et al.; Strain-softening of concrete in uniaxial compression, vol. 30, 1997.

[7] Birtel, V.; Mark, P.; Parameterised Finite Element Modelling of RC Beam Shear Failure, Abaqus Users' Conference, 2006: pp. 95–108.

[8] Kupfer, H.; Hilsdorf, H.; Rush, H.; Behaviour of Concrete Under Biaxial Stresses, ACI Journal, 1969, Vol. 66: pp. 856–66.

[9] CEN.; Eurocode 2: Design of concrete structures - Part 1-1: General rules and rules for buildings, Bruxelles: 2004.

[10] Popovics, S.; A numerical approach to the complete stress-strain curve of concrete, Cement and Concrete Research, 1973, Vol. 3: pp. 583–99.

[11] Pavlović, M.; Marković, Z.; Veljković, M.; Bucrossed D Signevac, D.; Bolted shear connectors vs. headed studs behaviour in push-out tests, Journal of Constructional Steel Research, 2013, Vol. 88: pp. 134–49.

[12] Hordijk, DA.; Local approach in fatigue of concrete. Delft University, 1991.

[13] Jankowiak, T.; Lodygowski, T.; Identification of parameters of concrete damage plasticity constitutive model, Foundations of Civil and Environmental …, 2005: pp. 53–69.

[14] Genikomsou, AS.; Polak, MA.; Finite element analysis of punching shear of concrete slabs using damaged plasticity model in ABAQUS, Engineering Structures, 2015, Vol. 98: pp. 38–48.

[15] Bompa, D V.; Onet, T.; Punching shear strength of RC flat slabs at interior connections to columns, Magazine of Concrete Research, 2016, Vol. 68: pp. 24–42.

[16] Najafgholipour, MA.; Dehghan, SM.; Dooshabi, A.; Niroomandi, A.; Finite element analysis of reinforced concrete beam-column connections with governing joint shear failure mode, Latin American Journal of Solids and Structures, 2017, Vol. 14: pp. 1200–25.

[17] Nana, WSA.; Bui, TT.; Limam, A.; Abouri, S.; Experimental and Numerical Modelling of Shear Behaviour of Full-scale RC Slabs Under Concentrated Loads, Structures, 2017, Vol. 10: pp. 96–116.

[18] Russell, JM.; Owen, JS.; Hajirasouliha, I.; Nonlinear behaviour of reinforced concrete flat slabs after a column loss event, Advances in Structural Engineering, 2018, Vol. 21: pp. 1–15.

[19] Navarro, M.; Ivorra, S.; Varona, FB.; Parametric computational analysis for punching shear in RC slabs, Engineering Structures, 2018, Vol. 165: pp. 254–63.

[20] fib.; fib Bulletin 42: Constitutive Modelling of High Strength/high performance concrete, 2008.

[21] CEB/FIP.; Ceb-Fip Model Code 1990, London: Thomas Telford; 1993.

[22] CEB/FIP.; Model Code 2010 - Volume 1, Bulletin 6, Lausanne, Switzerland: Internation Federation for Structural Concrete (fib); 2012.

[23] Drakatos, IS.; Muttoni, A.; Beyer, K.; Internal slab-column connections under monotonic and cyclic imposed rotations, Engineering Structures, 2016, Vol. 123: pp. 501–16.

[24] Almeida, A.; Marreiros, R.; Ramos, AP.; Ornelas, M.; Alcobia, B.; Behaviour of RC Flat Slabs with Stirrups under Reversed Horizontal Cyclic Loading, Magazine of Concrete Research, 2019.

6. CONCLUSIONS AND RECOMMENDATIONS

6.1 Conclusions

This chapter presents the conclusions that arise from this research, presenting first the ones based on the experimental results, followed by the non-linear numerical investigations.

The conclusions based on the experimental results are divided into three groups: specimens without shear reinforcement subjected to vertical loading only, specimens without shear reinforcement subjected to combined vertical and horizontal loading, specimens with shear reinforcement subjected to combined vertical and horizontal loading. For each group, composed by two specimens with different position of the opening, results of a reference slab without opening provided by a previous experimental campaign performed in the Structural Laboratory of the NOVA School of Science and Technology are also used for comparison.

Besides the comparison of experimental results between slabs with and without openings is valuable, differences in terms of concrete compressive strength of each specimen do not allow to outline accurate conclusions. For this reason, with the aim to evaluate the influence of the opening adjacent to the column on the response of the slab column connection, the investigation by means of nonlinear numerical analysis was used. In this case, assuming

equal mechanical characteristics of both concrete and reinforcement for all the specimens, the comparison of results provided by slab with and without opening results is effective.

The nonlinear numerical analysis is also used to investigate the influence of vertical loading distribution in the Lisbon setup on the response of specimen. The need of this investigation arises from the experimental results provided by the specimen SO2-01 subjected to vertical loading only, with the opening placed on the east side. Besides the difference in terms of concrete compressive strength, results provided by this specimen showed as expected a lower influence of the opening placed on the East side than North side. The numerical analysis allowed to evaluate how the distribution of vertical loading could influence the behaviour of the specimens under both gravity loading only and combined gravity and lateral loading.

Finally, a numerical model of an internal slab column connection is developed and the effects provided by the presence of openings are evaluated.

6.1.1 Effects of openings on punching failure due to vertical loading

According to the experimental results, the specimen SO1-01 showed a sensible reduction of the punching strength due to the presence of the opening when compared to the reference slab, while the specimen SO2-01 was scarcely affected by the opening.

The reason of this apparent contradiction is essentially found in the asymmetric distribution of vertical loading provided by the Lisbon setup. Since in the Lisbon setup the vertical loading is applied along the North-South direction, the presence of the opening adjacent to the column on the East side results less influential than the opening placed on the North side.

According to the numerical analysis, if a symmetric distribution of vertical loading is provided (Modified Lisbon setup) the two series of opening SO1 and SO2 provide the same punching strength. According to the Modified Lisbon setup, the punching strength provided by slabs with the opening was about 20% lower than that provided by the reference slab. This reduction coincides with the reduction of the control perimeter, due to the presence of the opening, calculated according to the EC2-2004.

Therefore, for vertical loading only the presence of openings results detrimental for the punching strength. The reduction of the punching strength is proved to be directly related to the reduction of the control perimeter as suggested by code provisions.

6.1.2 Effects of opening on punching failure due to combined vertical and horizontal loading on slabs without shear reinforcement

According to experimental results, when combined gravity and horizontal loading are applied to slabs without shear reinforcement, the presence of the opening seems to have a lower influence compared to that showed for vertical loading only. The specimens with opening SO1-02 and SO2-02 failed by punching for a drift of 1%, as the reference slab. The maximum unbalanced moment showed by the three specimens resulted about 75 kNm except for that exhibited by the specimen SO1-02 for southward loading. In this case the maximum unbalanced moment resulted about 46% lower than the reference slab.

The asymmetric behaviour provided by the specimen SO1-02 is due to the presence of the opening along the loading direction and it is the result of different flexural capacities according to the horizontal loading directions North and South. Indeed, for southward horizontal loading there has no tensile reinforcement passing through the column while for northward horizontal loading two 12mm hooked rebars are anchored in the column zone.

Compared to the experimental evidence, the numerical analysis provides slightly different results. Adopting the same material characteristics and the same vertical loading (V_g=194 kN) the specimens with opening show lower capacity than the reference slab. The maximum unbalanced moment provided by the reference slab results about 78 kNm. Considering northward loading, the presence of the opening provides a reduction of the maximum unbalanced moment of about 20% when compared to the case without opening. For southward loading, the series SO1 gives a reduction of 79% for the Lisbon setup and a reduction of 55% for the Modified Lisbon setup.

Considering the more realistic distribution of vertical loading, provided by the Modified Lisbon setup, the ultimate drift achieved by the reference slab is equal to 1.59%. For the specimen SO2-02 with opening placed on the East side, the ultimate drift results equal to 1.31%. The specimen SO1-02 with opening placed on North side provides an ultimate drift equal to 1.37% for northward loading and 0.88% for southward loading. For southward loading the reduction in terms of ultimate displacement provided by the opening results about 15-20% while for southward loading the opening on the North side gives a reduction of about 45%.

It should be noted that the cyclic loading tends to flatten the differences between the tests while the monotonic loading tends to highlight the differences. Indeed, if two specimens have similar characteristics, the cyclic failure of both specimens is expected to be reached in

the same step loading (same drift) while the monotonic failure is expected to be achieved for different horizontal drifts.

In conclusion, considering both experimental and numerical results, for slab column connections without shear reinforcement subjected to combined gravity and horizontal loading, the presence of an opening adjacent to the column plays a detrimental role if the lateral loading is applied in the opposite direction of the opening. For instance, if the opening is placed on the North side of the column and the loading is direct to South the percentage reduction in terms of maximum unbalanced moment could achieve the 55% when compared to the reference slab without openings. The percentage reduction in terms of ultimate displacement could achieve 45%.

For horizontal loading direct to East, West or North, the presence of the opening is less detrimental especially in terms of ultimate horizontal drift. The reduction in terms of maximum unbalanced moment is expected to be lower than 20%, while the ultimate horizontal drift is expected to be almost the same of slabs without opening.

These considerations are referred to a square opening, placed adjacent to the column, with a size equal to 80% of the column size. For larger opening sizes effects are expected to be higher. However, larger opening sizes are not recommended to be placed adjacent to columns.

6.1.3 Effects of opening on punching failure due to combined vertical and horizontal loading on slabs with shear reinforcement

According to experimental results, in case of combined gravity and horizontal loading applied to slabs with shear reinforcement, the presence of the opening affects the flexural capacity and, as consequence, the punching strength of the slab column connection. Considering northward drifts, the maximum unbalanced moment achieved by the specimen SO1-03 results equal to 83 kNm, about 33% lower than the reference specimen (123 kNm), while SO2-03 achieved 100 kNm, about 19% lower than the reference specimen. This difference in terms of flexural capacity, between the two specimens with openings, has been probably accentuated by the higher gravity loading of the specimen SO1-03 ($V_{g,SO1\text{-}03}$ = 214 kN, $V_{g,SO2\text{-}03}$ = 194 kN) and by the higher cyclic damaging effect due to the presence of the opening on the North side. For southward drifts, the maximum unbalanced moment achieved by the specimen SO1-03 (54 kNm) resulted 56% lower than that achieved by the reference specimen (124 kNm). With regards to the ultimate drift, the reference specimen achieved 4%, the

specimen with the opening placed on North side (SO1-03) reached 2.5%, while the specimen with the opening on the East side (SO2-03) reached 5.0%.

Despite the presence of the openings, specimens reached large horizontal drifts thanks to the presence of the shear reinforcement. Closed stirrups were designed, according to the EC2-2004, to provide a contribution in terms of punching strength at least equal to that provided by the concrete ($V_s \geq V_c$). Thanks to the insertion of shear reinforcement the specimens did not fail by punching and reached their flexural capacity.

The numerical analysis provides almost the same results of the experimental activity. As for the previous case, material characteristics are assumed equal for all the specimens, like the vertical loading, assumed equal to V_g=190 kN. Considering the Modified Lisbon setup, the maximum unbalanced moment provided by the reference slab results about 128 kNm. For northward loading, both specimens with opening provided a maximum unbalanced moment equal to about 100 kNm, 22% lower than the reference slab. For southward loading, the series SO1 gives a reduction of maximum unbalanced moment equal to 58% compared to the reference slab.

In conclusion, considering both experimental and numerical results, for slab column connections with shear reinforcement subjected to combined gravity and horizontal loading, the presence of an opening adjacent to the column plays a detrimental role especially if the lateral loading is applied in the opposite direction of the opening. For instance, if the opening is placed on the North side of the column and the loading is direct to South the reduction in terms of maximum unbalanced moment could achieve the 58% when compared to the reference slab without openings.

For horizontal loading direct to East, West or North, the reduction in terms of maximum unbalanced moment is expected to be lower than 25% of the peak moment achieved by the slab without openings. The ultimate horizontal drift is expected to be almost the same of slab without opening if shear reinforcement is properly designed. In this case, as discussed above, the contribution to the punching strength provided by shear reinforcement (V_s) was set to be at least equal to that provided by the concrete only (V_c) as follows $V_s \geq V_c$.

As for the previous case, these considerations are referred to a square opening, placed adjacent to the column, with a size equal to 80% of the column size. For larger opening sizes effects are expected to be higher. However, larger opening sizes are not recommended to be placed adjacent to the columns.

6.1.4 Considerations on the Lisbon setup

As shown previously, results of the experimental gravity loading tests highlighted some uncertainties regarding the reliability of the Lisbon setup. The specimen SO1-01, with the opening placed on the North side of the column, showed a sensible reduction of the punching strength when compared to the reference slab MLS, while the specimen SO2-01 apparently was not affected by the presence of the opening in the East side of the column. This inconsistence is essentially due to the distribution of gravity loading around the support provided by the Lisbon setup.

To investigate the behaviour and the reliability of the Lisbon setup a numerical model, providing a modified distribution of vertical loading, was developed. This model, named Modified Lisbon setup, provided the same vertical punching strength for the two series SO1 and SO2 with the opening placed on North and East side, respectively. Without openings the Lisbon setup and the Modified Lisbon setups provided almost the same punching strength. These results show how the distribution of vertical loading has a low influence for slab without openings, while it affects the vertical punching strength when openings are placed adjacent to the column.

However, for combined vertical and horizontal loading the distribution of vertical loading seems to have a lower influence on the response of slab column connections with openings. Indeed, both Lisbon and Modified Lisbon setup provided almost the same results except for the series SO1 for southward loading. In this case the two setups showed very different results. Compared to the reference slab the reduction in terms of peak moment resulted equal to 79% for the Lisbon setup and 55% for the Modified Lisbon setup. In presence of shear reinforcement, the influence of the vertical loading distribution resulted even lower, indeed the two setups provided almost equal results.

In conclusion, the response of slab column connection without openings was found to be scarcely affected by the distribution of the vertical loading, proving the reliability of the Lisbon setup. In presence of openings the influence of the vertical loading distribution was strongly found for gravity loading only. In this case experimental results provided by the Lisbon setup should be compared with numerical results provided by the Modified Lisbon setup. For combined gravity and horizontal loading this influence becomes very small and experimental results provided by the Lisbon setup are perfectly reliable.

6.1.5 Behaviour of internal slab column connections with openings adjacent to the column

The Lisbon setup was developed in the NOVA School of Science and Technology and represents one of the few attempts to comply the boundary conditions of a continuous flat slab subjected to combined gravity and horizontal loading. This setup allows equal vertical displacements and equal rotations at the opposite North-South slab borders. The specimen represents in longitudinal direction the slab between the mid-span lines, while in transverse direction is limited to 22% of the span length. It could be said that the specimen of the Lisbon setup represents a 4000 mm flat slab span, or 2/3 scale of a real flat slab 6000 mm span.

Beside a square specimen would be better for representing the actual behaviour of an internal slab column connection, the rectangular shape of the specimen was imposed by reasons of space and handling in the structural laboratory. The rectangular shape poses important challenges with regards to the compliance of constraint and loading conditions along the East-West direction.

Thanks to the numerical model of the Modified Lisbon setup, effects of the loading distribution against the response of the slab column connection have been investigated. The reliability of the Lisbon setup results confirmed for slab subjected to combined gravity and horizontal loading.

However, for a deeper investigation of the behaviour of an internal slab column connection, a new numerical model has been developed. This model, named Continuous setup, is the attempt to replicate the actual behaviour of the reference flat slab. The entire slab is modelled from midspan to midspan in both directions.

For gravity loading only, the Continuous setup provides a punching strength 15% higher than the Lisbon setup. Furthermore, the punching strength results independent from the position of the opening (North or East) and the detrimental effect provided by the latter results about 20% of the punching strength without opening, as found for the Modified Lisbon setup. This value corresponds to the reduction of control perimeter calculated according to EC2-2004.

For combined gravity and horizontal loading without shear reinforcement, the Continuous setup without openings provides a maximum unbalanced moment 73% higher than the Lisbon setup. The ultimate drift results equal to 1.59%, about 21% than that provided by the Lisbon setup (1.31%).

For northward loading, the presence of the opening in the Continuous setup provides a reduction of the maximum unbalanced moment of about 25% when compared to the case without opening. The reduction in terms of ultimate drifts results about 20% for both series SO1 and SO2. For southward loading, the series SO1 gives a reduction of 55% in terms of maximum unbalanced moment and a reduction of 50% in terms of ultimate drift.

For combined gravity and horizontal loading with shear reinforcement, the Continuous setup without openings gives a yielding moment about 35% higher than the Lisbon setup. For the Complete setup the presence of openings induces a substantial reduction of the yielding moment, for northward loading this reduction is about equal to 25% while for southward loading the series SO1 leads to a reduction equal to 55%.

In conclusion, the numerical model of the Continuous setup is the attempt to replicate the actual behaviour of an internal slab column connection. Compared to the Lisbon setup, this model shows higher flexural capacity, but it provides the same behaviour of the Lisbon setup with regards to the presence of openings. Furthermore, the two setups provide similar results in terms of ultimate horizontal drift.

Therefore, the experimental results provided by the Lisbon setup give a valuable information about the behaviour of an actual slab column connection with or without opening adjacent to the column.

6.2 Recommendations for future research

This research is focused on the effects provided by the presence of an opening placed adjacent to the column on the behaviour of an internal slab column connection. The opening size is chosen equal to 0.8 times the size of the column. More research could be done on openings with different sizes, the location of the opening from the column could be also investigated by testing appropriate specimens.

The experimental activity of this research was performed by using the Lisbon setup developed in the NOVA School of Science and Technology. A new test setup with square specimens could be developed for achieving a greater complying of the actual boundary conditions of an internal slab column connection. However, since experimental programs are expensive and time-consuming future research should include nonlinear finite element analysis. The calibration of a cyclic model is recommended for future research. Thanks to this model a deeper investigation of the behaviour of a slab column connection could be achieved.

REFERENCES

Aalami, B.; Moment Rotation Relation Between Column and Slab, ACI Journal, 1972, Vol. 69: pp. 263–9.

ACI Committee 318.; Building Code Requirements for Structural Concrete (ACI 318M-14) and Commentary (ACI 318RM-14), Farmington Hills, U.S.A.: 2014.

ACI-ASCE Committee 421.; ACI 421.2R-10 Guide to Seismic Design of Punching Shear Reinforcement in Flat Plates, 2010.

Alexander, SB.; Shear and moment transfer at column-slab connections, ACI Special Publication, 2017, Vol. 315: pp. 1–22.

Alexander, SDB.; Simmonds, SH.; Bond Model for Concentric Punching Shear, ACI Structral Journal, 1992, Vol. 89: pp. 325–34.

Allen, BF.; Darvall, P.; Lateral Load Equivalent Frame, ACI Journal, 1977, Vol. 74: pp. 294–9.

Almeida, A.; Marreiros, R.; Ramos, AP.; Ornelas, M.; Alcobia, B.; Behaviour of RC Flat Slabs with Stirrups under Reversed Horizontal Cyclic Loading, Magazine of Concrete Research, 2019.

Almeida, AFO.; Inacio, MMG.; Lucio, VJG.; Ramos, AP.; Punching behaviour of RC flat slabs under reversed horizontal cyclic loading, Engineering Structures, 2016, Vol. 117: pp. 204–19.

American Concrete Institute.; Building Code Requirements for Structural Concrete (ACI 318-19), 2019.

Anil, Ö.; Kina, T.; Salmani, V.; Effect of opening size and location on punching shear behaviour of two-way RC slabs, Magazine of Concrete Research, 2014, Vol. 66: pp. 955–66.

ASCE.; Seismic Evaluation and Retrofit of Existing Buildings (ASCE 41-13), ASCE/SEI 4, American Society of Civil Engineers; 2014.

Banchik, CA.; Effective beam width coefficients for equivalent plane frame analysis of flat-plate structures. University of California, Berkeley, 1987.

Birtel, V.; Mark, P.; Parameterised Finite Element Modelling of RC Beam Shear Failure, Abaqus Users' Conference, 2006: pp. 95–108.

Bompa, D V.; Onet, T.; Punching shear strength of RC flat slabs at interior connections to columns, Magazine of Concrete Research, 2016, Vol. 68: pp. 24–42.

Borges, LLJ.; Melo, GS.; Gomes, RB.; Punching Shear Strength of Reinforced Concrete Flat Plates with Openings, ACI Structral Journal, 2013, Vol. 110: pp. 547–56.

Broms, CE.; Design method for imposed rotations of interior slab-column connections, ACI Structural Journal, 2009, Vol. 106: pp. 636–45.

Bu, W.; Polak, MA.; Effect of openings and shear bolt pattern in seismic retrofit of reinforced concrete slab-column connections, Engineering Structures, 2011, Vol. 33: pp. 3329–40.

CEB/FIP.; Ceb-Fip Model Code 1990, London: Thomas Telford; 1993.

CEB/FIP.; Model Code 2010 - Volume 1, Bulletin 6, Lausanne, Switzerland: Internation Federation for Structural Concrete (fib); 2012.

CEN.; EN 12390-13 Testing hardened concrete Part 13: Determination of secant modulus of elasticity in compression, Bruxelles: 2013.

CEN.; EN 12390-3 Testing hardened concrete Part 3: Compressive strength of test specimens, Bruxelles: 2009.

CEN.; EN 12390-6 Testing hardened concrete Part 6: Tensile splitting strength of test specimens, Bruxelles: 2000.

CEN.; Eurocode 2: Design of concrete structures - Part 1-1: General rules and rules for buildings, Bruxelles: 2004.

Corley, WG.; Jirsa, JO.; Equivalent Frame Analysis For Slab Design, ACI Journal, 1970, Vol. 67: pp. 875–84.

Corley, WG.; Sozen, MA.; Siess, CP.; The Equivalent Frame Analysis for Reinforced Concrete Slabs, Urbana, Illinois: 1961.

Di Stasio, J.; Van Buren, MP.; Transfer of Bending Moment between Flat Plate Floor and Column, ACI Journal, 1960, Vol. 32: pp. 299–314.

Drakatos, I.; Beyer, K.; Muttoni, A.; Lateral Force Resisting Mechanisms in Slab-Column Connections : an Analytical Approach, 2nd European Conference on Earthquake Engineering and Seismology, 2014: pp. 11.

Drakatos, IS.; Muttoni, A.; Beyer, K.; Internal slab-column connections under monotonic and cyclic imposed rotations, Engineering Structures, 2016, Vol. 123: pp. 501–16.

Drakatos, IS.; Muttoni, A.; Beyer, K.; Mechanical model for drift-induced punching of slabcolumn connections without transverse reinforcement, ACI Structural Journal, 2018, Vol. 115: pp. 463–74.

El-Salakawy, E.; Polak, MA.; Soliman, MH.; Slab-column edge connections subjected to high moments, Canadian Journal of Civil Engineering, 1998, Vol. 25: pp. 526–38.

El-Salakawy, EF.; Polak, MA.; Soliman, MH.; Reinforced concrete slab-column edge connections with openings, ACI Structural Journal, 1999, Vol. 96: pp. 79–87.

Elshafiey, TMF.; Hussein, M.; Abdel-Aziz, M.; Behaviour of Flat Slabs With Openings Adjacent to Columns. Struct. Faults Repair 14th Int. Conf., Edinburgh: 2012.

European Committee for Standardization.; EN 10080 Steel for reinforcement of concrete - Weldable reinforcing steel - General, 2005.

European Committee for Standardization.; Eurocode 8: Design of structures for earthquake resistance - Part 1: General rules, seismic actions and rules for buildings Eurocode, 2004.

fib.; fib Bulletin 42: Constitutive Modelling of High Strength/high performance concrete, 2008.

Genikomsou, AS.; Polak, MA.; Finite element analysis of punching shear of concrete slabs using damaged plasticity model in ABAQUS, Engineering Structures, 2015, Vol. 98: pp. 38–48.

Ha, T.; Lee, M-H.; Park, J.; Kim, D-J.; Effects of openings on the punching shear strength of RC flat-plate slabs without shear reinforcement, Structural Design of Tall and Special Buildings, 2015, Vol. 24: pp. 895–911.

Han, S-W.; Park, Y-M.; Kee, Js-H.; Stiffness Reduction Factor for Flat Slab Structures under Lateral Loads, Journal of Structural Engineering, ASCE, 2009, Vol. 135: pp. 743–50.

Hawkins, NM.; Bao, A.; Yamazaki, J.; Moment Transfer from Concrete Slabs to Columns, ACI Structural Journal, 1989, Vol. 86: pp. 705–16.

Hognestad, E.; Elstner, RC.; Hanson, JA.; Shear Strength of Reinforced Structural Lightweight Aggregate Concrete Slabs, Journal Proceedings, 1964, Vol. 61: pp. 643–56.

Hordijk, DA.; Local approach in fatigue of concrete. Delft University, 1991.

Hwang, S.; Moehle, JP.; Models for Laterally Loaded Slab-Column frames, ACI Structural Journal, 2000, Vol. 97: pp. 345–53.

Jankowiak, T.; Lodygowski, T.; Identification of parameters of concrete damage plasticity constitutive model, Foundations of Civil and Environmental …, 2005: pp. 53–69.

Kupfer, H.; Hilsdorf, H.; Rush, H.; Behaviour of Concrete Under Biaxial Stresses, ACI Journal, 1969, Vol. 66: pp. 856–66.

Lee, J.; Fenves, GL.; Plastic-Damage Model for Cyclic Loading of Concrete Structures, Journal of Engineering Mechanics (ASCE), 1998, Vol. 124: pp. 892–900.

Liberati, EAP.; Marques, MG.; Leonel, ED.; Almeida, LC.; Trautwein, LM.; Failure analysis of punching in reinforced concrete flat slabs with openings adjacent to the column, Engineering Structures, 2019, Vol. 182: pp. 331–43.

Lubliner, J.; Oliver, J.; Oller, S.; Oñate, E.; A plastic-damage model for concrete, International Journal of Solids and Structures, 1989, Vol. 25: pp. 299–326.

Luo, YH.; Durrani, a. J.; Conte, JP.; Equivalent Frame Analysis of Flat Plate Buildings for Seismic Loading, Journal of Structural Engineering, 1994, Vol. 120: pp. 2137–55.

Luo, YH.; Durrani, AJ.; Equivalent Beam Model for Flat-Slab Buildings-Part 1 : Interior Connections, ACI Structral Journal, 1995, Vol. 92: pp. 115–24.

Mamede, N.; Ramos, A.; Faria, D.; Experimental and Parametric 3D Nonlinear Finite Element Analysis on Punching of Flat Slabs with Orthogonal Reinforcement, Engineering Structures, 2013, Vol. 48: pp. 442–57.

Mast, PE.; Stresses in Flat Plates Near Columns, ACI Journal, 1970, Vol. 67: pp. 761–8.

Megally, S.; Ghali, A.; Design considerations for slab-column connections in seismic zones, ACI Structural Journal, 1994, Vol. 91: pp. 303–14.

Megally, S.; Ghali, A.; Punching Shear Design of Earthquake-Resistant Slab- Column Connections, ACI Structural Journal, 2000, Vol. 97: pp. 720–30.

Moe, J.; Shearing Strength of Reinforced Concrete Slabs and Footings under Concentrated Loads., Journal of Portland Cement Association, Research and Development Laboratories, 1961, Vol. D47: pp. 130.

Mowrer, RD.; Vanderbilt, MD.; Shear Strength of Lightweight Aggregate Reinforced Concrete Flat Plates, Journal Proceedings, 1967, Vol. 64: pp. 722–9.

Muttoni, A.; Punching shear strength of reinforced concrete slabs without transverse reinforcement, ACI Structural Journal, 2008, Vol. 105: pp. 440–50.

Muttoni, A.; Ruiz, MF.; Bentz, E.; Foster, S.; Sigrist, V.; Background to fib Model Code 2010 shear provisions - part II: punching shear , Structural Concrete, 2013, Vol. 14: pp. 204–14.

Muttoni, A.; Ruiz, MF.; The levels-of-approximation approach in MC 2010: Application to punching shear provisions, Structural Concrete, 2012, Vol. 13: pp. 32–41.

Muttoni, A.; Schubfestigkeit und Durchstanzen von Platten ohne Querkraftbewehrung, Beton- Und Stahlbetonbau, 2003, Vol. 98: pp. 74–84.

Muttoni, A.; Schwartz, J.; Behavior of Beams and Punching in Slabs without Shear Reinforcement, IABSE Colloquium, 1991, Vol. 62: pp. 703–8.

Najafgholipour, MA.; Dehghan, SM.; Dooshabi, A.; Niroomandi, A.; Finite element analysis of reinforced concrete beam-column connections with governing joint shear failure mode, Latin American Journal of Solids and Structures, 2017, Vol. 14: pp. 1200–25.

Nana, WSA.; Bui, TT.; Limam, A.; Abouri, S.; Experimental and Numerical Modelling of Shear Behaviour of Full-scale RC Slabs Under Concentrated Loads, Structures, 2017, Vol. 10: pp. 96–116.

Navarro, M.; Ivorra, S.; Varona, FB.; Parametric computational analysis for punching shear in RC slabs, Engineering Structures, 2018, Vol. 165: pp. 254–63.

Oliveira, DC.; Gomes, RB.; Melo, GS.; Punching shear in reinforced concrete flat slabs with hole adjacent to the column and moment transfer, Revista IBRACON de Estruturas e Materiais, 2014, Vol. 7: pp. 414–67.

Pan, A.; Moehle, JP.; Lateral displacement ductility of reinforced concrete flat plates, ACI Structural Journal, 1989, Vol. 86: pp. 250–8.

Park, YM.; Han, SW.; Kee, S-H.; A modified equivalent frame method for lateral load analysis, Magazine of Concrete Research, 2009, Vol. 61: pp. 359–70.

Pavlović, M.; Marković, Z.; Veljković, M.; Bucrossed D Signevac, D.; Bolted shear connectors vs. headed studs behaviour in push-out tests, Journal of Constructional Steel Research, 2013, Vol. 88: pp. 134–49.

Pecknold, DA.; Slab Effective Width for Equivalent Frame Analysis, ACI Journal, 1975, Vol. 72: pp. 135–7.

Popovics, S.; A numerical approach to the complete stress-strain curve of concrete, Cement and Concrete Research, 1973, Vol. 3: pp. 583–99.

Regan, PE.; Shear Reinforcement of Flat Slabs. Int. Work. Punching Shear Capacit. RC Slab, Stockholm: 2000, p. 99–107.

Regan, PE.; Ultimate limite state principles. In: fib (fédération internationale du béton / the International Federation for Structural Concrete), editor. fib Bull. 2, Struct. Concr. Textb. Behav. Des. Performance; Vol. 2 Basis Des., 1999, p. 320.

Roll, F.; Zaidi, STH.; Sabnis, G.; Chuang, K.; Shear Resistance of Perforated Reinforced Concrete Slabs, ACI Special Publication, 1971, Vol. 30: pp. 77–101.

Russell, JM.; Owen, JS.; Hajirasouliha, I.; Nonlinear behaviour of reinforced concrete flat slabs after a column loss event, Advances in Structural Engineering, 2018, Vol. 21: pp. 1–15.

Sagaseta, J.; Muttoni, A.; Ruiz, MF.; Tassinari, L.; Non-axis-symmetrical punching shear around internal columns of RC slabs without transverse reinforcement, Magazine of Concrete Research, 2011, Vol. 63: pp. 441–57.

Simulia.; Abaqus 6.11 Theory Manual 2011: pp. 1172.

Stamenkovic, A.; Chapman, JC.; Local strengthlat column heads in flat slabs subjected t o a combined vertical and horizontal loading, Proceedings of the Institution of Civil Engineers, 1974, Vol. 57: pp. 205–32.

Tassinari, L.; Poinçonnement non symétrique des dalles en béton armé. Ecole Polytechnique Fédérale de Lausanne, 2011.

Teng, S.; Cheong, HK.; Kuang, KL.; Geng, JZ.; Punching shear strength of slabs with openings and supported on rectangular columns, ACI Structural Journal, 2004, Vol. 101: pp. 678–87.

Van Mier, JG.; Shah, SP.; Arnaud, M.; Balayssac, J.; Bascoul, A.; Choi, S.; et al.; Strain-softening of concrete in uniaxial compression, vol. 30, 1997.

Van Mier, JGM.; Part II : Load-Histories, Materiaux et Constructions, 1986, Vol. 19: pp. 190–200.

Vanderbilt, MD.; Corley, WG.; Frame analysis of concrete buildings, Concrete International, 1983, Vol. 5: pp. 33–43.

Vecchio, FJ.; Collins, MP.; The modified compression-field theory for reinforced concrete elements subjected to shear, ACI Journal Proceedings, 1986, Vol. 83: pp. 219–31.

Walraven, JC.; Fundamental analysis of aggregate interlock, Journal of Structural Engineering, ASCE, 1981, Vol. 107: pp. 2245–70.

Westergaard, HM.; Moments and stresses in slabs, Journal Proceedings, 1921, Vol. 17: pp. 415–538.